BULK ORIENTATION OF AGRICULTURAL FILLER-POLYPROPYLENE COMPOSITES

by

Zena Sin-Nga Ng

A thesis
presented to the University of Waterloo
in fulfillment of the
thesis requirement for the degree of
Master of Applied Science
In
Chemical Engineering

Waterloo, Ontario, Canada, 2008

AUTHOR’S DECLARATION

I hereby declare that I am the sole author of this thesis. This is a true copy of the thesis, including any required final revisions, as accepted by my examiners.

I understand that my thesis may be made electronically available to the public.

_____

ABSTRACT

When two or more individual materials combine to form a new material with improved characteristics, a composite is created. The two major components in a thermoplastic composite are the polymer, such as polypropylene (PP), and the filler, such as minerals like calcium carbonate and talc, or agricultural crop by-products like wheat straw, soy hull and soy stems. The main advantages of using agricultural fillers (AgFillers) in polypropylene are cost reduction and modulus improvement, without drastically increasing the specific gravity of the composite. These properties can be further enhanced by subjecting the composite to the bulk orientation process, in which the polymer chains align to give superior strength to the material, while the presence of polar AgFillers contributes to a reduction in material density.

The objective of this research was to systematically study the relationships between the components and properties of AgFiller-PP composites, and their contributions to property modifications. Three types of AgFillers, wheat straw (WS), soy hulls (SH) and soy stems (SS) were studied, along with two PP types, virgin PP (vPP) and recycled PP (rPP), and mixtures of the two PP types. Non-oriented composites with a composition ratio of 40 wt% AgFiller to 60 wt% PP were tested for their morphology, chemical, thermal, rheological and mechanical properties. Similar properties of oriented composites with 20 wt% wheat straw filler and 80 wt% PP were also examined.

The type of AgFiller was found to play a significant role in determining the rheological and mechanical properties of non-oriented AgFiller-PP composites. Scanning electron microscopy (SEM) showed that AgFillers had the tendancy to align lengthwise when subjected to the extrusion process. Depending on the fiber alignment within the filler with respect to the lengthwise direction of the filler, each AgFiller contributed differently to the composites' properties. Stem-based AgFillers like WS and SS had fiber alignment parallel to the lengthwise direction, and the composites created had higher viscosity and higher flexural modulus. On the other hand, shell-based AgFillers like SH had fiber alignment perpendicular to the filler's length, and were found to have less contribution to viscosity increase. Fourier transform Infrared (FTIR) spectroscopy using attenuated total reflectance (ATR) technique showed that a skin layer of PP congregated on the surface of all the non-oriented AgFiller-PP composites, regardless of the AgFiller used.

The main contribution of PP polymer type was to the rheological properties of non-oriented AgFiller-PP composites. The presence of rPP also appeared to slightly improve the immiscibility between polar AgFillers and nonpolar PP polymer, according to SEM image analysis. The viscosity of the composites decreased linearly with increasing amount of rPP, because the rPP tested had significantly lower viscosity than the vPP chosen. No statistically significant conclusions could be drawn on the mechanical property changes due to large experimental variance that existed in the data.

Bulk orientation of AgFiller-PP composites was shown to provide significant reduction in the material's density as well as improvement in physical properties. Experimental results of oriented wheat straw-PP composites showed that wheat straw was highly comparable, perhaps even more superior, to wood fibers as filler for oriented PP composites. The ability to produce oriented wheat straw-PP composites using the same technology and conditions as producing oriented wood-plastic composites affirmed the feasibility for commercialization of oriented wheat straw-PP composites, and by means contributing to setting a milestone in the scientific research of AgFiller-thermoplastic biocomposites.

ACKNOWLEDGEMENTS

I would like to express my sincere gratitude to Dr. Leonardo Simon, my supervisor, for providing me with the opportunity for graduate research, and for his guidance. I would like to further thank Dr. Larry Erickson and Dr. Frank Maine for sharing their insights and expertise on the project subject.

I thank my lab colleagues and friends, Aaron Law, Anthony Shin and Paula Kruger for the inspiration and support given to me over the length of my research. I specially thank my family for believing in me and providing much needed reassurance at difficult times and when I was in doubt.

Finally, I would like to acknowledge the financial support provided by the Ontario Ministry of Agriculture, Food and Rural Affairs (OMAFRA); and the industrial sponsors, A.Schulman and Green Forest, for their in-kind donations.

DEDICATION

I dedicate this thesis to *Bruce*, my fiancé, who has shown me immense love and patience, and supported me the entire length of my studies.

TABLE OF CONTENTS

LIST OF TABLES

LIST OF FIGURES

SELECTED ABBREVIATIONS

AgFiller – agricultural filler
PP – polypropylene
iPP – isotactic polypropylene
vPP – virgin polypropylene
rPP – recycled polypropylene
SH – soy hull
SS – soy stem
WS – wheat straw
WPC – wood plastic composite
g *prefix* – ground
o *prefix* – oriented
PVC – poly vinyl chloride
PLA – poly lactic acid
$CaCO_3$ – calcium carbonate
FTIR – Fourier transform infrared
ATR – attenuated total reflection
DSC – differential scanning calorimetry
TGA – thermal gravimetric analysis
XRD – X-ray diffraction
MFI – melt flow index
SEM – scanning electron microscopy
wt% - percentage in weight basis
L – length (mm)
W – width (mm)
D – thickness (mm)
K – K-value of β form crystal fraction
T_m – melting temperature (°C)
T_c – temperature of crystallization (°C)
X_c – percentage of crystallinity (%)
ΔH – heat of fusion (J/g)
ΔH° - specific heat of fusion (J/g)
d_p – penetration depth (μm)
n – refractive index

CHAPTER 1 INTRODUCTION

A composite combines two or more individual materials and extracts selected benefits of each constituent to create a more superior substance. In a thermoplastic composite, the polymer acts as the matrix or continuous phase, in which filler is dispersed. Despite disadvantages brought upon by high specific gravity, most traditional choices of fillers are mineral based, such as calcium carbonate and talc, mainly due to their abundance, low cost, and reinforcing abilities from the fillers' high strength and stiffness. Other well known examples of thermoplastic composites are glass-fiber reinforced plastic (FRP) and wood plastic composite (WPC).

Agricultural filler-polypropylene (AgFiller-PP) composites receive reinforcement in both strength and stiffness from fillers originated from crops such as wheat and soy, while maintaining the formability and stability of the polypropylene matrix. Everyday consumer products such as furniture, automotive parts and decking material can be made of composites using processing techniques such as injection molding and extrusion. Occasionally, compounding and masterbatching are used as an intermediate step to convert a recipe of numerous raw materials into one single material prior to being extruded or molded. Compound materials obtained from the compounding process contain exact amounts of ingredients per their formulations and can be directly used in downstream processes. A masterbatch material, on the other hand, is a concentrated version of the recipe, and requires dilution using additional polymer resin when used in the downstream processes.

In addition to the use of reinforcing fillers, the physical properties of polypropylene can also be improved by orienting the polymer using forming or drawing techniques. By means of bulk orientation, the backbone of the polymer chain uncoils and becomes straightened, allowing subsequently applied stresses to be distributed over strong covalent C-C bonds, thus increasing the strength, stiffness and impact resistance of the material.

1.1 Motivation

In recent years, increasing environmental awareness has prompted the development and use of "green" materials in consumer products, as part of the effort to promote renewability of resources and to lower the emission of harmful greenhouse gases. Currently, the most common thermoplastic materials such as polyethylene and polypropylene are derived from fossil fuels, a non-renewable resource that produces a heavy carbon footprint. Attempts in developing a bio-based polymer to replace commodity thermoplastics have had little success due to the inability of these bio-based polymers to compete economically (Mohanty, 2002). On the other hand, agricultural activities consistently provide sources of renewable bio-based filler that can readily be incorporated into existing polymer systems. By replacing portions of petroleum-based thermoplastic with fillers obtained from agricultural crop residues in the making of composite materials, society's dependence on fossil fuels may be eased.

Concurrently, there has been a continuous effort in the automotive industry to seek high strength raw materials that are also light weight, in order to improve the gas mileage and efficiency of vehicles. The low specific gravity of agricultural fillers makes possible the development of a light weight composite that at the same time possesses high flexural stiffness, thus giving the material an added advantage over composites filled with inorganic fillers. In the construction industry, wood plastic composites (WPC) have successfully gained market acceptance as a replacement of traditional wood products such as beams and panels. Advantages of WPC products include durability, non-splintering characteristics and high stiffness. However, the supply of timber-based fillers has its constraints due to the fact that trees require decades to grow into marketable size. In contrast, most agricultural crops are grown and harvested annually, rendering the supply of AgFillers boundless. This has prompted many research efforts to investigate the feasibility of AgFillers as replacements to wood fillers to alleviate timber dependency (Sanadi, 1995; Chen, 1998; Panthapulakkal, 2006).

1.2 Objective and Scope

The goal of this research is to serve as a step towards the development of an AgFiller-PP composite that is environmentally friendly, by using renewable raw materials and reducing the amount of petroleum-based plastic in the composition. The composite created would possess desirable properties suitable for its intended applications. It would create new market opportunities for the agricultural sector as a feedstock supplier for non-food applications, and the manufacturing sector as a consumer.

This thesis discusses the relationships between the components and properties of AgFiller-PP composites, determined through a series of systematic studies. The first portion of the study investigated how the selection of AgFiller and PP matrix types affects the rheological, thermal, chemical and mechanical properties of the composite. The second section of the project studied the effect of bulk orientation on the formation of microscopic voids in the composite, and the changes in density and mechanical properties brought upon as a result.

While AgFiller-PP composite is the material of interest for investigation, it is not in the scope of this project to study in detail the biology of the AgFillers used. Only aspects pertinent to the composites' performance, including the surface morphology and thermal stability of the filler, were examined. It is also beyond the scope of this thesis to discuss the effects brought upon by additives or components in the composite other than the polymer and filler.

1.3 Document Outline

This thesis contains seven chapters, as follows:

CHAPTER 1 - introduces the reader to the thesis topic by stating the motivation, objective and scope of the research, and outlines the document with a brief description for each chapter.

CHAPTER 2 - provides an overview of research on AgFiller-thermoplastic composites by other scientific efforts documented by literature. The compositions, processes, applications and properties of AgFiller-PP composites are reviewed.

CHAPTER 3 - explains the systematic approach undertaken in this research. This section describes all materials and methods used in conducting experiments.

CHAPTER 4 - contains a presentation of experimental results to the characterization of AgFiller-PP composites prior to bulk orientation for morphology, chemical, thermal, chemical and physical properties. The importance of AgFiller type selection is discussed.

CHAPTER 5 - presents experimental results to the characterization of non-oriented AgFiller-PP composites for morphology, chemical, thermal, chemical and physical properties. This chapter discusses the effects of varying the composition of the PP polymer matrix on the properties of the composities.

CHAPTER 6 - investigates the effect of the bulk orientation process on the properties of AgFiller-PP composites. The role that AgFillers play in determining the properties of oriented composites is examined, and the feasibility of using AgFillers as a replacement of wood fibers in making oriented composites is assessed.

CHAPTER 7 - contains concluding remarks and describes the contributions this research has made to the study of AgFiller-thermoplastic biocomposite materials. Recommendations for future work in this area of research are also presented in this section.

CHAPTER 2 LITERATURE REVIEW

2.1 Polymer Composites Filled with Agricultural By-Products

The incorporation of fillers into polymer systems has been practiced for over a century (Johnson, 1997), since the mass production of commodity plastics became possible. Up until the mid-1990s, the research and use of lignocellulosic material as filler mostly focused on wood fibers (Sanadi, 1995). In recent years, agricultural by-products have received increased attention as alternative fillers due to their low cost and abundance. Table 1 shows the global availability of major categories of lignocellulosic reinforcing materials that are suitable for use as fillers, where straw and stalk materials combined produce natural fibers in quantities that surpass wood fibers.

Table 1: Global availability of sources for lignocellulosic fibers (Rowell, 1997)

Material	World volume (million dry metric tons)
Wood	1750
Straw (wheat, rice etc)	1145
Stalk (corn, cotton etc)	970
Core (jute, kenaf, hemp)	8
Bast (jute, kenaf, hemp)	2.9
Leaf (sisal, abaca etc)	0.48

Researchers have used terms such as natural fillers or fibers (Salemane, 2005; Schemenauer, 2007), agro-fibers (Johnson, 1997), agro-plastics (Johnson, 1997), eco-composites (Bogoeva-Gaceva, 2007) and bio-composites (Mohanty, 2002; Alemdar, 2007) to describe this novel filler and the composites produced. Literature documenting this area of research revealed that both thermoplastic (Digabel, 2004; Crespo, 2007) and thermoset (Borda, 1999; Jacob 2006) polymers have been used as the matrix of plastic composites, depending on the intended applications of the composite. Meanwhile, the selection of AgFiller varies mainly according to local crop availability. For example, in Asia, bamboo and rice crops are abundant and therefore,

bamboo fibers (Mi, 1997; Chen, 1998) and rice husk fillers (Yang, 2004) have been studied greatly in the region. On the other hand, corn, wheat and soy account for the majority of domestic agricultural activity in the province of Ontario in Canada (OMAFRA, 2007).

Some researchers, such as Schirp *et al.* (2006), Jacob *et al.* (2006) and Panthapulakkal and Sain (2006), utilized AgFillers in the form of fibrous reinforcements. In such cases, the length to width (L:D) aspect ratio of the filler is of great importance, and the types of crops chosen typically belong to the bast or straw categories like kenaf, sisal and wheat straw, where high aspect ratios can be obtained. The resultant composites have enhanced modulus and strength, and are often compared to those reinforced with glass fibers (Rowell, 1999). Although the presence of the fibers provided improved mechanical properties of the composite (Jacob, 2006), the steps required to prepare the fibers can be complex and costly, often involving both mechanical and chemical treatments (Panthapulakkal, 2006). A more economical approach is to incorporate AgFillers into composites in the form of particulate fillers, similar to a flour, to replace the use of traditional mineral fillers such as calcium carbonate, mica and talc. The outcome of this practice is a composite with increased tensile and flexural moduli but little improvement on the strength of the composite (Rowell, 1999). The mechanical strength of rice husk filler-PP composites was found by Yang *et al.* (2004) to decrease as filler loading increases, and becomes unacceptable when the filler loading surpasses 40 wt%.

2.1.1 POLYPROPYLENE AS MATRIX OF COMPOSITES

Polypropylene (PP) is a semi-crystalline thermoplastic obtained from the Ziegler-Natta polymerization process. It is a polymer containing fundamental building blocks of propylene monomer, whose chemical structure is shown in Figure 1.

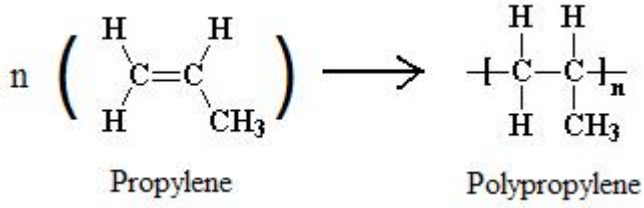

Figure 1: Schematics of polypropylene polymerization

PP is classified as a commodity thermoplastic due to its versatility in applications. The large annual production quantity contributes to its low cost of approximately $0.50 USD/lb (Johnson, 1997), making it greatly competitive against newly engineered plastics and biopolymers like poly-lactic acid (PLA) or bio-alcohols (Mohanty, 2002). As a thermoplastic, PP can be melted and shaped repeatedly, giving it an extra advantage in terms of recyclability. The molecular weight, tacticity and crystallinity are important characteristics that dictate the final properties of the polymer.

The molecular weight of PP is directly related to the chain lengths of the polymer as well as the amount of branching of the polymer. PP with longer chains, hence higher molecular weight, generally has higher physical properties but also becomes increasingly difficult to process. In fact, molecular weight of PP is positively related to its viscosity, which is further correlated inversely to melt flow index (MFI), a term more commonly used by industry (Maier, 1998). In addition, PP with higher molecular weights possesses higher tensile strength and stiffness, as lamellar thickness increases and shish-kebab (β-form) crystal structures are formed (Stern, 2007).

The crystallinity of PP is also dependent on the material's tacticity, or stereochemistry. PP can be isotactic, syndiotactic or atactic in nature, depending on the way the pendant methyl groups are arranged along the polymer backbone. Isotactic PP is the most common PP material available commercially, and is obtained when all methyl groups are configured identically on the same side of the polymer chain. On the other hand, when the methyl groups are configured in an alternating manner, syndiotactic PP is produced. The third type, atactic PP, contains randomly attached monomers and shows no specific arrangements (Maier, 1998).

The crystallinity of isotactic PP (iPP) is the highest among the three stereochemical configurations of PP due to its high level of molecular order. Three main forms of crystals, α, β and γ types, are created as the helical polymer chains fold into lamellae and grow to yield spherulites (Maier, 1998). The crystallization behaviour of PP has been a research interest for many groups, as it is dependent on the thermal history, such as cooling rate, and mechanical history, such as production techniques (injection molding, ram extrusion, die drawing etc), of the polymer. It is shown in the research by Gradys *et al.* (2005) that increasing cooling rate resulted in α-modifications and an increase of β-form crystals in iPP. Earlier work by Yin *et al.* (2004) studied the formation

of γ crystals in biaxially oriented PP films, and determined that in their case, cooling rate was more influential in the development of the crystal than the effect of stretching. Die drawing processes are also found to cause increases in the crystallinity of PP (Chaffey, 1997).

2.1.1.1 Virgin Polypropylene (vPP)

Virgin polypropylene (vPP) refers to PP material that is newly synthesized, and has never been previously made into any product. This material is mostly pure in nature, with occasional trace amounts of monomer and additive residues from the manufacturing process. vPP possesses characteristics most resemble its inherent design properties, such as viscosity and physical properties, based on which the material is marketed commercially. vPP can be further categorized into homopolymer, which is used extensively in many processes including extrusion and injection molding, random copolymer, which is less viscous compared to homopolymers due to lower crystallinity and higher chain mobility, and impact copolymer, which is designed to provide additional impact resistance for critical applications such as structural and automotive products (Maier, 1998). vPP can be purchased in Ontario at a cost of approximately $1680/ton (Jagarnauth, 2007).

2.1.1.2 Recycled Polypropylene (rPP)

Recycled PP (rPP) can be sorted into two types, namely post-industrial (pre-consumer) and post-consumer rPP, each of which can be further categorized into four groups (primary, secondary, tertiary and quaternary) according to their quality compared to virgin material, with “primary rPP” being of the best quality identical to that of virgin plastic, and “quaternary rPP” being of the lowest quality that is destined for incineration (La Mantia, 2002). While post-industrial rPP is typically graded as primary rPP due to its homogeneous nature, post-consumer rPP is often downgraded because it has been negatively impacted by degradation and contamination, and is less desirable by plastic processors. Two major groups of recyclable post-consumer waste are packaging materials and automotive scrap. Dairy containers, crates and totes, as well as used car

parts such as bumpers and lead battery casings are examples of recyclable post-consumer PP materials. Other applications that provide sources of rPP include non-wovens and slit tape fabrics.

The highly heterogeneous nature of post-consumer rPP remains the biggest challenge in deeming PP recycling a feasible process. The versatility of PP leads to production of goods in numerous applications, but at the same time makes the collection of PP waste strenuous, and output rate for rPP from specific sources (such as margarine tubs) is limited. In many occasions, rPP also suffered various degrees of degradation by chain scission during the first stages of processing, resulting in lower molecular weight than the original virgin PP resins (Maier, 1998). In turn, the lower molecular weight decreases the physical properties and crystallinity of products made using rPP.

Currently, the most common application for post-consumer rPP is in the production of recycled plastic lumber (RPL). Other applications include the manufacture of crates, bins and other type of containers. The use of post-consumer rPP in medical and food packaging industries is not widely practiced due to stringent restrictions by the FDA (Food and Drug Administration) or other federal health ministrations (CFSAN, 2006; Health Canada, 2003).

In Ontario, recycled waste made of PP has little value to local industries. For example, the Region of Peel Material Sorting Facility produces bales of rPP/HDPE mix with an 80:20 mix ratio. A portion of this recyclate is purchased by a sole local customer, while the remainder is exported overseas to China and to the USA, at a cost of approximately $150 per ton (Jagarnauth, 2007).

2.1.2 WHEAT AND SOY RESIDUES AS FILLER OF COMPOSITES

AgFillers obtained from both wheat and soy sources are lignocellulosic in nature, meaning that these fillers, like most plant materials, contain cellulose, hemicellulose, pectin and lignin as part of their compositions. In general, the composition of natural fiber fillers is 60-80% cellulose, 5-20% lignin (Saheb, 1999), with the remainder composed of hemicellulose, inorganics such as silica, and moisture (Golbabaie, 2007). Cellulose, a naturally occurring linear polymer, aggregates into microfibrils that are highly crystalline

and is the source of added strength and stiffness (Helbert, 1996; Alemdar, 2007). Meanwhile, lignin, a phenolic polymer, of up to 5 wt% provides antioxidation effects when added to PP, and enhances antioxidation when used in combination with commercial phenolic antioxidant additives (Gregorova, 2005).

In 2004, over four million tons of soy and wheat crops were produced in Ontario Canada (Stem Biomass Available from Major Ontario Crops (OMAFRA, 2007)). Of which, the majority in mass is considered a by-product (Table 2) and has only few applications such as fertilizers and animal feed. The large amount of stem material available from corn, soy and wheat crops as by-products is potentially excellent filler material at low cost.

Table 2: Stem Biomass Available from Major Ontario Crops (OMAFRA, 2007)

Crop	Production (t, 2004)	Stem Material (t)	Recoverable Stem Biomass (%)	Total Recoverable Stem Biomass (t)
Corn	5,334,300	4,735,700	70%	3,315,000
Soybean	2,476,600	2,000,000	90%	1,800,000
Wheat	1,676,400	3,840,000	75%	2,880,000

2.1.2.1 Wheat Straw (WS)

Wheat straw (WS) typically contains 35-40% cellulose, 45-55% hemicelluose and 15-20% lignin. Its similar cellulose content to wood (Csoka, 2008) makes it a reasonable candidate for study as an AgFiller. Figure 2 shows the morphology of the cross sectional surface of a wheat straw of the “soft white winter” strain grown in Ontario.

Figure 2: Micrograph of cross-section of wheat straw (Golbabaie, 2007)

Currently, most of the wheat straw harvested is used as animal feed and bedding. The remainder is generally considered waste and is left on the fields to be composted back into the land. By estimation based on average annual production of various types of wheat throughout the year, Ontario wheat straw carries a cost of $0.10-0.15/lb as an AgFiller, competitive to inorganic fillers of which the cost ranges at $0.05-0.50/lb (Kruger, 2007), especially when specific gravity differences of the two types of filler are also put under consideration.

The use of wheat straw as a particulate AgFiller in wheat straw-PP composites was studied extensively by Kruger (2007), where filler loading, water absorption properties, mechanical properties and interaction with additives were investigated. The study confirmed that wheat straw, like most other agricultural fillers, has weak resistance to water absorption and low compatibility with the polymer. The use of coupling agents can alleviate the problem of filler-polymer incompatibility, while water absorption can be reduced by lowering the processing temperature of the composite. It was also determined that the loading and aspect ratio of the wheat straw filler have great influence to the final properties of the composite. In terms of mechanical properties, Kruger concluded that fiber loading in the composite is positively related to flexural modulus, and inversely correlated to yield strength.

In addition to particulate fillers, wheat straw was also tested as filler in other forms. The use of lignocellulosic residues of wheat straw after acid treatment as fillers in polypropylene-polyethylene copolymer and in poly (butylenes adipate-co-terephthalate) copolyester was examined by Digabel *et al.* (2004). More recently, Alemdar and Sain (2007) extracted nanofibers from wheat straw and characterized their morphology chemical and thermal properties.

2.1.2.2 Soy By-products

Soybean production makes up for a significant portion of crops grown in Ontario. The advantage of using soybean by-product as a source of AgFiller is its abundance, since as much as 90% by weight of a soybean crop is its stem (OMAFRA, 2007), and close to an additional 1% is soy hull (Ashraf, 1988), both of which can be used as AgFiller at little cost. Figure 3 illustrates the schematics of a typical soy production and the sources for AgFillers. In addition to soy stems (SS) and soy hulls (SH), spent soy flakes (SSF) produced at the end of oil extraction processes can also be used as an AgFiller, although the investigation of its feasibility is beyond the scope of this thesis.

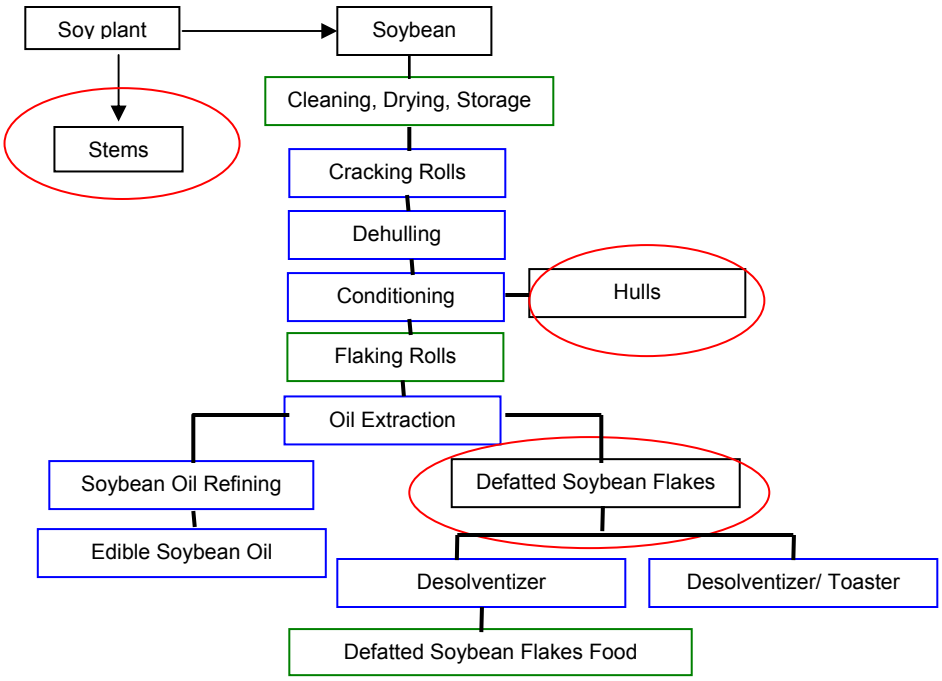

Figure 3: Soy production schematics (Wilke, 1979)

2.1.2.2.1 Soy Stems (SS)

Soy stem or soy stalk (SS) (Figure 4), of which a composition analysis showed that it contains 40% α-cellulose, 20% hemicellulose and 20% lignin (Wang, 2007), is a material greatly overlooked by the agricultural industry as a source of revenue. Although 90% of a soybean plant is of stem material (OMAFRA, 2007), there were currently few applications for soy stems except uses for animal feed or as compost. One novel application for soy stems was launched in a project named Project Soy, led by students at the University of Guelph, Ontario, who fabricated fashion attire using the fabrics constructed from soy stem material (University of Guelph, 2007). For applications as fillers in thermoplastic composites, nanofibers were extracted from soy stem by Wang and Sain (2007) using chemical treatment, and formed into composites with PVA (poly vinyl alcohol) and PE (polyethylene) as polymer matrices.

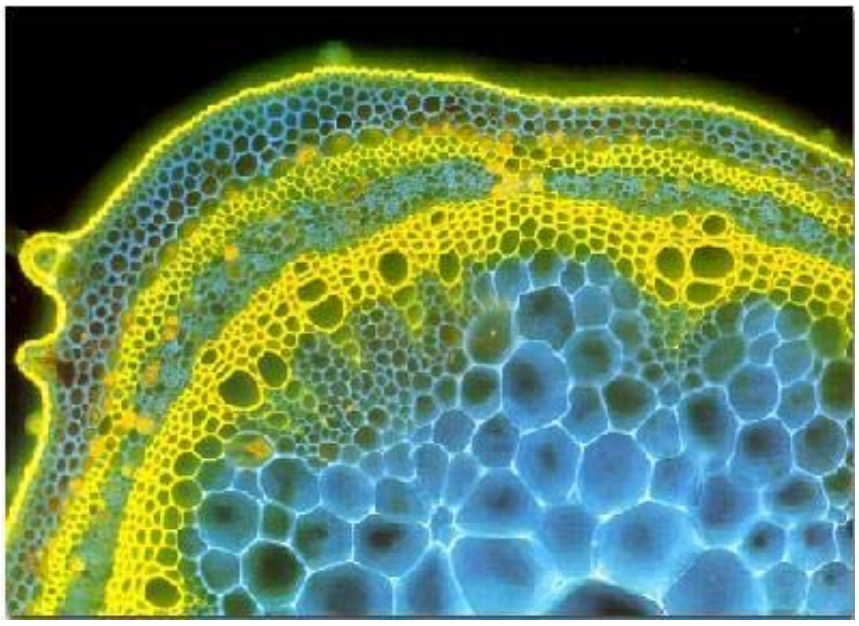

Figure 4: Micrograph of transverse section of soybean stem, stained with two fluorochromes to show distribution of cellulose (blue) and lignin (yellow). 50x mag. (Gates, 1985)

2.1.2.2.2 Soy Hulls (SH)

Soy hull (SH), also referred to as soy seed coat, accounts for 8% of a soybean's weight (Ashraf, 1988). Unlike stem materials, the cellulose-hemicellulose-lignin ratios of soy hulls vary greatly depending on the genotype of the soybean. One literature cited that soy hulls obtained from Illinois USA contains 42-49% cellulose, 29-34% hemicellulose and 1.4-2.7% lignin (Ashraf, 1988), while another suggested that the cellulose, hemicellulose and lignin compositions are 56%, 12% and 18% respectively for soy hulls obtained from Ontario grown soybeans (Alemdar, 2008). Most soy hulls recovered from soybean processing is used as cattle feed by farmers and has very little value. In the past, scientists have studied the possibility of using soy hulls as a human food source (Muzilla, 1989) as well as a source of more valuable materials such as pectin (Monsoor, 2001). In the research of biocomposites, efforts have recently been made to extract nano-sized fibers from soy hull for use as reinforcements in thermoplastic composites (Alemdar, 2008). However, a majority of the material remains underutilized, and therefore its application as an AgFiller is considered an excellent opportunity to explore new markets for the soybean industry.

2.2 Processes for Producing AgFiller-PP Composites

2.2.1 EXTRUSION

Extrusion is a continuous process that is widely used in making products with long shapes, such as beams, profiles or panels, and pipes. It is also the most common process for preparing AgFiller-PP compounds or masterbatches prior to further processing into consumer goods. During extrusion, a recipe of raw materials is fed into the heated extruder barrel, in which one or two screws convey and mix the material as it melts. Single screw and co-rotating twin screw extruders are common in processes that require little shear mixing, while counter-rotating twin screw extruders are used when high dispersion of material is desired (Holbery, 2006). Material exits the barrel through a shaping die and is subsequently cooled. At the end of an extruder line, secondary equipment such as pelletizers, cutting saws and orientation tooling can be installed according to application needs (A.Schulman, 2007; Newson, 2002).

PP of high molecular weight (or low MFI) can be processed by extrusion as relatively low flow restrictions are imposed onto the material by the process. Many researchers have studied the relationship between extrusion processing and the properties of PP composites. Chiu and Shyu (1987) and Sanomura *et al.* (2007) examined the effects of extrusion parameters on, respectively, the morphology and mechanical properties of glass-fiber reinforced PP composites. Results of their work showed that fiber length can be controlled by adjusting extruder temperature and speed, while crystallinity is independent of processing parameters (Chiu, 1987). Meanwhile, extrusion parameters affect fiber alignment within the polymer, which in turns determine the mechanical characteristics of reinforced PP composites (Sanomura, 2007).

2.2.2 BULK ORIENTATION

Newson and Maine (2002) define oriented thermoplastics as “thermoplastic polymers that have been processed in such a way as to straighten the polymer chain backbone so that when the polymer molecule experiences an applied stress, this stress is applied to the carbon-carbon bond in the chain backbone and not to just uncoiling the polymer helix. The result of this molecular orientation is an increase in strength, stiffness and impact strength of the polymer”. Ajji *et al.* (1998) extensively investigated various orientation techniques, which included rolling, roll-drawing and solid state forming, and their effects on the properties of various thermoplastics. The effects of orienting process parameters such as draw ratio, extrusion speed, roll gaps were also studied. They determined that draw ratio contributes to increases in polymer crystallinity and mechanical properties in the longitudinal direction. These findings agreed with earlier research regarding crystallinity changes of oriented polypropylene (Taraiya, 1988; Chaffey, 1997).

Patents, US2005171246 (Maine, 2005) and US2006057348 (Maine, 2006), describe the manufacture of thermoplastic composites by bulk orientation with wood fillers and reactive fillers respectively. The technology employs a set of inline orientation tooling at the end of a regular extrusion facility (Figure 5), where the extruded material is reheated to slightly below its melting point and die drawn to a desired ratio.

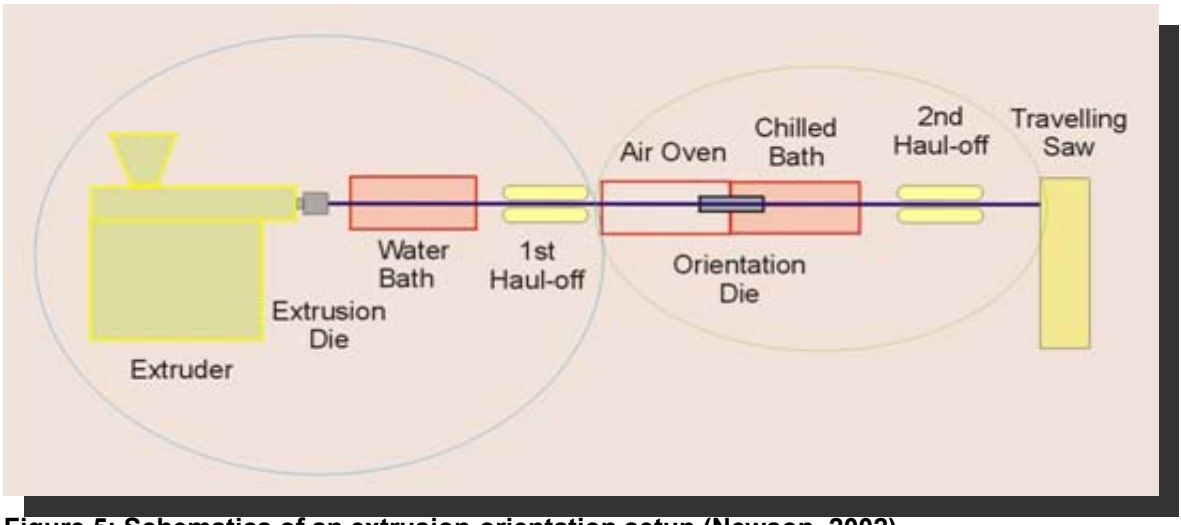

Figure 5: Schematics of an extrusion-orientation setup (Newson, 2002)

When Newson and Maine oriented WPC by drawing, the natural incompatibility between hydrophilic filler and hydrophobic polymer caused a separation of the two phases and resulted in the generation of microscopic gaps, with the wood fiber acting as the nucleus for void formation. The consequence of such void formation is a reduction in the composite's density. The magnitude of density decrease is found to be proportional to the loading of fillers, as shown in Figure 6.

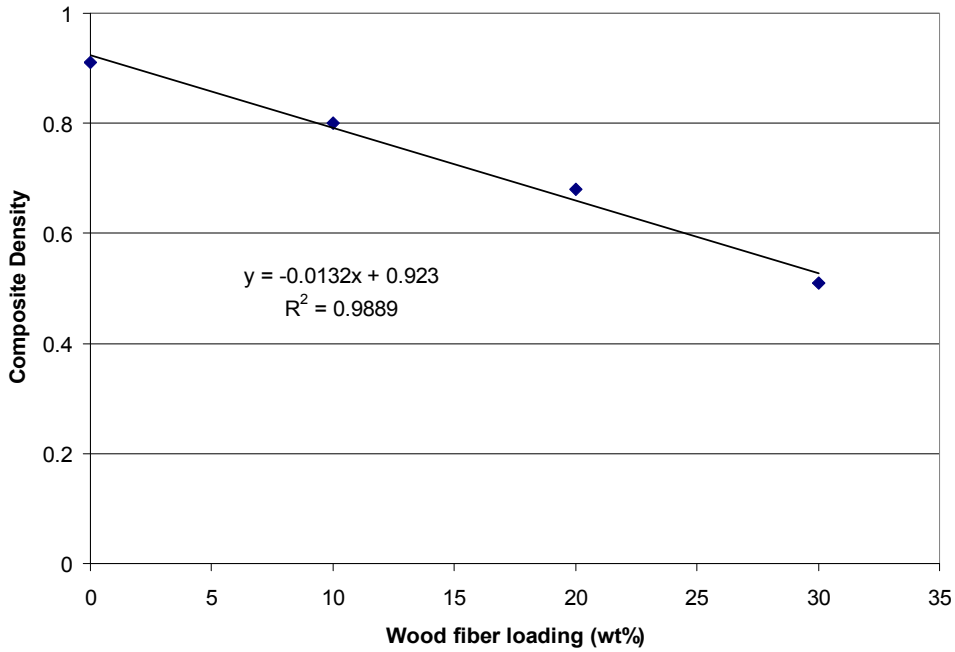

Figure 6: Density change of oriented WPC due to fiber loading (Newson, 2004)

Draw ratio, or reduction ratio, refers to the dimensional reduction that occurs during the orientation process. Increasing die drawing ratio was determined to increase the dynamic modulus of polypropylene rods, for draw ratio up to 18.2 (Taraiya, 1987). Later studies of die drawn polypropylene sheets showed similar findings that modulus is proportional to draw ratio in the draw direction (Chaffey, 1997).

2.2.3 OTHER PROCESSES

Although it is beyond the scope of this thesis to study in detail other processes in making AgFiller-PP composites, these techniques should be made aware of nonetheless. Thermoforming or press-molding is often employed in producing composites with a thermoset polymer matrix, or in making mat-like thermoplastic composites (Holbery, 2006). Sheets of prefabricated polymer are inserted into a heated mold press, which then sandwich a layer of AgFiller. The mold then applies pressure to produce a laminate composite.

Injection molding is a semi-continuous processing technique widely used by the automotive and consumer product manufacturing industries. The first section of the injection molding machine consists of the feeding zone and a heated barrel, in which a single screw extruder is equipped. In this section the material is melted, mixed and conveyed to the nozzle section of the machine. At the injection point, the process mechanism is similar to a plug flow system, where a fixed portion of the material is transferred into the mold for shaping. The fixed portion is known as “shot size”. Some advantages of the injection molding process are dimensional tolerance and fast cycles (Holbery, 2006). However, because of small injection ports and gates, the process induces high shear to the material and can trigger degradation of shear sensitive components. In most scenarios, raw materials are in the form of premixed compounds to ensure cleaniness of the process. When processing AgFiller-PP composites, moisture is a crucial aspect to be addressed. AgFiller-PP compounds must be dried prior to feeding into the injection molding machine, otherwise excess moisture could cause catastrophic explosions as pressure builds up inside the barrel of the injection molding machine when the moisture vaporizes (A. Schulman[1], 2007). Panthapulakkal *et al.* (2005) prepared WS-PP composites by injection molding and performed property characterization. They observed that the injection molding process yielded inferior strength of composites

containing WS fibers prepared by chemical treatment than that prepared by mechanical treatment.

2.3 Applications of AgFiller-PP Composites

Applications of AgFiller-PP composites are greatly influenced by the properties of the material. For instance, injection molding facilities in the automotive industry have the ability to process only material with low viscosities, while extrusion processes for manufacturing consumer products have larger operating windows. However, extruded goods designed for structural construction applications may require higher mechanical properties than those made for non-structural applications. An example of consumer products produced from WS-plastic composite is office furniture as shown in Figure 7. For construction applications, Environ Biocomposites manufactures panels made of thermoplastics and wheat straw and sunflower hulls (Environ, 2008). In 2006, Holbery and Houston showcased automotive components such as door panels produced from kenaf-PP mats (Figure 8). On the other hand, oriented WPC successfully found markets in structural construction applications, such as in producing pedestrian bridges (Figure 9).

Figure 7: Office furniture made of wheat straw-recycled plastic composite (Baltix, 2004)

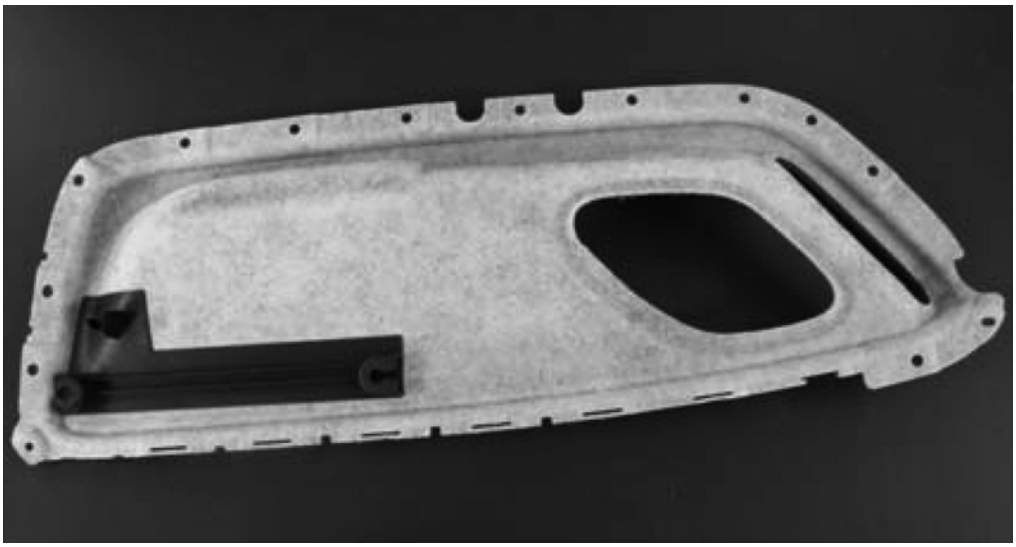

Figure 8: Automotive component made of 50% kenaf/50% PP (Holbery and Houston, 2006)

Figure 9: Bridge, located in Millbrook, Ontario, constructed using oriented wood-plastic-composite material (Everarch, 2008)

2.4 Properties of AgFiller-PP Composites

2.4.1.1 Rheological Properties

As most thermoplastic composites are processed by melt-mixing (Kruger, 2007), rheological properties are an important aspect with regards to AgFiller-PP composites because it reflects the ability to successfully process the material. In the melt-mixing process for preparing AgFiller-PP composites, heat and shear are the main contributors to the melting of the polymer phase, but at the same time cause damage and possibly degradation of the AgFiller. Futhermore, problems such as segregation and clogging may arise due to differences in bulk density and geometry between the polymer and AgFiller.

Melt flow index (MFI), documented by ASTM D1238, is the most common method in testing viscosity characteristics of thermoplastics including polypropylene. Expressed in standardized units of g/10min, MFI is inversely correlated to viscosity and is related to the molecular weight of the material tested. The higher the MFI value, the less viscous the test material is. Other methods commonly used to study rheological properties of polymer melts include the use of torque rheometers (Kruger, 2007), capillary

rheometers, slit rheometers (Son, 2007), or online electrical (amperage) and mechanical (torque) readings from the processing equipment.

Studies on various natural fiber-PP composites showed that the addition of AgFillers results in an increase in viscosity of the composite material, as indicated by MFI decreases (Schemenauer, 2000) or torque increases (Kruger, 2007) . Different types of AgFillers are found to have varied influence on viscosity changes. Schemenauer *et al.* (2000) further showed in their work that among coir, jute and kenaf, jute fibers had the most significant impact in raising viscosity, while coir fibers were the least influential.

2.4.1.2 Thermal Properties

One disadvantage of combining AgFillers with thermoplastics is that AgFillers have thermal stabilities below the processing temperature of many thermoplastics. For instance, the use of AgFillers such as wheat straw, which has a degradation onset of 200^{o}C (Kruger, 2007), can prove to be a challenge when mixed in with polypropylene during processing, of which typical temperature profiles of 190-230^{o}C are used. The difficulty increases when thermoplastics of higher melting point, such as Nylon, are the desired polymer matrix.

The degradation of AgFillers is undesirable and the consequences include loss in mechanical strength, increased brittleness and darkening of the composite. The release of odour can also be detected (Saheb, 1999). To avoid AgFiller degradation, adjustments were made to test protocols and processing conditions to attain lower temperature profiles, as exemplified by the MFI experiments carried out by Schemenauer *et al.* (2000), in which the test temperature was lowered from 230^{o}C, as stated in the ASTM D1238 standard, to 190^{o}C. According to Zurale and Bhide (1998), it was necessary to manipulate the extruder speed and the temperatures at each extruder zone in order to successfully produce prototype composite pipes using coconut shell powder and PVC (poly vinyl chloride).

Also important in studying AgFiller-PP composites are the melting and crystallization behaviours. Crystalline structures give order on the molecular level and are a source of the polymer's strength. Therefore, a high percentage of crystallinity is desired

(Alemdar, 2008). Crystallinity can be manipulated by adding fillers that serve as nucleating agents, as shown in the study by Albano *et al.* (2004), where it is demonstrated that composites containing inorganic particulate fillers showed increases in crystallization temperature as well as percentage of crystallinity when compared to pure PP. The most commonly used method for studying melting and crystallization is by differential scanning calorimetry (DSC), where heat flow is measured over a range of temperature change and any transition caused by phase change is recorded. X-ray diffraction (XRD) is also a useful tool for studying crystallinity of polymers. Changes in crystalline structures among various polymorphs (α, β and γ types) can be studied by identifying characteristic peaks from diffraction patterns. Mi *et al.* (1997) showed that the addition of bamboo fibers into PP causes the formation of β crystals, and the ratio of the heights of α and β peaks recorded from the XRD pattern can be used to estimate crystal fractions in the composite.

2.4.1.3 Density

The main drawback of using inorganic materials as fillers is their high densities or specific gravities, which results in heavy and non user friendly composites. In comparison, AgFillers like wheat straw and soy stem have significantly lower densities, giving weight advantages mainly in logistics. The lighter weight of AgFiller-thermoplastic composites also allows them to penetrate markets in which light weight is of great importance, such as in the automotive industry. By replacing glass fiber with flax straw fibers in PP composites at 25 wt% filler loading, Hornsby *et al.*[2] (1997) observed a density reduction from 1076 kg/m^3 to 986.8 kg/m^3. Similarly, the specific gravity of kenaf-PP composites with 50 wt% kenaf is 1.007, competitive to talc-PP composites with 40 wt% filler, which has a specific gravity of 1.27 (Rowell, 1999).

The density of AgFiller-PP composites can be further reduced by bulk orientation, based on a polarity mismatch between filler and polymer. Die-drawn oriented WPC containing 30 wt% wood fibers has a relative density of 0.52, approximately half that of traditional WPC with higher fiber loading, which has a relative density of 0.97 at 50 wt% filler (Newson, 2002).

2.4.1.4 Mechanical Properties

The mechanical properties of an AgFiller-PP composite are the most important aspects in determining the end-use applications of the materials. For example, automotive and construction industries require high mechanical strength and stiffness, while decorative and non-structural panels have lower requirements on physical properties. The four mechanical properties most studied are tensile or yield strength, Young's modulus of elasticity (tensile modulus), flexural modulus and impact strength. Figure 10 illustrates a summary of mechanical test results of AgFiller-PP composites studied by Rowell *et al.* (1999), showing that AgFiller-PP composites often possess higher tensile and flexural properties, but suffer losses in impact resistance.

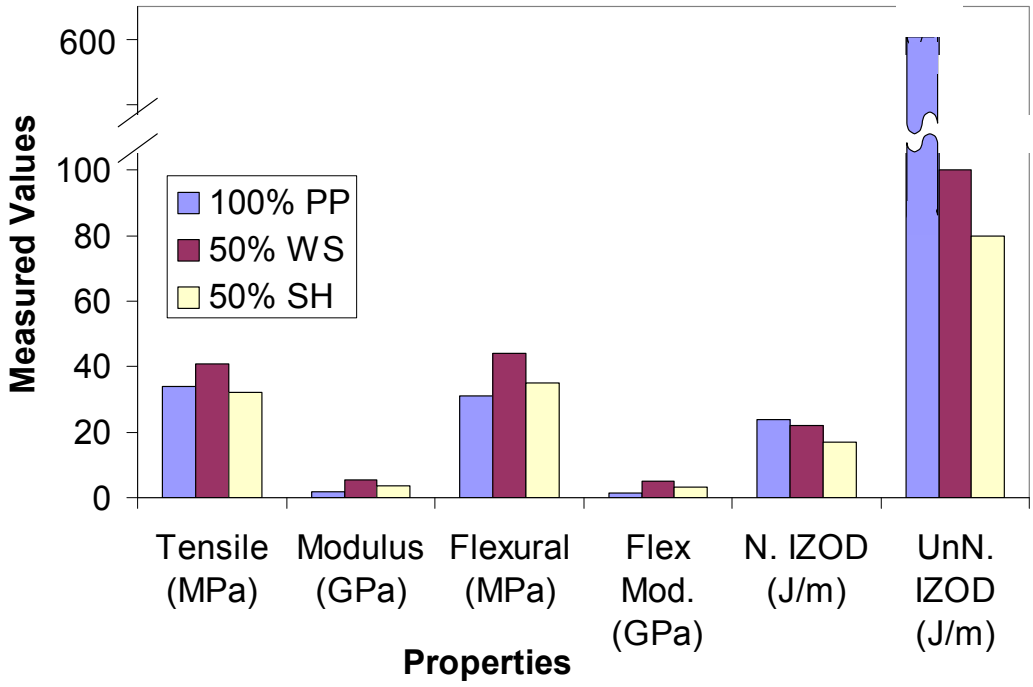

Figure 10: Mechanical properties of various AgFiller-PP composites (Rowell, 1999)

It was Joseph *et al.* (1996) who suggested that the inherent mechanical strength and stiffness of AgFiller, the strength and chemical stability of the polymer, and the effectiveness of polymer-filler bonding are the determining factors to the mechanical performance of natural fiber filled plastic composites. This is further supported by the work of Crespo *et al.* (2007), in which was shown that the particle size of almond husk

fillers and plasticizer levels separately contributes to changes in tensile strength, tensile modulus and Shore D hardness of the almond husk filler-PVC plastisol composites produced.

The benefits of mechanical property improvement of AgFiller-thermoplastic composites are further complemented by the low specific gravity of the AgFiller when specific properties are of interest (Kruger, 2007). Specific properties are calculated values that are obtained by dividing the property values by the specific gravity of the composite. When comparisons are made in specific properties, many natural fibers present competitiveness to high strength reinforcing materials like glass fibers, although their absolute properties are inferior (Table 3).

Table 3: Specific gravity, modulus and specific modulus of natural fibers compared to glass fiber (Saheb, 1999)

Fiber	Specific Gravity	Modulus (GPa)	Specific Modulus (GPa)
Jute	1.3	55	38
Flax	1.5	27	50
Sunhemp	1.07	35	32
Glass Fiber E	2.5	72	28

CHAPTER 3 EXPERIMENTAL

Figure 11 shows the experimental plan for this project. The design involves studying two polymers to be combined with four AgFillers. Two types of processing, batch extrusion and extrusion-orientation, are planned to study the changes in composite properties prior to and after orientation. The properties of interest and testing involved are also illustrated in the figure.

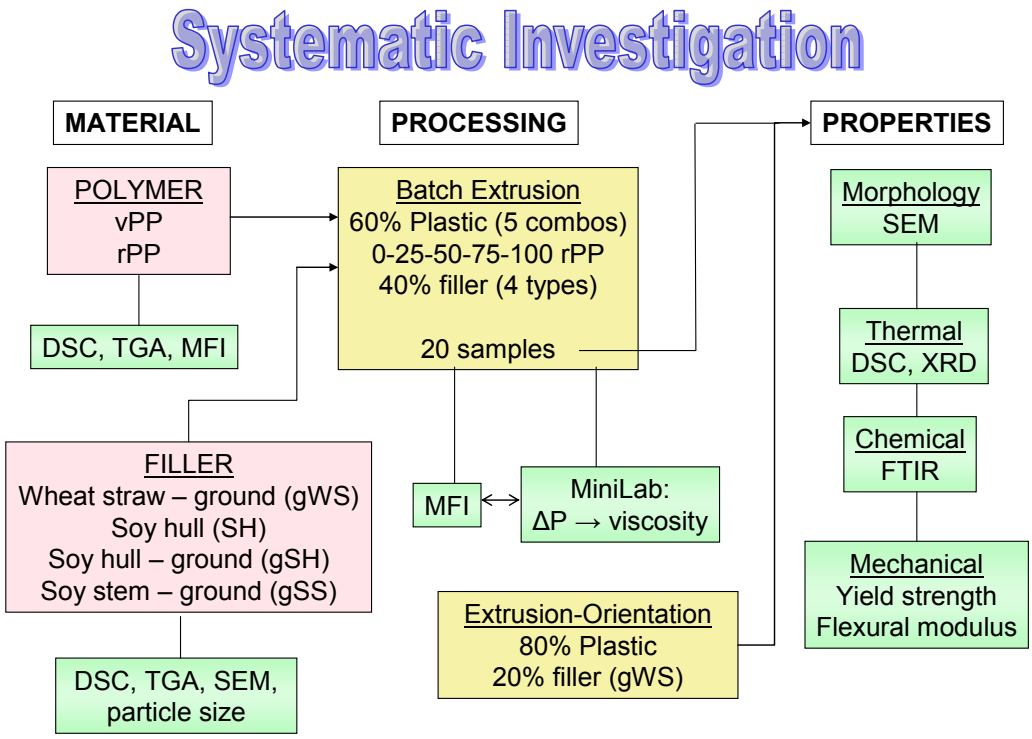

Figure 11: Project planning and design schematics

3.1 Materials

3.1.1 AGRICULTURAL FILLER (AgFiller)

Wheat straw and two parts of the soy plant, bean hulls and stems, were used as AgFillers in this study.

The wheat straw (WS) used was grown in Aberfoyle, Ontario, and was harvested in 2005. It is of variety Pioneer 25R47. A sample of wheat straw contains mostly straw and

leaf, however, on occasion one may find also husks attached on the tips of the wheat plant.

The soy hulls (SH) received for testing were donated by Bunge Inc., as a by product of their soybean crushing and extraction operation in Hamilton, Ontario. The soybeans from which the hulls were extracted were locally grown in Ontario in 2005. The hulls received have a flake-like geometry, of approximately 1-3 mm in diameter.

The soy stems (SS) obtained were grown in Elora, Ontario in 2005. In a sample of soy stems, one may find a combination of soy pods, stem stalks as well as leaves. The genotype of the plant from which these soy stems were collected is uncertain, due to the fact that this plant was the experimental result of combining several breeding lines studied by researchers at the University of Guelph.

3.1.2 POLYPROPYLENE (PP) MATRIX

A high viscosity PP impact copolymer (grade PP2407, donated by A. Schulman Inc.) was used as the polymer matrix of non-oriented AgFiller-PP composites. This PP material is denoted in this work as virgin PP, or vPP. It has a density of 0.9 g/cm^3 and a melt flow index of 1.5 g/10min (230^{o}C, 2.16 kg), according to the material's technical data sheet.

A random sample of post-consumer PP recyclate (rPP) was collected from the Region of Peel Material Sorting Facility, Ontario. This rPP sample consists mainly of food containers for items such as ice cream, butter and theatre concessions. These containers were cleaned with detergent and bleach solutions, and sorted into various categories as shown in Figure 12. Non-PP components in the sample were removed.

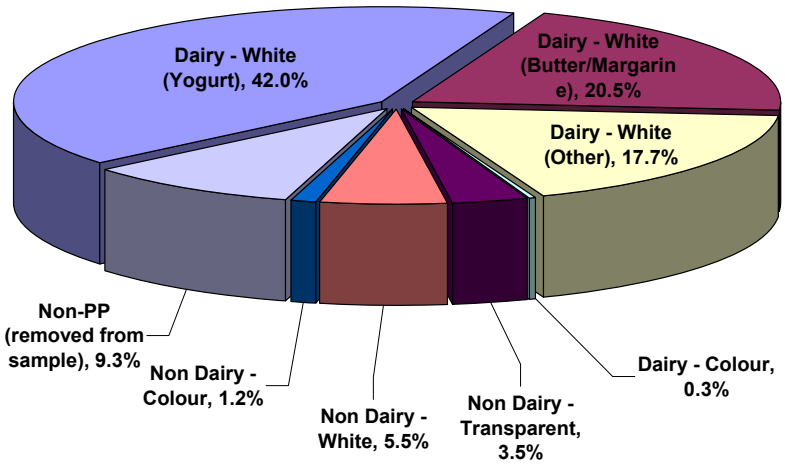

Figure 12: Composition of recycled PP sample

3.1.3 MATERIALS FOR ORIENTATION TRIAL

Pellet-form PP homopolymer (donated by A.Schulman Inc.) with a melt flow index of 4 g/10min (230°C, 2.16 kg) was used as a polymer matrix, while gWS of two particle sizes (coarse and fine) were used as AgFiller. Although it is not in the scope of this thesis to study the effects of additives, antioxidants (CIBA Irganox 1010 and CIBA Irgafos 168) were mixed into the composite materials during the compounding step in scale-up trials. This was done to safeguard the industrial sponsors' equipment in subsequent extrusion and orientation processes. The recipe for masterbatch is shown in Table 4. The masterbatch was then mixed with pure PP resin to reduce filler concentration by 50 wt% prior to extrusion, such that the resultant extruded billet contained 20 wt% gWS filler.

Table 4: Composite masterbatch recipe

Ingredient	Loading (wt%)
PP homopolymer	59.70
gWS	40.00
Antioxidant Irganox 1010	0.15
Antioxidant Irgafos 168	0.15

3.2 Processing Methods

3.2.1 GRINDING

Due to the large sizes of the AgFillers received, a size reduction step was required prior to being used to process into composites. Wheat straw and soy stem materials were first cut into approximately 5cm long segments before feeding into the grinder. Because of smaller sizes, soy hull material was fed into the grinder directly without the need of pre-cutting.

A rotary grinder (Thomas-Wiley Laboratory Mill, Model 4, 800 RPM) fabricated of stainless steel was used to grind up the materials to their proper sizes. Grinding of each material was done at 30-45 minutes intervals, with 1-2 hours intermissions to allow machine cooling, at a yield of approximately 60g/interval. A total of 500-800 g was ground up for each material. In order to minimize contamination, the machine was thoroughly cleaned when grinding of one material was completed, and before grinding of a different material began. The ground material was screened through a mesh with 0.5 mm openings, and collected at the exit of the grinder. The prefix “g” was added to each filler that underwent the grinding process, and were re-designated as gWS, gSH and gSS to distinguish them from the original material as received.

rPP was cut from its container forms into 5 cm long, 1 cm wide pieces prior to grinding. The amount of each type of recycled PP cut was representative of the mass fraction of each component similar to that shown in Figure 3, after adjusting for the removal of non-PP portions (9 wt%). The pieces were immersed into liquid nitrogen for 3 minutes in small portions, then removed and ground up using a bench-size grinder (Black & Decker coffee bean grinder). The ground rPP was then sieved through a mesh screen with 1 mm openings to remove excessively large pieces.

3.2.2 COMPOUNDING

An AgFiller (gWS, SH, gSH or gSS) was hand-blended with a polymer (vPP, rPP or mixture of the two) at a ratio of 40 wt% AgFiller to 60 wt% polymer. The blend was fed into the Haake Minilab Microcompounder (Minilab), a co-rotating conical extruder with a cycle/flush option. The Minilab was set at 190^{o}C, running at 30 RPM in flush mode. As

the material was conveyed by the Minilab screws, melting and mixing took place. A homogenized melt exits at the flush orifice at the end of the Minilab in the form of strands. These strands were then cut to smaller (approximately one inch long) pieces, and then pelletized using a bench-size grinder (Black & Decker coffee bean grinder).

Large scale compounding was carried out with the assistance of our industrial sponsor, A.Schulman Inc. in St. Thomas, Ontario, using a twin screw extruder equipped with a water trough for cooling and a strand pelletizer. The extruder's temperature profile was adjusted to maintain the compound's melt temperature beneath 210^{o}C to prevent degradation of the filler.

3.2.3 COMPRESSION MOLDING

Pelletized compound was molded into plaques or bars of desired sizes using molds and cover plates comprised of aluminum or steel. First, a measured amount of the pelletized compound was placed inside the mold cavity, sandwiched between two cover plates wrapped in aluminum foils, and was preheated at 190^{o}C for 10 minutes to fully melt the material. Then the compound was pressed using 10,000 lb_f of pressure in the mold for 3 minutes, during which the pressure was released and re-established at the first minute mark to allow volatiles and entrapped air bubbles to escape. At the end of compression, the set of plates, with the sample within, was removed and let cool to room temperature. Once cooled, the molded specimens were removed and inspected for voids and other defects. Only samples with no major visible defects were kept for use in property characterization experiments.

3.2.4 BULK ORIENTATION

Prototype samples were produced by our industrial sponsor, Green Forest Composites in Nevada, Missouri, using a twin-screw extruder equipped with inline orientation tooling setup. The operating conditions for orientation are proprietary. Standard "one-by-two" beams were made during the trial for characterization.

3.3 Property Characterization Methods

3.3.1 RHEOLOGY

3.3.1.1 Melt flow Index (MFI)

A Dynisco LR7001 MFI tester was used to obtain the MFI of PP and PP-based composites, using conditions of 230^{o}C and 2.16 kg weight-load through a standard 8 mm die. Following ASTM D1238, method A, approximately 10 g of pelletized sample was loaded in for testing in each experiment. The material was subjected to a melt time of 360 seconds, after which 5 sample cuts were made. 4-6 samples were collected and their MFI values were averaged for analysis.

3.3.1.2 Apparent Shear Viscosity

Testing was performed in a similar setting as in the compounding procedure using the Haake Minilab micro compounder: extruder temperature of 190^{o}C, extruder speed of 30 RPM and 5 g of PP-AgFiller dry blend. For viscosity measurement, the Minilab was set to "cycle" mode, such that all material was directed into the slit channel (Figure 13). One minute was counted after the last of the test material was loaded to allow steady state to establish, and ΔP data was recorded for the following one minute. The data was averaged prior to being used in further calculations.

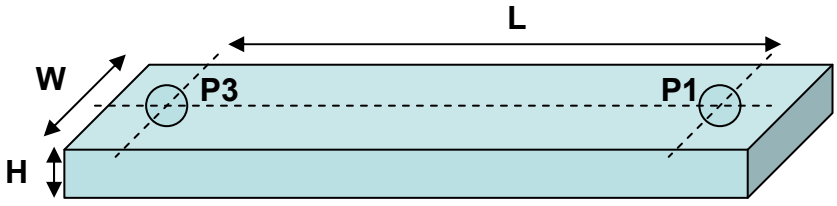

Figure 13: Rectangular slit geometry

In a channel with rectangular slit geometry such as the one found in the Minilab, the resultant shear stress across the channel is determined by the formula:

$$\tau = \frac{\Delta P \cdot H}{2L} \tag{1}$$

where

ΔP = P1 – P3
H = height of flow channel (1.5 mm)
L = length of flow channel (between pressure transducers, 64 mm)
W = width of flow channel (10 mm)
τ = shear stress

The shear rate is calculated as:

$$\dot{\gamma} = \frac{6Q}{WH^2} \tag{2}$$

where

Q = volumetric flow rate

Due to the lack of equipment specifications, Q could not be definitively determined. To allow further analysis, an assumption was made, that the Minilab test chamber was fully filled at steady state during the experiment, and therefore Q remained constant when the equipment is operating at the above-specified conditions, regardless of the type of material that is under testing.

Finally, shear viscosity is represented by the ratio of shear stress to shear rate, expressed as a function of Q^{-1}, a constant:

$$\eta = \frac{\tau}{\dot{\gamma}} = \left(\frac{\Delta P \cdot W \cdot H^3}{12L} \right) \cdot \left(\frac{1}{Q} \right) \tag{3}$$

Relative comparisons were then made among samples tested under the same operating conditions.

3.3.2 DENSITY

The density (or specific gravity) of composites were measure using the technique of water immersion, following ASTM D2395 Procedure B. First, the dry weight of a sample was measured using an analytical balance. Next, the sample was suspended using a non water absorbing string, and submersed in deionized water using a sink weight. The displaced weight of the sample was measured. The relative density of the sample was then calculated as:

$$Relative\ Density = \frac{Dry\ Weight}{Dry\ Weight - Displaced\ Weight} \tag{4}$$

3.3.3 FIBER EXTRACTION

To study the damages on AgFiller fibers due to processing, fibers were separated from the polymer matrix by xylene extraction. A 41 screen ashless filter paper was folded into an envelope, in which approximately 0.5g composite sample is placed. The envelope was then sealed with a staple, and was suspended into a flask of boiling xylene (175 mL) using a thread. A condenser was attached to the top of the flask such that evaporating xylene could be recovered. The extraction lasted 24 hours, during which the solvent was replaced with new xylene on hour 4, 12 and 16. After 24 hours, the envelope containing AgFillers was removed from the flask, and dried inside a ventilated fume hood for 24 hours.

3.3.4 MORPHOLOGY

The morphology of AgFiller-PP composites was studied by scanning electron microscopy (SEM), using a LEO SEM scanning electron microscope equipped with a Gemini field emission column. A small piece of each sample was sliced using a knife cutter in the cross-sectional direction, and was affixed to an aluminum stub using double-sided conductive tape. The sample was sputter coated with gold at a thickness of approximately 10 nm prior to loading into the SEM. EHT was set to 20 kV and WD at 10 mm at the beginning of scans, and the parameters were adjusted accordingly to obtain optimal image resolution.

3.3.5 THERMAL PROPERTIES

3.3.5.1 Thermal Gravimetric Analysis (TGA)

Thermal gravimetric analysis (TGA) was performed to determine the degradation onset of each AgFiller and PP in their neat form. A TA Instrument SDT 2960 Simultaneous DTA-TGA machine was used to perform the experiments. Small amounts (approximately 10 mg) of each sample were placed in platinum crucibles, which were then loaded into the apparatus. Prior to any data recording, each sample was then heated from ambient to 40^{o}C, then held isothermal for 10 minutes for equilibrium to establish. Upon completion of the isothermal step, the sample was heated at 10^{o}C/min to 600^{o}C in an oxidative environment filled with air. The equipment was then air cooled to ambient before beginning the next set of experiments.

3.3.5.2 Differential Scanning Calorimetry (DSC)

Differential scanning calorimetry (DSC) was used to study the melting and crystallization behaviours of selected samples. The DSC equipment used was the Q10 model, made by TA Instruments. A small amount of sample (approximately 10 mg) was cut from a larger pellet or strand at a random location. The sample was then placed in an aluminum pan, crimp-sealed and loaded into the DSC chamber purged with nitrogen. The test was

carried out in three steps. First, a heating step from ambient (23^{o}C) to 210^{o}C at 10^{o}C/min. This step was performed to remove any thermal history of the composite and was excluded from any analysis. The sample was then held isothermally at 210^{o}C for 5 min. The second step involved cooling the sample from 210^{o}C to 30^{o}C at 10 °C/min. After the second step the sample was again held isothermally at 30^{o}C for 5 min. The final heating step from 30^{o}C to 210^{o}C, at 10^{o}C/min, would again melt the material. Crystallization and melting information were gathered from data produced in step (2) and (3).

3.3.5.3 X-ray Diffraction (XRD)

X-ray diffraction (XRD) experiments were performed using a Bruker D8 Focus apparatus. Film samples with approximately 0.65 mm thickness were placed on the sample holder and secured with clay putty at the bottom. Up to 5 samples were loaded into the apparatus for testing simultaneously. X-ray intensity was set to 40 mV, and scanning was made for 2θ range from 5^{o} to 30^{o}, at resolution of 0.05 per step, and scan speed of 1 step per second. The spectrum recorded was smoothed to a 0.2 factor using the Bruker EVA analysis program to remove noise in the baselines.

3.3.6 CHEMICAL PROPERTIES

The surface chemistry of the composites was studied using fourier transform infrared spectroscopy (FTIR) by attenuated total reflection (ATR). A Bruker FTIR Tensor 27 with Harrick MVP2 model ATR attachment was used. Scans were made at 4 cm^{-1} resolution and 32 scans were made on each sample. Samples used for testing were thick films prepared by hot-pressing, with an average thickness of 0.65 mm. The spectrum recorded was smoothed to 13 point index using the Bruker OPUS computer program.

3.3.7 MECHANICAL PROPERTIES

Experiments to determine the flexural properties of the non-oriented composites were carried out following ATSM D790 specifications for procedure A. The instrument used for testing is MiniMat 2000 miniature material tester (Minimat), equipped with a load cell of 200 N. Due to equipment constraints, test specimens were obtained by cutting compression molded of 63.00 x 12.75 x 3.00 mm dimensions into halves, such that each test specimen was approximately 31.68x12.75x3.00 mm. The support span was fixed at 18.25 mm. This allowed a support span (length) to thickness ratio of approximately 6:1.

Larger industrial prototype samples of oriented gWS-PP composite were tested using an MTS-810 universal tester, equipped with a 50 kN load cell. Because all samples had similar thickness, a single value of 252 mm was set as the support span, achieving the 16:1 support span (length) to thickness in compliance with ASTM D790 standard. Similarly, a single value of 6.50 mm/min was calculated to be the proper crosshead travel speed to obtain a strain rate of 0.01 mm/(mm·min).

CHAPTER 4 EVALUATION OF AgFILLERS IN NON-ORIENTED COMPOSITES

The differences in types, sizes and geometries of AgFillers produced from different crop materials are critical in determining the properties of the biocomposites produced. In this chapter, gWS, SH, gSH and gSS AgFillers were studied for their morphologies, and their roles in affecting the morphological, thermal, chemical, rheological and mechanical properties of the composites made using each type of AgFiller and vPP were investigated. The AgFiller-vPP composites each contained 60 wt% polymer and 40 wt% filler. Samples were prepared in the laboratory by compression molding pellets obtained from batch extrusion. This sample preparation technique produced non-oriented composites.

4.1 Property Characterization

4.1.1 MORPHOLOGY

Figure 14 to Figure 16 show respectively SEM micrographs of gWS, gSH and gSS fillers prior to compounding with PP polymer. From the figures, it was observed that gWS and gSS had similar morphology with splinter-like appearances, and major axis (length) to minor axis (width) aspect ratios of greater than one. On the other hand, gSH fillers had disc-shaped geometry with aspect ratios of approximately one. Furthermore, the fiber orientations of gWS and gSS were along the length axis, while that of gSH was along the depth axis.

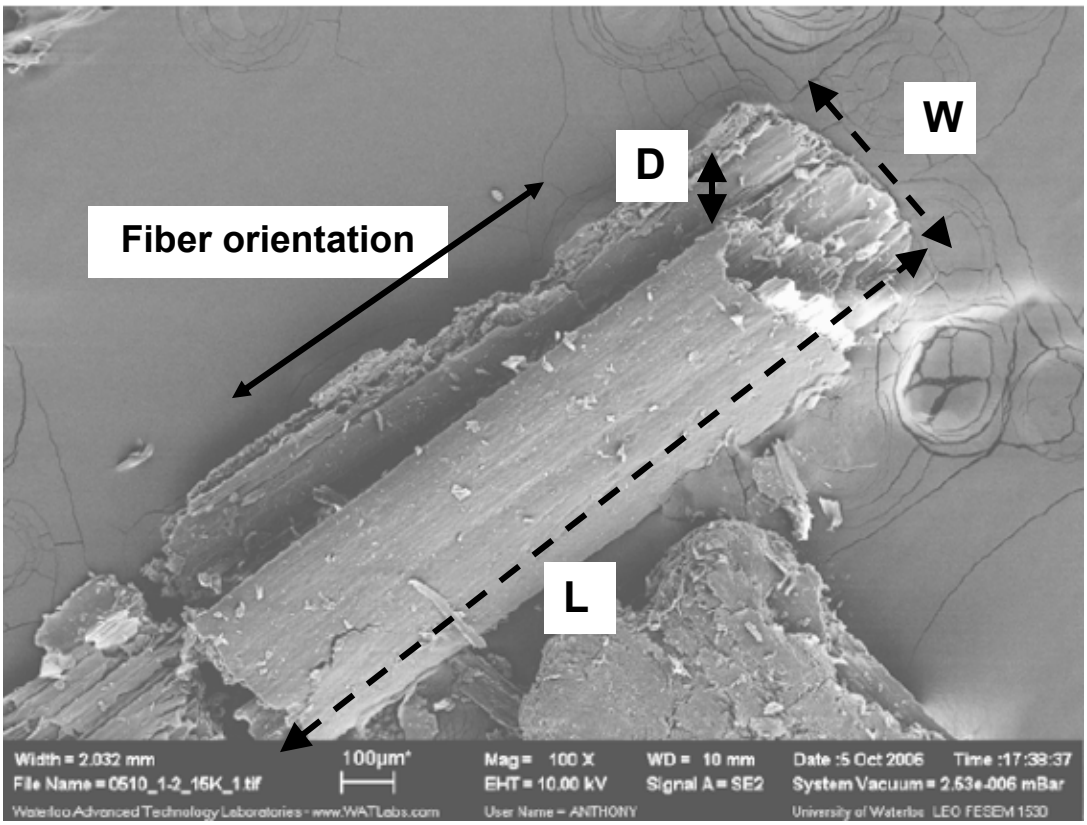

Figure 14: SEM of gWS filler prior to compounding, mag = 100x (Kruger, 2007)

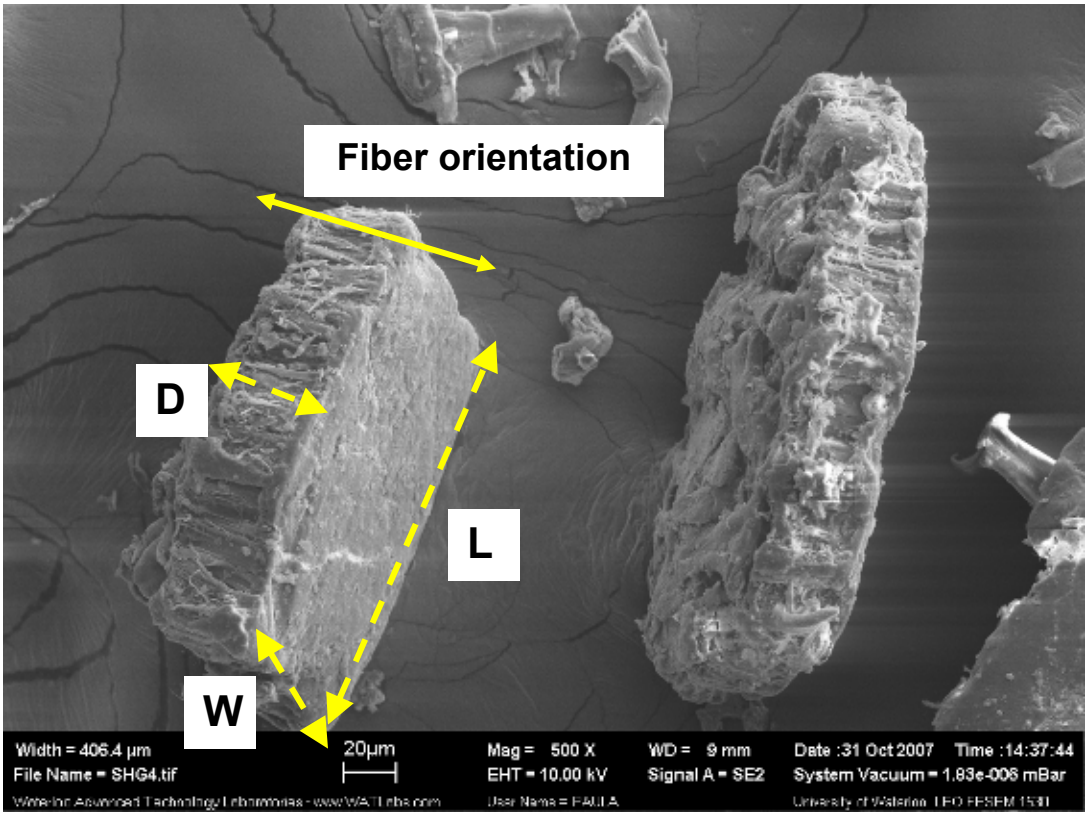

Figure 15: SEM of gSH filler before compounding, mag = 500x

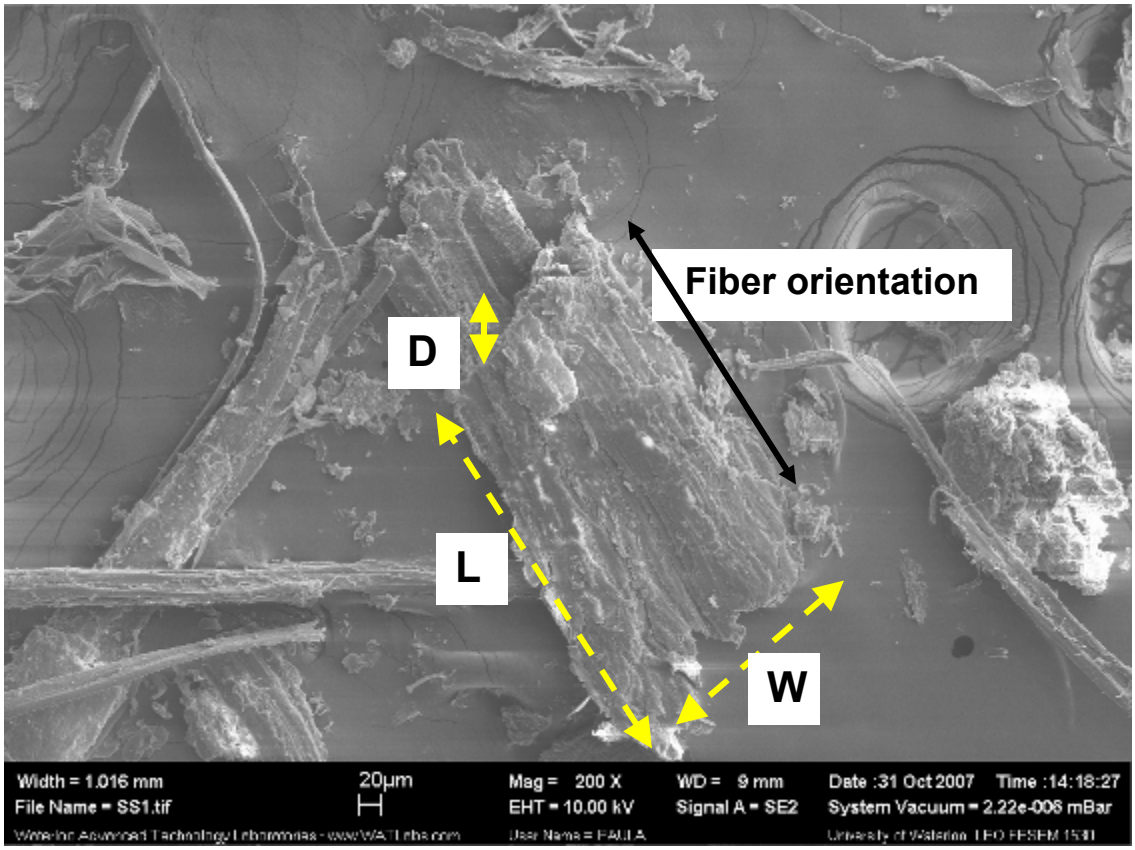

Figure 16: SEM of gSS filler before compounding, mag = 200x

Figure 17 illustrates the fracture surface of gWS-PP, where a fiber that was embedded lengthwise into the polymer matrix has been pulled out. Similar observations had been recorded for gSS-PP composites. It was apparent that gWS-PP and gSS-PP composite materials after compounding show significant fiber protrusion where the composite was broken apart. This is because the fillers were buried lengthwise, and the fracture took place perpendicular to the fiber orientation of the filler, which also affected the level of fiber pullout. On the other hand, the SEM micrograph of SH-PP composite (Figure 18) showed that the SH filler was also embedded lengthwise, but since the fiber orientation of the filler is in the direction of its depth, there was no fiber pullout at the fracture surface. Instead, the filler broke off evenly at the same level as the polymer. Kruger (2007) also observed differences in breakage mechanism of WS fibers from the PP matrix in coupled WS-PP composite. She attributed the observation to the stronger

forces between filler and matrix as a result of chemical coupling, than the forces along the WS fiber.

It is also apparent in Figure 17 and Figure 18 that empty gaps were present at the filler-polymer interface, as shown by the dark voids photographed. This confirmed indications that the fillers and the polymer are not compatible in nature. As the composite cooled from processing and the polymer solidified, volumetric contraction took place and the polymer shrank away and separated itself from the filler surface (Hornsby[2], 1997).

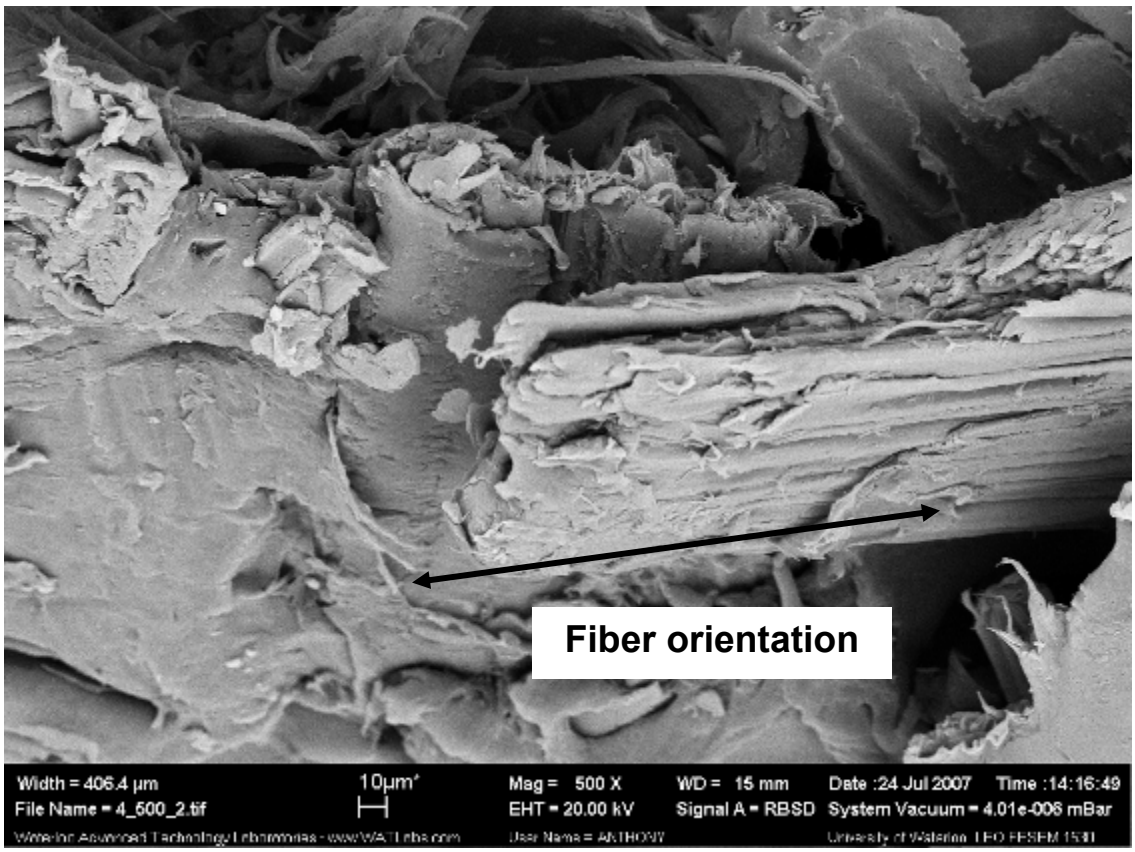

Figure 17: SEM of gWS-PP composite, mag = 500x

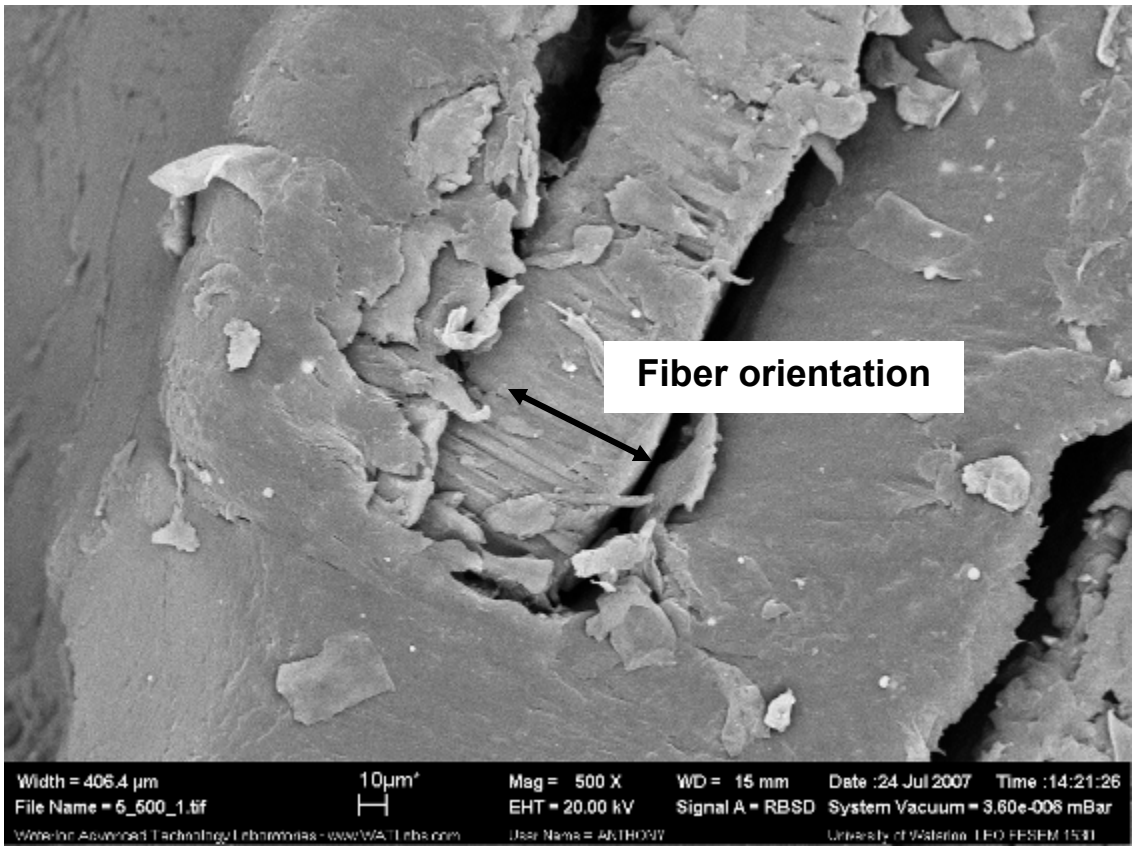

Figure 18: SEM of SH-PP composite, mag = 500x

In Figure 19, the cross sectional surface of a gSS-PP composite granule is illustrated. It shows that the AgFiller was distributed randomly throughout the composite. There was no evidence of filler aggregation as suggested by Salemane and Luyt (2006). There was however a preference for the AgFiller to align in the lengthwise direction along the granule. This is attributed to the fact that resistance to shear and flow is minimal in this particle arrangement. gWS-PP and SH-PP also demonstrated the same lack of specific order in filler distribution.

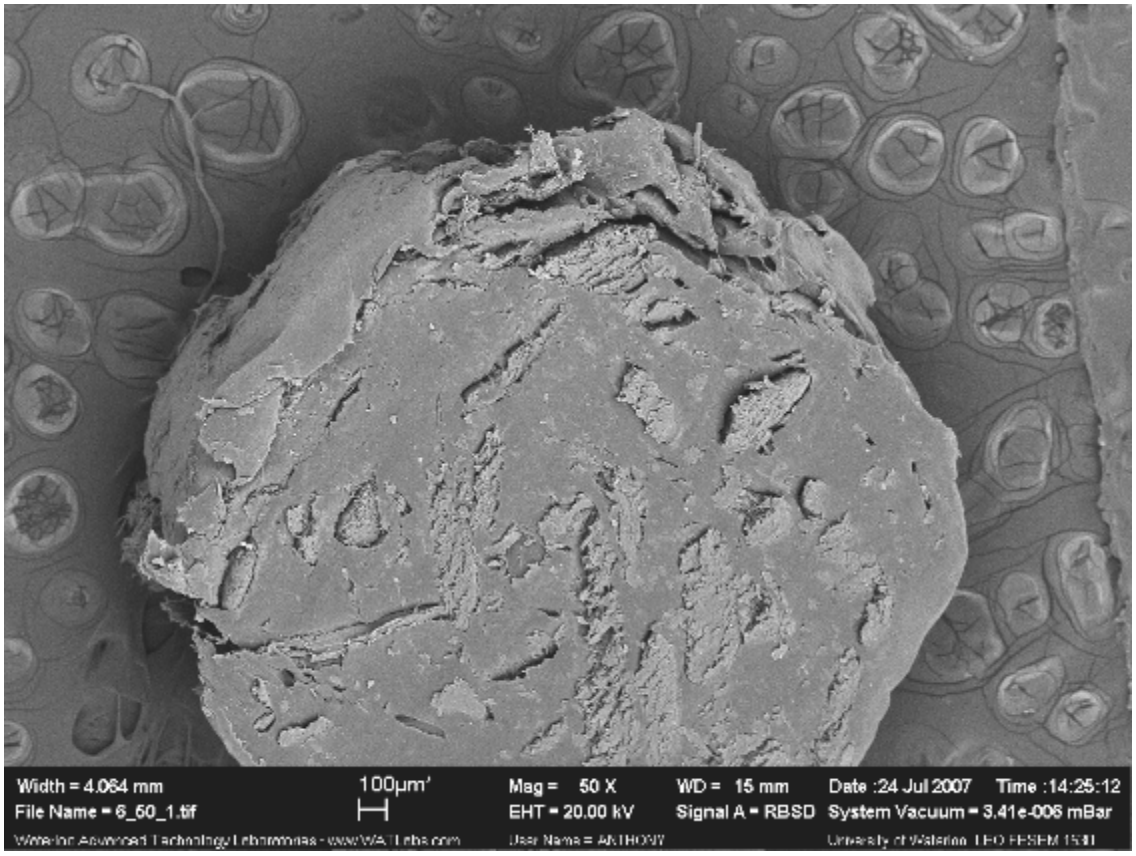

Figure 19: SEM of gSS-PP composite, mag = 50x

4.1.1.1 Fiber Damage Incurred During Processing

Figure 20 to Figure 22 show extracted AgFillers from each of gWS-PP, gSH-PP and gSS-PP composites from compounded granules. It was observed that all three AgFillers suffered some form of surface damage, such as the cracking observed in gSH, and peeling as found in gWS and gSS. There were also more fines found in the extracted AgFillers, especially in gSS (Figure 22). While these damages are mainly attributed to shear forces applied during the extrusion process, other factors may include fiber degradation caused by thermal and chemical treatments during the extraction step (Kruger, 2007).

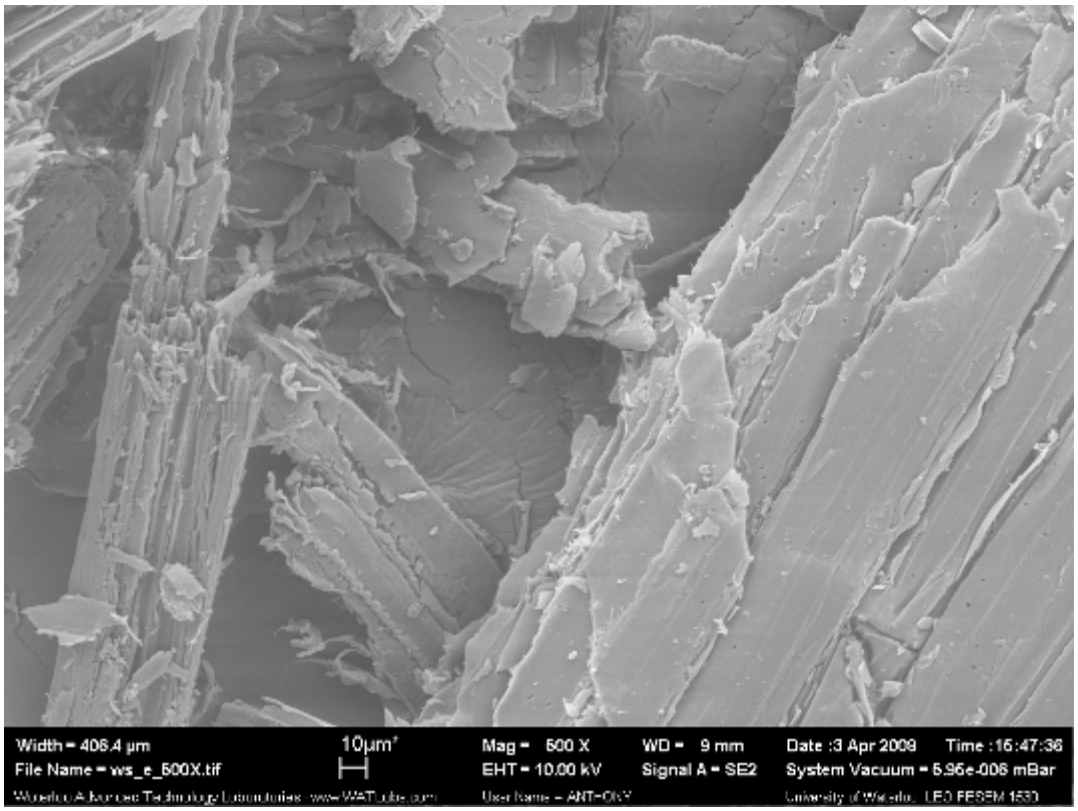

Figure 20: gWS fibers extracted from gWS-PP composite

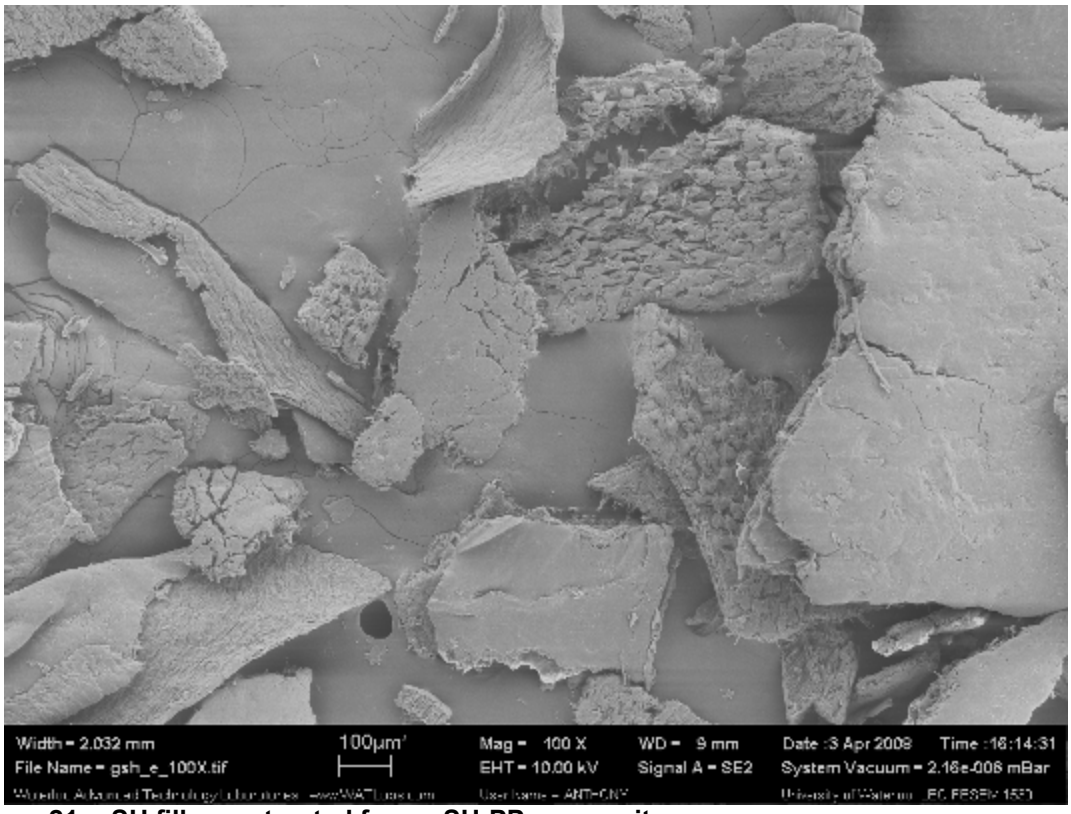

Figure 21: gSH fillers extracted from gSH-PP composite

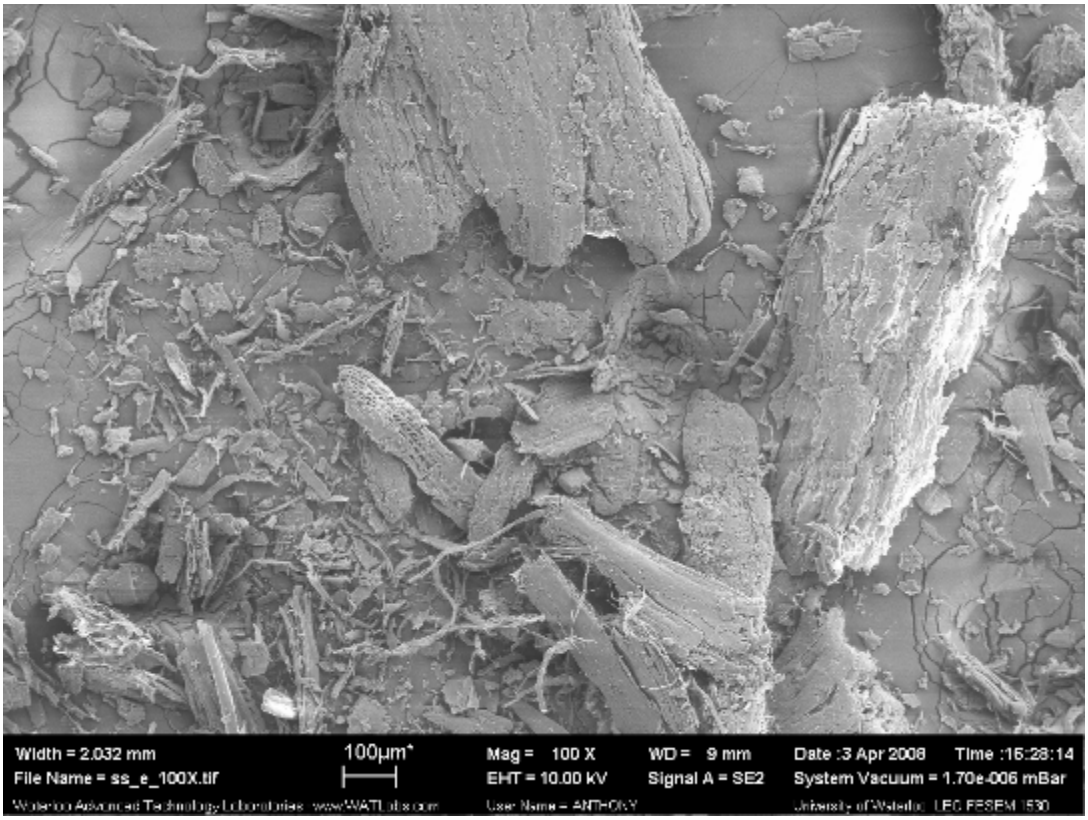

Figure 22: gSS fibers extracted from gSS-PP composite

Among the three AgFillers studied, SH was found to be the most brittle in nature, and it was expected that it would have sustained the most damage during processing. Therefore, the change in the size of this AgFiller's major axis, or length, was investigated, and the results are illustrated in Figure 23. It was confirmed that the extrusion process had resulted in a reduction in filler size, especially in SH, where most particles (47%) were over 2 mm in length prior to extrusion. After processing, filler particles with lengths between 0.25-0.5 mm had increased from 6% to 19%, a 3-fold increase. In addition, it was discovered that the particle size distribution of SH after processing was similar to that of gSH after processing, especially in the 0.25-0.75 mm and 1.00-2.00 mm ranges. This showed that the extruder had the capability of crushing SH fillers and equalizing their particle sizes. Based on this observation, it was determined that unlike WS and SS which require grinding from large stalks into useable fillers, the grinding of SH fillers prior to extrusion is not necessary.

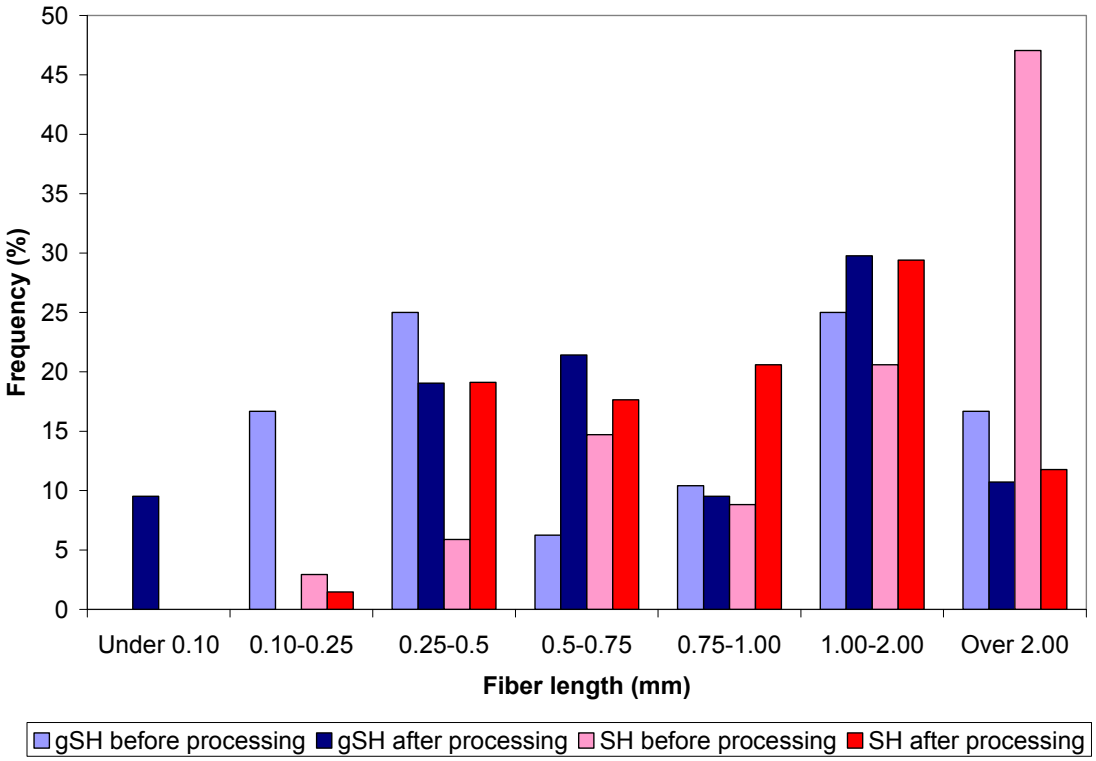

Figure 23: Histogram of the lengths of SH and gSH AgFillers before and after processing

4.1.2 THERMAL PROPERTIES

4.1.2.1 Thermal Gravimetric Analysis (TGA)

The stability of each AgFiller of interest was studied using TGA because it is an important aspect in determining the suitability of the AgFiller for the selected polymer matrix. Schemenauer *et al.* (2000) reported the need to lower the temperature for their rheological experiments on kenaf-PP composites to prevent degradation. Table 5 summarizes the temperatures of degradation onset of AgFillers tested in an atmospheric environment, while the full results of the experiment are documented in Appendix B. Table 5 shows that gWS and gSS had similar thermal stabilities, while gSH degraded at a significantly lower temperature. Considering that most PP processes operate at temperature ranges of approximately 190-230^{o}C, the thermal stability of SH was only marginal.

Table 5: AgFiller degradation onset temperature determined by TGA

AgFiller	Degradation onset temperature (^{o}C)
Wheat straw (gWS)	217
Soy Hull (gSH)	195
Soy Stem (gSS)	220

The low thermal stability of SH AgFiller was further demonstrated by significant discoloration of SH-PP composite material when heated to 230^{o}C and held isothermal for 10 minutes. gWS-PP and gSS-PP also showed discoloration under the same conditions, but to a lesser extent. The degradation of AgFiller inside the composite is undesirable mainly because of the negative effects on the aesthetics of the composition due to discoloration and the generation of a strong odour. There is also evidence that overheating of fibers to 200^{o}C would soften the fibers, resulting in deteriorations of mechanical properties, such as modulus, of the composite (Hornsby[1], 1997).

4.1.2.2 Differential Scanning Calorimetry (DSC)

During the cooling step (step 2) of the DSC experiment, distinctive peaks would form as crystallization takes place and the crystallization temperature can be determined. Figure 24 graphically illustrates the cooling endotherms of gWS-PP, SH-PP, gSH-PP, gSS-PP composites and pure vPP, while Table 6 summarizes the onset and peak crystallization temperatures extracted from the figure.

As shown in Figure 24 and Table 6, a shift in crystallization temperature was detected for all AgFiller-PP composites when compared to that of pure PP. Specifically, crystallization of the composites occurred at higher temperatures. The reason for the change in crystallization temperature is that the AgFiller served as nucleating agents to promote formation of spherulite crystals, similar to the way mineral fillers increases T_c of talc-PP composites (Albano, 2004).

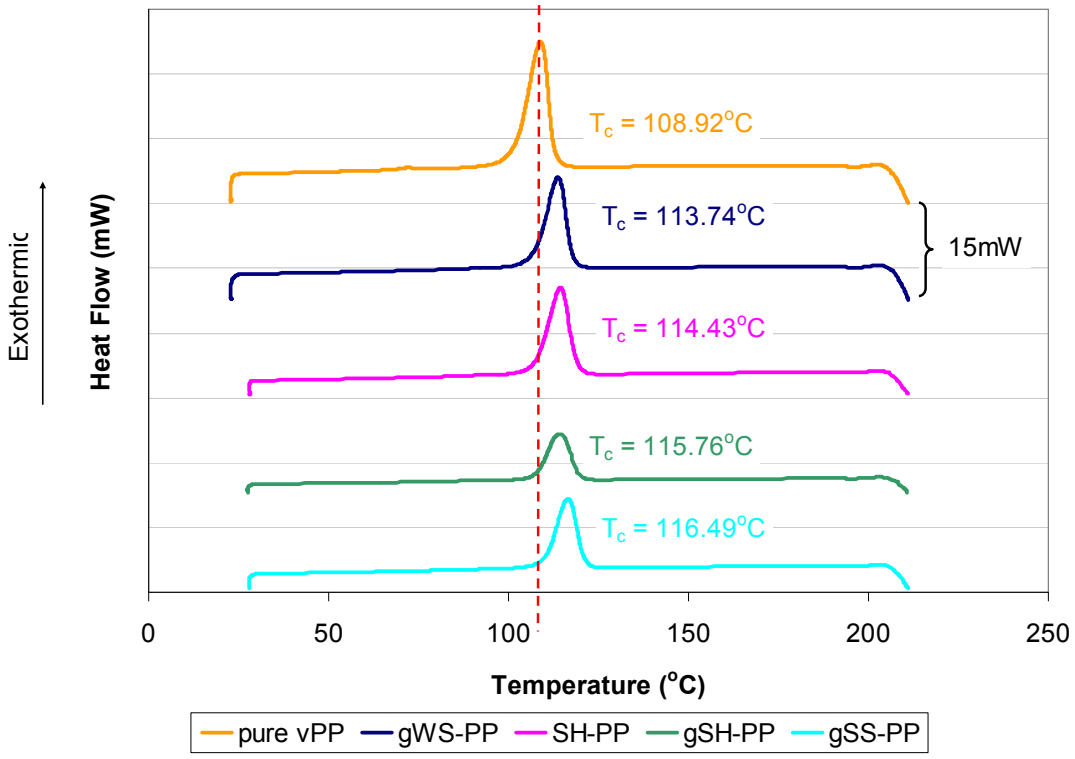

Figure 24: DSC curves during cooling step for AgFiller-PP composites and pure vPP

Table 6: Crystallization temperature of AgFiller-PP composites and pure vPP

Composite	T_c onset (°C)	T_c peak (°C)
Pure vPP	112.6	108.9
gWS-vPP	117.7	113.7
SH-vPP	119.0	114.4
gSH-vPP	119.6	114.3
gSS-vPP	121.1	116.5

The reheating step (step 3) forms characteristic peaks from which the sample's melting point of the composite was recorded. Crystallinity was also calculated from data of peak areas. The percentage of crystallinity in a composite material is determined by:

$$X_C = \frac{\Delta H}{\Delta H^o} \cdot \frac{100}{w} \quad (5)$$

Where X_c is the percentage of crystallinity, ΔH is the heat of fusion of the PP composite, ΔH^o is the heat of fusion of 100% crystalline PP, and w is the polymer weight fraction in

the composite (Digabel, 2004). According to references (Kruger, 2007; Salemane, 2005), ΔH^o of 209 J/g was used for calculation.

Figure 25 compares the melting endotherms of AgFiller-PP composites and pure PP. It could be seen that the melt point did not experience any changes, regardless of AgFiller type used. On the other hand, the data in Table 7 showed that composites containing gWS, SH or gSH had increased crystallinity when compared to pure PP as suggested by literature (Albano, 2004). One exception was gSS-PP, which showed little change in crystallinity from pure PP. Studies of crystallization effects of PP composites filled with calcium carbonate ($CaCO_3$) of different particle sizes showed that $CaCO_3$ of smaller particle sizes resulted in lower composite crystallinity (Zhang, 2006). This inferred that after processing, gSS-PP contained the highest amounts of fines among all the composites, supporting the particle size and morphology results previously presented.

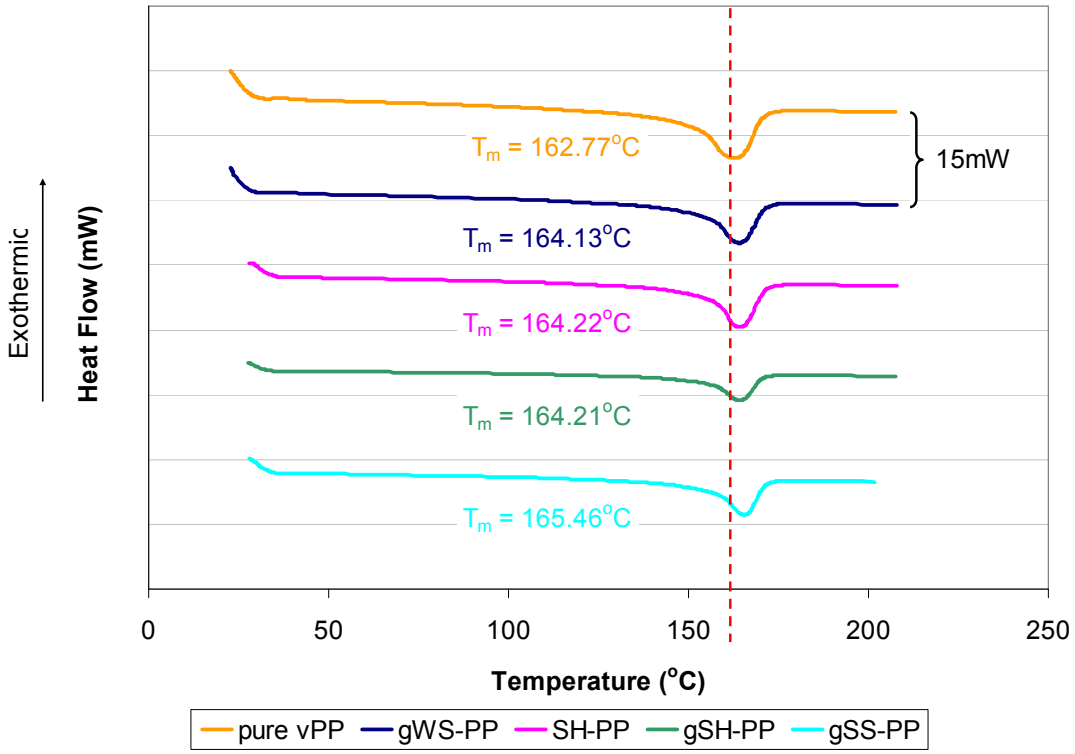

Figure 25: DSC curves during second heating step for AgFiller-PP composites and pure vPP

Table 7: Melting temperatures and crystallinity of AgFiller-PP composites and pure PP

Composite	T_m onset (°C)	T_m peak (°C)	Crystallinity (%)
Pure vPP	150.5	162.8	38
gWS-vPP	154.0	164.1	48
SH-vPP	155.7	164.2	48
gSH-vPP	154.8	164.2	45
gSS-vPP	155.9	165.5	39

To validate the repeatability of the experiment, two gSH-PP composites were tested in separate runs to study the uncertainty regarding DSC testing of non-oriented AgFiller-PP composites. Results tabulated in Table 8 show that melting temperature and crystallization temperature were very repeatable with standard deviations of less than 1%. Crystallinity results showed higher uncertainty and the error margin based on standard deviation was close to 10%. This is explained by the fact that crystallinity is a calculated values based on parameters such as sample weight and the mass fraction of polymer within the samples. Each of these parameters presents a significant level of uncertainty due to the small quantity of test specimen used in a DSC experiment (5-10 mg).

Table 8: Repeatability test for gSH-PP composite

	T_m-onset (°C)	T_m-peak (°C)	T_c-onset (°C)	T_c-peak (°C)	Crystallinity (%)
Run #1	154.8	164.2	119.6	114.3	45
Run #2	155.3	164.0	120.5	115.9	51
Average	155.0	164.1	120.0	115.1	48
Standard Deviation	0.3	0.1	0.7	1.1	4

4.1.2.3 X-ray Diffraction (XRD)

The XRD diagrams of non-oriented gWS-PP, SH-PP, gSH-PP and gSS-PP composites are shown in Figure 26. A number of peaks were identified, but only some were of importance. It was confirmed with a background scan that the peaks found when 2θ angle is between 25-30° belonged to the clay putty used to secure the sample to the sample holder during scanning. These irrelevant peaks were neglected from analysis. Furthermore, the thickness and opacity of the sample was found to have an influence on

the spectrum intensity, as shown by the gSH-PP spectrum in Figure 26, where the sample was thinner than the others. This, however, did not appear to have affected the ratios of peak heights.

According to Yi *et al.* (1997), the most important peaks in the diagram were the three equatorial α-form peaks at (110), (040) and (130) planes, and the (300) β-form peak. The K-value is defined as the β fraction in all crystal forms, and can be calculated using the height of each crystal peak and the equation:

$$K = \frac{H_\beta}{H_\beta + (H_{\alpha 1} + H_{\alpha 2} + H_{\alpha 3})} \tag{6}$$

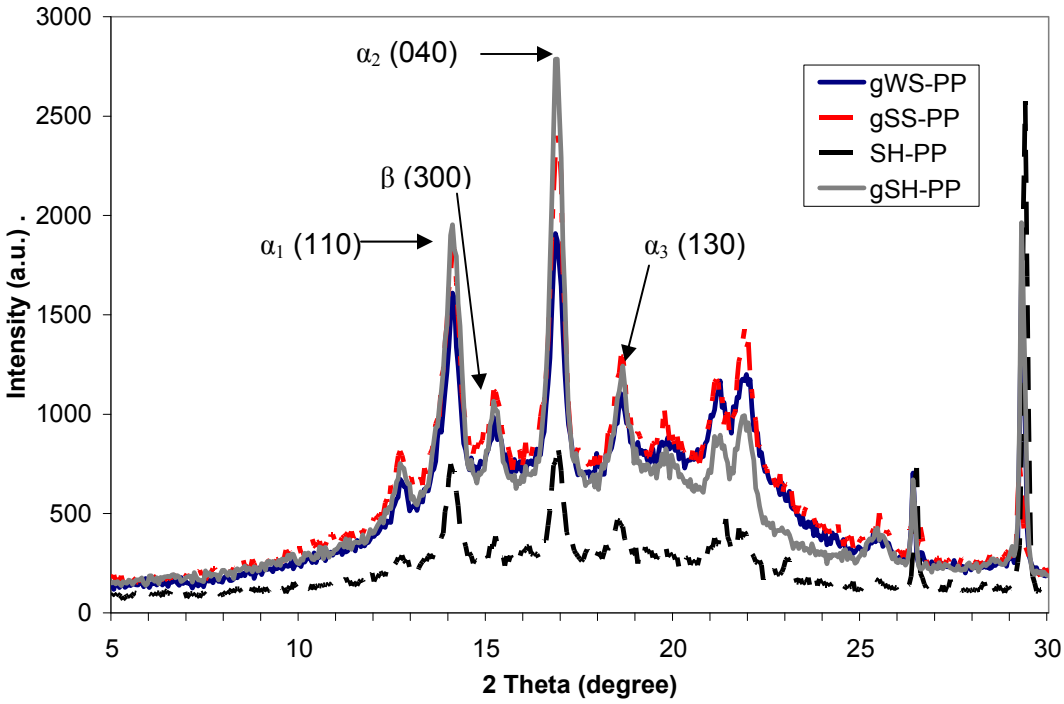

Figure 26: XRD patterns of gWS-PP, SH-PP, gSH-PP and gSS-PP composites

The K-value of each AgFiller-PP composite is presented in Table 9. After translating the K-values into percentages, the β-form fractions of AgFiller-PP composites were determined to range between 15% and 17.5% These K-values obtained were similar to those determined for bamboo fiber-PP composites containing m-MAPP coupling agent (0.15) but lower than the K-value of 0.35 reported for uncoupled bamboo fiber-PP

(Yi, 1997). Both K-values were considered by Yi as a moderate level of β-crystal formation when compared to K-values of up to 0.95 in PP containing β-nucleators.

Table 9: K-value of non-oriented AgFiller-PP composites

Composite	$H_{\alpha 1}$	$H_{\alpha 2}$	$H_{\alpha 3}$	H_{β}	K-value
gWS-PP	1610	1909	1104	984	0.175
SH-PP	749	846	462	385	0.158
gSH-PP	1954	2787	1242	1065	0.151
gSS-PP	1844	2401	1288	1111	0.167

Further comparisons in K-values of stem-based AgFiller against shell-based AgFiller showed that both gWS and gSS had slighter higher (1.5-2.5%) K-values than gSH filler. On the other hand, reducing the size of filler by grinding SH into gSH prior to processing did not cause any significant changes in the amount of β-form crystals in the composite.

Peak deconvolution is often performed to calculate the degree of crystallinity of materials by isolating the sharp crystalline peaks and the broad amorphous halo from an XRD curve (Saujanya, 2002; Chaffey, 1997; Rabiej, 1993). Using the Lorentzian peak fitting function in the Origin 8 data analysis software, an attempt was made to identify and resolve the characteristic peaks of the XRD scans of each AgFiller-PP composite. Results similar to that illustrated in Figure 27 were obtained. It was observed that the software was unable to provide enough degrees of freedom for manipulation, and therefore the mathematical fit using the Lorentzian distributions was inadequate for describing all the crystalline peaks of interest in the XRD curve, as highlighted by the circled sections in Figure 27. The width of some peaks identified was considered too large, and resulted in different height-to-width ratios for the peaks. This, in turns, led to under-estimations of the amount of amorphous fraction while over-estimating the crystalline amount. As a result, the calculated crystallinity values for some samples were found to be significantly higher than the values determined using DSC data (Table 10). It is suggested that additional work is required to fully interpret and understand the results generated by the XRD deconvolution analyses.

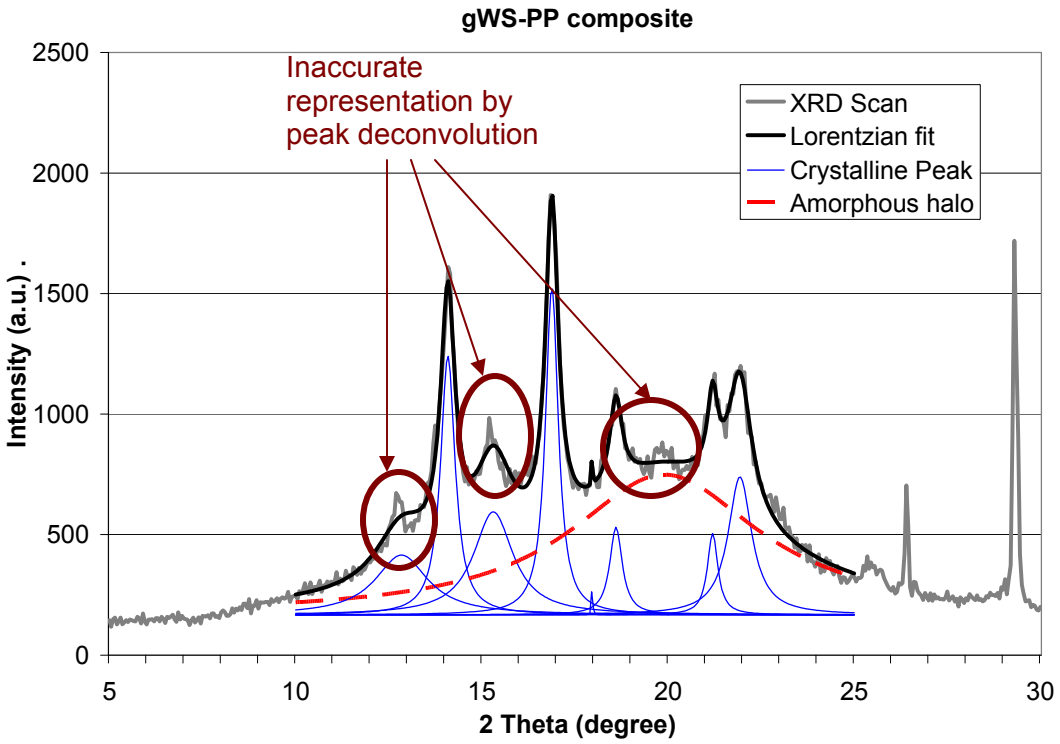

Figure 27: XRD peak deconvolution of gWS-PP composite to identify crystalline and amorphous fractions of the material for the calculation of percent crystallinity

Table 10: Comparison of crystallinity of AgFiller-PP composites, and of pure vPP, as determined by XRD and DSC

Material	Crystallinity (%) determined by XRD	Crystallinity (%) determined by DSC
gSHPP	64	48
SHPP	74	48
SSPP	52	39
WSPP	47	48
vPP	72	38

4.1.3 CHEMICAL PROPERTIES

4.1.3.1 Fourier Transform Infra-red Spectroscopy (FTIR)

The surface chemical composition of AgFiller-PP composites were studied by FTIR using the attenuated total reflection (ATR) technique. According to the penetration depth expression (equation 7) defined by Harrick (1967), the sampling depth of using this nondestructive technique was estimated to be 0.85 microns (Pike Technologies, 2005).

$$d_p = \frac{\lambda_1}{2\pi(\sin^2\theta - n_{21}^2)^{1/2}} \quad (7)$$

Where d_p denotes the penetration depth, λ_1 the wavelength of irradiation, θ the incident angle, and n_{21} the refractive index from medium (2) to medium (1).

At the depth penetrated by the ATR's radiation, the recorded spectra of AgFiller-PP composites showed identical peaks to pure vPP in the fingerprinting region (Figure 29), despite the fact that each composite contained an AgFiller which had a characteristic spectrum distinct from that of vPP polymer (Figure 28). Many characteristic peaks of pure isotactic PP, including those at 1175cm^{-1}, 1000 cm^{-1}, 975 cm^{-1}, 900 cm^{-1}, 850 cm^{-1} and 810 cm^{-1} (Lamberti, 2003), were found on the composite spectra, while characteristic peaks for WS and SH fibers at 1238 cm^{-1}, 1200 cm^{-1} and 1058 cm^{-1} (Alemdar, 2008) were not detected. The assignment and significance of these characteristic FTIR peaks are presented in Table 11.

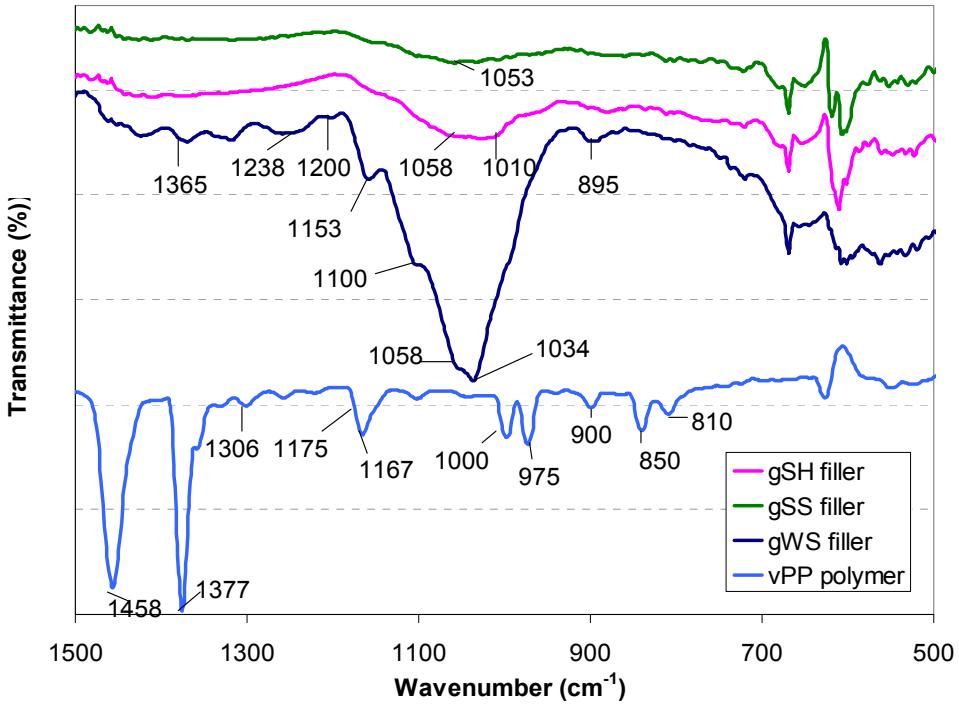

Figure 28: ATR-FTIR spectra of AgFillers compared to that of vPP polymer

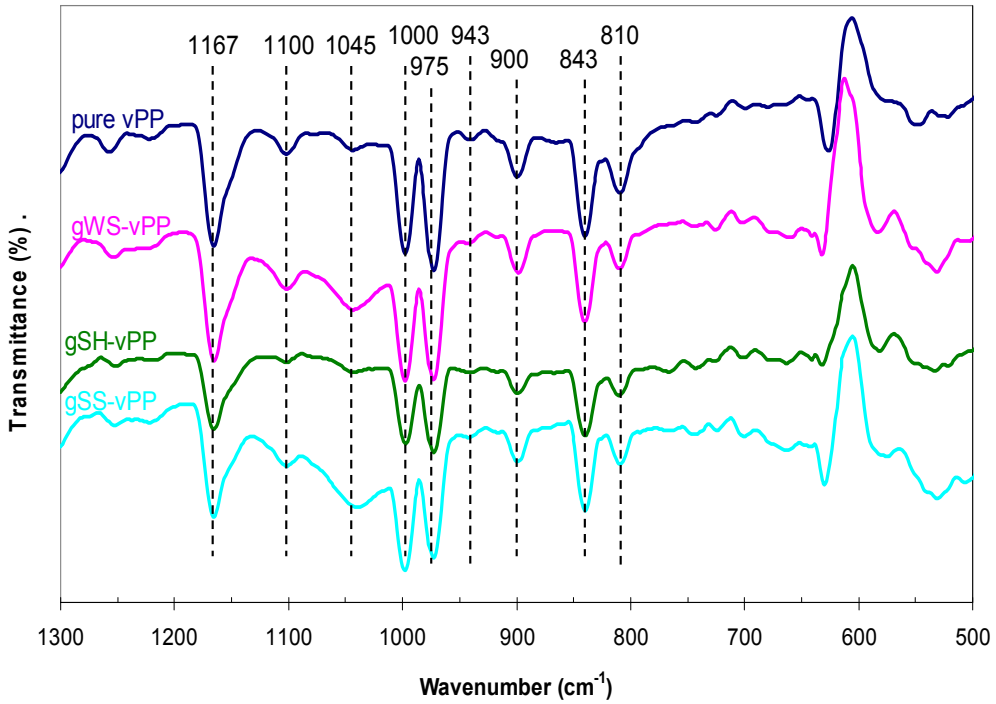

Figure 29: ATR-FTIR spectra of AgFiller-PP composites and pure PP

Table 11: Selected FTIR peak identification and assignment

Peak Band (cm^{-1})	Assignment	Material	Reference
1458	Methyl asym. bend	PP	Coates, 2000
1377	Methyl sym. bend	PP	Coates, 2000
1238	C-H, O-H, CH_2 bend	SH	Alemdar, 2008
1200	C-O stretch	WS	Alemdar, 2008
1058	1^o alcohol C-O stretch	WS, SH	Alemdar, 2008; Coates, 2000
1000	Isotactic PP vibration	PP	Lamberti, 2003; Ozzetti, 2001
850	CH_2 skeletal stretch	PP	Lamberti, 2003; Gatos, 2007

A possible explanation for this observation is that a skinning effect took place when the composite was produced, during which the AgFiller migrated away from the surface, which was filled with PP, the continuous phase. The magnitude of this effect would be large enough to exceed the sampling depth of ATR-FTIR.

To verify repeatability of the experiment, each sample was scanned 3 times, and no variations in peak positions were found. Variations in peak intensities among samples

were observed on occasion, but since the ATR-FTIR experiment performed was intended for qualitative but not quantitative analysis, the variation was considered unimportant. All ATR-FTIR curves can be found in Appendix D.

4.1.4 RHEOLOGICAL PROPERTIES

4.1.4.1 Apparent Shear Viscosity

A relative comparison of the apparent shear viscosity of AgFiller-PP composites and pure vPP is shown in Figure 30. As predicted based on many literature references (Schemenauer *et al.*, 2000; Kruger, 2007; Zurale and Bhide, 1998), the result of the experiments demonstrated that all four composites studied were more viscous than vPP. In particular, gWS-PP and gSS-PP had the highest and similar viscosities. The effect of grinding SH filler into gSH prior to extrusion was shown to slightly increase the viscosity of the composite. The increase was not significant enough to raise the viscosity of composite filled with shell materials (SH) to the same level as that filled with stalk materials (WS or SS).

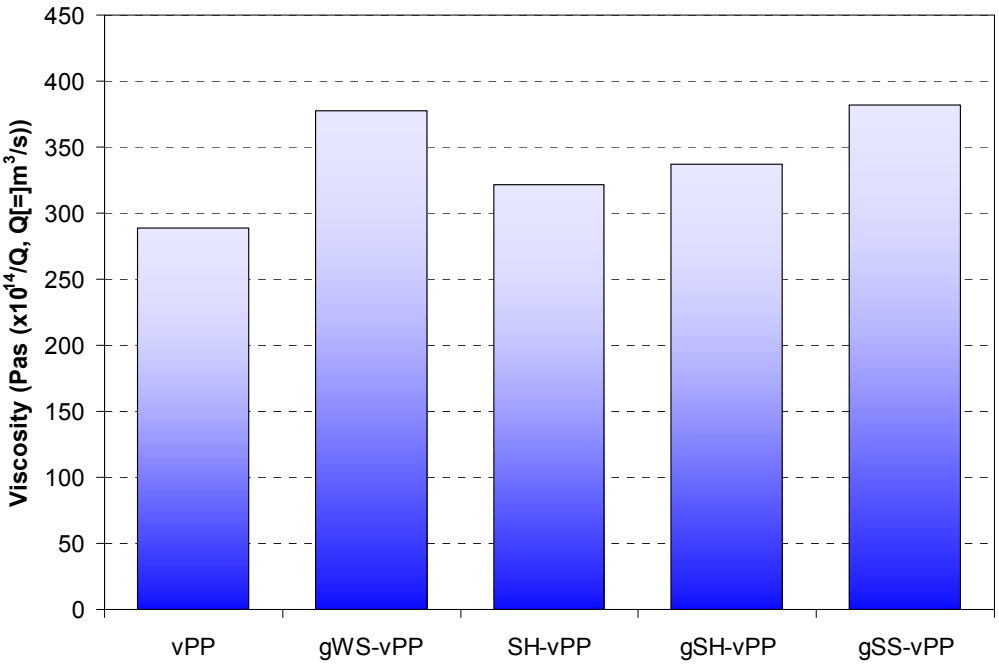

Figure 30: Relative comparisons in apparent shear viscosities of AgFiller-PP composites and pure vPP

Table 12: Experimental variance for Minilab testing

	Melt Temperature (°C)	Minilab Screw Speed (RPM)	ΔP (bar)
Set Value	**190.00**	**30.00**	**--**
gWS-PP #1	189.89	30.00	33.23
gWS-PP #2	189.99	30.01	31.24
Average	189.94	30.01	32.24
Standard Deviation	0.07	0.01	1.41
vPP #1	189.83	30.00	25.12
vPP #2	189.94	30.02	24.12
Average	189.89	30.01	24.62
Standard Deviation	0.08	0.01	0.71

Repeatability of the experiment was assured by testing each of gWS-PP composite and pure vPP twice and checking for any significant deviations. As seen in Table 12, variations on factors controllable by the apparatus, including temperature and running speed, were minimal. The deviation on the measured value ΔP was approximately 5% for gWS-PP and under 3% for pure PP, both considered acceptable for the purpose of this analysis.

4.1.4.2 Melt Flow Index (MFI)

Melt flow index (MFI) is a more commonly applied indicator for the viscosity of polyolefins than melt viscosity. MFI is inversely related to both melt viscosity and molecular weight of the material. Noting that there was a deviation in the actual MFI of vPP tested in the laboratory (2.65) from the literature value (1.50), Table 13 compares the laboratory recorded MFI of each AgFiller-PP composite material against that of vPP. It was shown that the stem-based fillers, gWS and gSS, had greater contribution in reducing the MFI of the material than shell-based SH and gSH fillers. These changes in MFI matched the viscosity changes observed previously in Figure 30 in an inverse relationship, exactly as theory predicted (Maier, 1998).

Table 13: MFI of vPP polymer and AgFiller-PP composites

	vPP polymer	gWS-vPP	gSS-vPP	SH-vPP	gSH-vPP
# specimens	6	5	5	4	5
Average MFI	2.65	0.84	1.04	2.03	2.14
Standard Deviation	0.04	0.15	0.11	0.25	0.29
95% Confidence	±0.03	±0.13	±0.10	±0.24	±0.25

4.1.5 MECHANICAL PROPERTIES

4.1.5.1 Flexural Properties

Figure 31 shows the change in stiffness when AgFiller was added to PP to form composites, with error bars showing one standard deviation. Based on average values of the property as displayed in the figure, it appeared that all four types of AgFiller-PP composites possessed higher flexural modulus than pure PP.

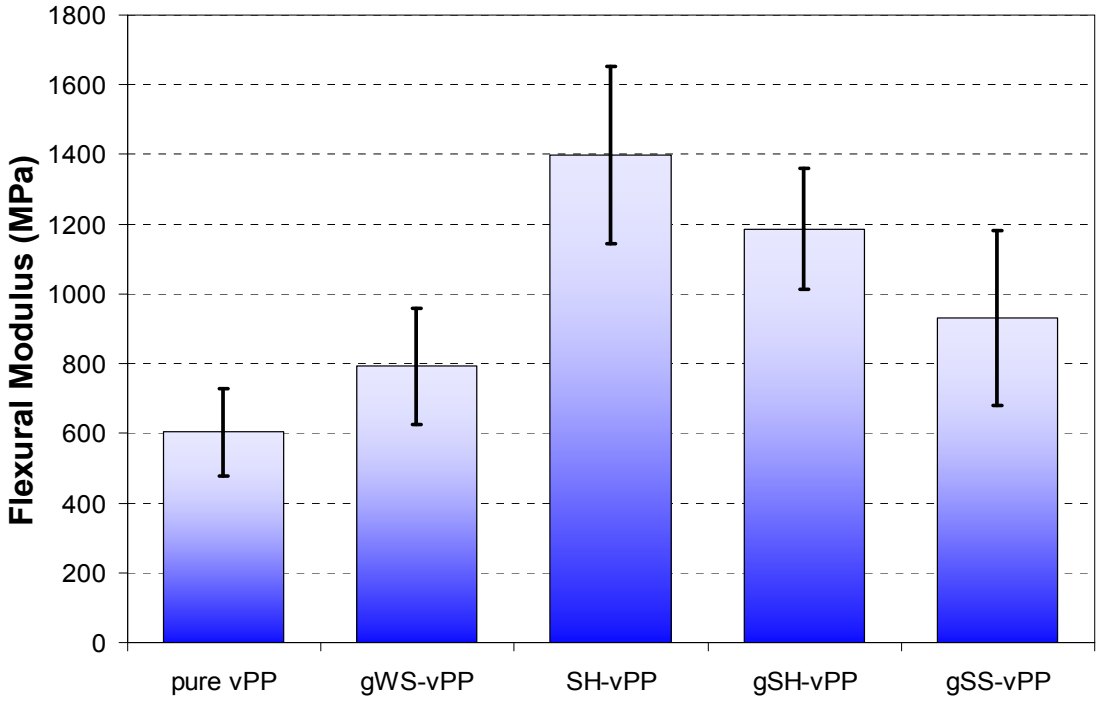

Figure 31: Flexural modulus of AgFiller-PP composites at 40 wt% filler, 60 wt% polymer; compared to 100 wt% virgin PP

A t-test was used to confirm this observation statistically by comparing the means of the flexural moduli between each composite and pure PP at 95% confidence level, using the null hypothesis H_0 that there is no difference in the means, i.e.:

$$H_0: \mu_{composite} - \mu_{PP} = 0$$

The alternative hypothesis H_1 was set based on observations made from the results shown Figure 31, in this case, that the mean flexural modulus of each composite was larger than that of pure vPP. The T-observed values were calculated and compared against the respective T-tabulated values, and when T-observed is greater than T-tabulated, the null hypothesis is rejected. The results of the t-test are summarized in Table 14. The ability to reject the null hypothesis in all cases shows that the mean of each AgFiller-PP composite's flexural modulus is significantly different from that of pure vPP.

Table 14: Summary of t-test result for significance in difference in flexural modulus means of composites and pure vPP

Composite	Alternative hypothesis H_1	Degree of Freedom	T-observed	T-tabulated (α=0.05)	Decision
gWS-vPP	$\mu_{composite} > \mu_{PP}$	10	2.30	1.81	Reject H_0
SH-vPP	$\mu_{composite} > \mu_{PP}$	4	5.69	2.13	Reject H_0
gSH-vPP	$\mu_{composite} > \mu_{PP}$	7	6.07	1.89	Reject H_0
gSS-vPP	$\mu_{composite} > \mu_{PP}$	5	2.60	2.02	Reject H_0

It seemed apparent from the trend shown in Figure 31 that, among all the composites, the material made using shell material (SH) showed the most improvement in flexural modulus, while stem materials (WS and SS) were less effective in modifying this property of the composite, and that soy hull grinding resulted in a decrease in composite stiffness when SH-PP and gSH-PP properties were compared. However, these differences can not be truly distinguished based on a failed analysis of variance (ANOVA) for determining the significance of between-sample variance over within-sample variance. Table 15 presents the result of the statistical test. By definition, an ANOVA test fails when the F-observed value is less than the F-tabulated value.

Table 15: ANOVA summary of f-test for the significance in variance of flexural modulus among and within AgFiller-PP composites

	Degree of Freedom	Sum of Squares	Mean Square	F-observed	F-tabulated
Between Samples	3	9.03×10^6	3.01×10^6	-7.63	Approximately 3.10
Within Sample	18	-7.10×10^6	-3.94×10^6	--	--

Figure 32 compares the yield strength measured at 0.2% offset among AgFiller-PP composites and pure PP. It was predicted according to literature (Rowell, 1999) that the yield strength should not be positively affected by the presence of AgFillers. This prediction was found true for all ground AgFillers (gWS, gSH and gSS), as determined by a t-test. The result of the statistical analysis (Table 16) showed that gWS resulted in a decrease in yield strength, while gSH and gSS had no contribution in affecting this property. On the other hand, the improvement in strength is statistically significant for composite made with SH (as received).

The result obtained for gWS-PP composite was further compared to the study performed by Kruger (2007). The observed decrease in yield strength of gWS-PP from that of pure vPP was in agreement with the trend found in Kruger's work.

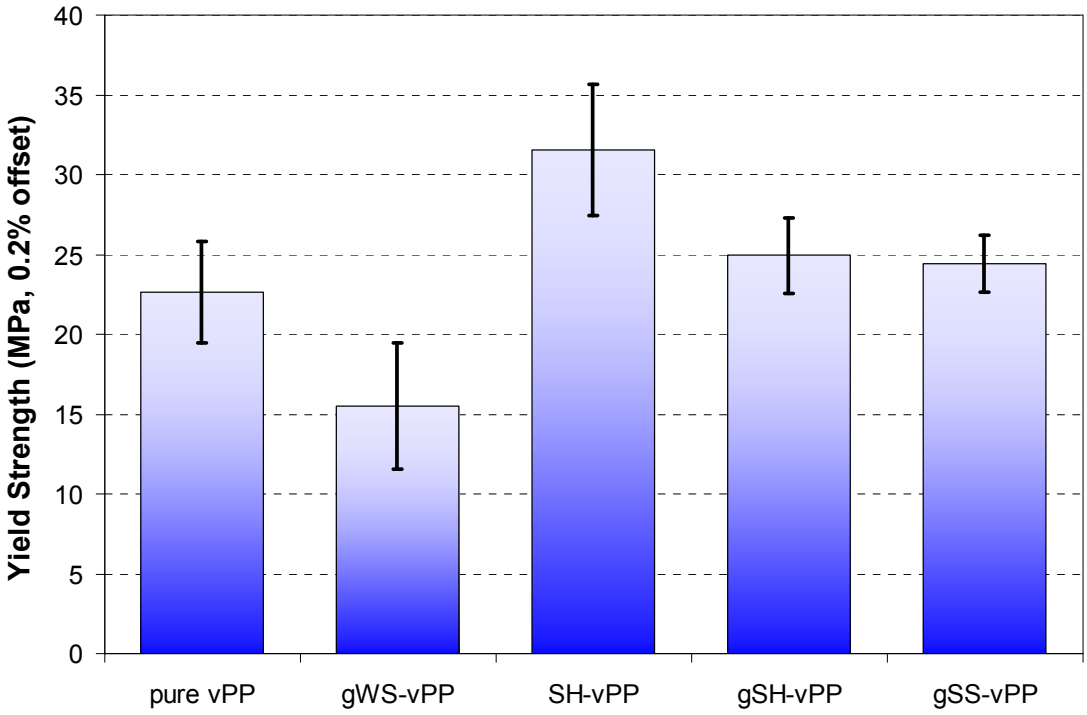

Figure 32: Yield Strength (0.2% offset) of non-oriented AgFiller-PP composites at 40 wt% filler, 60 wt% polymer; compared to 100 wt% virgin PP

Table 16: Summary of t-test result for significance in difference in yield strength means of composites and pure vPP

Composite	Alternative hypothesis H_1	Degree of Freedom	T-observed	T-tabulated (α=0.05)	Decision
gWS-vPP	$\mu_{composite} < \mu_{PP}$	10	3.58	1.81	Reject H_0
SH-vPP	$\mu_{composite} > \mu_{PP}$	6	3.60	1.94	Reject H_0
gSH-vPP	$\mu_{composite} > \mu_{PP}$	7	1.30	1.89	Fail to reject H_0
gSS-vPP	$\mu_{composite} > \mu_{PP}$	6	1.10	1.94	Fail to reject H_0

4.2 Chapter Summary

In this chapter, the effects of AgFiller type on the properties of AgFiller-PP composites were investigated. Four types of AgFillers, gWS, SH, gSH and gSS were studied.

SEM micrographs presented excellent visual evidence that the morphology of shell type AgFiller (SH) is greatly different than that of stalk type AgFiller (WS and SS), especially in terms of AgFiller alignment, where fiber orientation with respect to the largest surface plain defined by the length-width axes was found to be opposite between the two types of AgFillers. When a composite sample was broken apart, it was shown that AgFillers with fibers aligned perpendicular to the fracture surface were pulled out from the polymer phase (as observed in gWS-PP and gSS-PP composites, while those with fibers aligned parallel to the fracture surface would break off level to the polymer (as observed in SH-PP composite). In terms of AgFiller distribution in the composites, no specific patterns were found and the distribution was determined to be random.

The thermal stabilities of AgFillers were found to be adequate, although marginal, for the production of AgFiller-PP composites. Discoloration was the first sign of degradation when processing conditions for the composite were above the stability of the AgFiller. The presence of AgFiller attributed to increases in crystallization temperature and crystallinity of the composite in comparison to pure PP, but had no effect on melting behaviour. Grinding of SH into gSH prior to compounding did not have any effects on the thermal properties of the composite.

ATR-FTIR demonstrated that a very thin layer of polymer was aggregated on the surface of the composite, giving the composite a structure similar to a core-shell material.

AgFillers were found to increase the viscosity of the composite. Stalk type WS and SS showed slightly greater impact on increasing composite viscosity than shell type SH. Grinding SH prior to processing contributed to little increase to composite viscosity.

From mechanical testing, it was determined that flexural modulus was increased with the use of AgFillers. On the other hand, tensile strength was found to suffer, or to experience no significant changes, in gWS-PP, gSH-PP and gSS-PP composites. However, the large variance within the samples prohibited any distinction among the composites.

CHAPTER 5 USE OF RECYCLED PP AS MATRIX OF NON-ORIENTED COMPOSITES

Recycling is an environmentally friendly practice that contributes to alleviating the dependence on fossil fuels. In this chapter, vPP was progressively replaced by rPP, and the composites resulted were examined for their morphologies, thermal, chemical, rheological and mechanical properties. The AgFiller-PP composites each contained 60 wt% total polymer and 40 wt% filler. Non-oriented composite samples were prepared in the laboratory by compression molding pellets obtained from batch extrusion.

5.1 Property Characterization

5.1.1 MORPHOLOGY

Figure 33, Figure 34 and Figure 35 show respectively the SEM micrographs of SH-PP composites of which the polymer matrix consisted of vPP only, of equal weight-fraction of respectively vPP and rPP, and of rPP only. Some extent of fiber pullout and void formation at the filler-polymer interface was observed in all three composites.

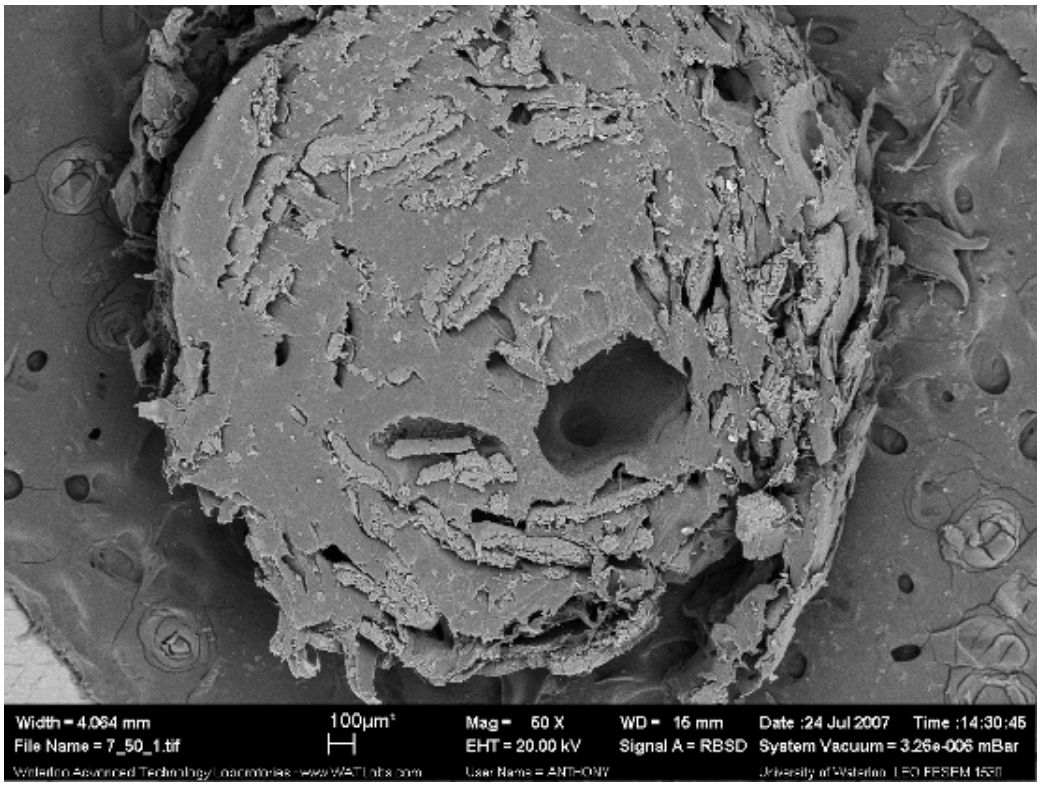

Figure 33: SEM of SH-PP composite with vPP only as polymer matrix, filled with 40 wt% AgFiller, mag = 50x

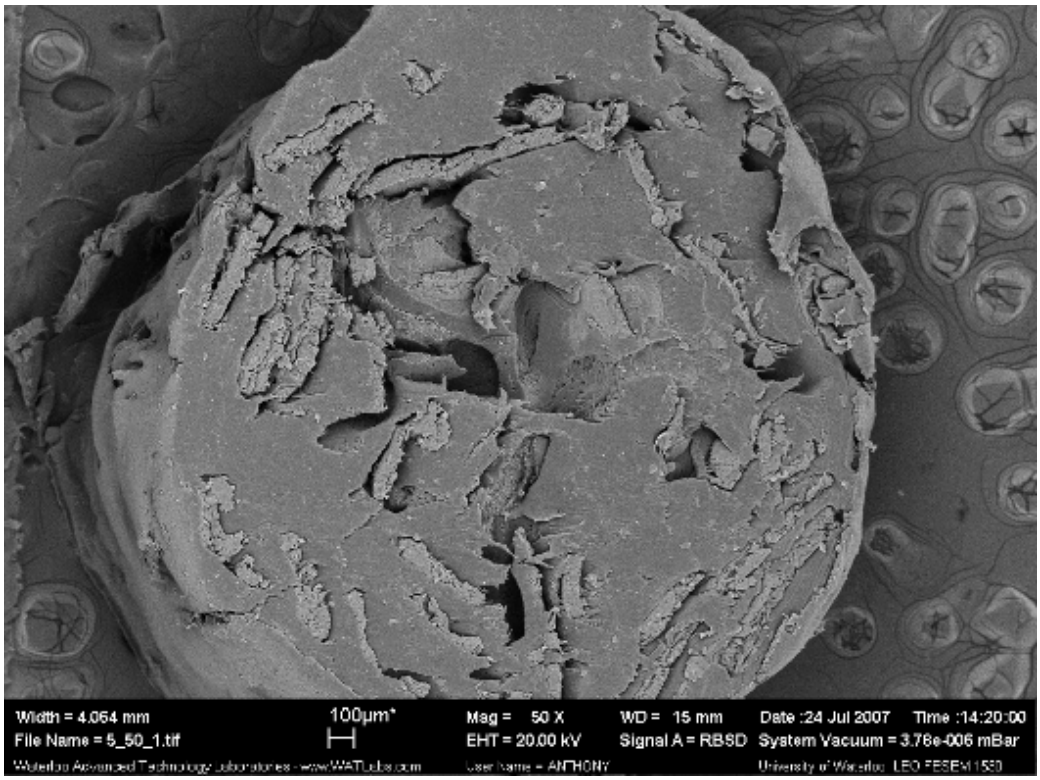

Figure 34: SEM of SH-PP composite with equal amount of vPP and rPP as polymer matrix, filled with 40 wt% AgFiller, mag = 50x

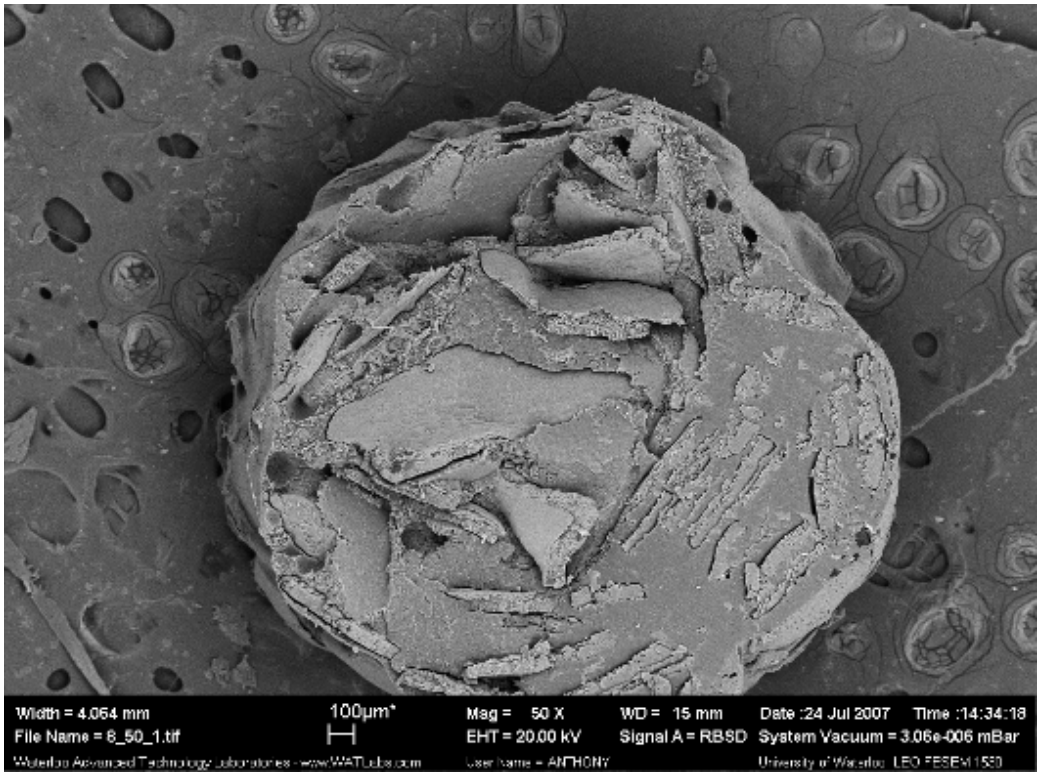

Figure 35: SEM of SH-PP composite with rPP as matrix as polymer matrix, filled with 40 wt% AgFiller, mag = 50x

It was observed that the number and width of separation between polymer and AgFiller decreased as more rPP was present in the polymer matrix, similar to observations made on natural fiber-PP composites containing coupling agents shown in the work by Jasso-Gastinel and Sanjuan-Raygoza (2007). Bearing in mind that the MFI of rPP was over 40 times higher than that of vPP, it is possible that such difference in viscosity allowed the rPP to better surround the AgFillers, thus resulting in fewer gaps. In addition, the sample of rPP was most likely to have contained processing residual additives such as lubricants and compatibilizers, or greasy contaminants such as oil and fat, from the polymer's first application. The presence of these additives and contaminants might have also played a role in allowing the polymer chains to arrange themselves easier to encapsulate the AgFiller. Despite the lesser extent of gaps being formed, the incompatibility between AgFiller and polymer remained. A close-up image of SH-rPP composite at the interface between AgFiller and PP is illustrated in Figure 36, showing clear void formation and lack of adhesion between the two phases.

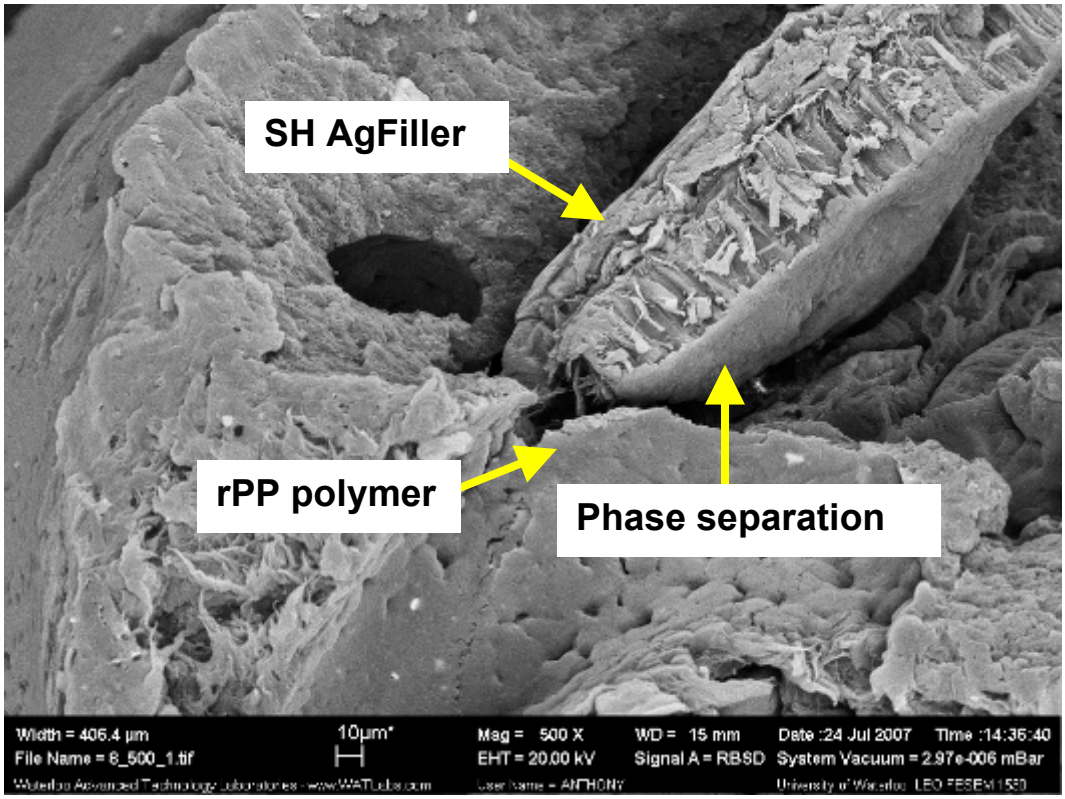

Figure 36: SEM of SH-rPP composite at AgFiller/polymer interface, filled with 40 wt% AgFiller, mag = 500x

5.1.2 THERMAL PROPERTIES

5.1.2.1 Differential Scanning Calorimetry (DSC)

DSC enthoderms of rPP showed distinct bimodal crystallization behaviour, with the primary crystallization onset temperature at 127.9°C and the primary and secondary peak crystallization temperatures at 121.7°C and 109.7°C respectively. In the study of die-drawn polypropylene by Taraiya *et al.* (1988), it was suggested that the presence of a second crystallization peak was likely due to the presence of copolymers. Since copolymers are common in injection molding applications to provide additional impact resistance (Maier, 1998), this explanation is plausible considering the source of the rPP tested was mainly injection molded food containers. In comparison, the crystallization behaviour of rPP was significantly different than that of vPP, which had only one crystallization onset at 112.6°C and peak T_c at 108.9°C.

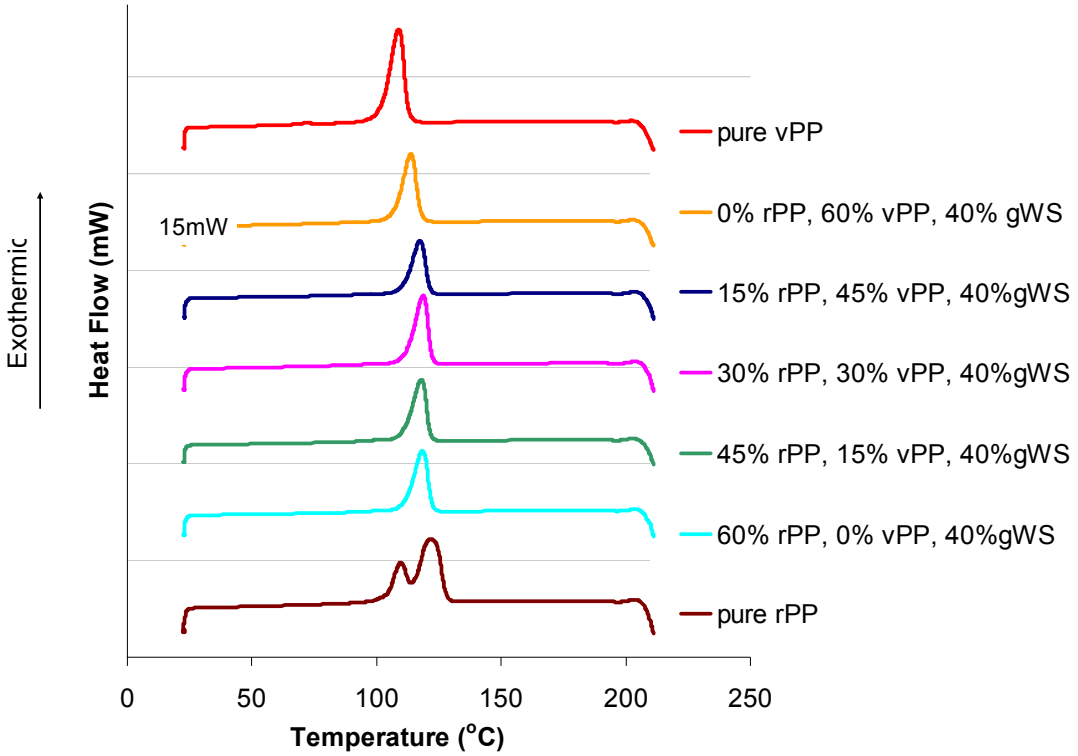

Figure 37: DSC endotherms during cooling step of experiment, for gWS-PP composite with increasing rPP content

The bimodal crystallization peaks were eliminated by the addition of AgFiller (Figure 37), and the resulting peak crystallization temperature of the composite was determined to be 118.4°C, a value in between the primary and secondary peak T_c of rPP. It was also shown in Figure 37 that, as the ratio of rPP in the composite increased, the peak crystallization temperature of the composite also increased. It was also possible to eliminate the secondary peak of rPP by mixing the polymer with vPP polymer, as shown in Figure 38.

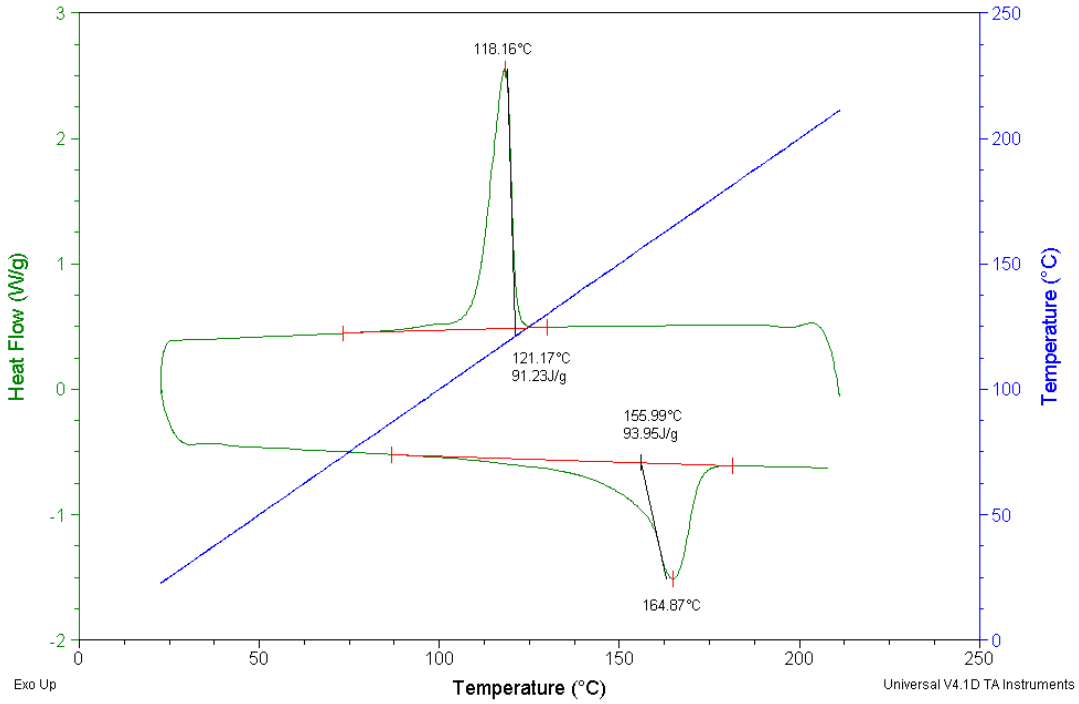

Figure 38: DSC endotherm of first cooling and second melting steps of 50:50 blend of vPP:rPP

The percent of crystallinity of AgFiller-PP composites were not greatly affected by the amount of rPP in the composition, as illustrated in Figure 39. All composites containing rPP, showed crystallinity similar to or lower than that of pure rPP, based on a typical range of ±3-5% of statistical significant difference among crystallinity values.

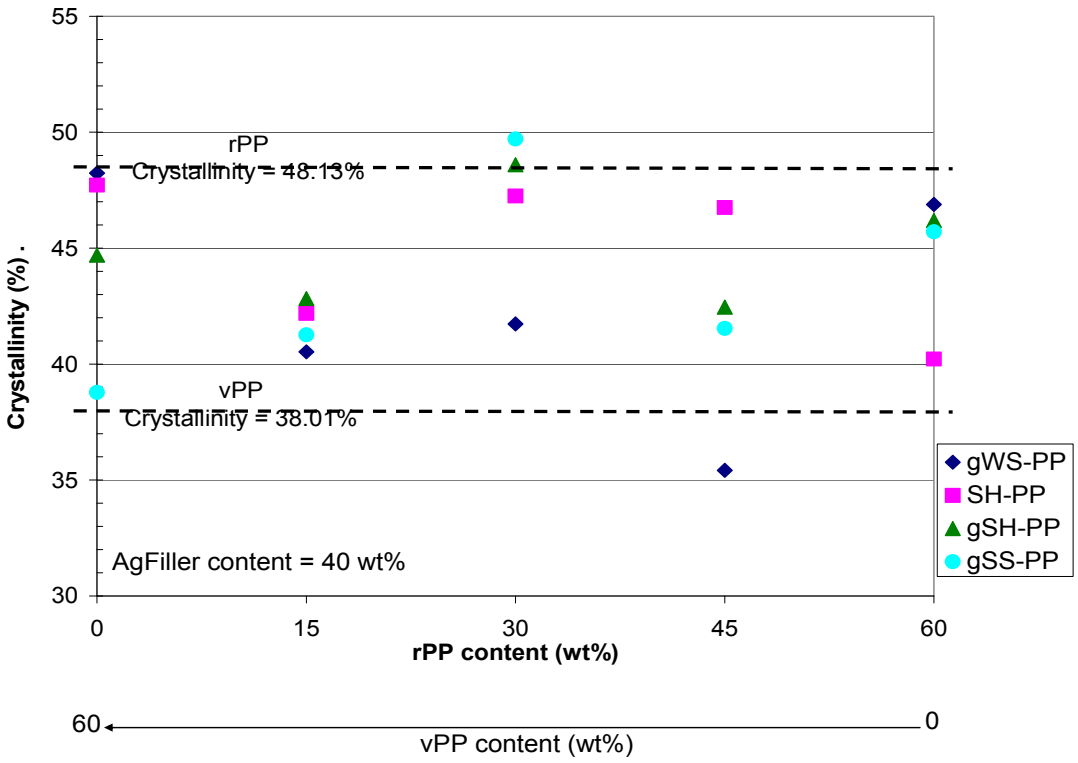

Figure 39: Crystallinity of AgFiller-PP composites at various rPP levels

5.1.2.2 X-ray Diffraction (XRD)

The X-ray diffraction patterns of gWS-PP containing rPP only, equal amounts of rPP and vPP, and vPP only, are shown in Figure 40. In the 2θ range between 10^{o} and 25^{o}, the peaks of α-form and β-form crystals were identified. The three samples showed baselines that overlapped extremely well, indicating the accuracy of the experiments. It was observed by comparing the three XRD patterns that gWS-rPP composites showed higher peak intensities for all peaks of interest than the other two composites studied.

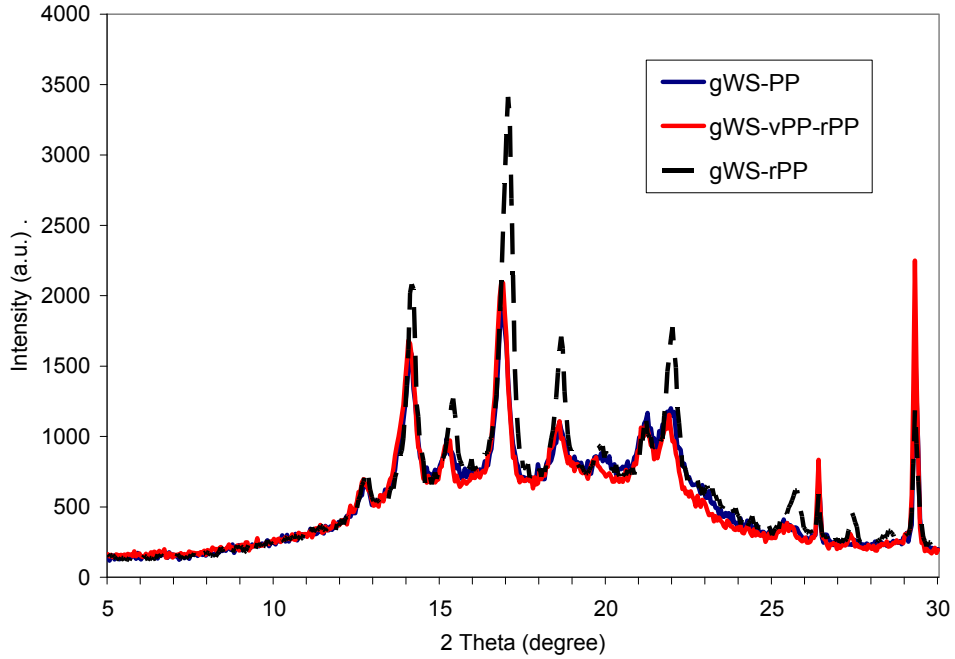

Figure 40: XRD diagrams for gWS-PP composites containing only vPP, 50:50 vPP:rPP and only rPP as polymer matrix

The fraction of β-form crystals was again calculated using equation (6) for each of the composites, and the results were summarized in Table 17. It was determined that the gWS-vPP sample had the highest β-form fraction of 17.5%, and the fraction decreased as the amount of rPP increased, to 15.0% as found in the gWS-rPP sample.

Table 17: XRD peak and K-value of gWS-PP composites containing various levels of rPP

Polymer composition	$H_{\alpha 1}$	$H_{\alpha 2}$	$H_{\alpha 3}$	H_{β}	K-value
vPP only	1610	1909	1104	984	0.175
50:50 vPP:rPP	1681	2090	1109	972	0.166
rPP only	2047	3412	1709	1269	0.150

5.1.3 CHEMICAL PROPERTIES

5.1.3.1 Fourier Transform Infra-red Spectroscopy (FTIR)

Figure 41 illustrates the comparison of ATR-FTIR spectra of SH-PP composites containing various levels of rPP in the composition. The spectra of the composites were further compared against those of pure rPP and vPP. From the figure, it was first determined that rPP displayed the same spectra as vPP, signifying that there were no differences in the surface chemical composition of the two polypropylene polymers. Secondly, similar to that previously observed in AgFiller-vPP composites, SH-PP composite yielded an ATR-FTIR spectrum identical to that of PP polymer. The change of rPP ratios did not contribute to any spectrum variations.

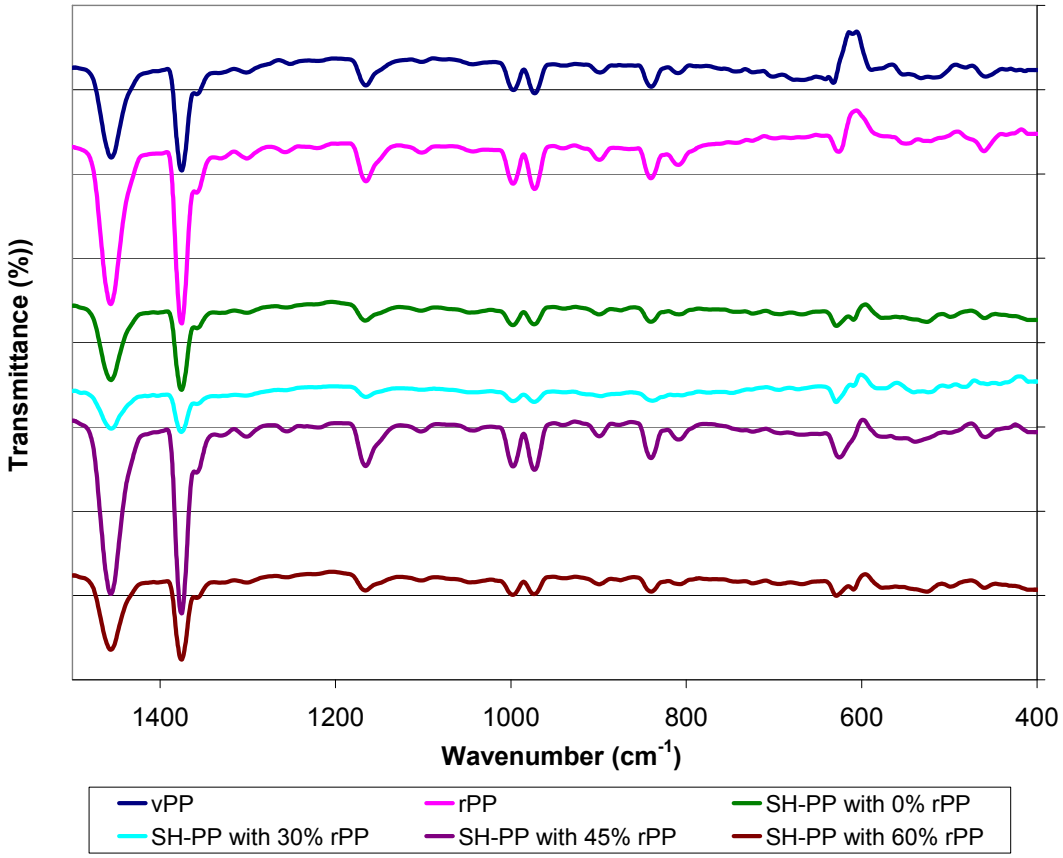

Figure 41: ATR-FTIR spectra of SH-PP composites containing rPP

5.1.4 RHEOLOGICAL PROPERTIES

5.1.4.1 Apparent Shear Viscosity

As shown in Figure 42, the apparent shear viscosity of AgFiller-PP composites was lowered by the addition of rPP in the composition. The effect of rPP on viscosity appeared to be a linear relationship. Overall, stalk filler-based composite, which included both gWS and gSS, possessed the highest viscosity for all levels of rPP present in the composite, while shell-based composite containing SH material was the least viscous. The rate of viscosity decrease to rPP content was consistently for gWS-PP, SH-PP and gSH-PP composites, while the rate of viscosity decrease was slightly greater for gSS-PP. Finally, it was shown that pre-grinding of SH had little effect on the viscosity change of the composite, regardless of rPP content.

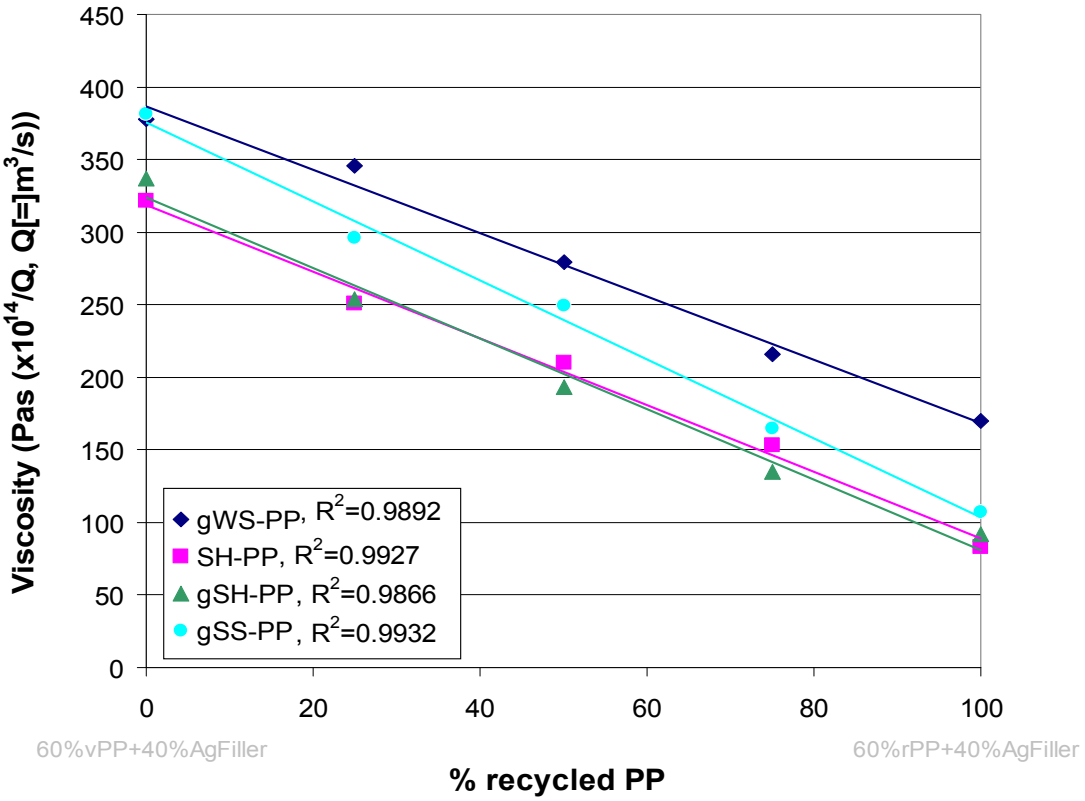

Figure 42: Relative comparison of apparent shear viscosity as rPP percentage increases in polymer matrix

5.1.4.2 Melt Flow Index (MFI)

Table 18 shows the MFI recorded for each AgFiller-PP composite of which the polymer matrix consisted of vPP only, of a 50:50 mixture of vPP and rPP, and of rPP only. The results were found to be consistent to the trends observed in Figure 42, that the composites containing higher levels of rPP were less viscous. It was also observed that as the MFI of the composite increased, the variance in the experimental data also increased. This was mainly due to the need to lower sample collection time in order to meet standard requirements, thus the experimenter's response time in cutting the samples played a more significant role in contributing to errors.

Table 18: MFI of AgFiller-PP composites with various AgFiller and polymer compositions

FILLER (40 wt%)	POLYMER (60 wt%)		
	vPP only	50:50 vPP:rPP	rPP only
gWS	0.84 ±0.13	2.84 ±0.12	9.60 ±0.70
SH	2.03 ±0.24	8.16 ±0.39	44.89 ±7.11
gSH	2.14 ±0.25	8.63 ±1.52	45.28 ±6.65
gSS	1.04 ±0.10	2.50 ±0.12	15.94 ±0.63

5.1.5 MECHANICAL PROPERTIES

5.1.5.1 Flexural Properties

Figure 43 to Figure 46 show respectively the flexural moduli of gWS-PP, SH-PP, gSH-PP and gSS-PP composites at varying levels of rPP. In contrast to the expectation that flexural modulus would decrease as rPP level increases (Jasso-Gastinel, 2007), there were no conclusive changes to flexural modulus of the composites.

Large degrees of variance were found in the samples tested. The result was overlapping of the confidence intervals of each sample, thus masking any trends to be observed. The variance is attributed to two main factors. First, the heterogeneous nature of rPP could be responsible for inconsistency among test specimens. Secondly, unavoidable defects found on the samples, such as sample shrinkage during the cooling step of compression molding, entrapped air bubbles, and the random distribution and alignment of fillers, account for other sources of experimental error.

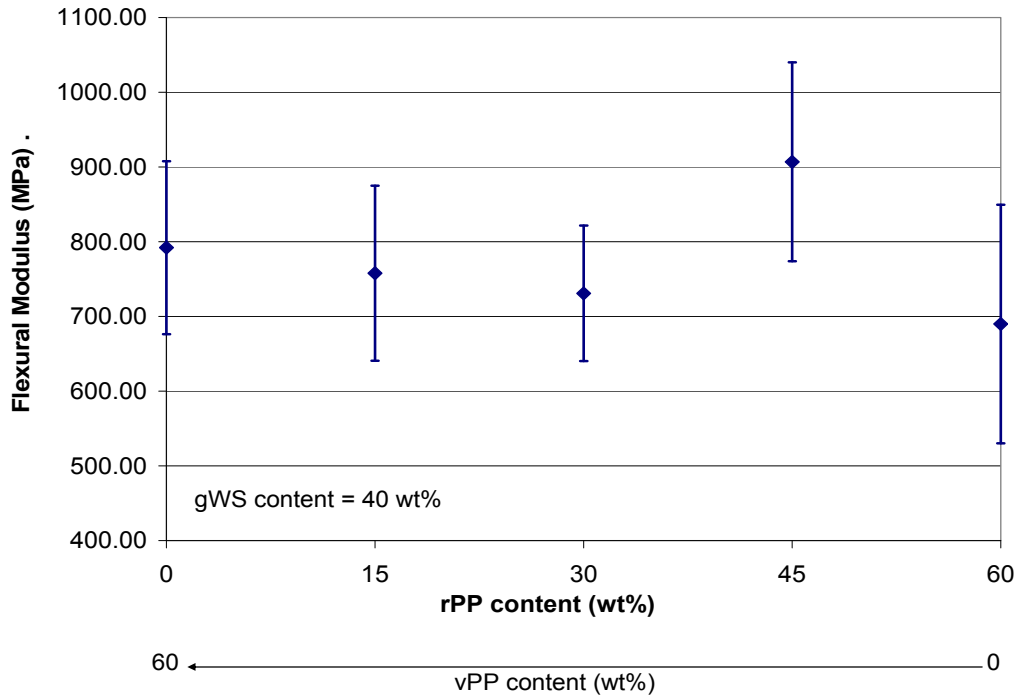

Figure 43: Flexural Modulus of gWS-PP composite at varying levels of rPP. Error bar represents 95% confidence interval

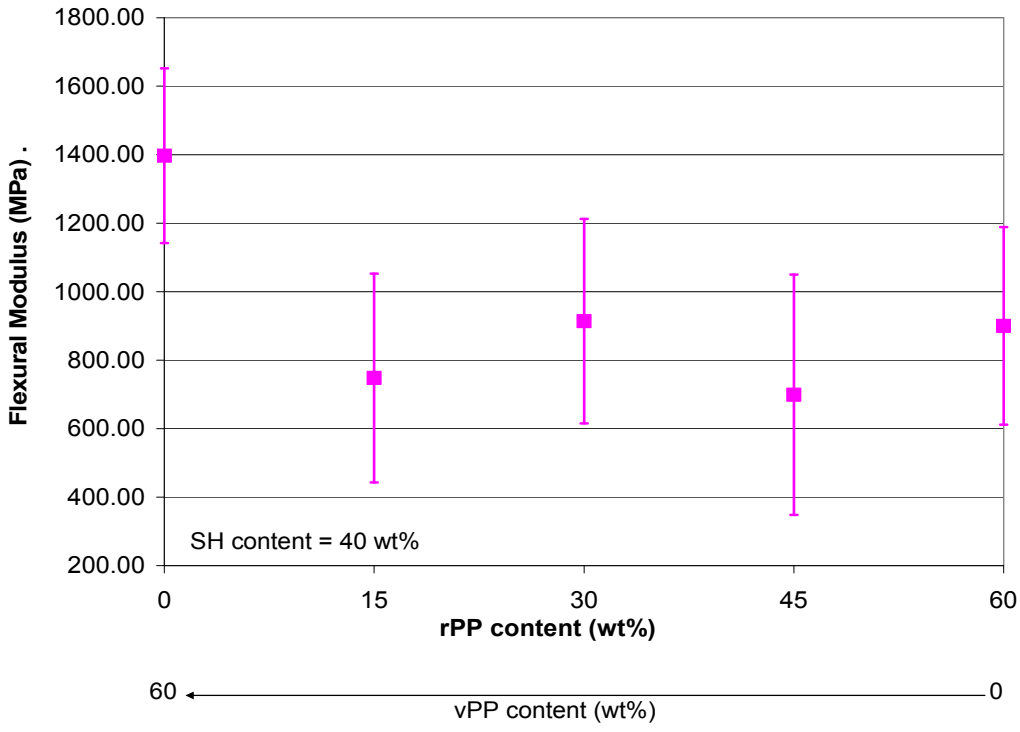

Figure 44: Flexural Modulus of SH-PP composite at varying levels of rPP. Error bar represents 95% confidence interval

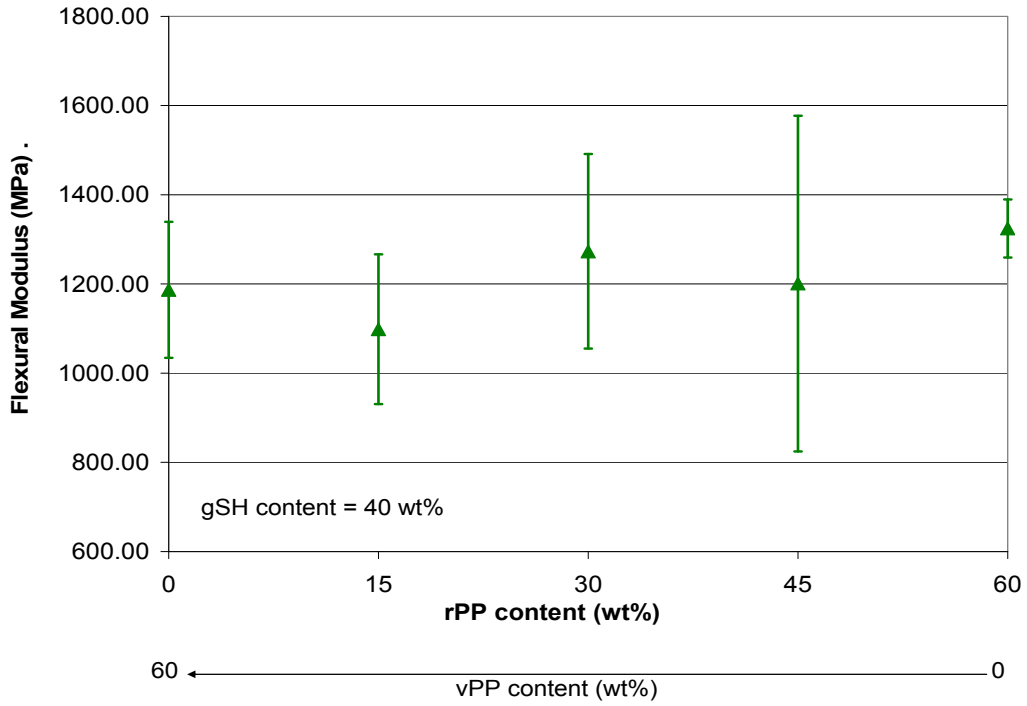

Figure 45: Flexural Modulus of gSH-PP composite at varying levels of rPP. Error bar represents 95% confidence interval

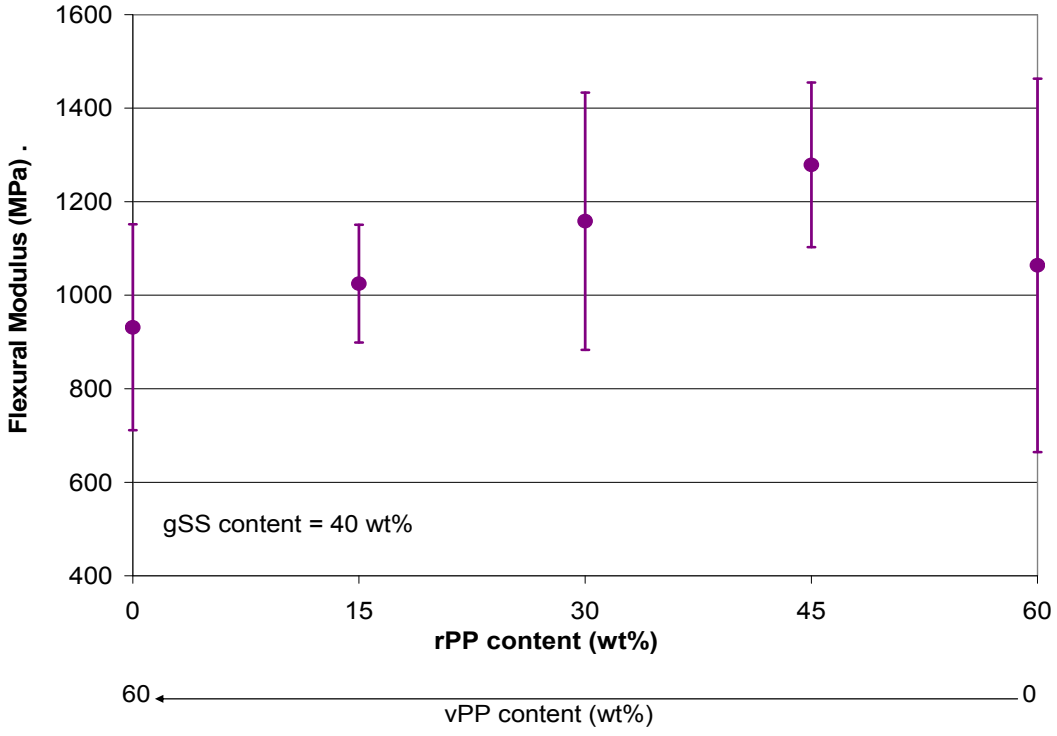

Figure 46: Flexural Modulus of gSS-PP composite at varying levels of rPP. Error bar represents 95% confidence interval

5.2 Chapter Summary

This chapter examined the role of PP polymer on the properties of AgFiller-PP composites. vPP, rPP and blends of the two formed the matrix of the composite, into which each of gWS, SH, gSH and gSS AgFillers were added.

SEM micrographs of SH-PP composites showed that rPP better encapsulated the fillers than vPP. The number and size of gaps, which signify incompatibility between polymer and filler phases, were lowered in the presence of increasing amounts of rPP. However, the use of rPP was not adequate in completely eliminating the phase separation, as shown by a close-up examination at the polymer/filler interface, and no physical or chemical bonding were found.

rPP polymer showed bimodal crystallization characteristics that were significantly different that the single-peak crystallization observed in vPP. The two peaks merged into one single peak upon mixing rPP with vPP, or by the addition of AgFillers. In terms of chemical composition, ATR-FTIR spectra revealed no difference between vPP and rPP, and the AgFiller-PP composites made of vPP, rPP or blends of the two all showed the same spectra as polypropylene, suggesting the presence of a polymer skin layer at the surface of the composites.

The viscosity of rPP was lower than that of vPP. By blending the two polypropylenes, a linear decrease in viscosity of each AgFiller-PP composite was observed as the rPP content in the composite increased. The effect of rPP on the rate of viscosity change were similar for gWS-PP, SH-PP and gSH-PP, while the viscosity decrease was more sensitive to rPP content for gSS-PP composites. rPP content had no correlation with AgFiller pregrinding regarding viscosity, as SH-PP and gSH-PP had almost identical viscosities at all rPP loading tested.

Due to higher viscosity of rPP, it was postulated that rPP had lower molecular weight than vPP and therefore AgFiller-PP composites containing higher levels of rPP would possess less strength and stiffness than those with more vPP. However, this was not observed in the results obtained from flexural testing, which suggested no statistically significant changes in the properties mainly due to the large variance present within the samples.

CHAPTER 6 ORIENTED AgFILLER-PP COMPOSITES CONTAINING WHEAT STRAW

One method to further enhance the properties of AgFiller-PP composites is by bulk orientation. During the orientation process, the entangled polymer chains straighten and align themselves to the pulling force, while the incompatibility between the polar AgFiller and non-polar polymer causes microscopic phase separation, producing pockets of empty space at the separation sites. The end result is a composite that is “twice as strong but half the weight” (Newson, 2004). In this chapter, oriented gWS-PP (o-gWSPP) composites are examined, and their properties are compared to those of oriented WPC and $CaCO_3$-PP composites. The o-WSPP samples were prepared by extrusion-orientation with the assistance of industrial sponsor Green Forest, Misouri. The composites contained 20 wt% gWS, 79 wt% vPP, and 1 wt% processing additives that include antioxidants and lubricants.

6.1 Property Characterization

6.1.1 MORPHOLOGY

An SEM micrograph of the cross-section surface along the extrusion-orientation direction of o-gWSPP composite is shown in Figure 47. Distinct strand-like morphology was observed in the polymer phase. PP fibers on the fracture surface were pulled out from the bulk, likely by shear forces during sample preparation. This is significantly different than the smooth and undefined polymer mass as seen in non-oriented AgFiller-PP composites, such as the polymer phase of SH-PP as shown in Figure 18.

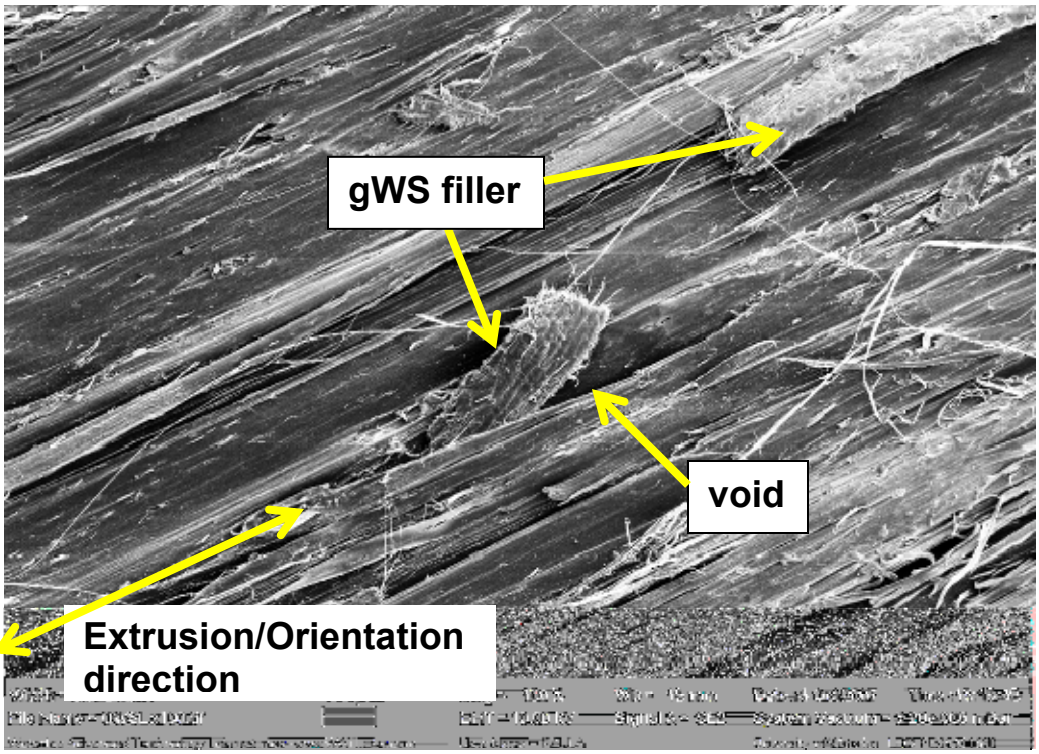

Figure 47: 100x mag oriented WS profile side surface cross section along the extrusion-orientation direction

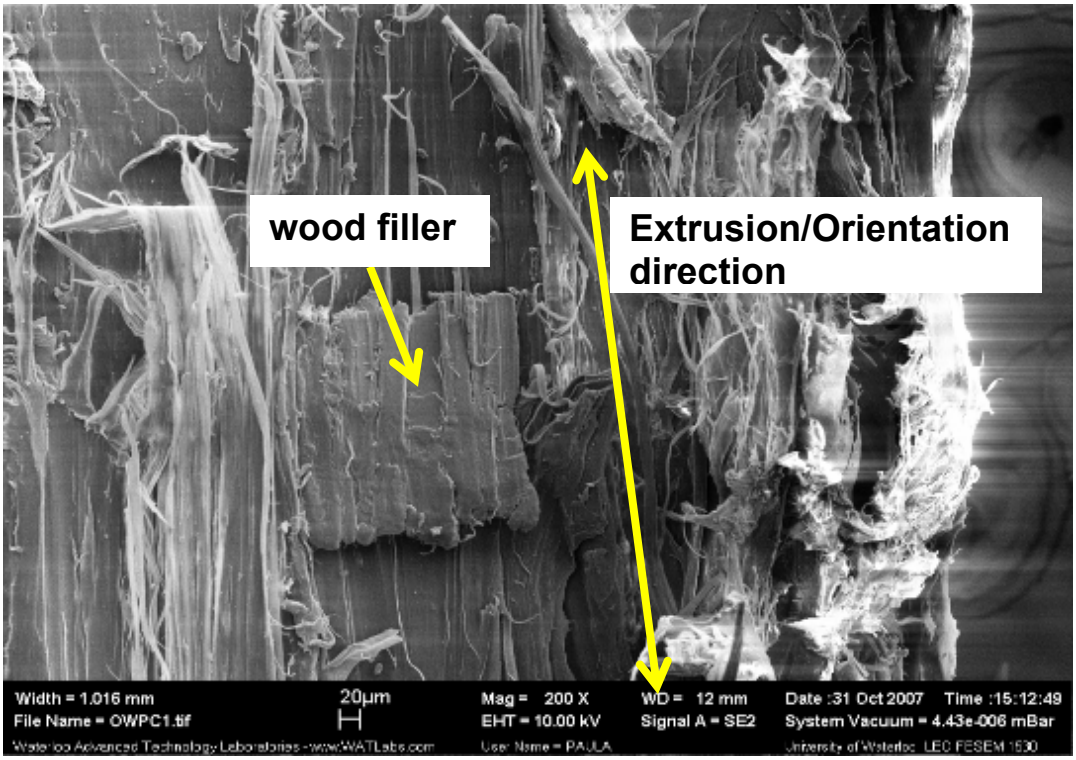

Figure 48: 200x mag oriented WPC profile side surface cross section along the extrusion-orientation direction

The morphology of o-gWSPP composite was compared to that of oriented WPC (Figure 48). Similar polymer fibrous structures and filler inclusions were observed in both composites.

Figure 48 also shows gWS fibers that were embedded lengthwise along the extrusion-orientation direction, similar to that observed in non-oriented AgFiller-PP composites. There was little adhesion between the filler and the polymer. As a result voids were formed and were observed in Figure 48 as darkened shades. According to Newson and Maine (2004), these voids caused weight reduction effects in the resulted composite, which was not possible to achieve by orienting pure PP.

There appeared to be a good degree of polymer realignment due to orientation. This was proven by attempting, and failing, to freeze-break a sample of the o-gWSPP composite orthogonally to the extrusion-orientation direction.

The gWS and wood fibers were extracted from the oriented composites to study the effects and damage incurred during processing. Figure 49 and Figure 50 show the SEM micrograph of gWS and wood fibers extracted from their respective oriented composites. It was shown that the extent of surface fiber damage was less severe than that observed in the lab scale samples. By comparison, gWS remained more intact, and had formed fewer fines, than wood fibers.

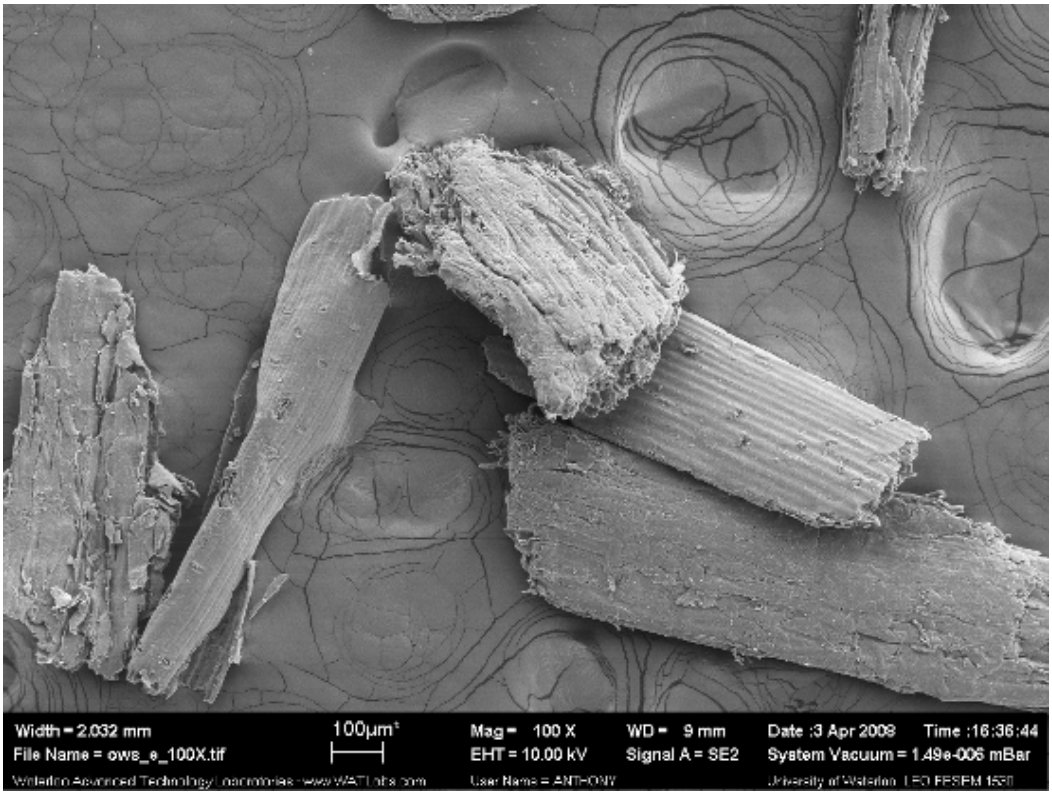

Figure 49: SEM of wheat straw filler extracted from oriented gWS-PP, mag = 100x

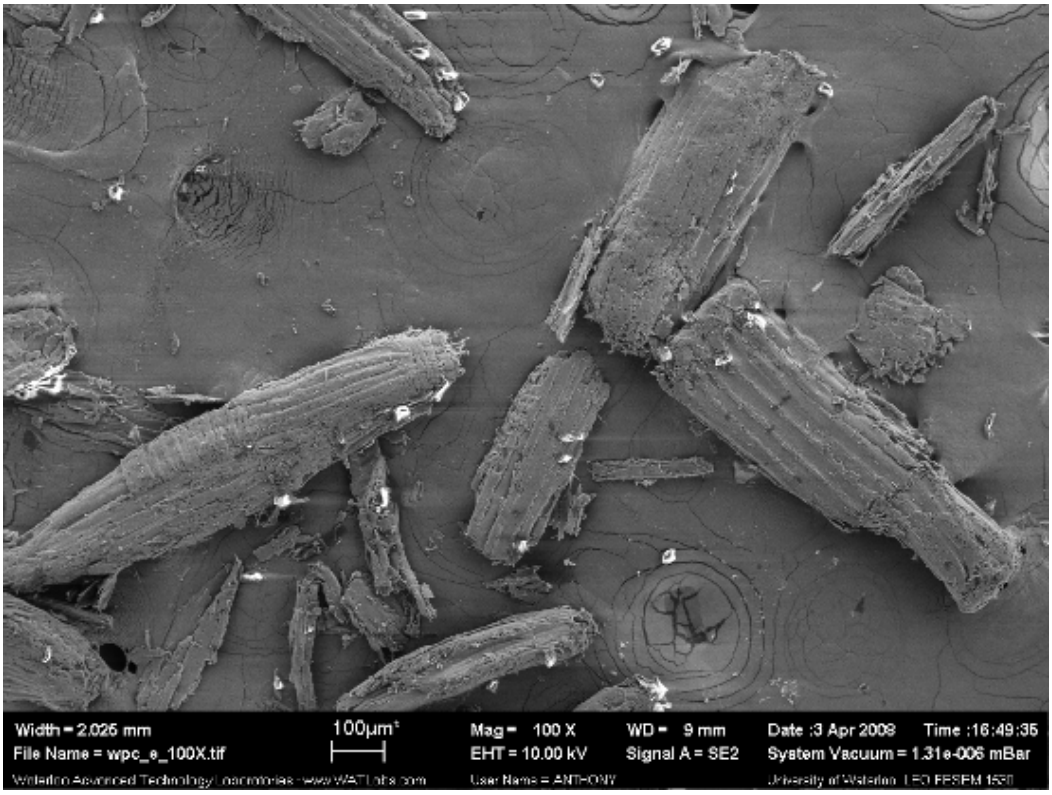

Figure 50: SEM of wood fiber extracted from oriented WPC, mag = 100x

A closer look at the extracted gWS (Figure 51) and wood fibers (Figure 52) confirmed that gWS had suffered less damage than the wood fiber. The hollow tube-like structures of gWS remained clearly identifiable, showing little effect from crushing and deformation. In addition, there were less fines or sheared fibers found on gWS than found on wood fiber. It also appeared that using the same extraction technique, more residual polymer remained on the wood fibers than on gWS.

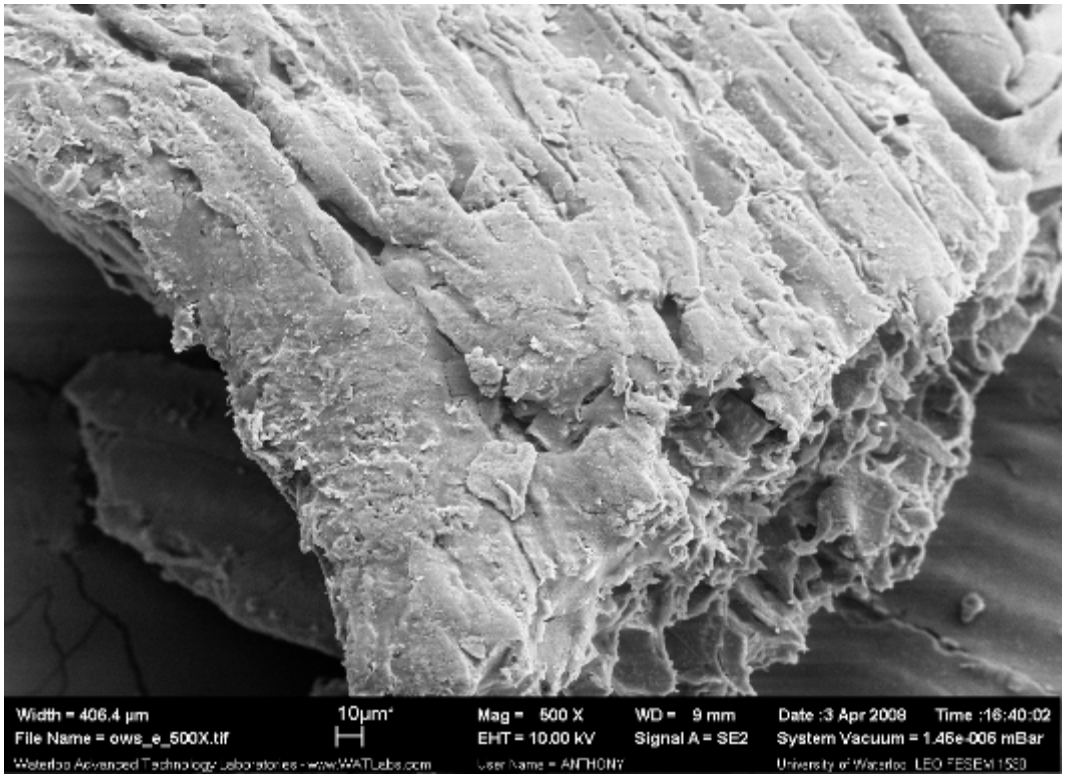

Figure 51: Close up SEM of wheat straw filler extracted from oriented ES-PP, mag = 500x

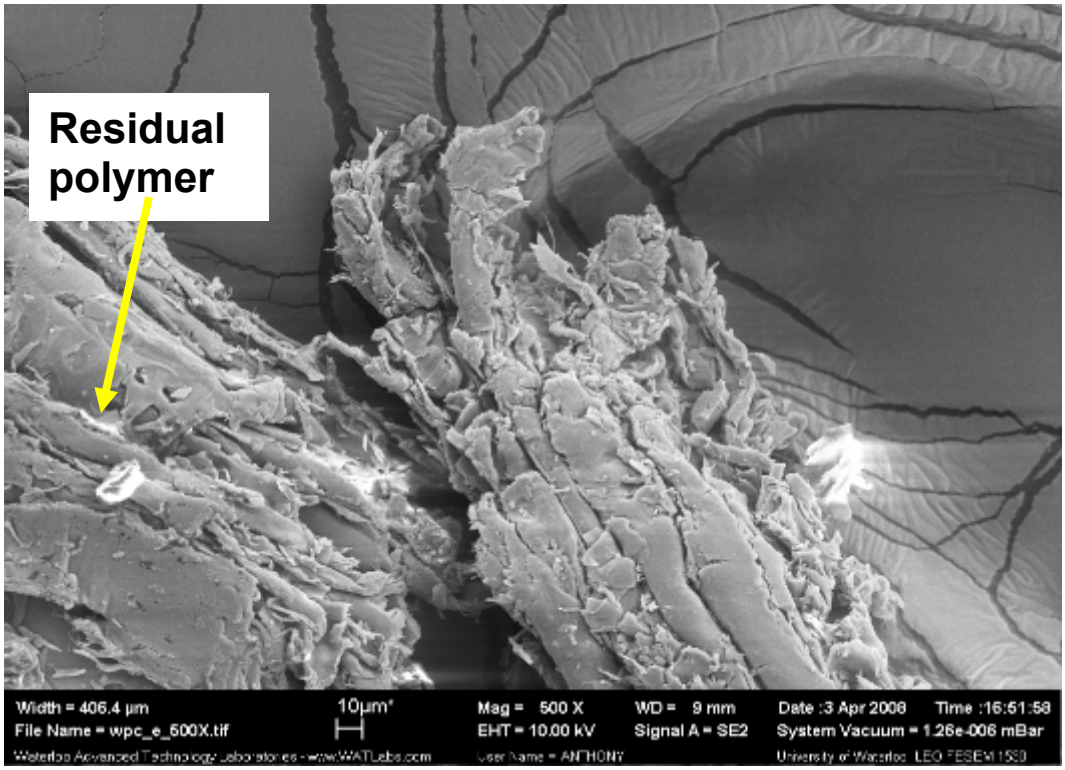

Figure 52: Close up SEM of wood fiber extracted from oriented WPC, mag = 500x

6.1.2 DENSITY

Experimental results of the changes in densities of gWS-PP and pure PP before and after orientation are presented in Table 19, with the exception that literature value was shown for non-oriented pure PP (A. Schulman[2], 2007). The tabulated data show that orientation caused a reduction of composite density in gWS-PP composites by 20% but imposed no effects on pure PP. Previous work on studying oriented WPC by Newson and Maine (2004) presented similar findings and explained this phenomenon they observed as a result of microscopic void formation originating at a nucleus provided by the wood fiber bundles. Extending their reasoning to AgFiller-PP composites led to a conclusion that the low compatibility between polar gWS filler and non-polar PP polymer resulted in the same type of void formation. Pulling forces applied to the composite during die-drawing orientation processes triggered the separation of the two phases, which if compressive forces, such as those encountered in ram-extrusion processes, were applied, no density reduction would result (Newson, 2002).

Table 19: Density change of gWS-PP composite due to orientation pure PP

Material	# samples tested	Density	
		Average	Standard Deviation
Non-oriented gWS-PP composite, 20% filled	4	0.956	0.0039
Oriented gWS-PP composite, 20% filled	4	0.759	0.0059
Non-oriented pure PP (literature data; A. Schulman[2], 2007)	n/a	0.905	n/a
Oriented pure PP	4	0.909	0.0046

Table 20 compared the densities of gWS-PP, WPC and PP filled with calcium carbonate ($CaCO_3$-PP) that had been oriented. Because the o-WPC sample available for testing contained higher levels of filler than o-gWSPP, literature data (Newson, 2004) was also included in the table for an o-WPC composite with equal amount of filler as o-gWSPP. It was determined that o-gWSPP outperformed o-$CaCO_3$-PP in weight reduction, and performed similarly, although slightly less effectively, to o-WPC. The accuracy of the experiments was found to be quite high, as shown by the low standard deviation resulted from testing four random specimens. The experimental data of o-$CaCO_3$-PP at 20% fill level and o-WPC at 30% fill level were also found to be in accordance with literature (Newson, 2004).

Table 20: Comparison of densities of oriented gWS-PP and other filled composites

Material (oriented)	# samples tested	Density	
		Average	Standard Deviation
gWS-PP profile 20% filled	4	0.759	0.0059
$CaCO_3$-PP 20% filled	4	1.052	0.0035
WPC profile 30% filled	4	0.509	0.0060
WPC composite 20% filled (literature data; (Newson, 2004)	n/a	0.680	n/a

6.1.3 MELTING & CRYSTALLINITY

6.1.3.1 Differential Scanning Calorimetry (DSC)

The thermal properties of an o-gWSPP billet were studied at various locations on the surface across the extrusion-orientation direction (Figure 53). It was postulated that due to the thickness of the sample, crystallization could have occurred differently at each location due to heat transfer constraints.

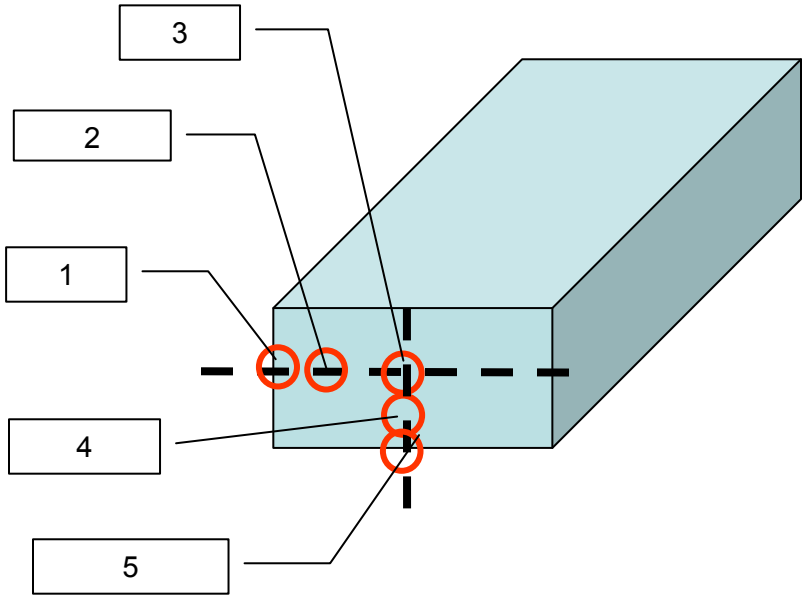

Figure 53: Location for sample collection on oWS-PP profile for DSC testing

Table 21 shows the melting and crystallization temperatures, both at onset and peak of the phase change, as well as the calculated percentage of crystallinity of o-gWSPP at the sample locations as specified in Figure 53. No change was observed in crystallization or melting temperatures of the composite as sampling location varied from the edge towards the center of the bar, both horizontally and vertically. On the other hand, the crystallinity of the composite was found to be marginally higher in the center than along the wall.

Table 21: Melting and crystallization temperatures, as well as crystallinity at various locations on the o-WSPP composite cross-sectional surface

Sampling Position	T_m onset	T_m peak	T_c onset	T_c peak	Crystallinity
1	153.3 ± 0.5	164.6 ± 1.1	116.6 ± 0.2	111.6 ± 0.6	52 ± 2
2	153.7 ± 0.4	163.7 ± 0.4	116.3 ± 0.7	112.0 ± 0.4	54 ± 2
3	153.2 ± 0.4	164.4 ± 0.8	116.8 ± 0.1	111.5 ± 0.7	54 ± 1
4	153.4 ± 0.4	164.3 ± 0.5	117.0 ± 0.1	112.1 ± 0.4	53 ± 2
5	153.7 ± 0.4	163.8 ± 0.5	117.2 ± 0.2	112.1 ± 0.2	53 ± 1

6.1.3.2 X-ray Diffraction (XRD)

Figure 54 shows the XRD diagrams of gWS-PP composite billet before entering the orientation process. This non-oriented sample (preO-WSPP) showed slightly different crystalline structures in the center and the surface skin. The intensities of peaks assigned to α (111) and α (131) were found to vary at the two locations. An additional peak at 2θ = 16.4° was found at the surface of preO-WSPP, which was absent in the center of the composite. On the other hand, γ phase peak, typically found at 2θ = 20.05° (Xu, 2003), was observed in the sample's center but not on the surface.

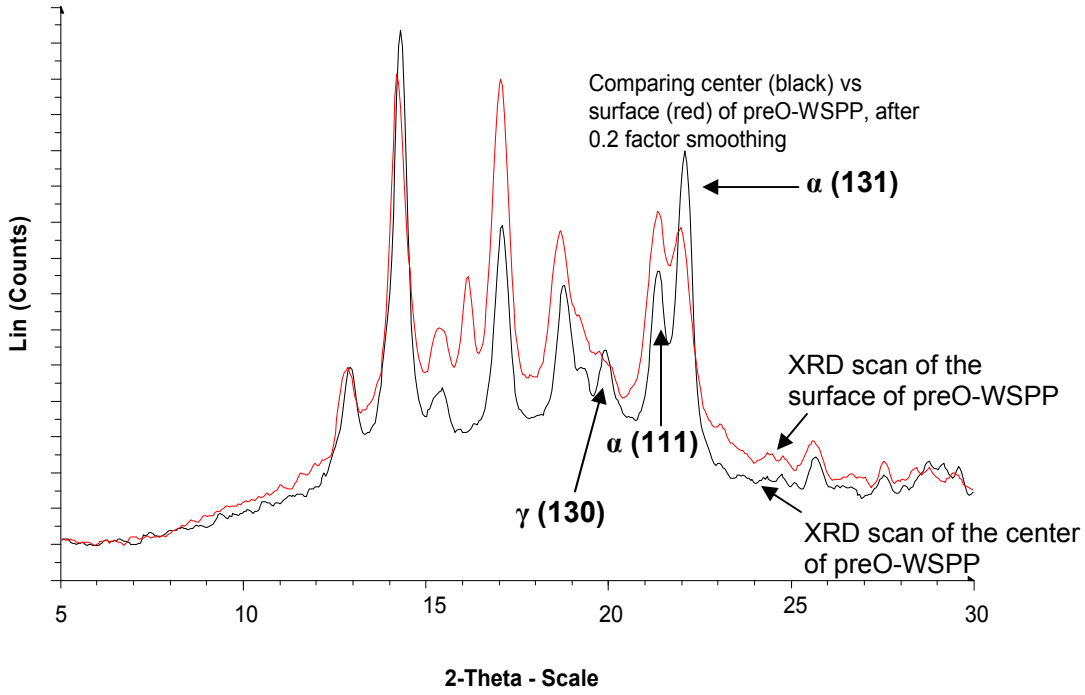

Figure 54: XRD pattern of the center and surface sections of WS-PP composite billet before orientation

After orientation, the XRD patterns of the o-gWSPP composite changed to those as shown in Figure 55. o-gWSPP at the surface showed an XRD pattern of higher intensity than that in the center of the oriented composite. Although lower in intensity, the peaks representing α, β and γ phases did not vary greatly in the center of the sample. By orienting the sample, however, the peak at 16.4^{o} found on the surface of the composite disappeared. Based on the comparison of β-fraction in terms of K-values (Table 22), there was little change observed from the surface (K = 0.130) to the center (K = 0.139).

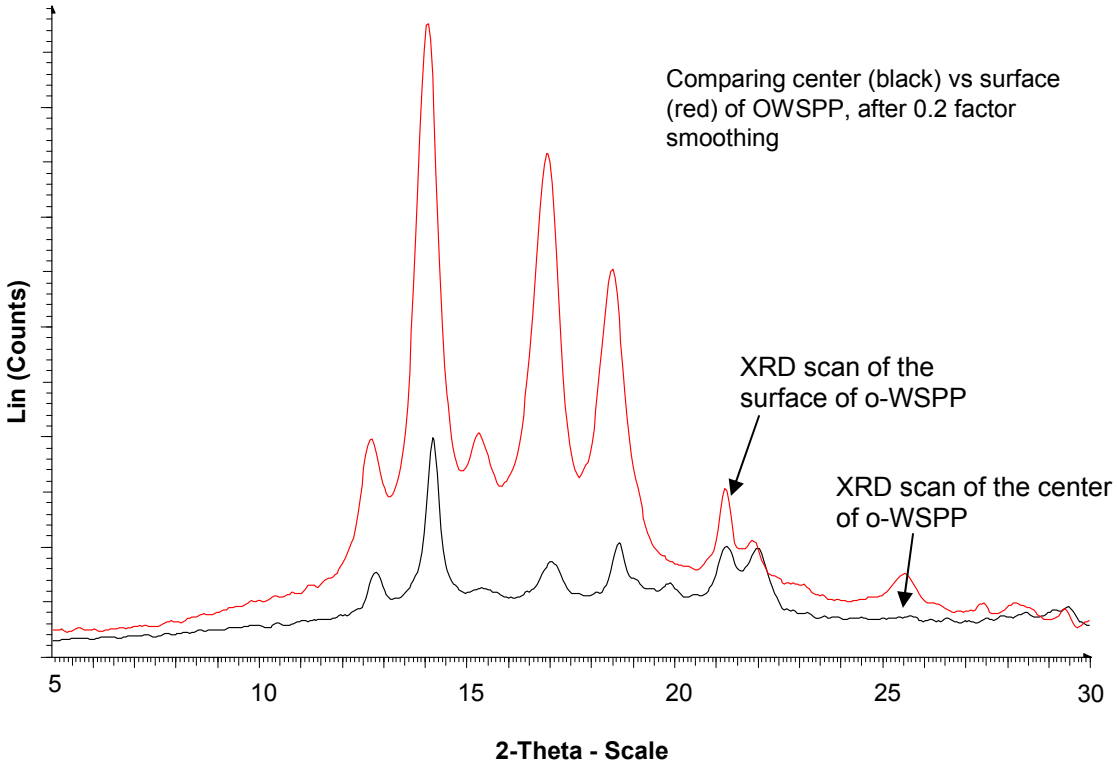

Figure 55: XRD pattern of the center and surface sections of oriented WS-PP composite

Table 22: β-fraction of gWS-PP composites at the center and surface of sample, before and after orientation

	α_1 (110)	α_2 (040)	α_3 (130)	β (300)	K-value
PreO-WSPP-center	1603	1005	827	550	0.138
o-gWSPP-center	2093	892	1082	656	0.139
PreO-WSPP-surface	1420	1428	999	756	0.164
o-gWSPP-surface	5815	4597	3552	2090	0.130

Further determined from data presented in Table 22, was that by orientation, the surface of the gWS-PP composite experienced a sharp decrease in β-fraction at the surface of the surface, while there was practically no change in K-value in the center of the composite. This intriguing result is explained by possible β-relaxation, such as that observed in drawn isotactic polypropylene in the work by Jawad and Alhaj-Mohammad (1994). In their work, it was determined that the intensity of β-peaks would decrease as draw ratio increased, and the peak would nearly disappear as the draw ratio approaches 16. An increase in draw ratio is usually achieved by increasing the speed of drawing, which means higher shear at the surface due to greater velocity gradient across the profile. This can be inferred to the o-gWSPP composite, where the surface of the sample would experience greater shear than the bulk at the center, and therefore would result in greater reduction in β phase than the bulk.

Crystal formation varies with the degree of orientation. Bulk orientation involves stretching in three dimensions that is found to occur in processes like die drawing. In 1988, Taraiya *et al.* determined that die drawn rods of draw ratio up to 20 contained disordered α modification. In addition, die drawn billets machined from isotropic PP rods was found to suffer a crystallinity decrease from 62.2% to 51.4% as draw ratio increased from isotropic to 10, during which β relaxation occured as amorphous relaxation (Jawad, 1994). On the other hand, cast PP films, or biaxially oriented PP (BOPP) films, are oriented in two dimensions, namely in the transverse and longitudinal directions. Yin *et al.* (2004) determined that γ crystals were present in cast PP films, and that stretching had no effects in the formation of these crystals. It was also determined that the formation of γ crystals deterred the transformation of the smectic phase into α crystals. PP fibers are considered to be oriented in a singular dimension, due to its infinitely large aspect ratio obtained from the fibers' very long (high length) but thin (low diameter) geometries. Jinan *et al.* (1989) observed the presence of monoclinic (α phase) and hexagonal (β phase) crystals with various magnitudes of orientation in melt spun PP fibers. In all cases, crystallization is also dependent on factors such as crystallization temperature and time, orientation or drawing speed, as well as the type and molecular weight of the polypropylene studied.

6.1.4 MECHANICAL PROPERTIES

As summarized in Table 23, the flexural modulus of oriented gWS-PP composite billets at 95% confidence was determined to be 2722±106 MPa. In comparison, the flexural modulus of oriented WPC containing equal amount of filler (20 wt%) was 2310 MPa (Newson, 2004). This translates to an 18% increase when gWS was used as filler instead of wood fiber.

Table 23: Flexural modulus and yield stress of oriented gWS-PP composite

	Flexural Modulus (MPa)	Max. Yield (MPa)	0.2% Offset Yield (MPa)
Average	2733	53.95	31.16
Standard Deviation	132	2.32	2.18
95% Confidence	106	1.86	1.74

Meanwhile, the maximum flexural strength and yield stress at 0.2% offset of the composite were 53.95±1.85 MPa and 31.15±1.74 MPa respectively, at 95% confidence. In comparison, Newson and Maine (2002) recorded the maximum flexural strength of oriented WPC to be 82.74 MPa. However, it was noted that the length to depth ratio of the samples tested by Newson and Maine was 8:1, lower than the 16:1 suggested by ASTM standard. The strain rate used for testing (1.2/s) was also much higher than ASTM standard (0.01/s). According to Karmaker and Prasad (2000), decreasing length to depth ratio from 16 to 8 creates interlamiar shear stress, resulting in decreases in flexural strength of approximately 14%, while the flexural modulus of samples with L:D of 8 was found to be approximately 7% less than that of samples with L:D of 16 (Crawford, 1984). Crawford and Yigsaw (1984) further determined that by lowering L:D from 16 to 8, the experimental errors were increased from 1.4% to 6%. On the other hand, increasing straining rate causes the resultant yield strength to rise. To validate this claim, retesting was done on oWS-PP samples with 8:1 L:D ratio at a straining rate of 1.2/min, since a strain rate of 1.2/s was so high, the calculated crosshead speed was beyond the capability of the equipment. Retest results showed that the maximum yield strength increased to 71.43 MPa from the originally recorded 54 MPa, and became more comparable to the literature value. It is postulated that higher values in yield strength might be obtained if the testing speed was further increased.

Another important factor that determines the mechanical properties of oriented composites is the draw ratio used. By increasing the draw ratio in a die drawing process, the modulus in the drawing direction would increase proportionally in the draw direction (Chaffey, 1997). The o-gWSPP composites tested had a draw ratio of approximately 5, while the work by Newson and Maine (2004) involved o-WPC with a draw ratio of 12. Therefore, it is suggested that by raising the draw ratio from 5 to 12, the mechanical properties of o-gWSPP composites may be further enhanced to surpass those of o-WPC.

6.2 Chapter Summary

This chapter studied the effect of bulk orientation on the properties of WS-PP composites containing 20 wt% gWS filler and 80% PP polymer. Prototype samples were manufactured on an industrial scale and the properties o-gWSPP were compared to those of o-WPC.

SEM micrographs showed that the orientation process generated distinct fibers in the polymer phase, and fillers were embedded in the polymer with a lengthwise alignment. Voids caused by filler-polymer incompatibility were observed. There was no difference in the morphology between o-gWSPP and o-WPC, although extracted fibers showed that gWS fillers better withstood the impacts of processing, and suffered less damages compared to wood fiber.

Significant density decrease was found in o-gWSPP, although to a lesser extent than o-WPC. DSC and XRD experiments showed differentials in crystallinity and crystal types across the composite's cross-sectional profile from the surface into the bulk of the sample. The crystallinity was higher in the center of the composite, where the β-phase fraction remained constant before and after orientation. On the other hand, β-relaxation at the surface of the composite caused a decrease in β-fraction during orientation.

The flexural modulus of o-gWSPP was marginally higher than that of o-WPC, while the maximum yield strength was found to be inferior. However, the differences in these two properties between o-gWSPP and o-WPC observed might not be true indicators as it was noted that there were discrepancies in the test procedures for o-gWSPP and o-WPC.

No major changes were made during industrial trials to the proprietary running conditions for manufacturing oriented WPC composites for producing o-gWSPP profiles by extrusion-orientation. This indicated "Proof of Concept" that the same process can be used to make both o-gWSPP and o-WPC composites, thus affirming the feasibility of the commercialization of oriented AgFiller-PP composites.

CHAPTER 7 CONCLUSIONS & RECOMMENDATIONS

7.1 Conclusions

Literature documentation on lignocellulosic filler-thermoplastic composite research was reviewed and the features of several agricultural fillers (AgFiller), as well as different types of polypropylenes (PP) were surveyed. Experiments were performed to prepare AgFiller-PP composites of various compositions and their properties, including morphology, thermal, physical, chemical and mechanical properties, were examined. Oriented composites made of wheat straw and PP were fabricated and their properties were studied and compared against oriented wood plastic composites.

The conclusions drawn based on the aforementioned research are as follows:

- Agricultural by-products like wheat straw, soy stems and soy hulls are excellent choices as fillers for producing natural fiber-thermoplastic composites, due to the materials' local abundance in Ontario and its low cost;

- The type of AgFiller, the type and quality of PP are of great importance in determining the end properties of non-oriented composites;

- Stem type AgFillers, such as wheat straw and soy stem, have length-wise fiber alignment and provide longitudinal reinforcement to non-oriented composites, while shell type AgFillers, such as soy hull, have depth-wise fiber orientation and are less effective as reinforcements;

- Soy hull AgFillers have the lowest thermal stability, and care must be taken when determining processing temperatures for the composites to avoid undesired degradation;

- Recycled PP has bimodal crystallization peaks, which can be converted into unimodal crystallization by mixing with virgin PP and by adding AgFillers;

- The addition of AgFillers increases the crystallization temperature, but has no effect on the level of crystallinity, of the polymeric phase in non-oriented composites;

- Viscosity of the composite increases with the addition of AgFillers, and decreases with the addition of recycled PP;

- In non-oriented composites, the yield strength decreases, while flexural modulus increases, with the addition of AgFillers, while no changes of statistical significance are observed in the properties with the addition of recycled PP;

- Phase separation occurs due to polarity incompatibility between AgFiller and polymer, which causes a skin polymeric layer to form on the surface on the composites, and generates a reduction in density when the composites undergo the orientation process;

- Crystallinity and crystal types change from the surface into the bulk across the composite's cross-sectional profile, with the center of the composite showing highest crystallinity and regularity in the amount of β-phase present;

- Mechanical properties and processibility of oriented WS-PP composites are comparable to those of oriented wood fiber-PP composites;

- Results of this work demonstrate feasibility of the use of AgFillers in making PP composites commercially, as supported by successful industrial scale trials for material processing and fabrication.

This work gave contribution to the scientific research in the field of biocomposites, and provided added values to agricultural byproducts, such as wheat straw and soy residues, when used as AgFiller. To demonstrate the feasibility for the commercialization of AgFiller-PP composites, two prototype chairs were fabricated using oriented WS-PP composites as the seating material (Figure 56). The chairs, together with a display shelf with samples and information, were placed on public display in the atrium of the Ontario Ministry of Agriculture, Food, and Rural Affairs (OMAFRA), located in Guelph Ontario, in December 2007 (Figure 57). The display information can be found in Appendix E.

Figure 56: Prototype chair using oriented WS-PP composite as seating material

Figure 57: OMAFRA public display of research on AgFiller-PP composites

7.2 Recommendations & Proposed Future Work

There is great potential for thermoplastic composites produced with agricultural fillers to replace existing commercial materials that are less environmentally friendly, and to create new markets in novel applications where thermoplastics failed to penetrate in the past due to lack of reinforcements. Research and understanding of the components which these composites are comprised of are essential for developing the proper composite specialized for its application.

In the work presented for this thesis, all AgFillers have received no chemical treatments to modify or enhance the material, and no additives have been used. However, a review of literature suggested that certain chemical modifications and use of additives can bring added benefits to the filler, while possibly creating other useful byproducts at the same time. One aspect of specific interest would be to tackle the issue regarding the low thermal stability of AgFillers, especially as observed in soy hulls. Improving the thermal stability of AgFillers would open new opportunities for the use of these materials in polymeric systems that require higher temperatures for processing, such as in poly vinyl chloride (PVC) and polyamides (Nylons).

It would be very useful to study the inclusion of other ingredients that are almost always present in the recipe for composites, such as colorants. Additionally, in the automotive industry, special aspects such as the paintability and weathering resistance of the material are often as important as the material's strength. Therefore, it may be of interest to investigate the likelihood of AgFiller-PP composites in meeting these special requirements.

Due to time constraints, it was not impossible to study in this work all properties that are of interest to this field of research. It would be of great interest to investigate the effects of AgFillers, polymer and orientation on other properties such as the impact strength of the composites produced. Literature has suggested that most fillers create concentrated stress points and therefore would lower impact resistance, whereas by orienting the polymer impact resistance would increase due to the specific alignment of the polymer chains. To study the interactions, and to find the optimal compromise, between these contributing factors would be a fascinating subject for research.

In this thesis, only one level of AgFiller (40 wt%) was studied because the focus was set at investigating the type not the loading of the fillers. To properly understand the contribution of each AgFiller to the properties of the composites, materials containing various levels of filler loading may be examined.

Finally, the level of our understanding of the bulk orientation process can be described as only a tip of the iceberg. There are still many details unknown regarding the kinetics and thermodynamics of the process. Further research should be conducted to increase our understanding the effects of orientation imposed on the composites. A good starting point would be to rescale the operation to a more friendly level, such as into a laboratory or pilot plant scale, to reduce lag time between preparation and execution due to logistics and scheduling issues.

REFERENCES

Albano C., Papa J., Ichazo M., Gonzalez J. and Ustariz C. "Characteristic of non-isothermal crystallization of polypropylene with and without talc". **Proceedings from POLYCHAR World Forum on Advanced Materials.** 11th. Denton TX, (2004).

Alemdar A. and Sain M. "Isolation and characterization of nanofibers from agricultural residues – wheat straw and soy hulls". **Bioresource Technology**. 99, 1664-1671, (2008).

A. Schulman Inc[1]. Personal communication, (2007).

A. Schulman Inc.[2] Technical data sheet for A.Schulman PP 2407. Retrieved from http://prospector.ides.com/datasheet.aspx?E=70966, (2007).

Ashraf H.L. and Lee H. "Effects of Soy Hull Flour on Soy Proteins Emulsions" **Journal of Food Science.** 53 (6)1766-1768, (1988).

Borda J., Teslery B. and Zsuga M. "Biologically Degradable Fiber-Reinforced Urethane Composites from Wheat Straw". ***Polymer Composites.*** 20(4), 511, (1999).

CFSAN/Office of Food Additive Safety. *Use of Recycled Plastics in Food Packaging: Chemistry Considerations*. Retrieved 2007 from http://www.cfsan.fda.gov/~dms/opa2cg3b.html, (2006).

Chaffey C.E., Taraiya A.K. and Ward I.M. "Orientation in Polypropylene Sheets Produced by Die-Drawing and Rolling". **Polymer Engineering & Science.** 37(11), 1774-1784, (1997).

Chen X., Guo Q and Mi Y. "Bamboo Fiber-Reinforced Polypropylene Composites: A Study of the Mechanical Properties". **Journal of Applied Polymer Science.** 69, 1891-1899, (1998).

Coates J. "Interpretation of Infrared Spectra, A Practical Approach". **Encyclopedia of Analytical Chemistry**. pp.10815-10837. John Wiley & Sons Ltd, Chichester, (2000).

Crawford R.J. and Yigsaw Y. "A study of the effect of test variables on the flexural modulus of plastics". **Journal of Materials Science Letters.** 3, 171-176, (1984).

Crespo J.E., Sanchez L., Parres F. and Lopez J. "Mechanical and Morphological Characterization of PVC Plastisol Composites with Almond Husk Fillers". **Polymer Composites.** 71-77, (2007).

Csoka L., Lorincz A. and Winkler A. "Sonochemically Modified Wheat Straw for Pulp and Papermaking to Increase its Economical Performance and Reduce Environmental Issues". **BioResouces** 3(1), 91-97, (2008).

Digabel F., Boquillon N., Dole P., Monties B. and Averous L. "Properties of Thermoplastic Composites Based on Wheat-Straw Lignocellulosic Fillers". **Journal of Applied Polymer. Science.** 93, 428-436 (2004).

Everarch Inc. “Products”. Retrieved 2008 from http://www.everarchbridge.com/, (2008).

Eviron Biocomposites Manufacturing LLC. “Products of Environ Biocomposites”. Retrieved 2008 from http://www.environbiocomposites.com/index.php, (2008).

Gates P. Image of “transverse section of soybean stem, stained with two fluorochromes to show cellulose (blue) and lignin (yellow)”. **Department of Botany, University of Durham**, UK. Retrieved 2007 from http://www.nikonsmallworld.com/gallery.php?grouping=year&year=1985&imagepos=8, (1985).

Gatos K.G., Minogianni C. and Galiotis C. “Quantifying crystalline fraction within polymer spherulites”. **Macromolecules**, 40, 786-789, (2007).

Golbabaie M. Masters Candidate, **Department of Plant Agriculture, University of Guelph**, Canada. Personal communication, (2007).

Gradys A., Sajkiewicz P., Minakov A.A., Adamovsky S., Schick C., Hashimoto T. and Saijo K. “Crystallization of Polypropylene at various cooling rates”. **Materials Science & Engineering. A.** 413-414, 442-446, (2005).

Gregorova A., Cibulkova Z., Kosikova B. and Simon P. “Stabilization effect of lignin in polypropylene and recycled polypropylene”. **Polymer Degradation & Stability**. 89, 553-558, (2005).

Harrick N.J. **Internal Reflection Spectroscopy**. Interscience Publishers, New York, (1967).

Health Canada. “*Federal regulations governing the use of packaging materials in food packaging applications”.* Retrieved 2007 from http://www.hc-sc.gc.ca/fn-an/legislation/guide-ld/recycled_guidelines-directives_recycle03_e.html, (2003).

Holbery J. and Houston D. “Natural-fiber-reinforced polymer composites in automotive applications”. **JOM**. 58(11), 80-86, (2006).

Hornsby[1] P.R., Hinrichsen E. and Taverdi K. “Preparation and properties of polypropylene composites reinforced with wheat and flax straw fibers – Part I Fibre characterization”. **Journal of Materials Science**. 32, 443-449, (1997).

Hornsby[2] P.R., Hinrichsen E. and Taverdi K. “Preparation and properties of polypropylene composites reinforced with wheat and flax straw fibers – Part II Analysis of composite microstructure and mechanical properties”. **Journal of Materials Science**. 32, 1009-1015, (1997).

Hoyle W. and Karsa D.R. *Chemical Aspects of Plastics Recycling*. Processings of the symposium on Chemical Aspects of Plastics Recycling, Manchester, 1996.

Jacob M., Francis B. and Thomas S. “Dynamical Mechanical Analysis of Sisal/Oil Palm Hybrid Fiber-Reinforced Natural Rubber Composites”. **Polymer Composites**. 671-680, (2006).

Jagarnauth C., Ross P., Tang H. and Thirmal C. “Feasibility of recycling polypropylene in Ontario” **ChE483 Fourth Year Group Design Project**, Univeristy of Waterloo, Ontario, (2007).

Jasso-Gastinel C.F. and Sanjuan-Raygoza R.J. “Reinforcing virgin, reprocessed or recycled polypropylene with agave fiber and a polymeric coupling agent”. **Proceeding of ANTEC 2007**, Cinninati OH, (2007).

Jawad S.A. and Alhaj-Mohammad M.H. “β-Relaxation of Drawn Isotactic Polypropylene in Terms of a Simplified Two Phase Model”. **Polymer International.** 35, 395-398, (1994).

Jinan C., Kikutani T., Takaku A. and Shimizu J. “Nonisothermal Orientation-Induced Crystallization in Melt Spinning of Polypropylene”. **Journal of Applied Polymer Science.** 37(9), 2683-2697, (1989).

Johnson D.A., Maclean W.D and Jacobson R. “Agro-Plastic Composites: Replacing Polypropylene and Polyethylene with Wheat Straw”. **Making a Business from Biomass in Energy, Enviornment, Chemicals, Fibers, and Materials.** 925-932, (1997).

Karmaker A. and Prasad A. “Effect of design parameters on the flexural properties of fiber-reinforced composites”. **Journal of material science letters**. 19, 663-65, (2000).

Kruger P.K. “Wheat Straw-Polypropylene Composites”. **MASc Thesis, University of Waterloo**, Ontario, (2007).

La Mantia, Francesco. **Handbook of Plastics Recycling**. Rapra Technology Ltd, 2002.

Maine F.W. and Newson W.R. “Method and Apparatus for Forming Composite Material and Composite Material Therefrom”. **US Patent US2005192382 A1-2005-09-01**, (2005).

Maine F.W. and Newson W.R. “Oriented Composite Thermoplastic Material with Reactive Filler”. **US Patent US2006057348 A1-2006-03-16**, (2006).

Maier C. and Calafut T. **Polypropylene. The Definitive User’s Guide and Databook**. Plastics Design Library, New York, (1998).

Mi, Y., Chen X. and Guo Q. “Bamboo Fiber-reinforced Polypropylene Composites: Crystallization and Interfacial Morphology”. **Journal of Applied Polymer Science** 64, 1267-1273, (1997).

Mohanty A.K., Misra M. and Drzal L.T. “Sustainable Bio-Composites from Renewable Resources: Opportunities and Challenges in the Green Materials World”. **Journal of Polymer & the Environment.** 10 (1/2), 19-26, (2002).

Newson W.R. and Maine F.W. “Advances in New WPC Technologies”. **Proceedings of Progress in Woodfibre-Plastic Composites 2004,** Toronto, May 23-24, (2002).

Newson W.R. and Maine F.W. “Second Generation Woodfiber-Polymer Composites”. **Proceedings of Progress in Woodfibre-Plastic Composites 2002,** Toronto, May 10-11, (2004).

OMAFRA. “Historical Provincial Estimate by Crop). Retrieved 2008 from http://www.omafra.gov.on.ca/english/stats/crops/estimate_metric_historical.htm, (2007).

Ozzetti R.A., Filho A.P., Schuchardt U. and Mandelli D. “Determination of Tacticity in Polypropylene by FTIR with Multivariate Calibration”. **Journal of Applied Polymer Science.** 85(4), 734-745, (2001).

Panthapulakkal S; Sain M. “Injection Molded Wheat Straw and Corn Stem Filled Polypropylene Composites”. ***Journal of Polymer & Environment.*** 14, 265, (2006).

Panthapulakkal S., Zereshkian A. and Sain M. “Preparation and characterization of wheat straw fibers for reinforcing application in injection molded thermoplastic composites”. **Bioresource Technology.** 97, 265-272, (2006).

Pike Technologies. “ATR Theory and Applications”. Pike **Technologies Application Note – 0402**. Retrieved 2008 from http://www.piketech.com/technical/app-notes.html, (2005).

Rabiej S. “Determination of the Crystallinity of Polymer Blends by an X-ray Diffraction Method”. **European Polymer Journal.** 29(4), 625-633, (1993).

Rowell R.M., Sanadi A.R., Caulfield D.F. and Jacobson R.E. “Utilization of Natural Fibers in Plastic Composites: Problems and Opportunities”. **Proceedings of International Symposium on Lignocellulosic-Plastic Composites.** 1st. Sao Paulo, March 13-15 1996. 23-51, (1997).

Rowell R.M., Sanadi A., Jacobson R. and Caulfield D. “Properties of Kenaf/Polypropylene Composites”. Retrieved 2007 from http://www.fpl.fs.fed.us/documnts/pdf1999/rowel99b.pdf, (1999).

Saheb D.N. and Jog J.P. “Natural Fiber Poly Composites: A Review”. **Advance In Polymer Technology.** 18(4), 351-363, (1999).

Salemane M.G. and Luyt A.S. “Thermal and mechanical properties of polypropylene-wood powder composites”. **Journal of Applied Polymer Science**. 100, 4173-4180, (2006).

Sanadi A.R., Caulfield D.F., Jacobson R.E., and Rowell R.M. “Renewable agricultural fibers as reinforcing fillers in plastics: mechanical properties of kenaf fiber-polypropylene composites”. **Ind. Eng. Chem. Res.** 34, 1889-1896, (1995).

Saujanya C., Tangirala R. and Radhakrishnan S. “Crystallization Behaviour in Poly(pryolyene) Containing Wollastonite Microfibrils”. **Macromolecular Materials and Engineering.** 287(4), 272-276, (2002)

Schemanauer J.J., Osswald T.A., Sanadi A.R., and Caulfield D.F. “Melt Rheolocial properties of natural fiber-reinforced polypropylene”. **Proceedings from ANTEC 2000**. 2206-2210, (2000).

Son Y. and Kim D.H. “Determination of Shear Viscosity and Shear Rate from Pressure Drop and Flow Rate Relationship in a Rectangular Channel”. **Proceedings from ANTEC 2007**. 1940, (2007).

Stern C., Frick A. and Weickert G. “Relationship Between the Structure and Mechanical Properties of Polypropylene: Effects of the Molecular Weight and Shear-Induced Structure”. **Journal of Applied Polymer Science.** 103, 519-533, (2007).

Taraiya A.K., Richardson A. and Ward I.M. “Production and Properties of Highly Oriented Polypropylene by Die Drawing”. **Journal of Applied Polymer Science.** 33, 2559-2579, (1987).

Taraiya A.K., Unwin A.P. and Ward I.M. “The Role of Differential Scanning Calorimetry and X-ray Diffraction in Identifying Crystal Continuity in Highly Oriented Samples of Die-Drawn Polypropylene”. **Journal of Polymer Science: Part B: Polymer Physics.** 26, 817-838, (1988).

University of Guelph. “Project Soy”. Retrieved 2008 from http://www.projectsoy.ca/en_index.html, (2007).

Wang B. and Sain M. “Dispersion of soybean stock-based nanofiber in a plastic matrix”. **Polymer Int.** 56, 538-546, (2007).

Wilke H.L. and Hopkins D.T.; Waggele D.H., (eds.); "Soy protein and human nutrition", New York Academic Press (1979).

Xu J., Guan F., Yasin T. and Fan Z. “Isothermal crystallization of metallocene-based polypropylenes with different isotacticity and regioregularity”. **Journal of Applied Polymer Science**. 90, 3215–3221, (2003).

Yang, H., Kim H., Son J., Park H., Lee B. and Hwang T. “Rice-husk flour filled polypropylene composites; mechanical and morphological study”. **Composite Structures.** 63, 305-312, (2004).

Yin B., Yang W., Yu Q. and Yang MI. “Flow-Induced Morphology of Cast Polypropylene”. **Polymer Engineering & Science.** 44(9), 1656, (2004).

Zhang J., Ding Q., Zhou N., Li L., Ma Z. and Shen J. “Studies on crystal morphology and crystallization kinetics of polypropylene filled with $CaCO_3$ of different size and size distribution” **Journal of Applied Polymer Science**. 101, 2437-2444, (2006).

Zurale M.M. and Bhide S.J. “Properties of fillers and reinforcing fibers”. **Mechanics of Composite Materials.** 34(5), 461-472, (1998).

APPENDIX A – SEM Micrographs

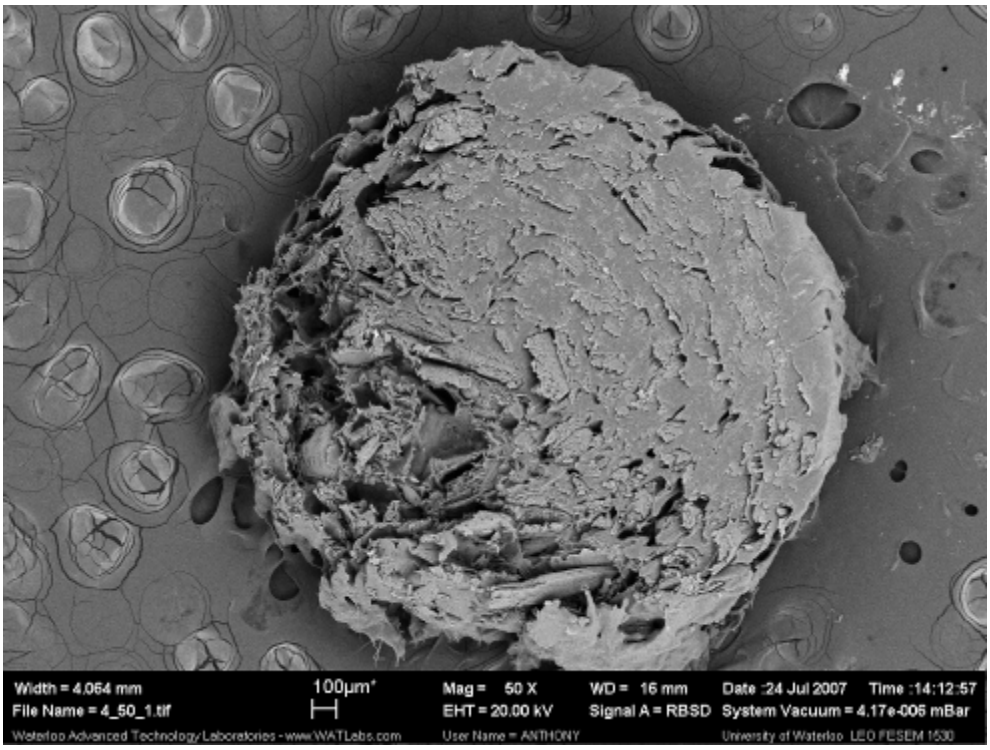

Figure A1.1: 50x mag of lab composite of 30vPP-30rPP-40WS

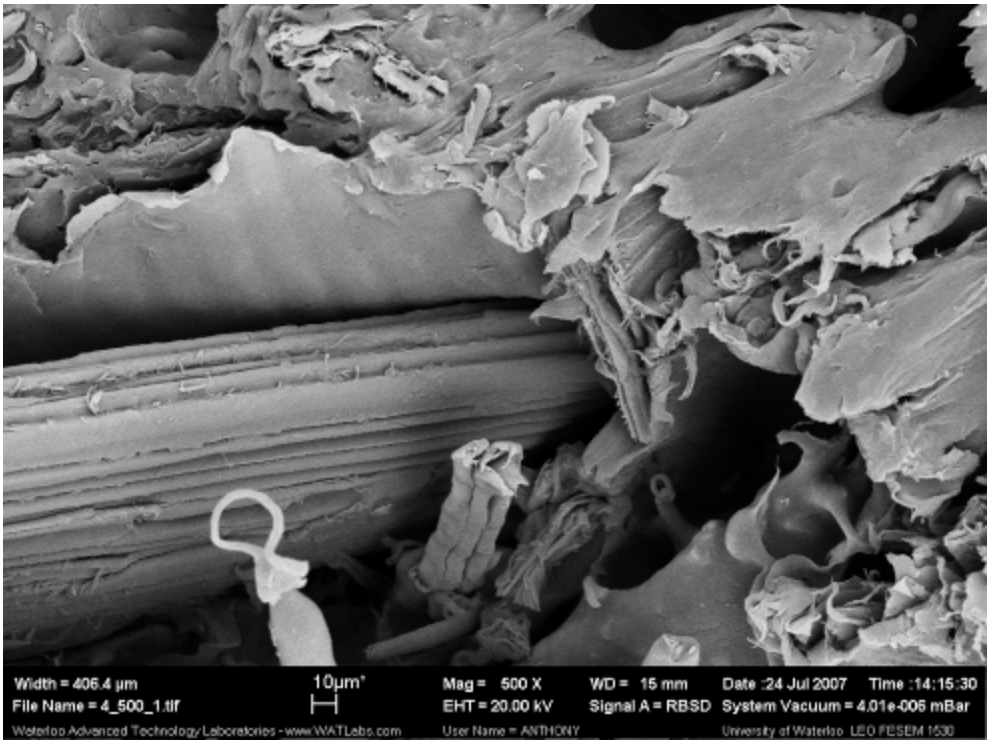

Figure A1.2: 500x mag of lab composite of 30vPP-30rPP-40WS

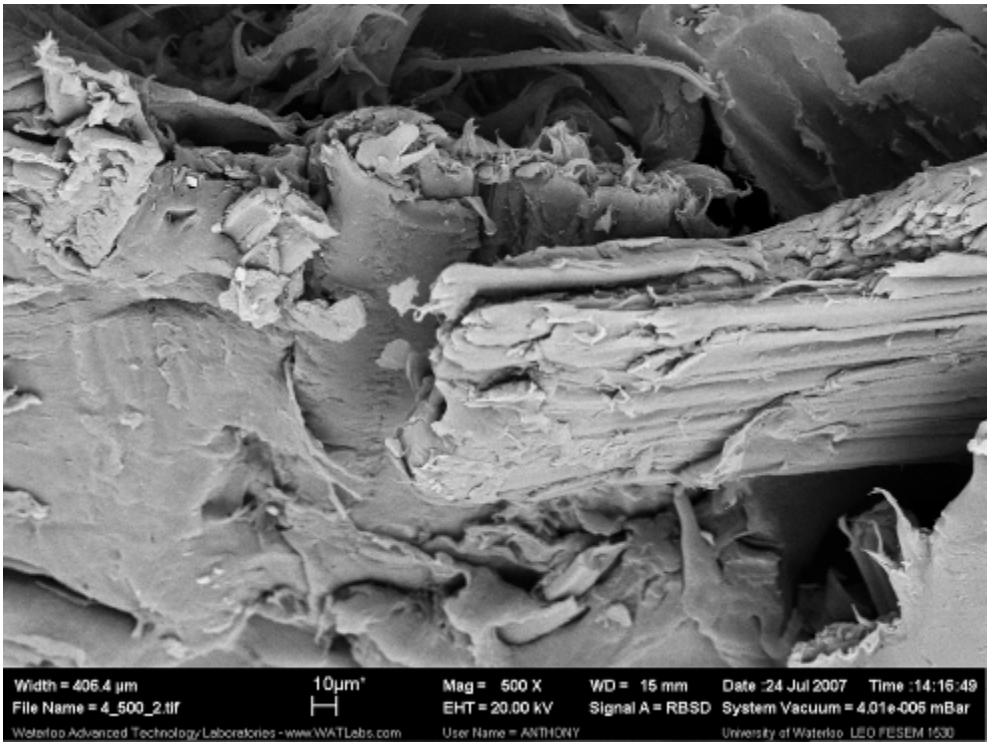

Figure A1.3: 500x mag of lab composite of 30vPP-30rPP-40WS. A look at another section of the sample to assess fiber damage.

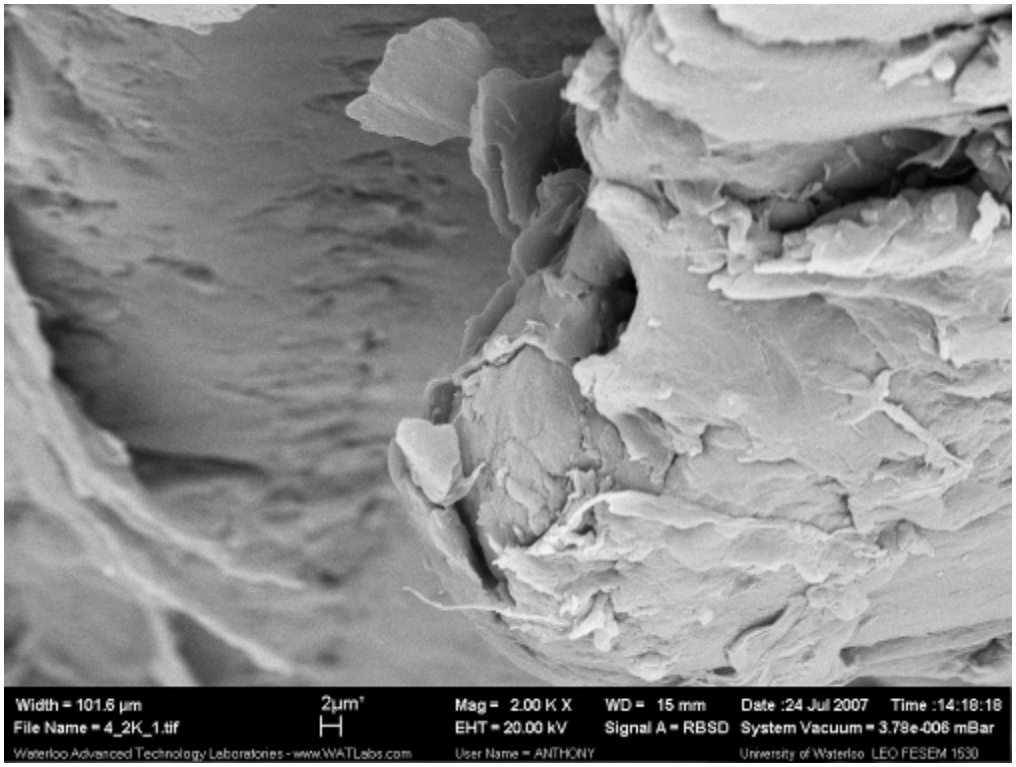

Figure A1.4: 2000x mag of lab composite of 30vPP-30rPP-40WS.

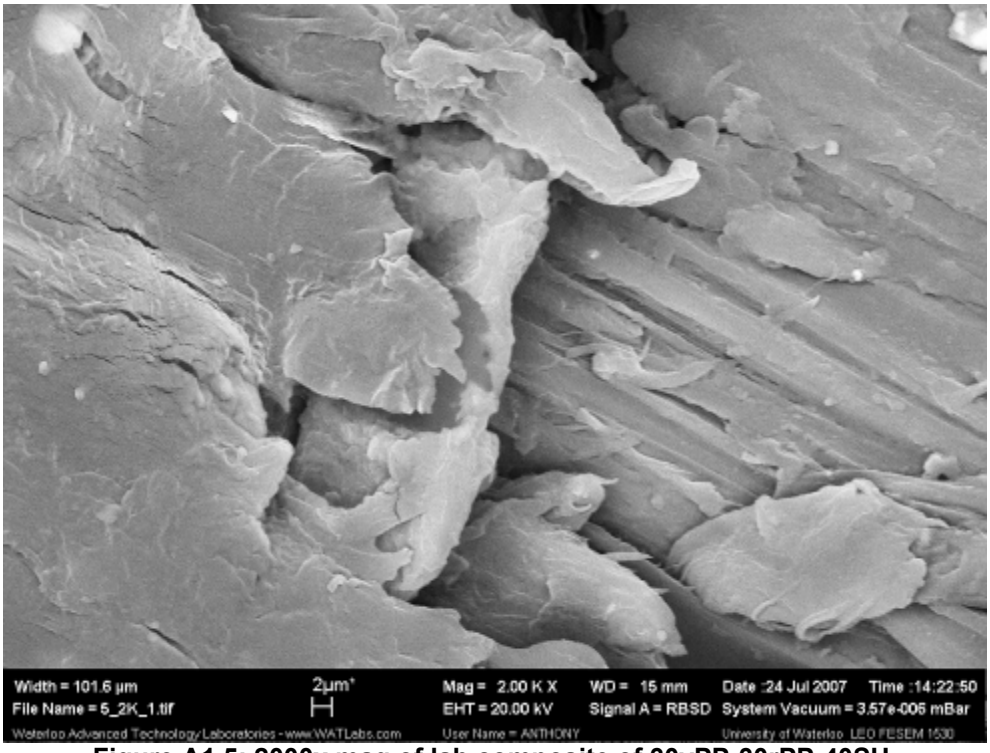

Figure A1.5: 2000x mag of lab composite of 30vPP-30rPP-40SH.

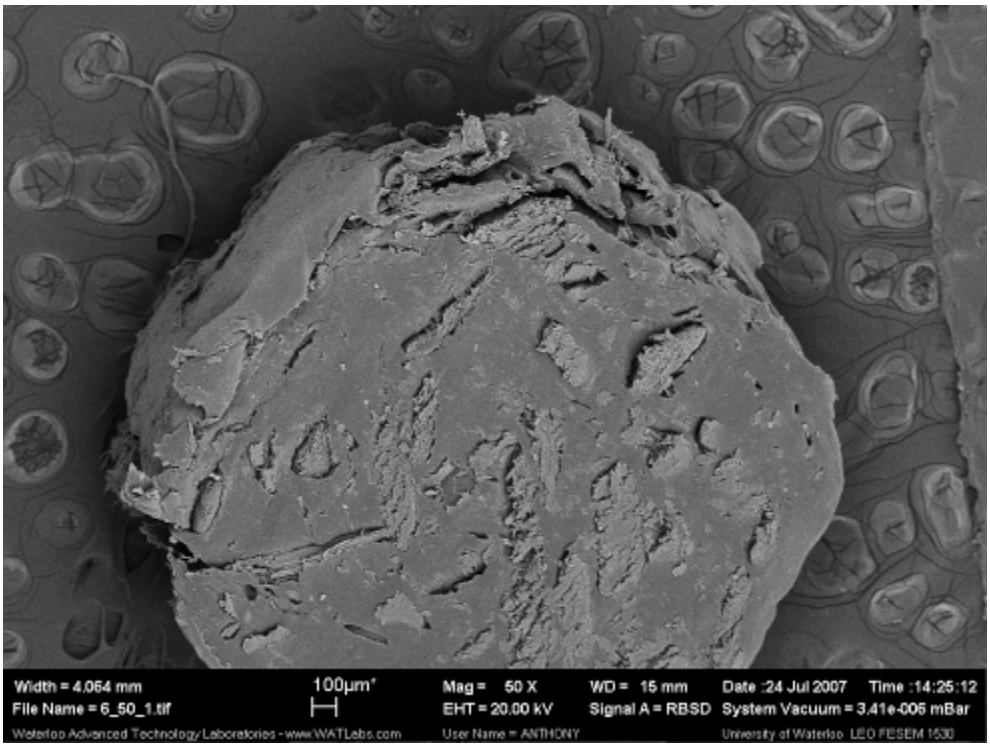

Figure A1.6: 50x mag of lab composite of 30vPP-30rPP-40SS.

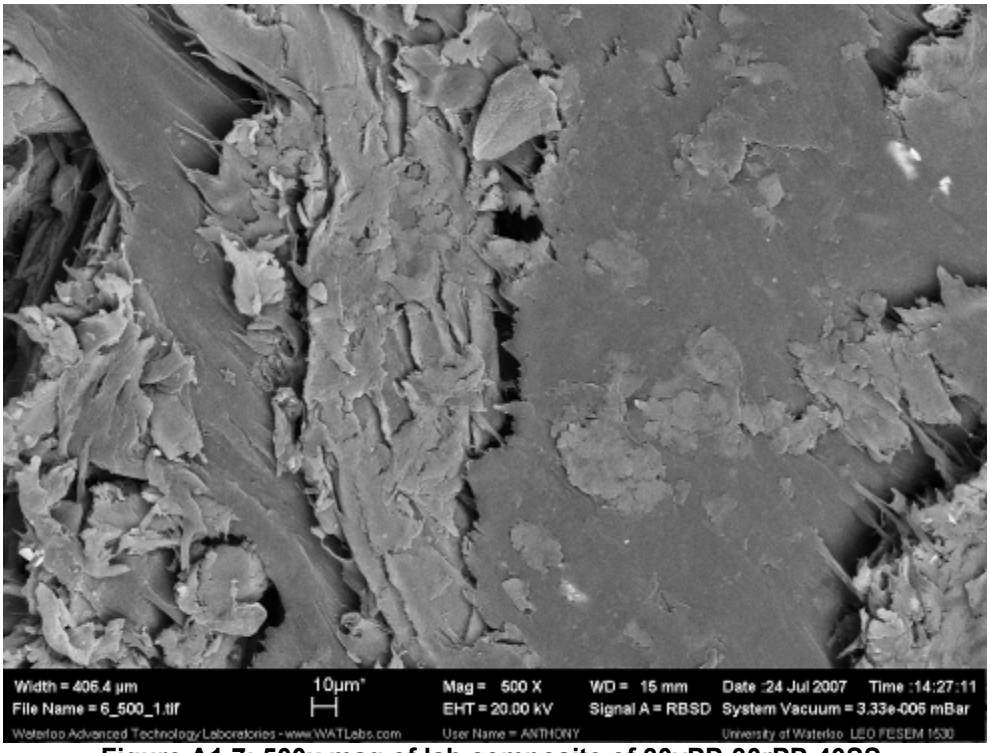

Figure A1.7: 500x mag of lab composite of 30vPP-30rPP-40SS.

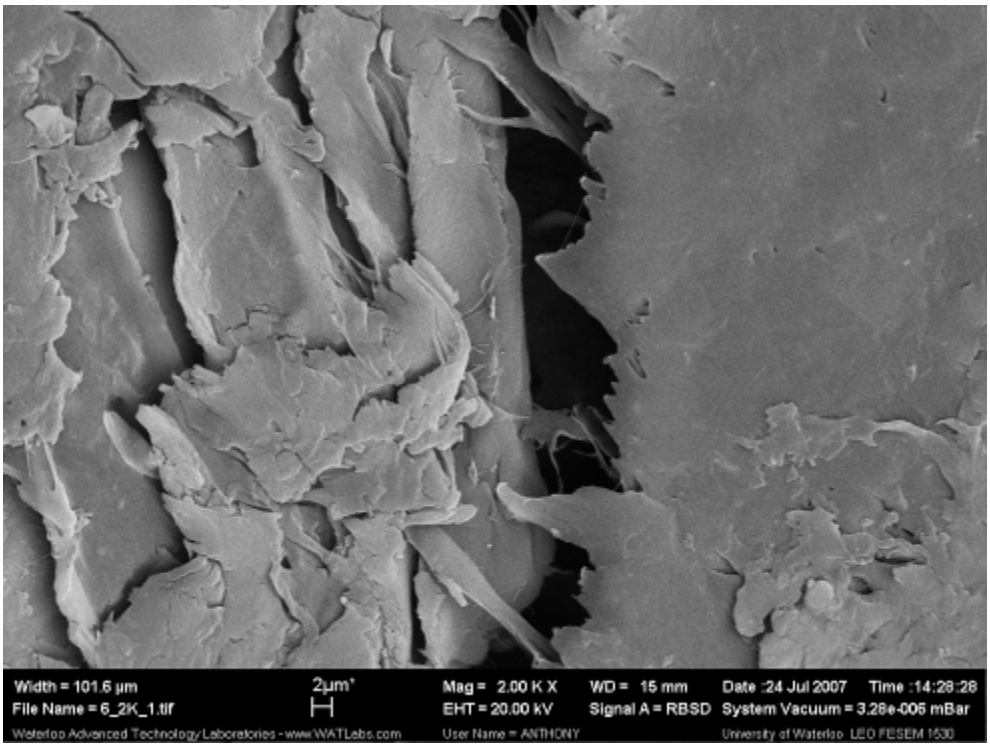

Figure A1.8: 2000x mag of lab composite of 30vPP-30rPP-40SS.

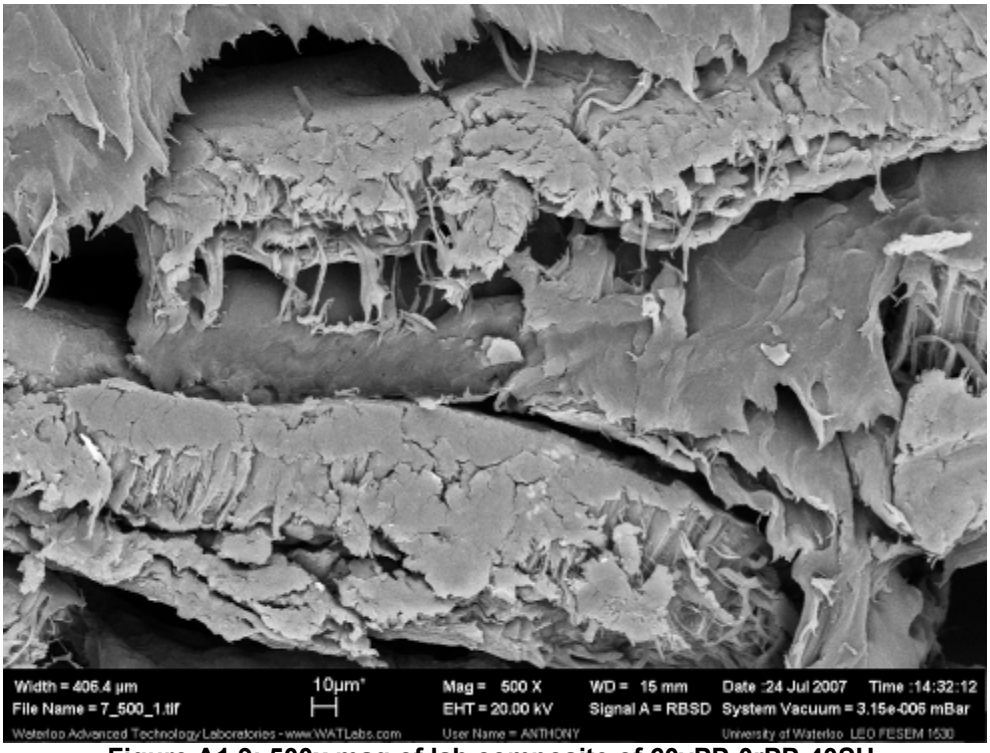

Figure A1.9: 500x mag of lab composite of 60vPP-0rPP-40SH.

Figure A1.10: 500x mag of lab composite of 0vPP-60rPP-40SH.

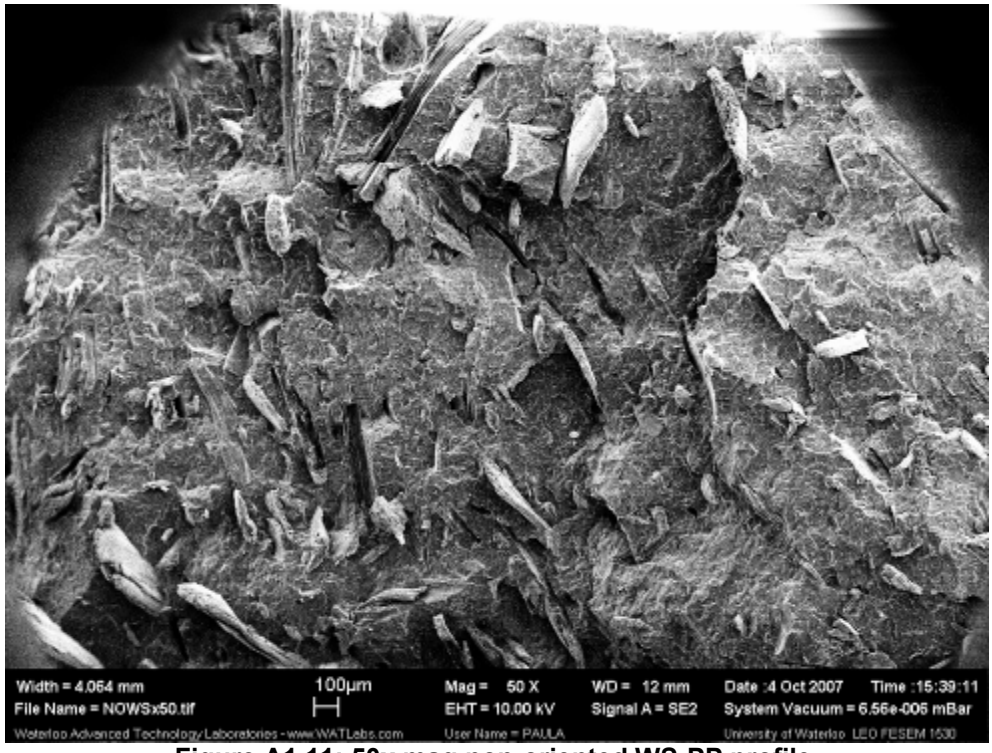

Figure A1.11: 50x mag non-oriented WS-PP profile.

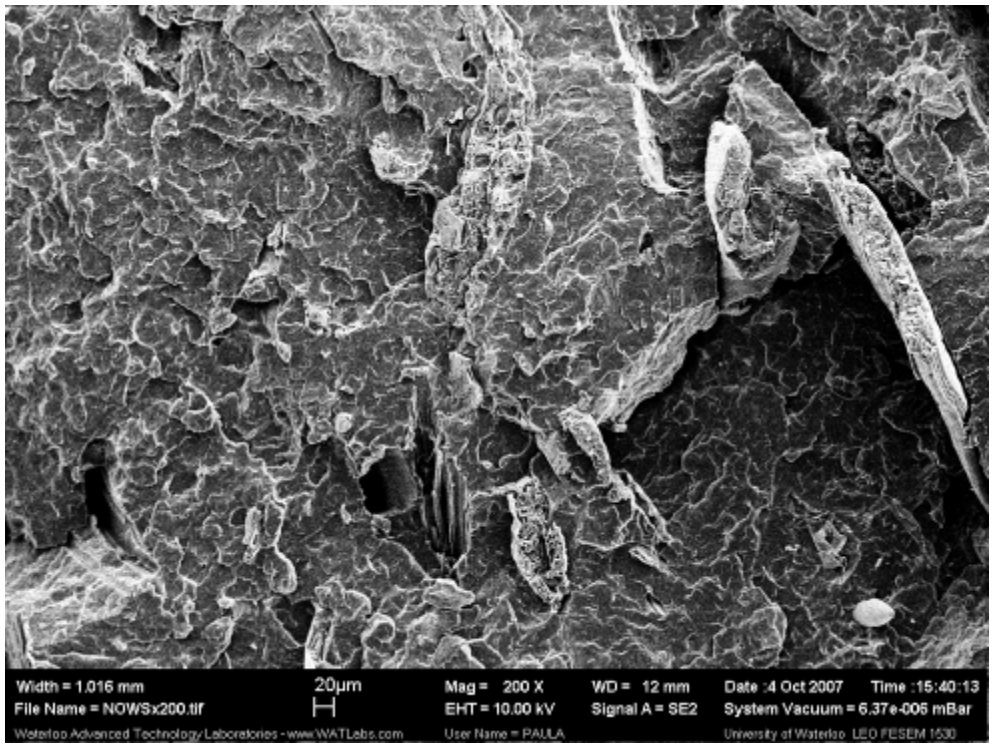

Figure A1.12: 200x mag non-oriented WS-PP profile.

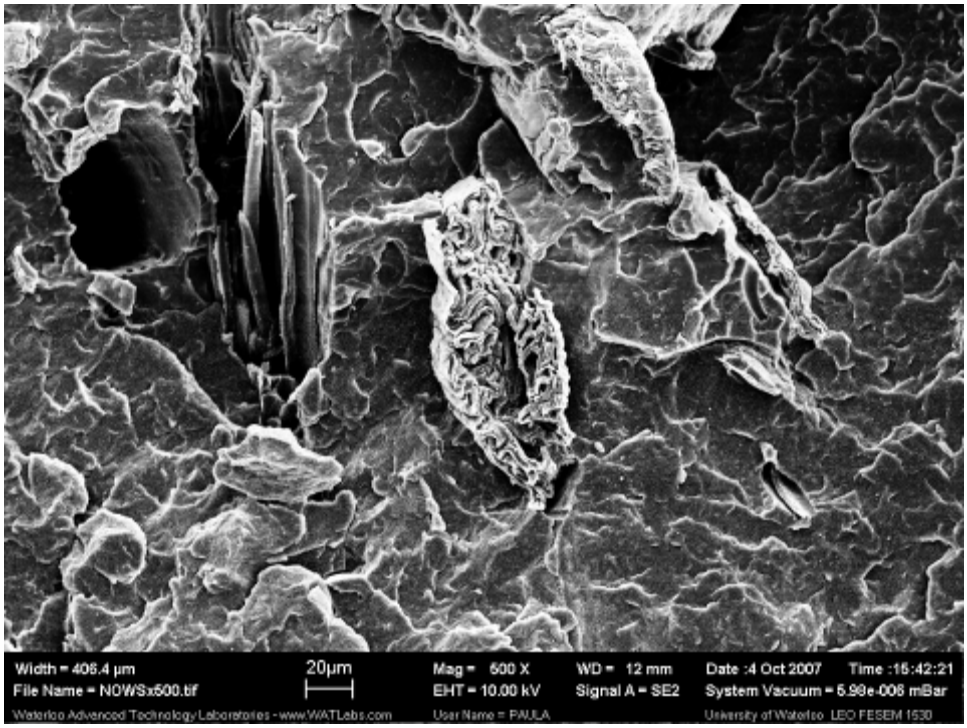

Figure A1.13: 500x mag non-oriented WS-PP profile.

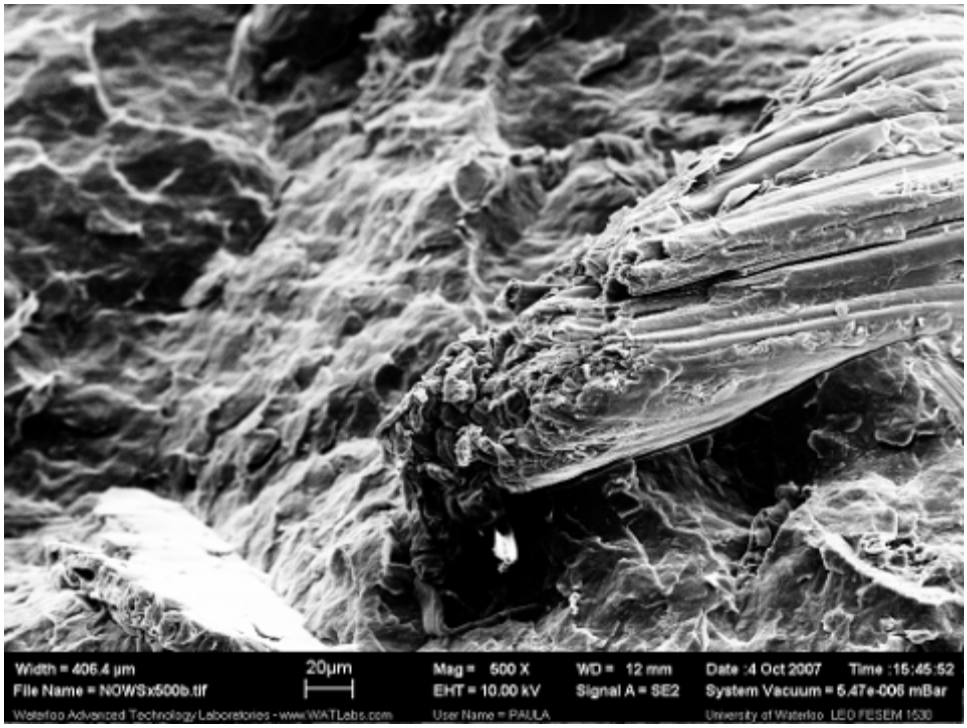

Figure A1.14: 500x mag non-oriented WS-PP profile, another look at fiber protruding.

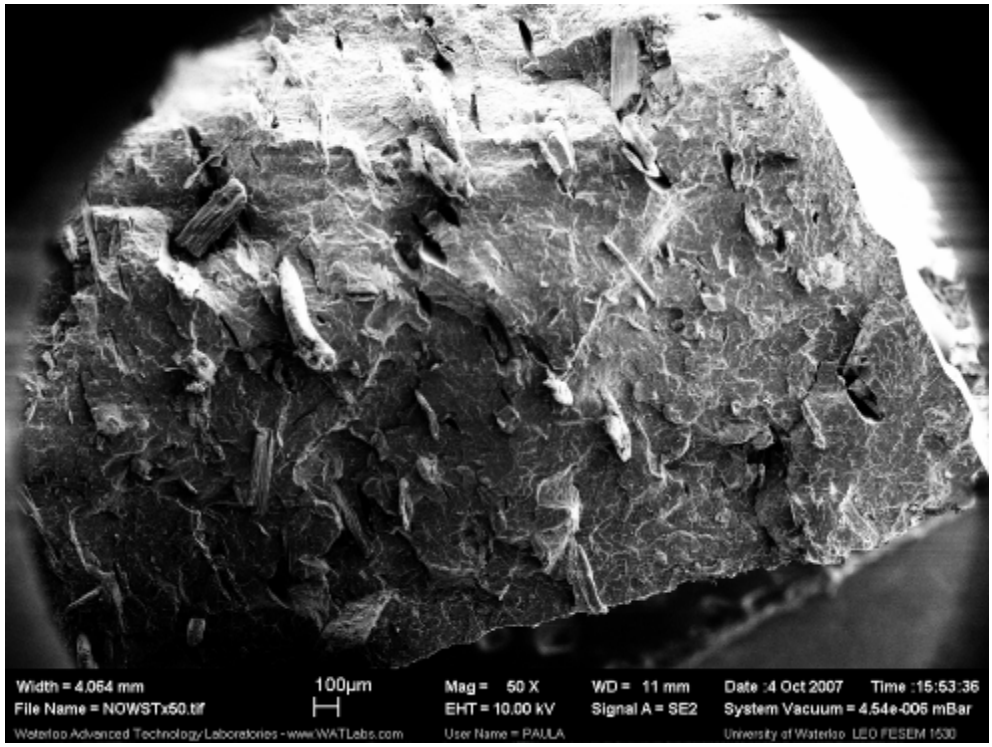

Figure A1.15: 50x mag non-oriented WS-PP profile, top of profile cross section.

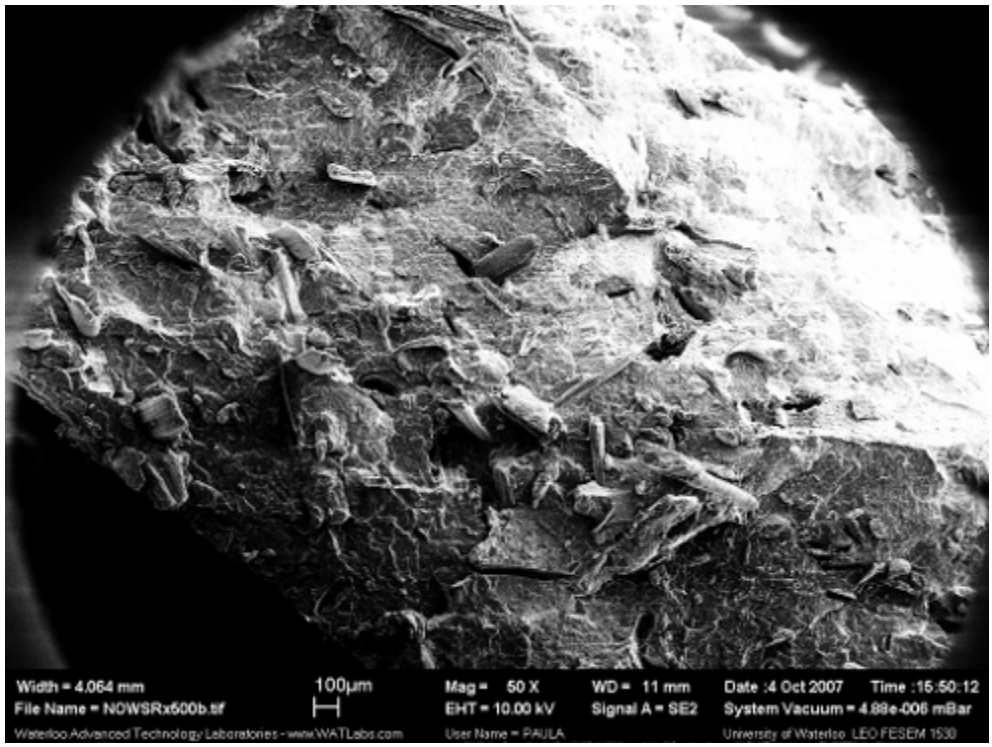

Figure A1.16: 50x mag non-oriented WS-PP profile, right of profile cross section.

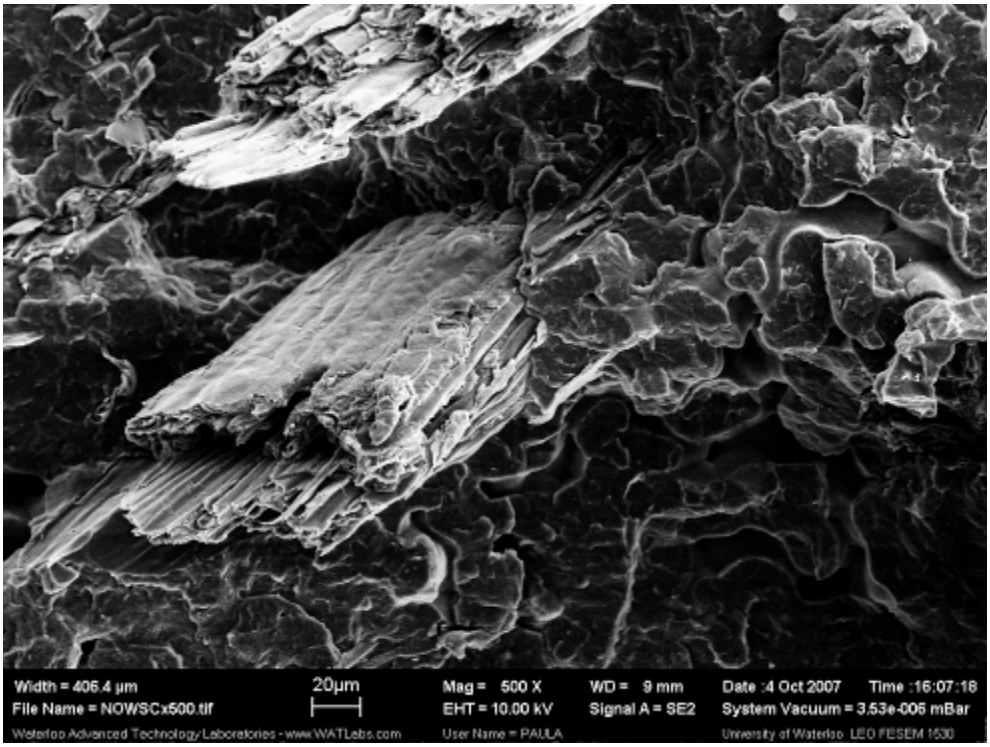

Figure A1.17: 500x mag non-oriented WS-PP profile, center of profile cross section.

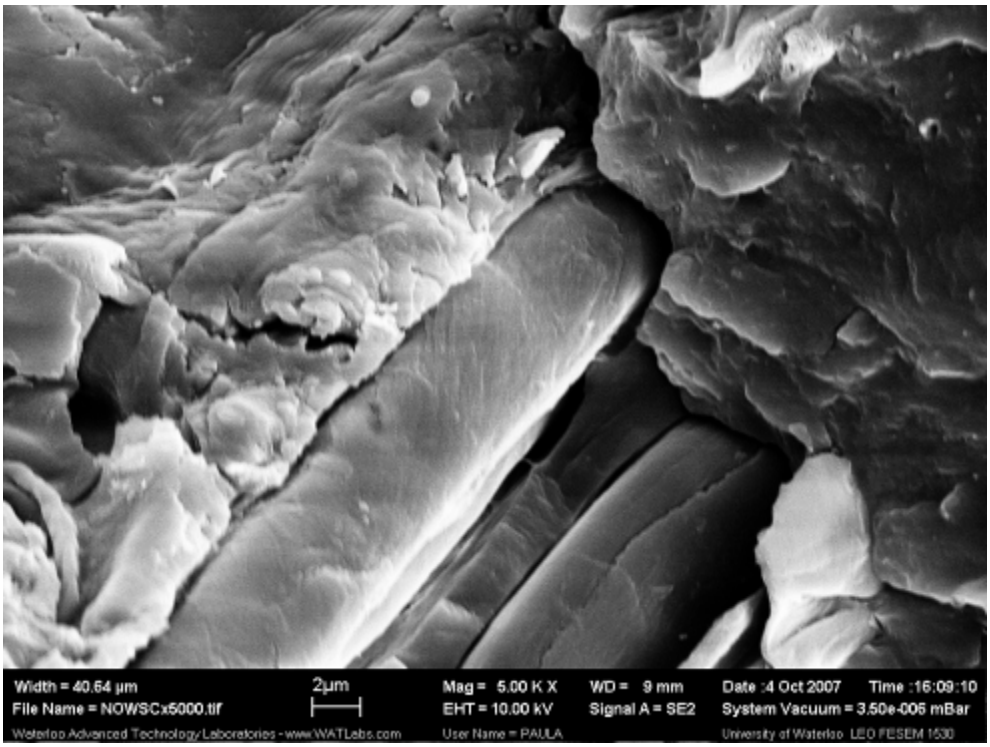

Figure A1.18: 500x mag non-oriented WS-PP profile, center of profile cross section.

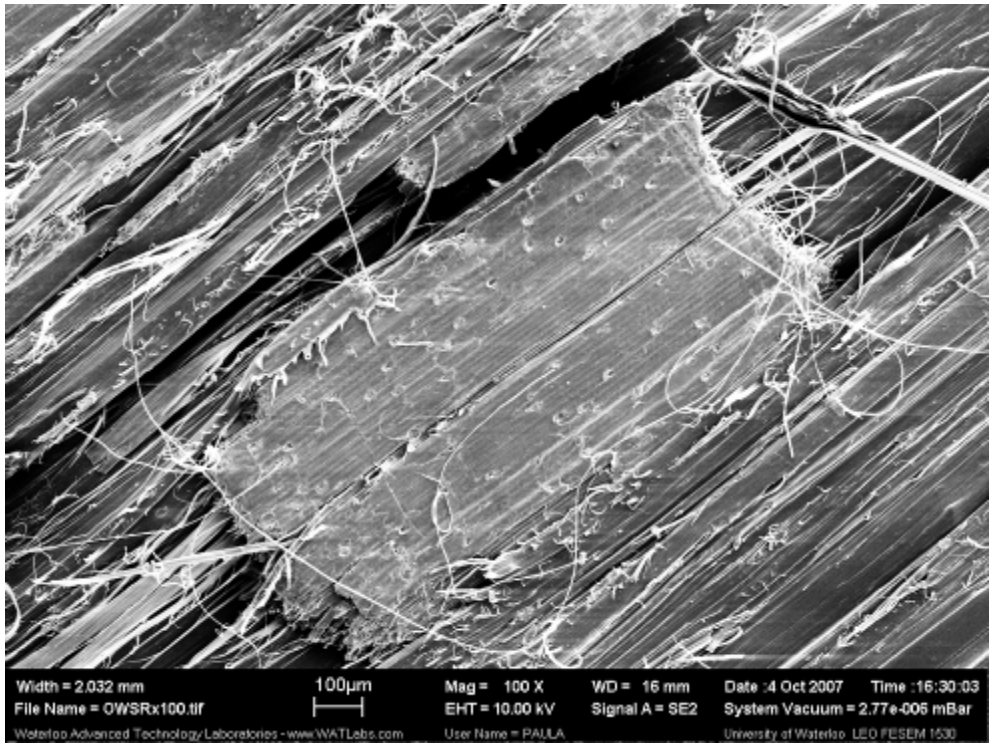

Figure A1.19: 100x mag oriented WS-PP profile, side surface of right profile cross section.

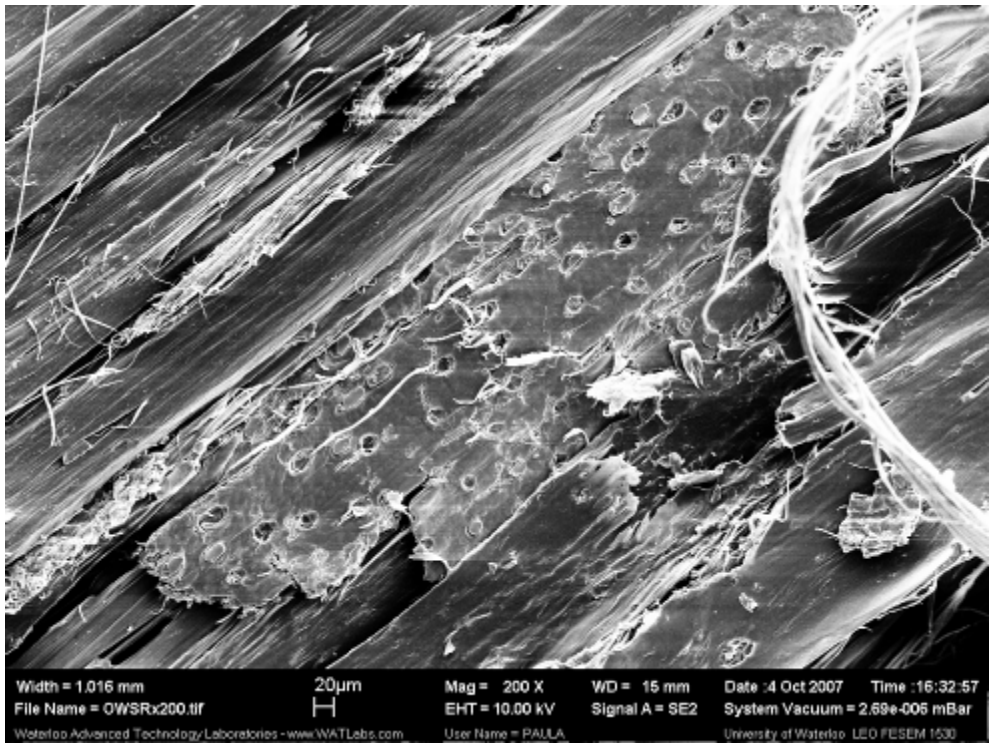

Figure A1.20: 200x mag oriented WS-PP profile, side surface of right profile cross section.

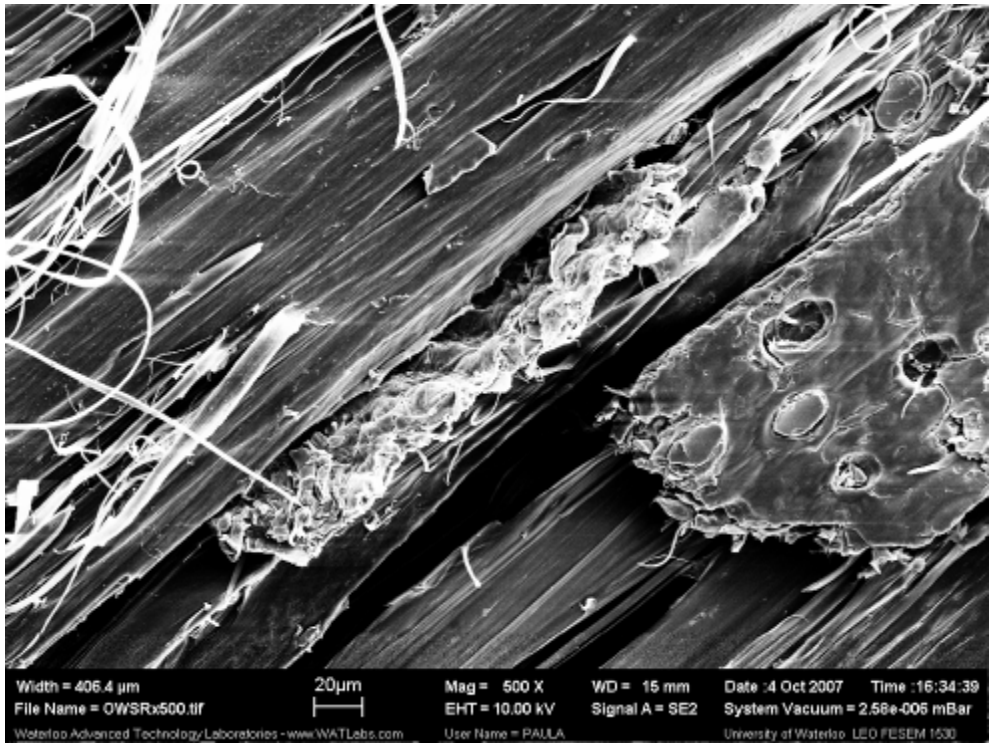

Figure A1.21: 500x mag oriented WS-PP profile, side surface of right profile cross section.

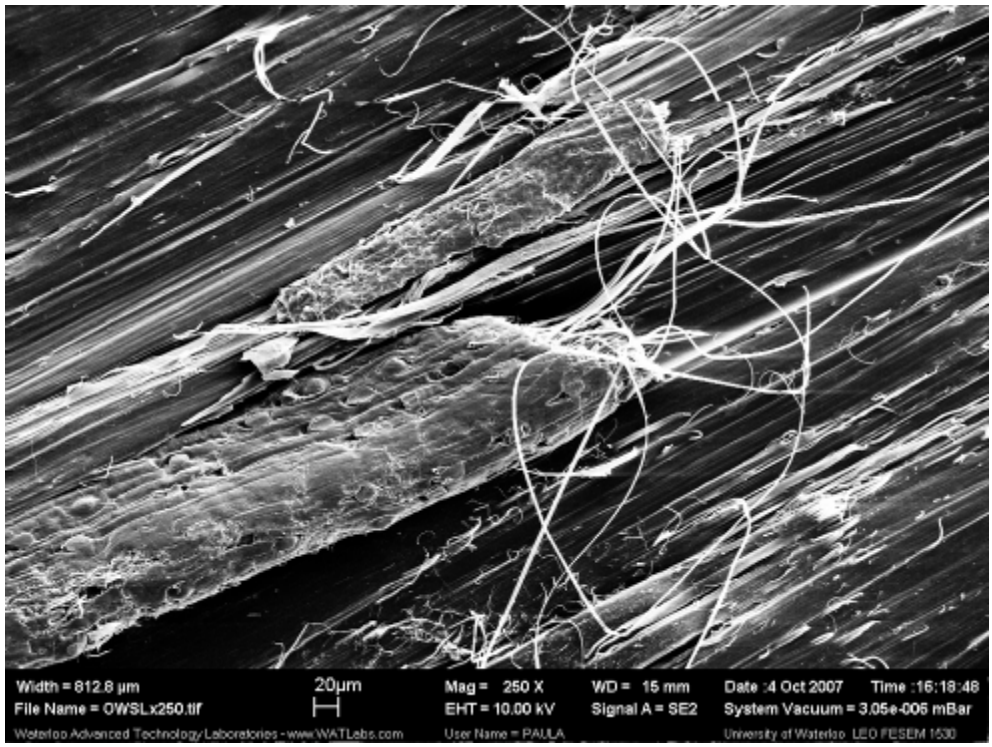

Figure A1.22: 250x mag oriented WS-PP profile, side surface of left profile cross section. Embedded wheat straw.

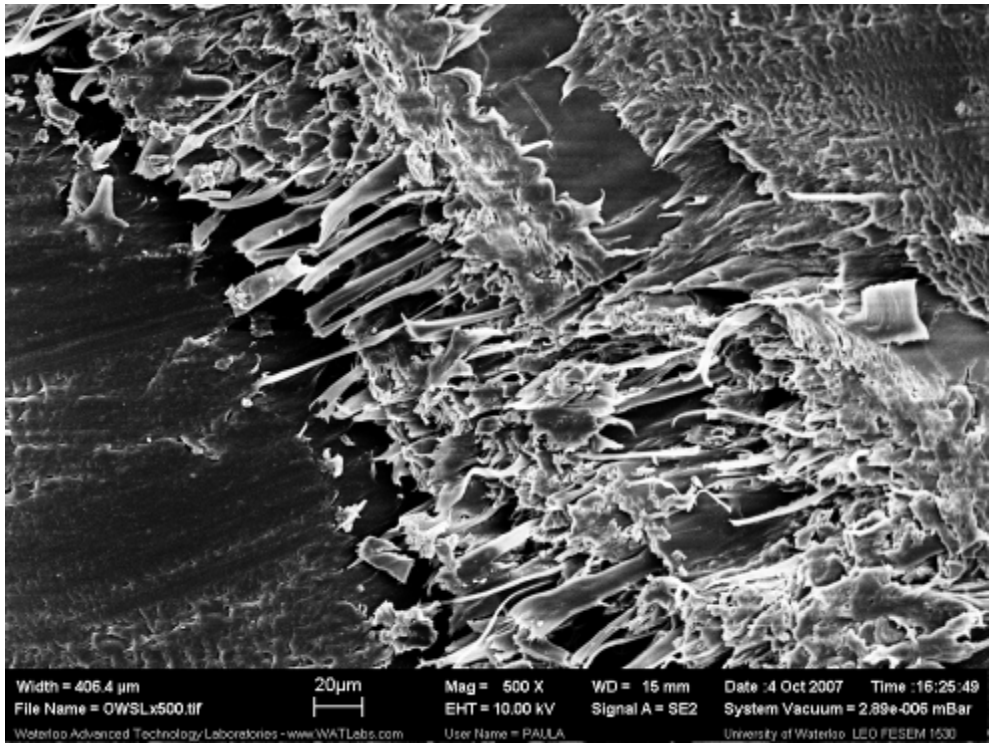

Figure A1.23: 500x mag oriented WS-PP profile, side surface of left profile cross section.

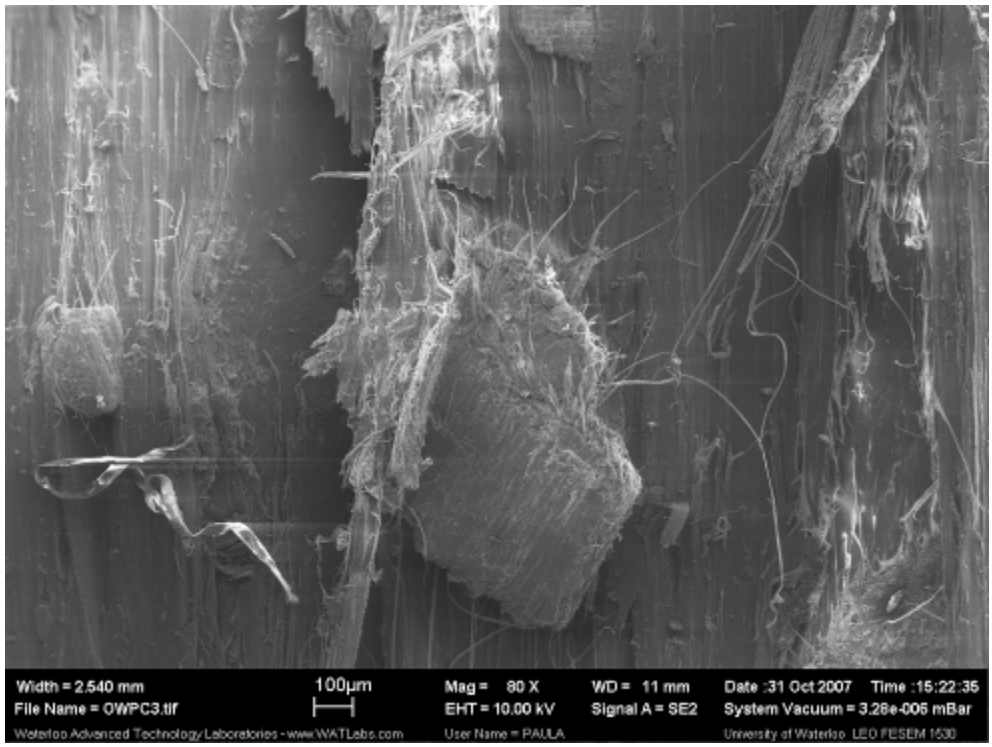

Figure A1.24: 80x mag oriented WPC profile, side surface of profile cross section.

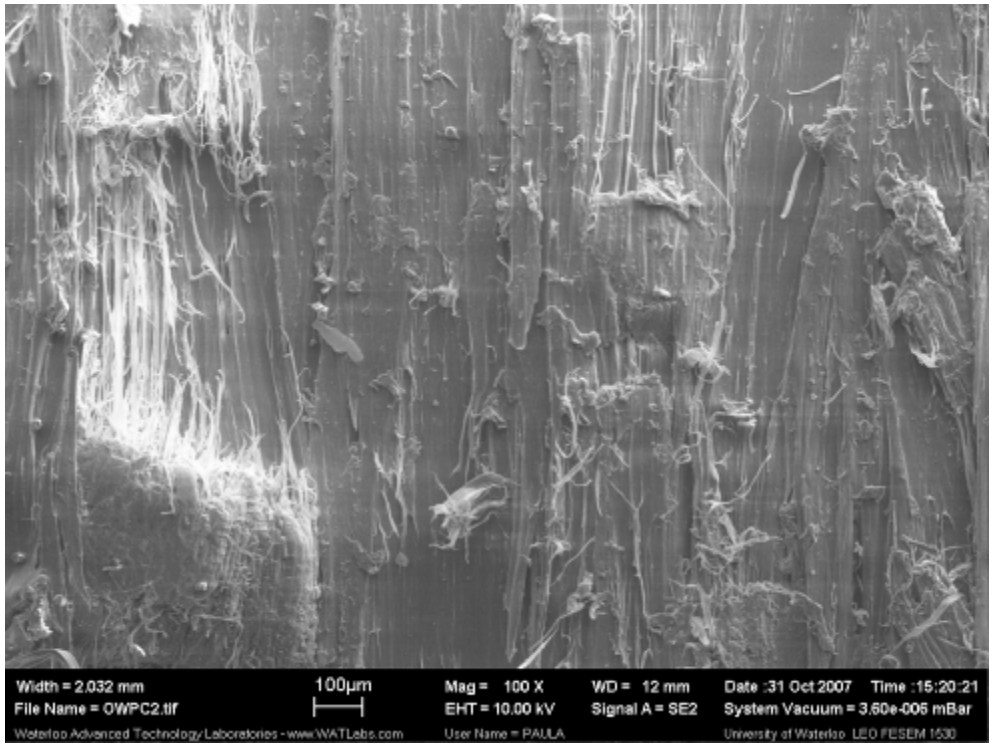

Figure A1.25: 100x mag oriented WPC profile, side surface of profile cross section.

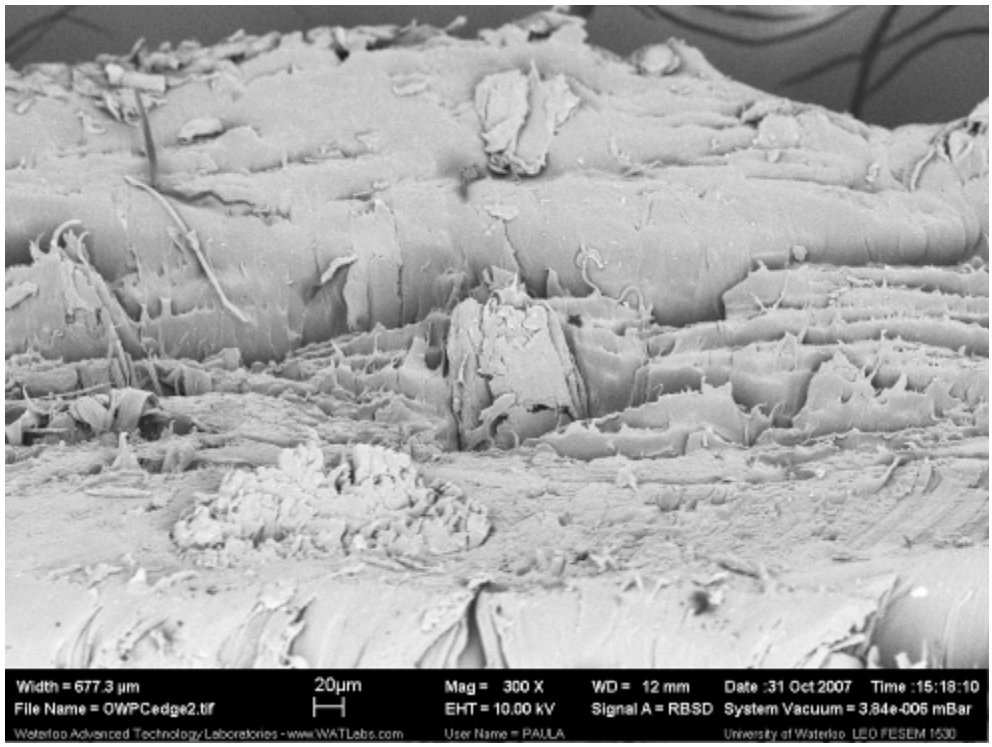

Figure A1.26: 300x mag RBSD mode oriented WPC profile, cross sectional edge of side surface of profile cross section.

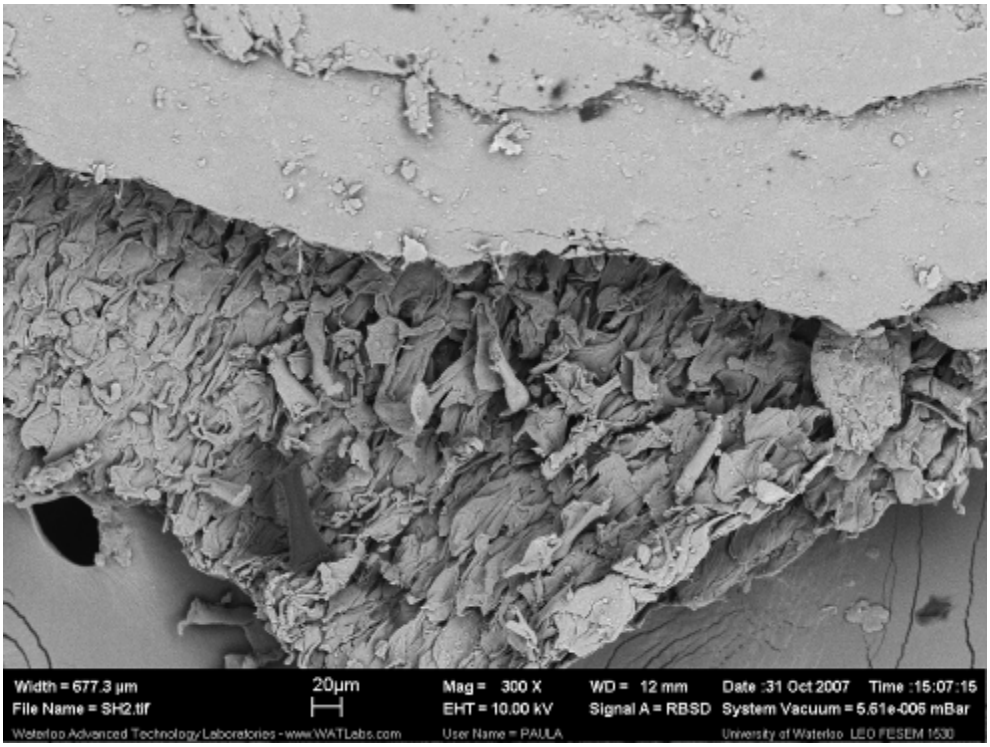

Figure A1.27: 300x mag of SH filler. Looking at edge of SH piece, which has strand-like structure. Outer hull (top surface) is smooth.

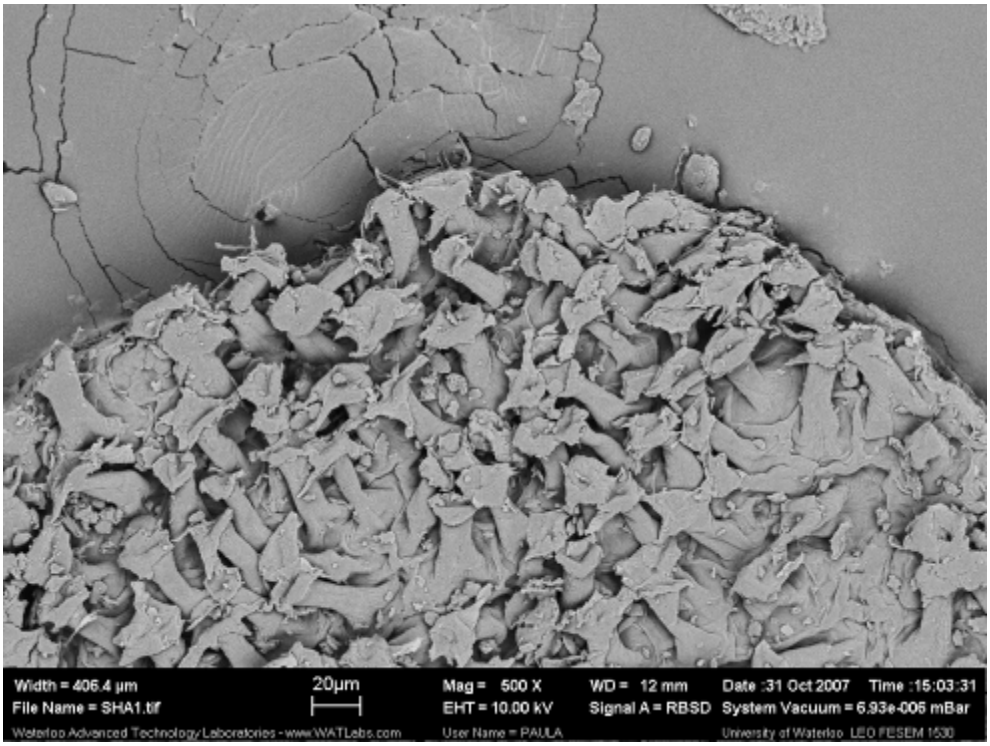

Figure A1.28: 500x mag of SH filler. Bottom surface (inner hull). Porous with distinct strand-like structures protruding outwards.

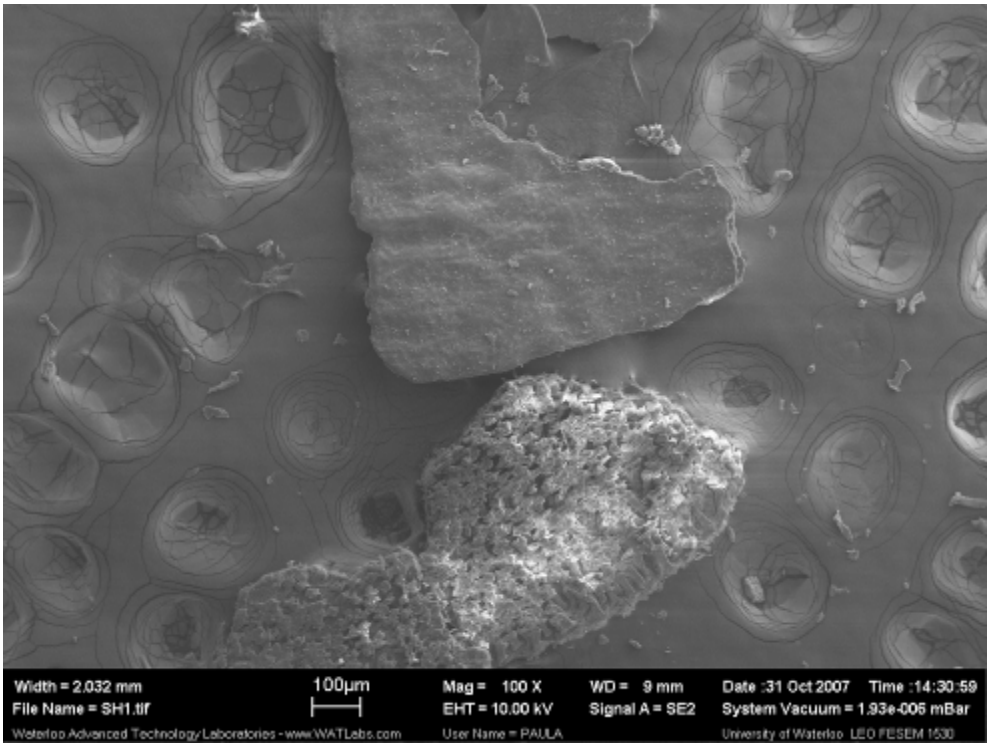

Figure A1.29: 100x mag of ground SH filler. Smaller pieces than raw SH. Top and bottom surfaces of SH have different textures. Top surface (outside of hull) is smooth, while bottom surface (inside of hull) is rough and porous.

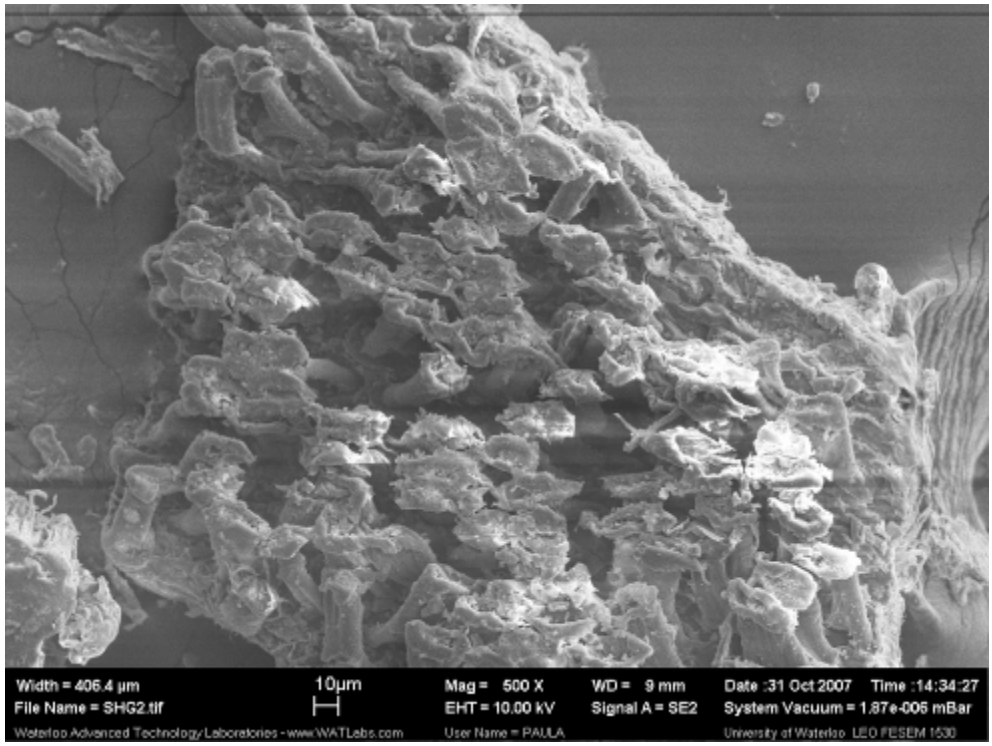

Figure A1.30: 500x mag of ground SH filler. Inner hull surface (porous strand-like).

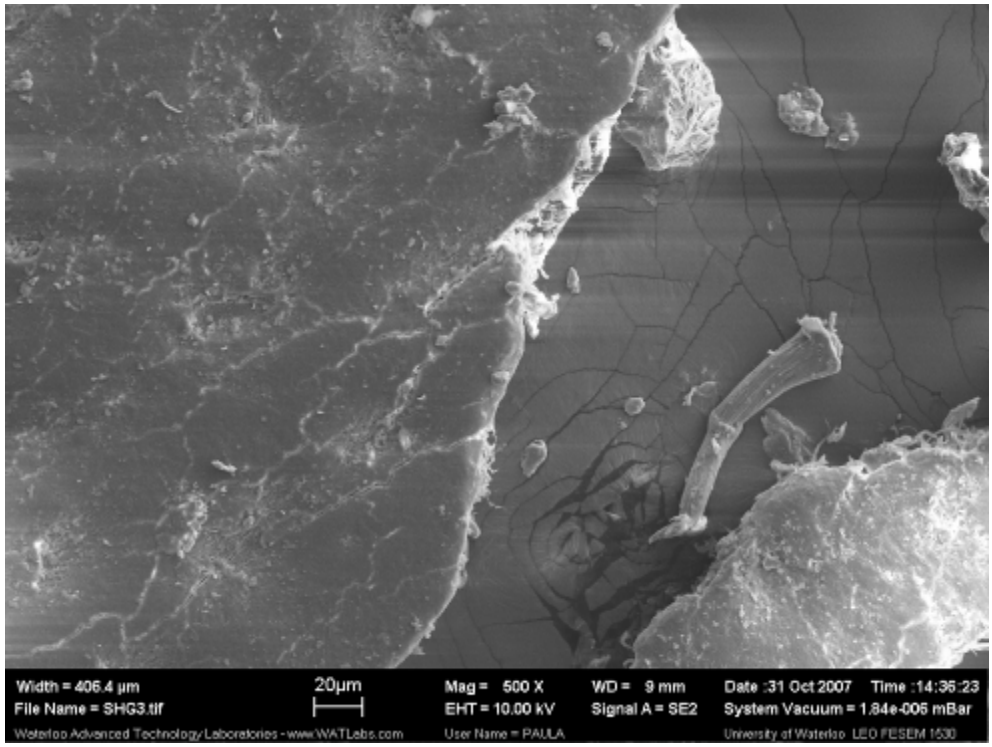

Figure A1.31: 500x mag of ground SH filler. Smooth outer hull, and separated strand of fiber.

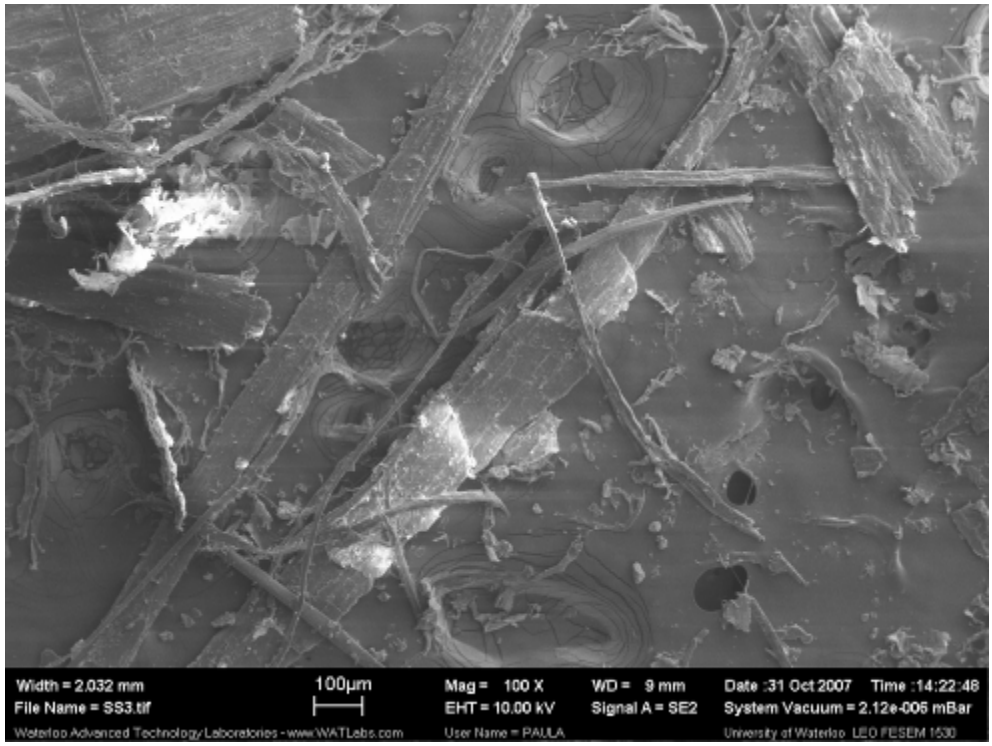

Figure A1.32: 100x mag SS filler.

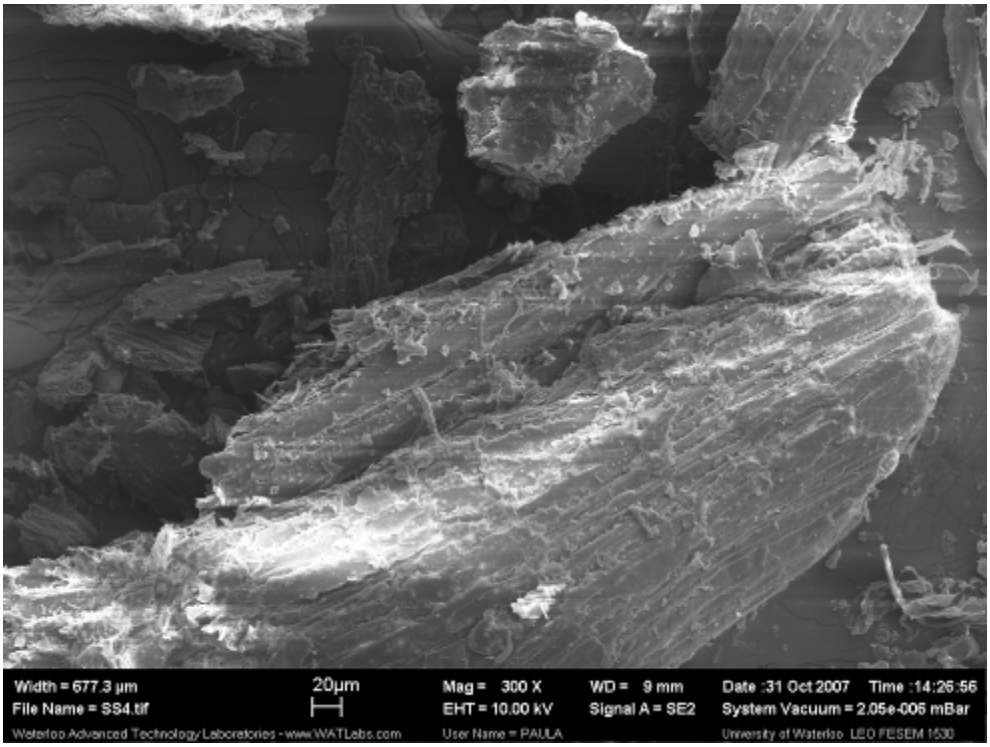

Figure A1.33: 300x mag SS filler.

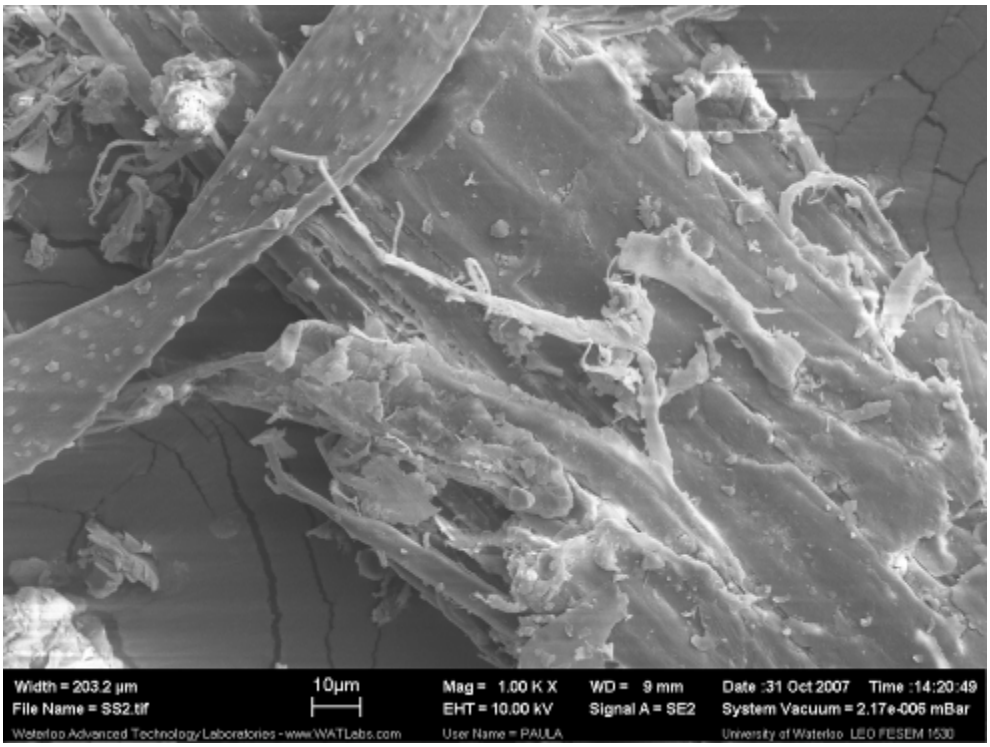

Figure A1.34: 1000x mag SS filler.

APPENDIX B –TGA Graphs

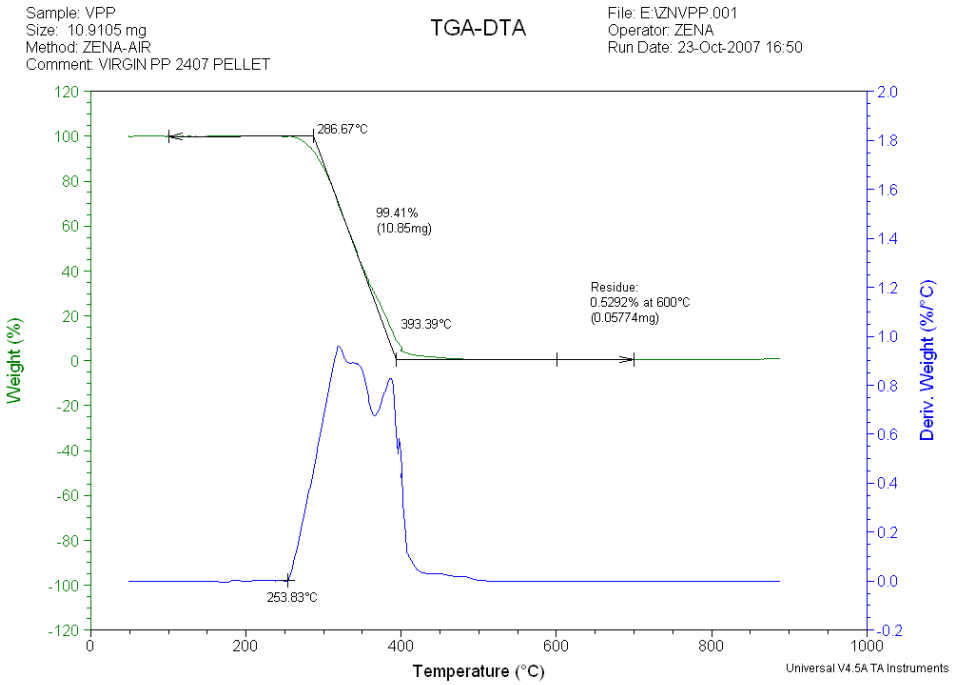

Figure A2.1: TGA (green) and DTA (blue) graph of vPP

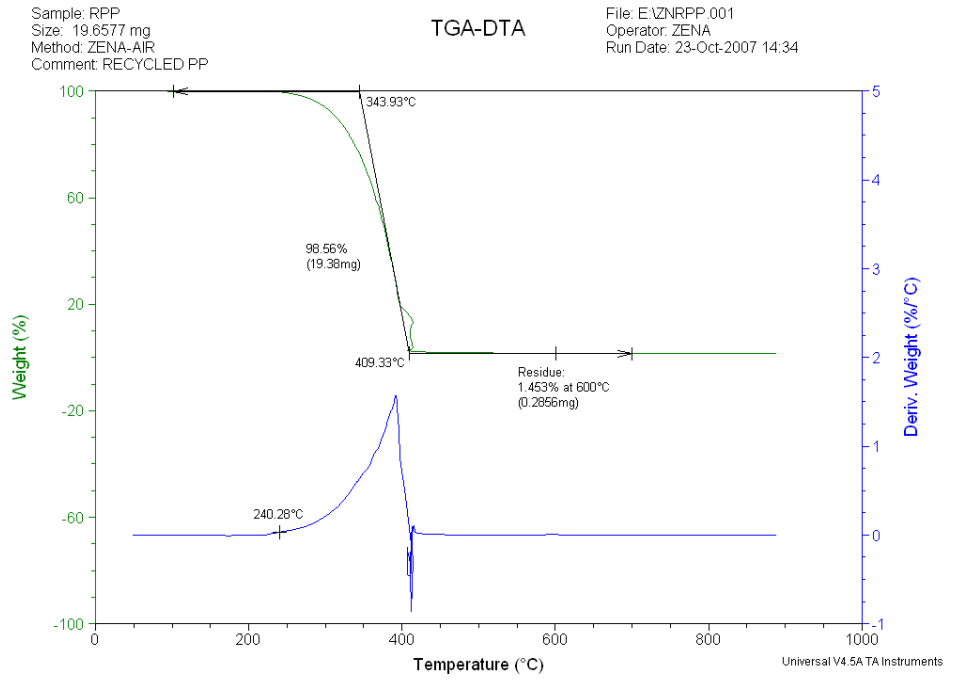

Figure A2.2: TGA (green) and DTA (blue) graph of rPP

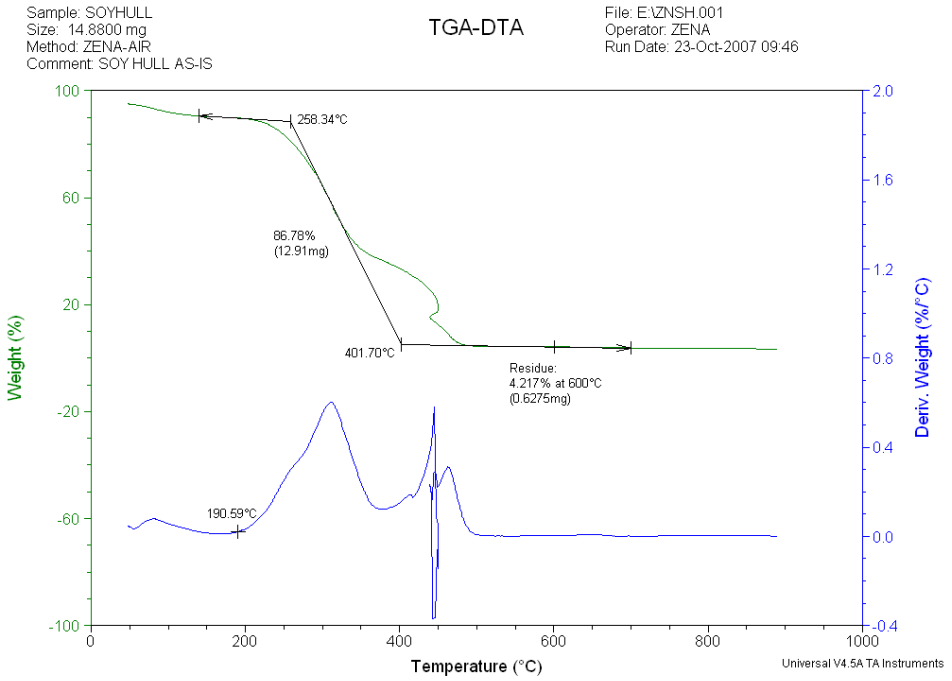

Figure A2.3: TGA (green) and DTA (blue) graph of SH filler

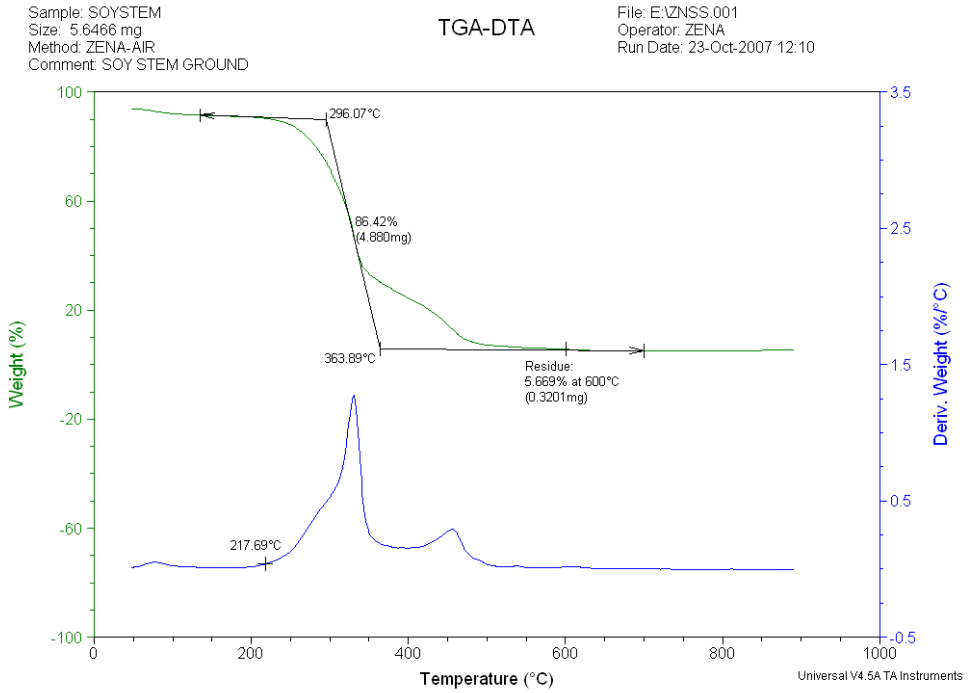

Figure A2.4: TGA (green) and DTA (blue) graph of SS filler

APPENDIX C – DSC Endotherms

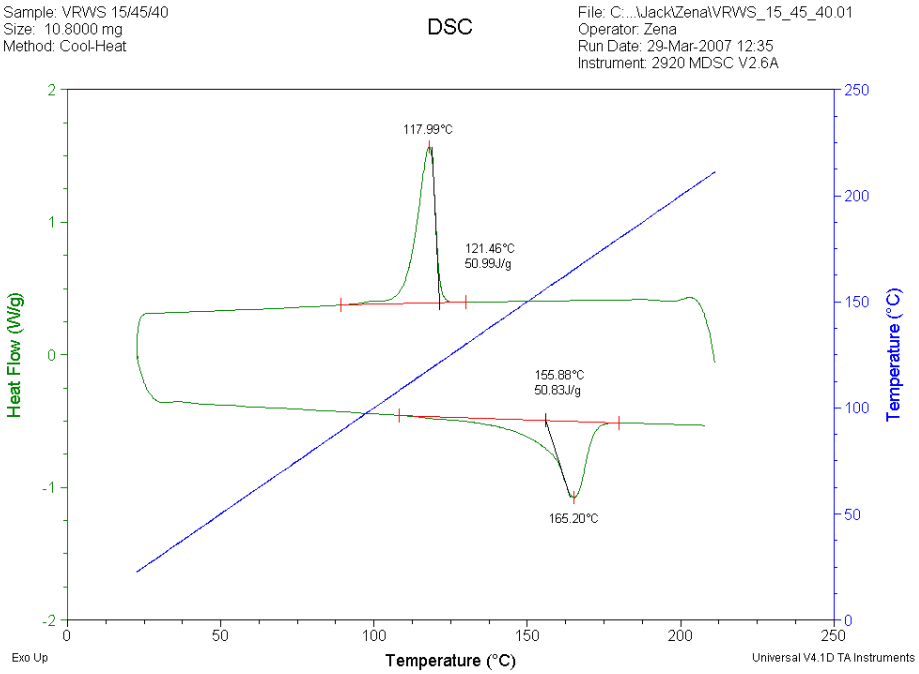

Figure A3.1: DSC endotherm for 40WS-15vPP-45rPP

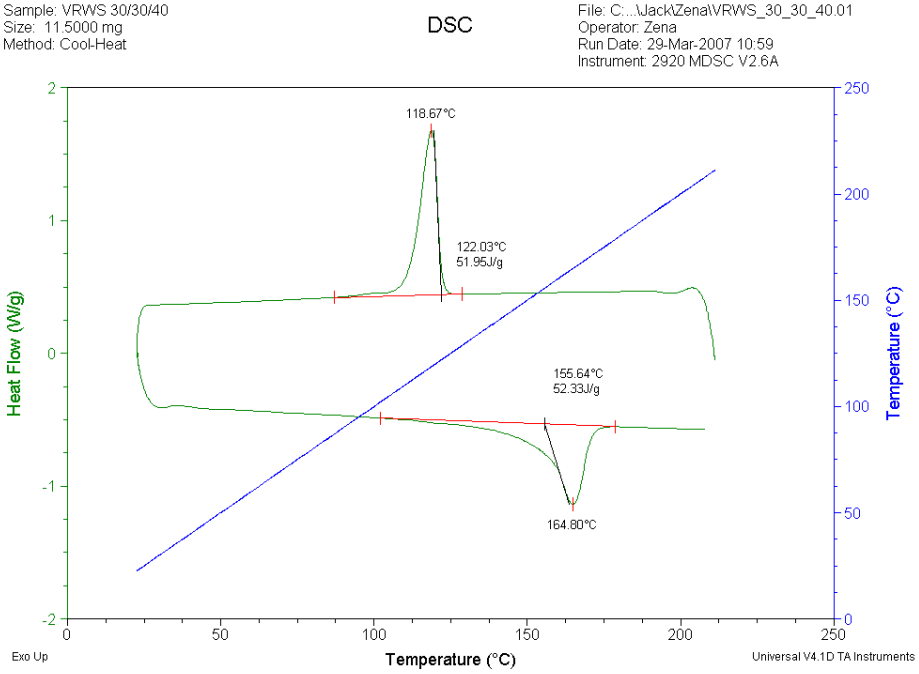

Figure A3.2: DSC endotherm for 40WS-30vPP-30rPP

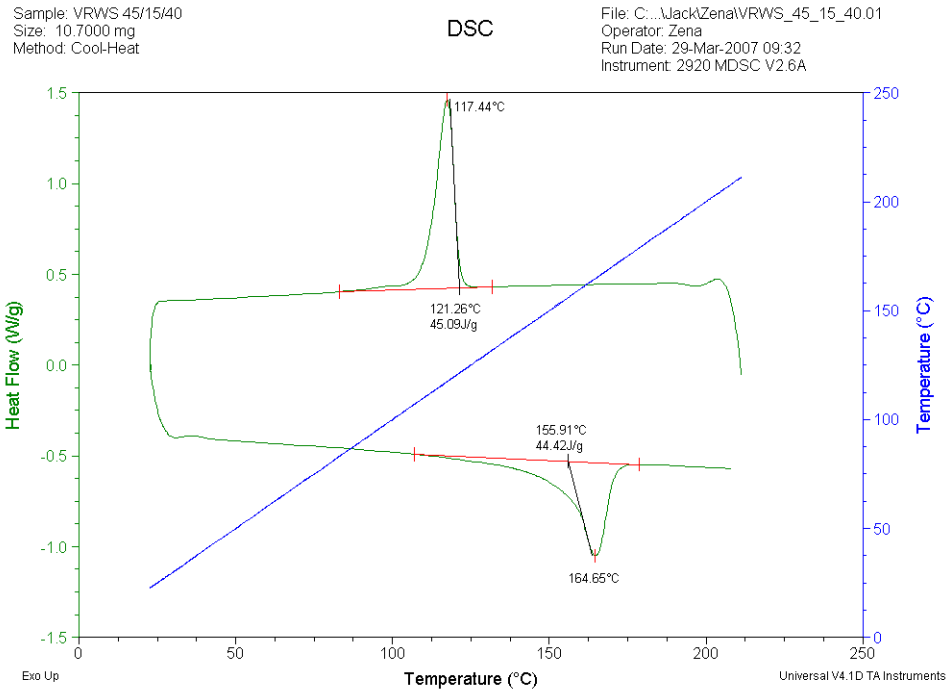

Figure A3.3: DSC endotherm for 40WS-45vPP-15rPP

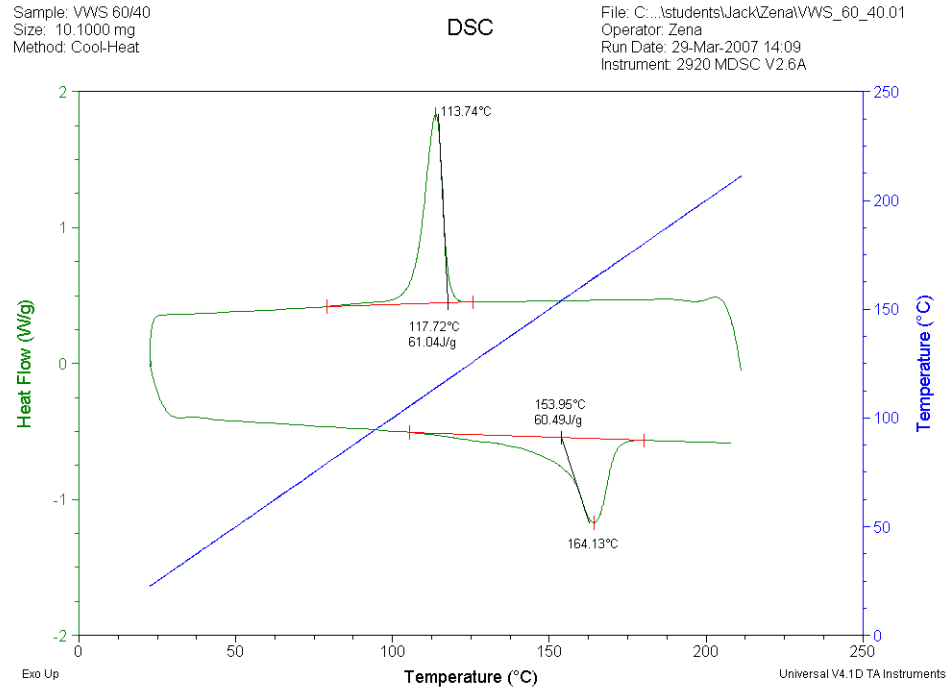

Figure A3.4: DSC endotherm for 40WS-60vPP-0rPP

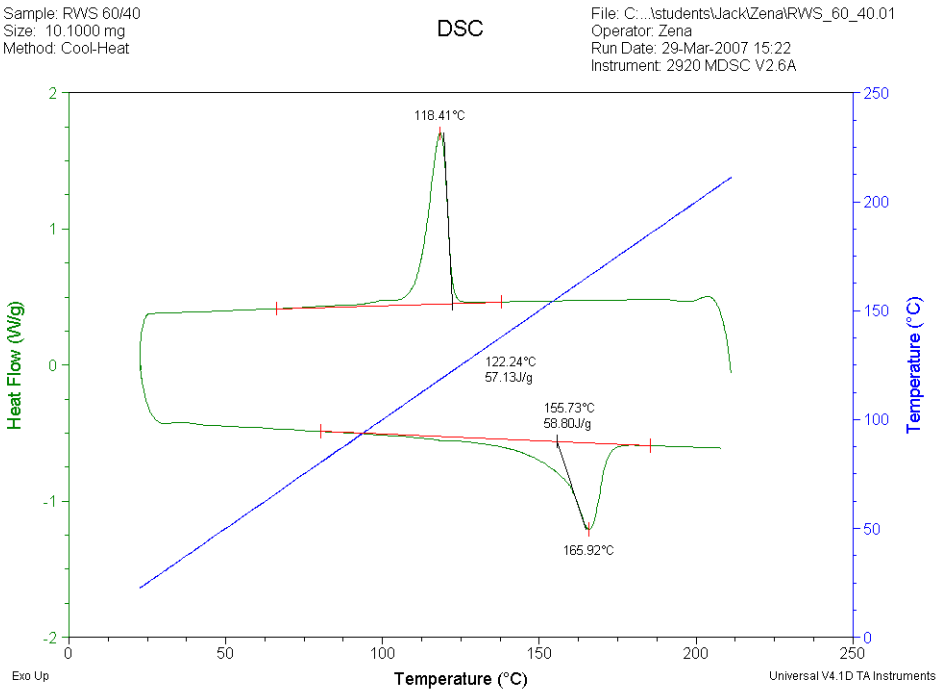

Figure A3. 5: DSC endotherm for 40WS-0vPP-60rPP

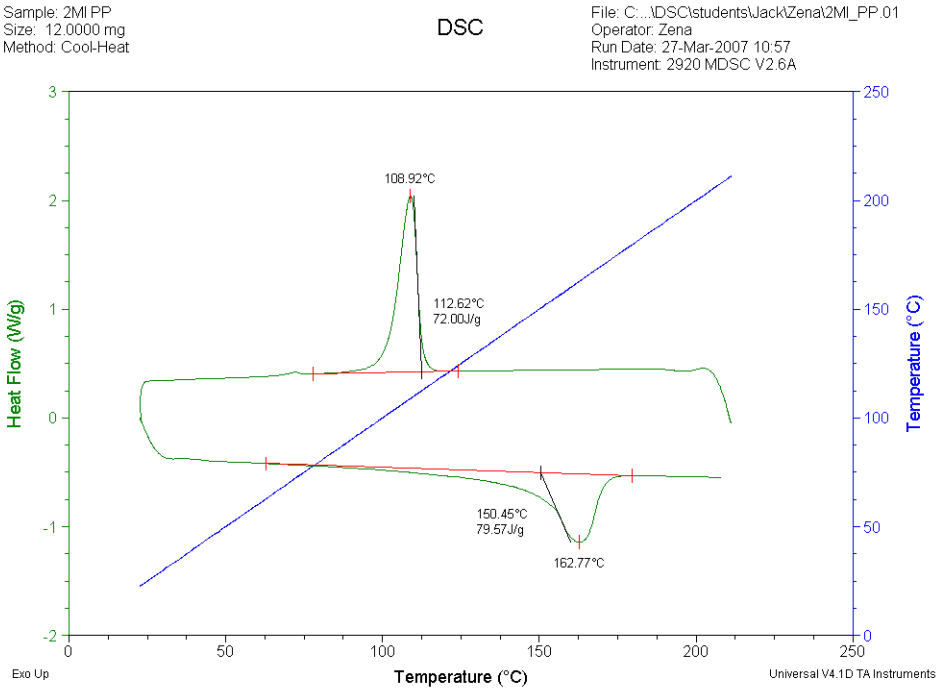

Figure A3. 6: DSC endotherm for vPP

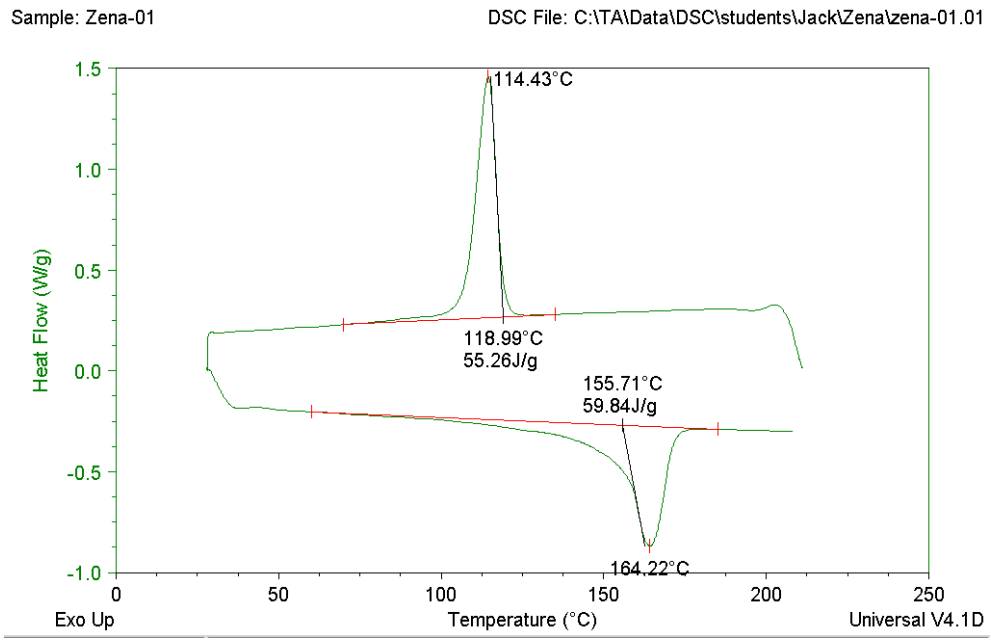

Figure A3.7: DSC endotherm for 40WS-60vPP-0rPP

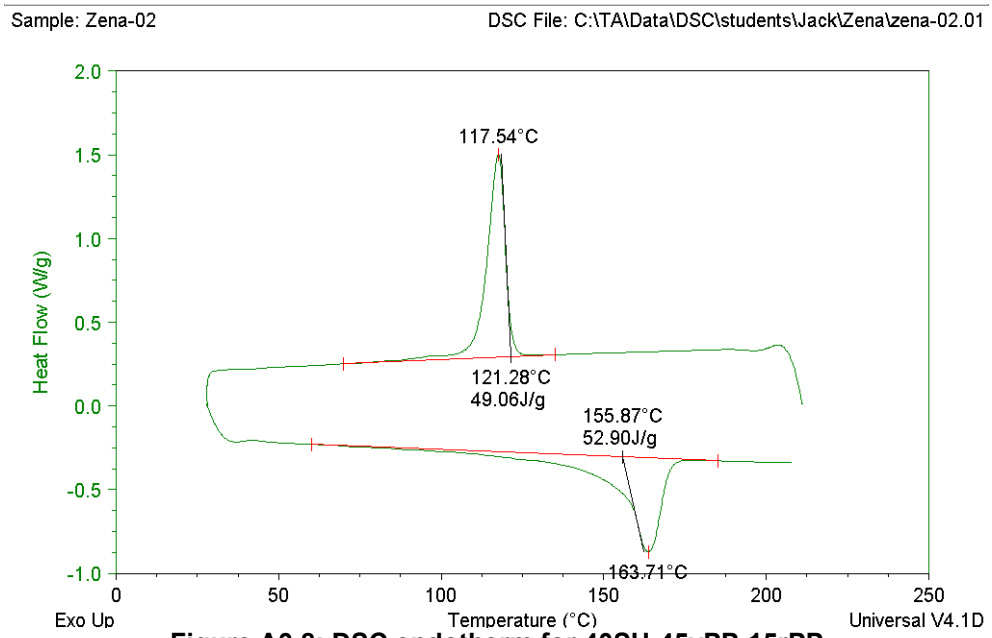

Figure A3.8: DSC endotherm for 40SH-45vPP-15rPP

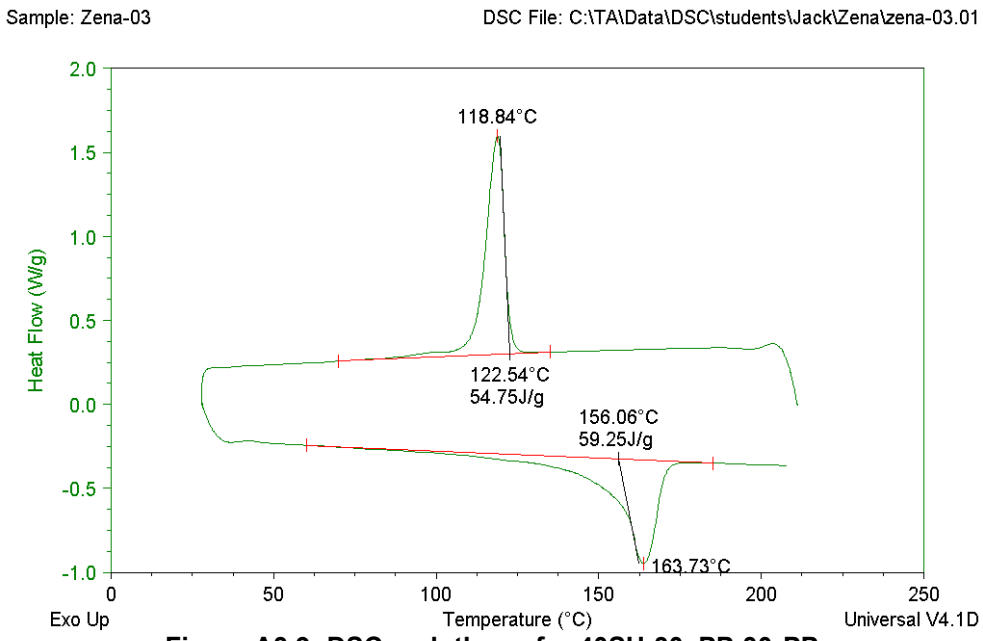

Figure A3.9: DSC endotherm for 40SH-30vPP-30rPP

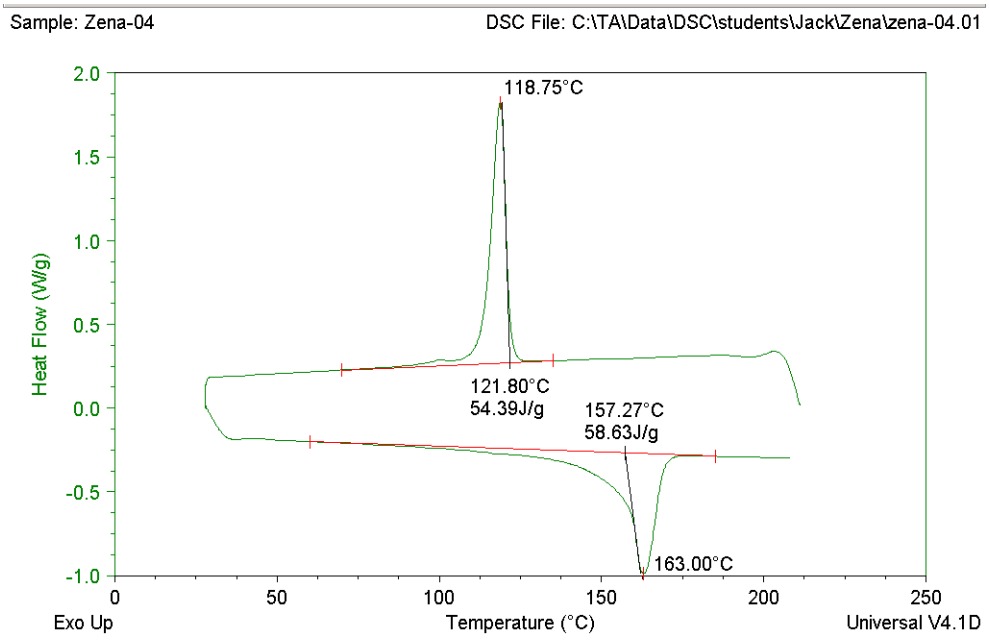

Figure A3.10: DSC endotherm for 40SH-15vPP-45rPP

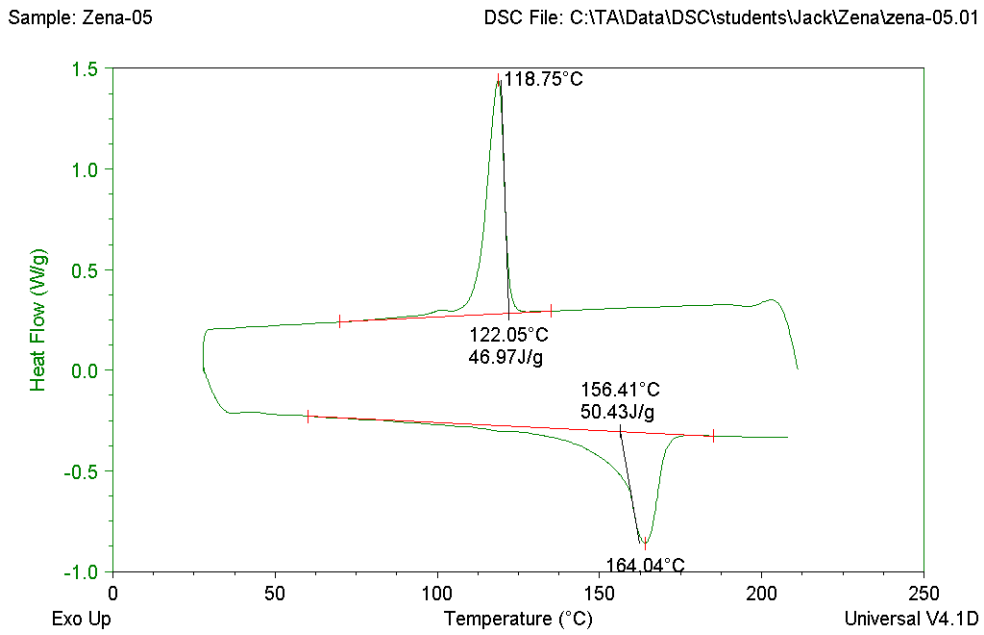

Figure A3.11: DSC endotherm for 40SH-0vPP-60rPP

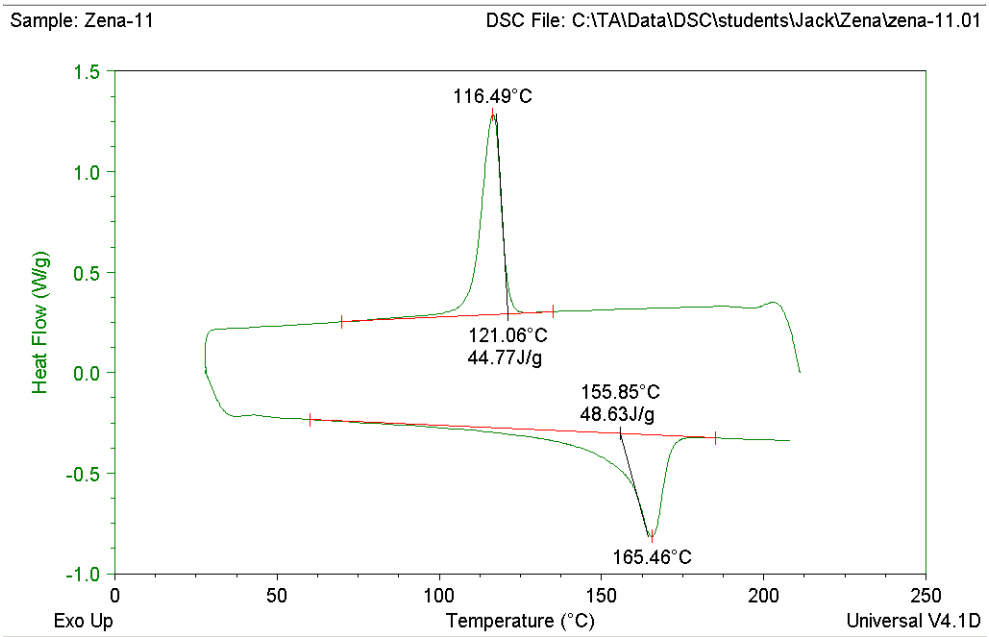

Figure A3.12: DSC endotherm for 40SS-60vPP-0rPP

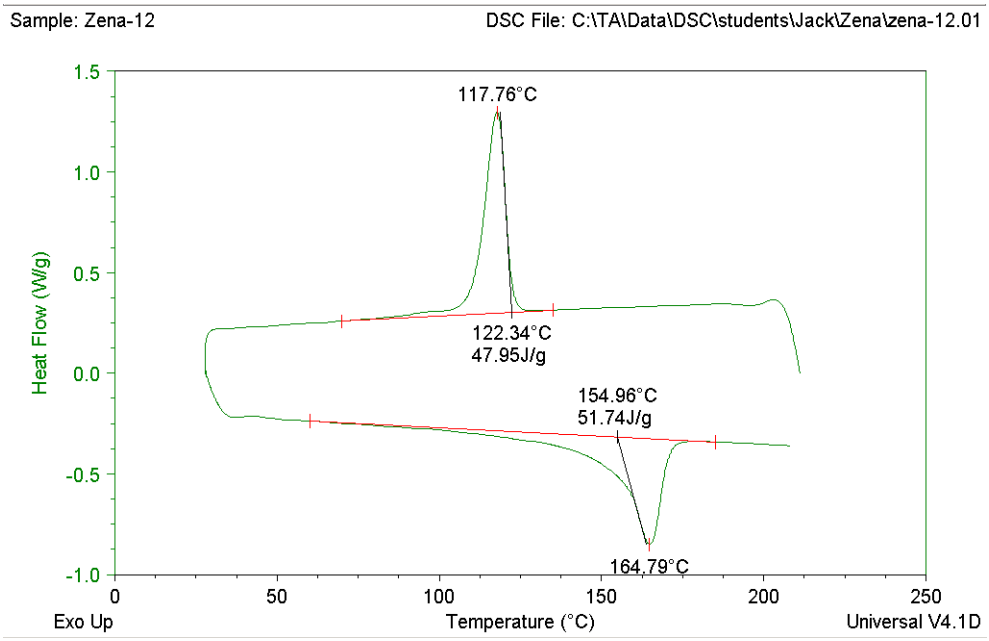

Figure A3.13: DSC endotherm for 40SS-45vPP-15rPP

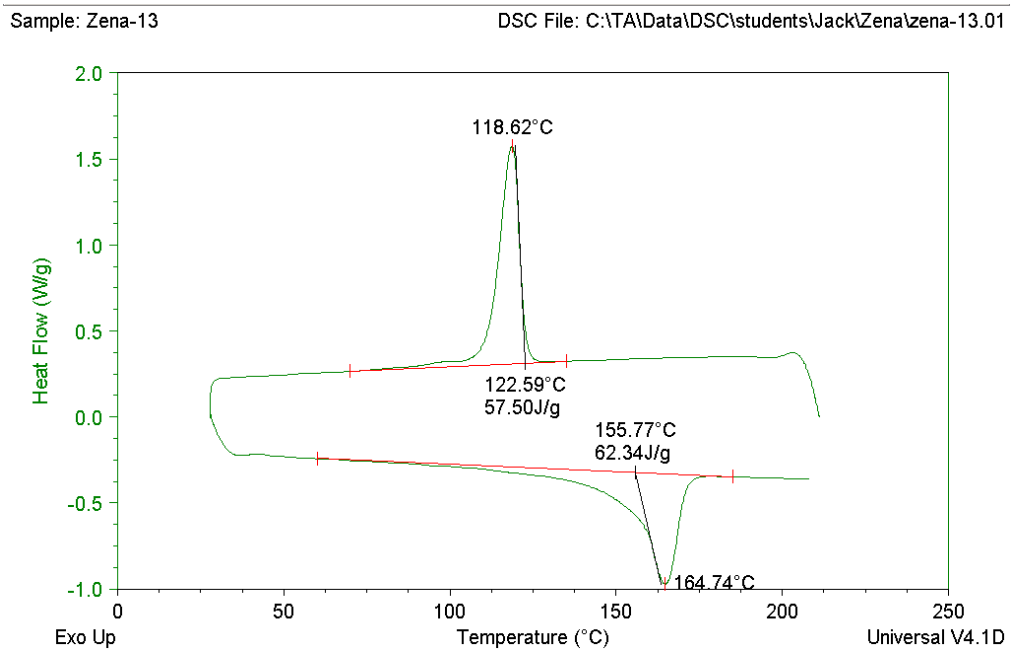

Figure A3.14: DSC endotherm for 40SS-30vPP-30rPP

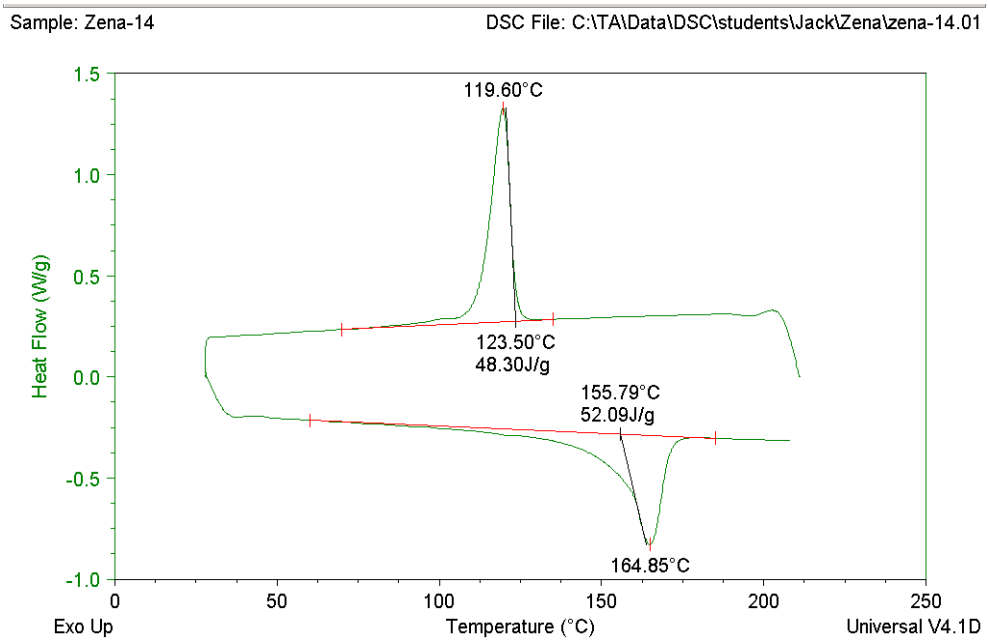

Figure A3.15: DSC endotherm for 40SS-15vPP-45rPP

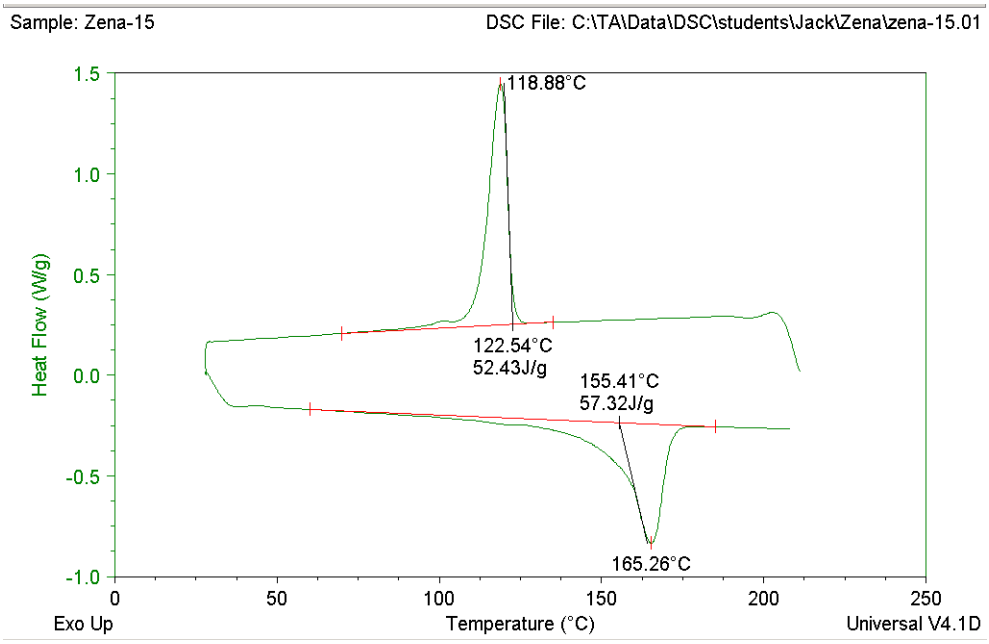

Figure A3.16: DSC endotherm for 40SS-0vPP-60rPP

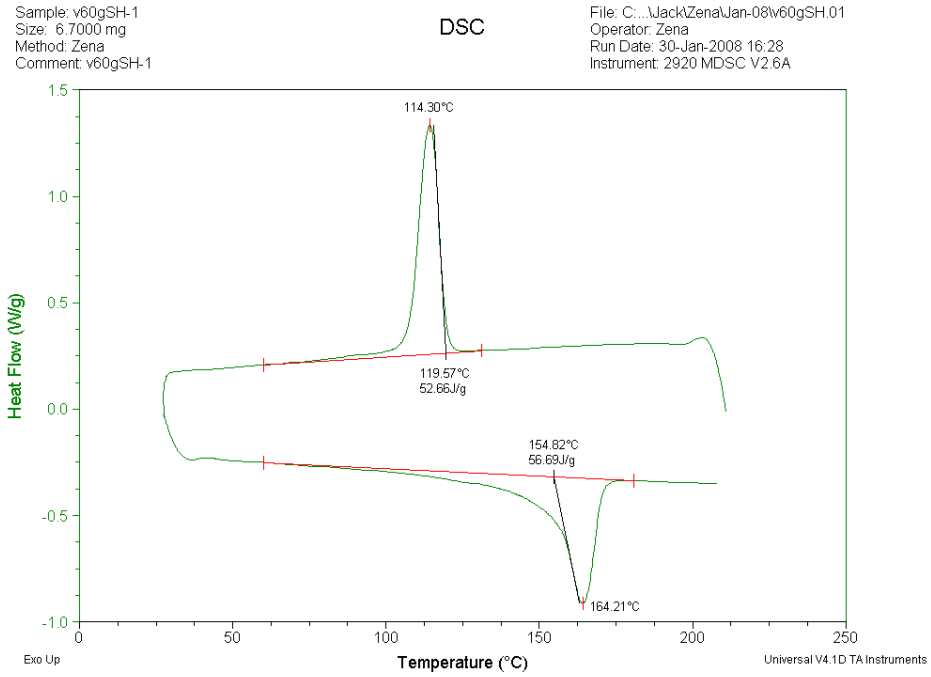

Figure A3.17: DSC endotherm for 40gSH-60vPP-0rPP

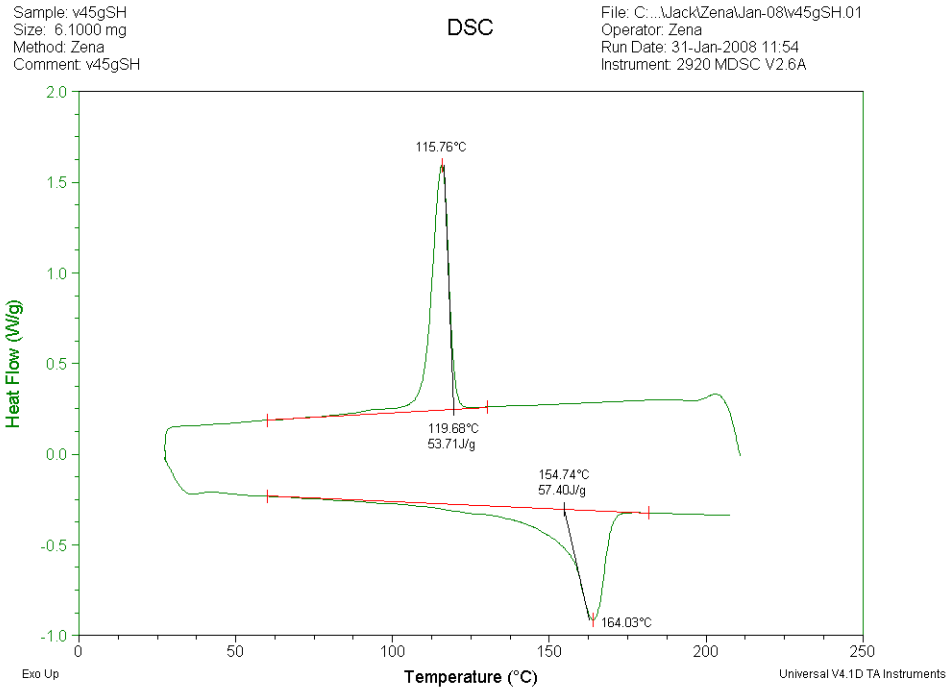

Figure A3.18: DSC endotherm for 40gSH-45vPP-15rPP

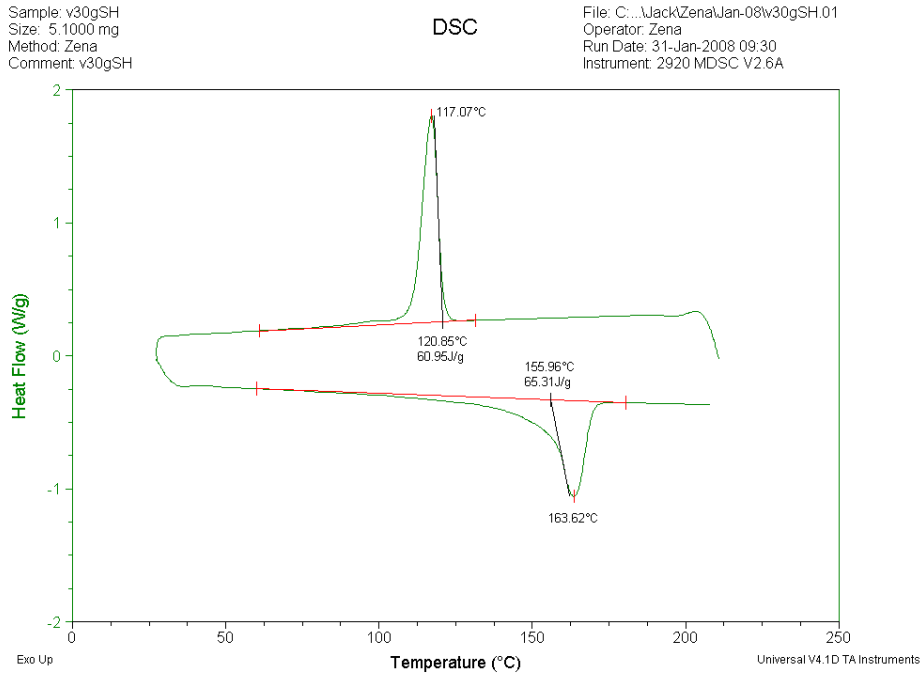

Figure A3.19: DSC endotherm for 40gSH-30vPP-30rPP

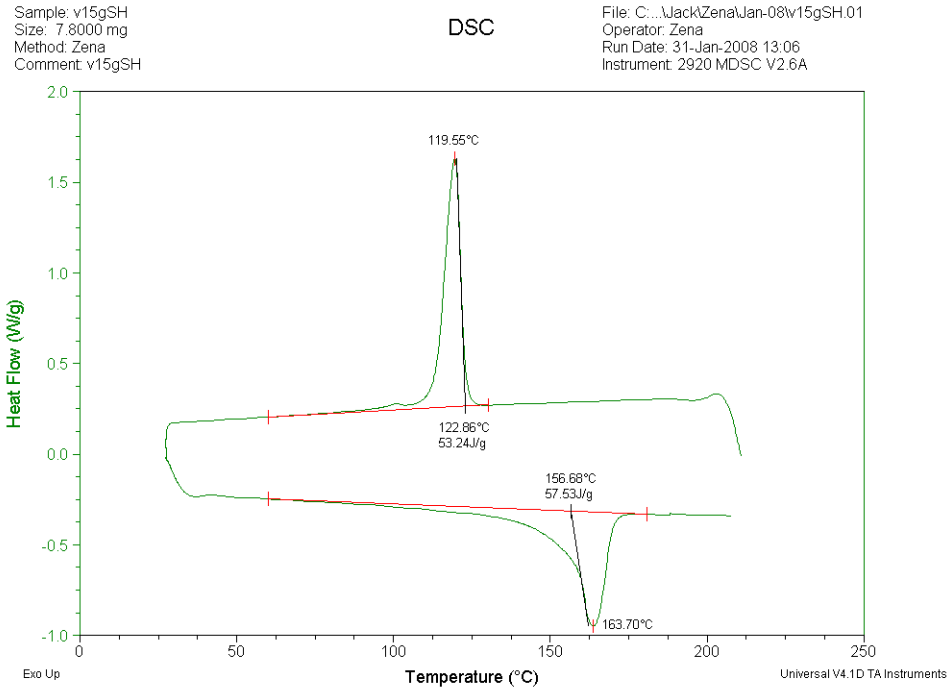

Figure A3.20: DSC endotherm for 40gSH-15vPP-45rPP

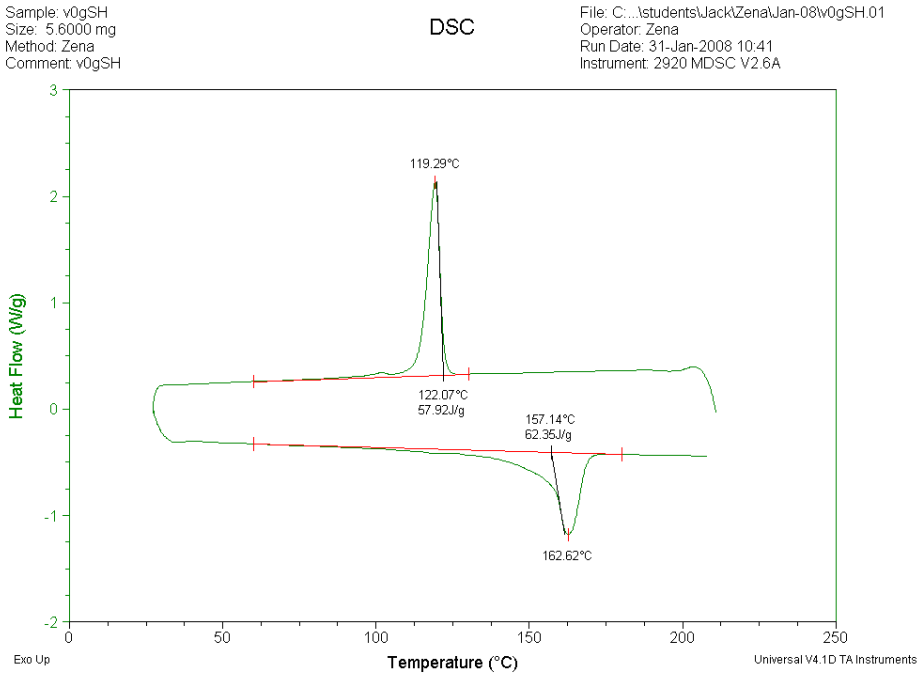

Figure A3.21: DSC endotherm for 40gSH-0vPP-60rPP

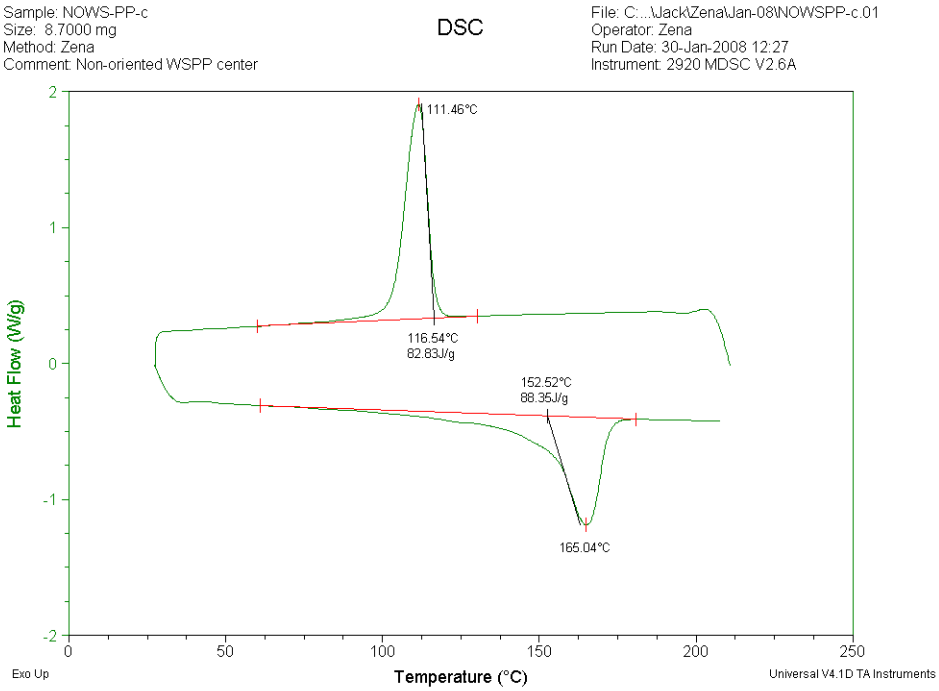

Figure A3.22: DSC endotherm for non-oriented WSPP center

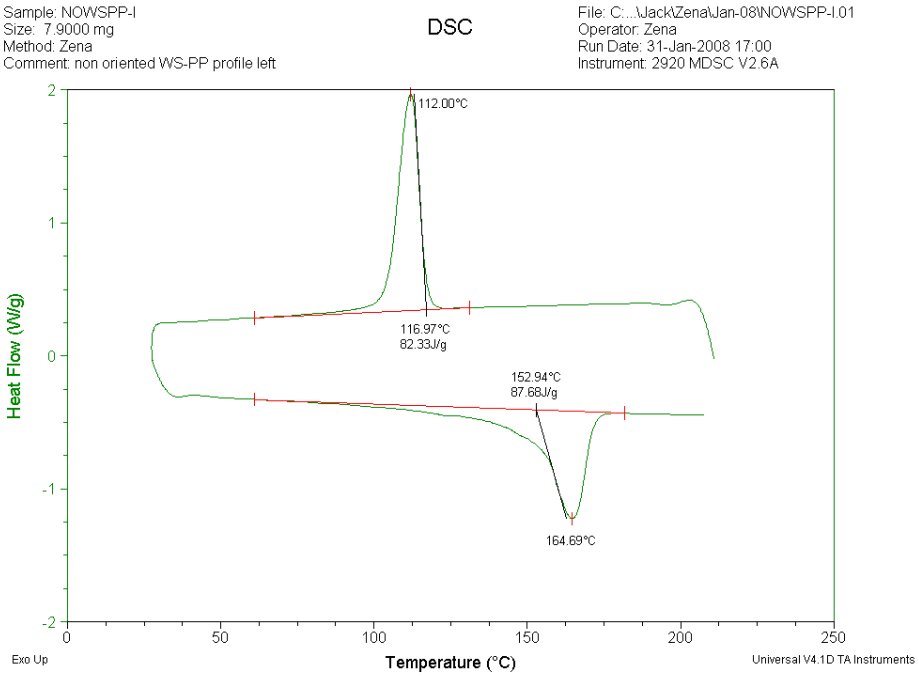

Figure A3.23: DSC endotherm for non-oriented WSPP left

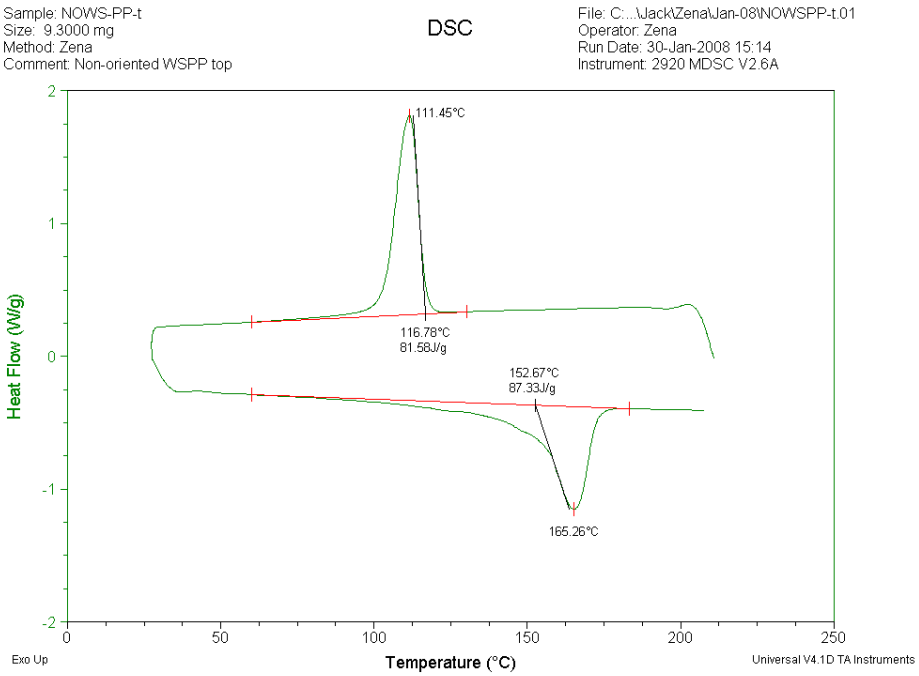

Figure A3.24: DSC endotherm for non-oriented WSPP top

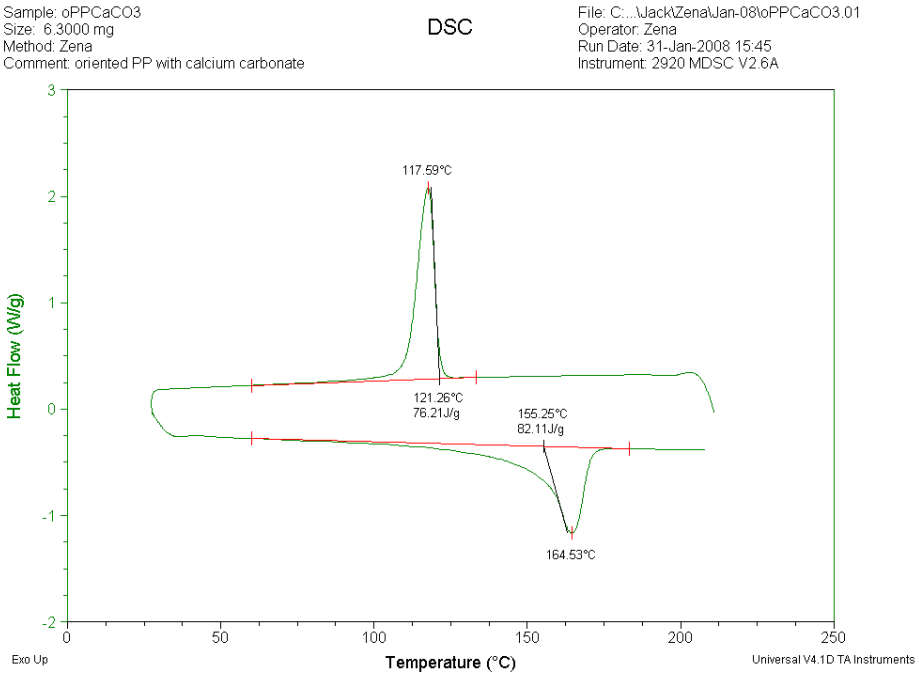

Figure A3 25: DSC endotherm for oriented CaCO3-PP

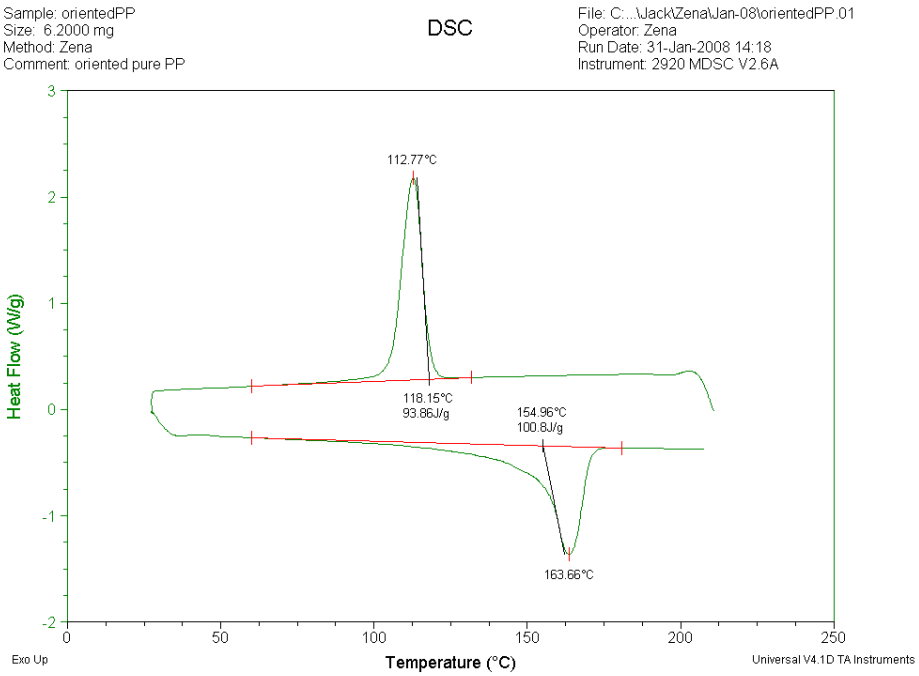

Figure A3.26: DSC endotherm of oriented PP

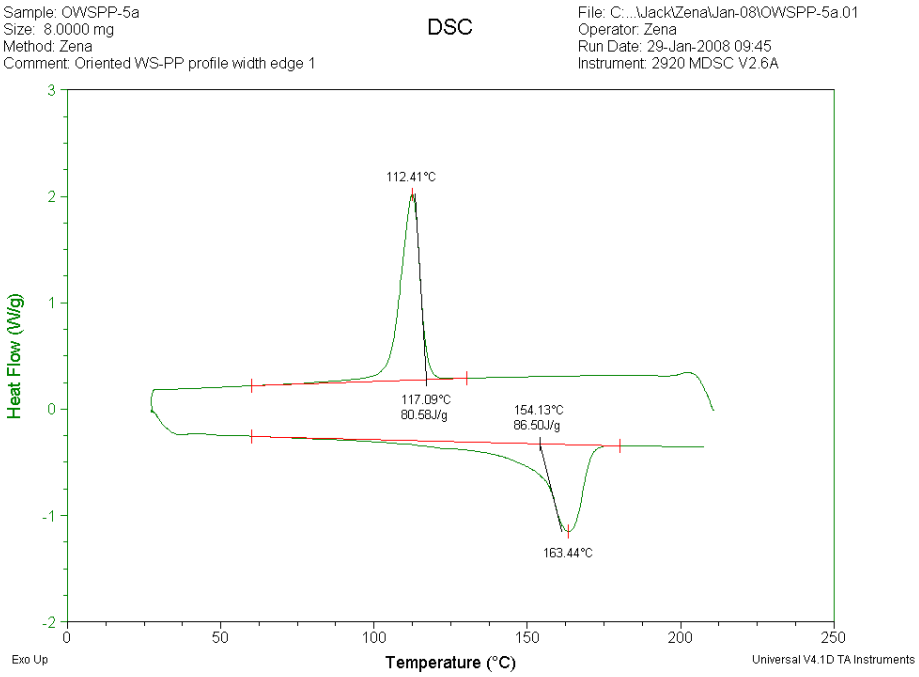

Figure A3.27: DSC endotherm for oriented WSPP width edge (position 1)

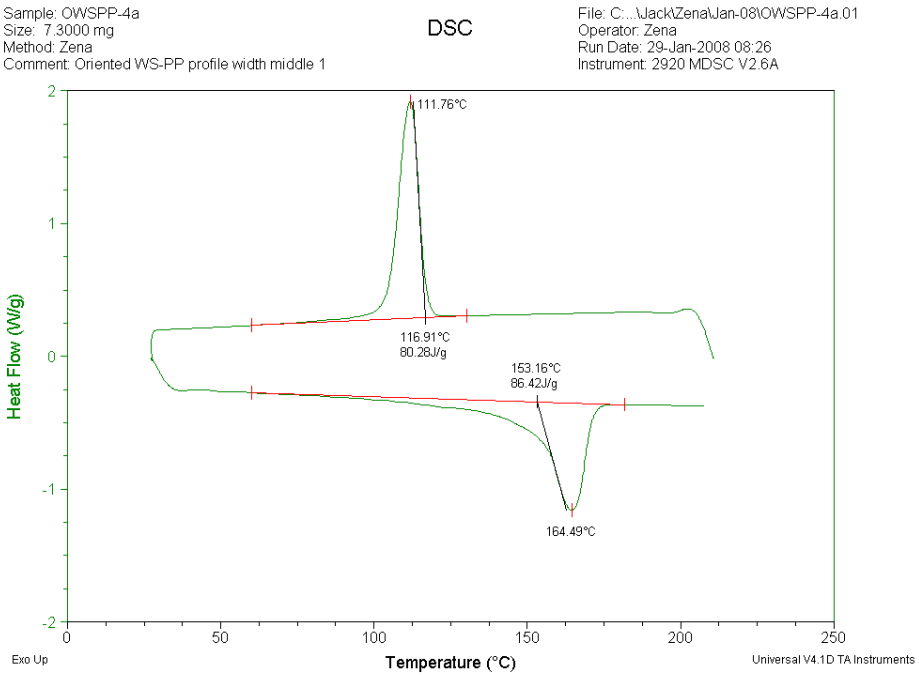

Figure A3 28: DSC endotherm for oriented WSPP widthmiddle (position 2)

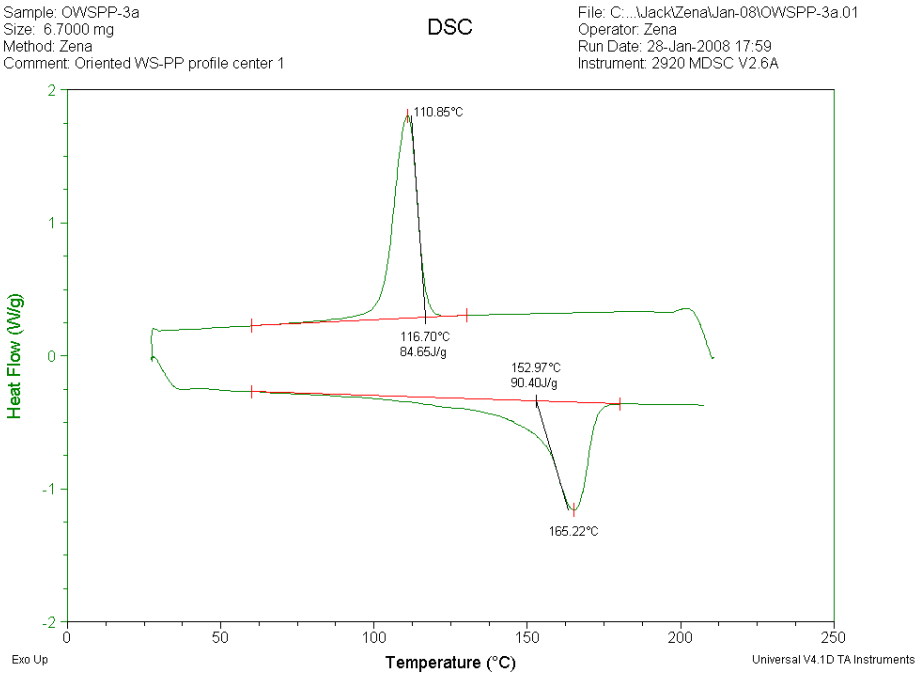

Figure A3.29: DSC endotherm for oriented WSPP center (position 3)

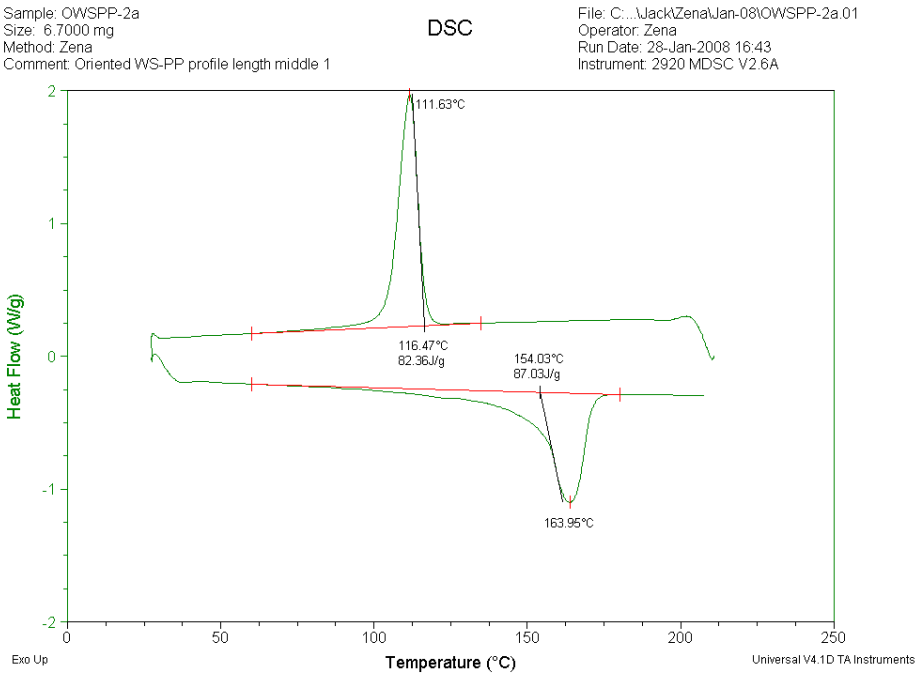

Figure A3.30: DSC endotherm for oriented WSPP length middle (position 4)

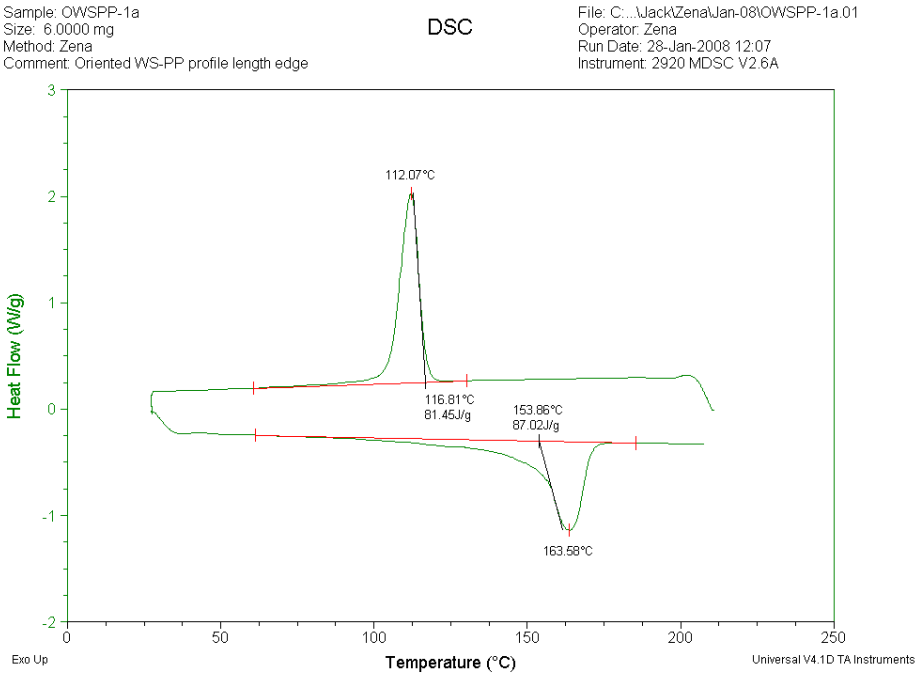

Figure A3.31: DSC endotherm for oriented WSPP length edge (position 5)

APPENDIX D – FTIR Spectra

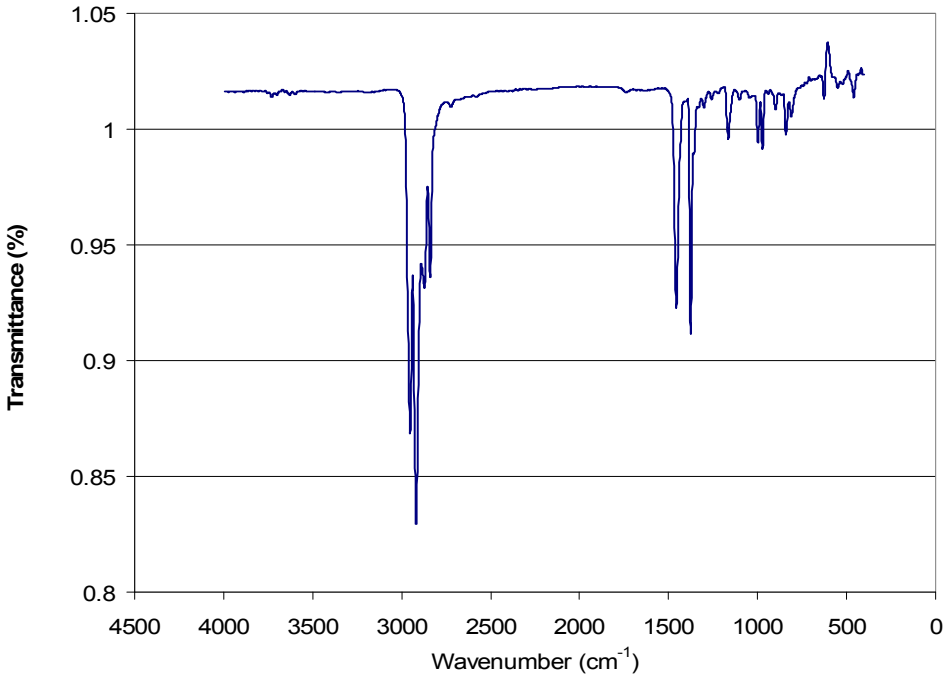

Figure A4.1: ATR-FTIR spectrum for vPP, sample #1

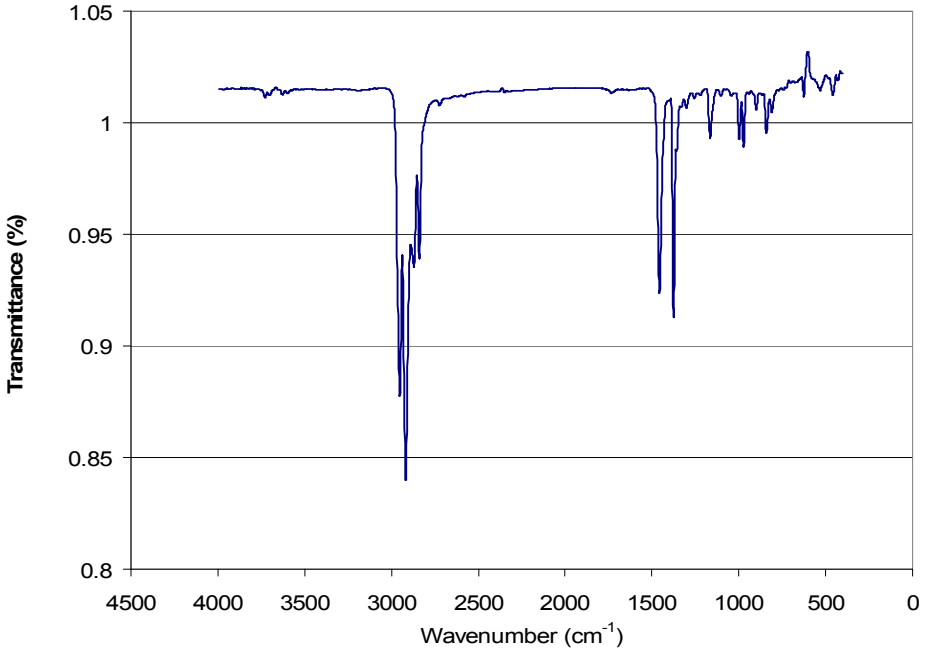

Figure A4.2: ATR-FTIR spectrum for vPP, sample #2

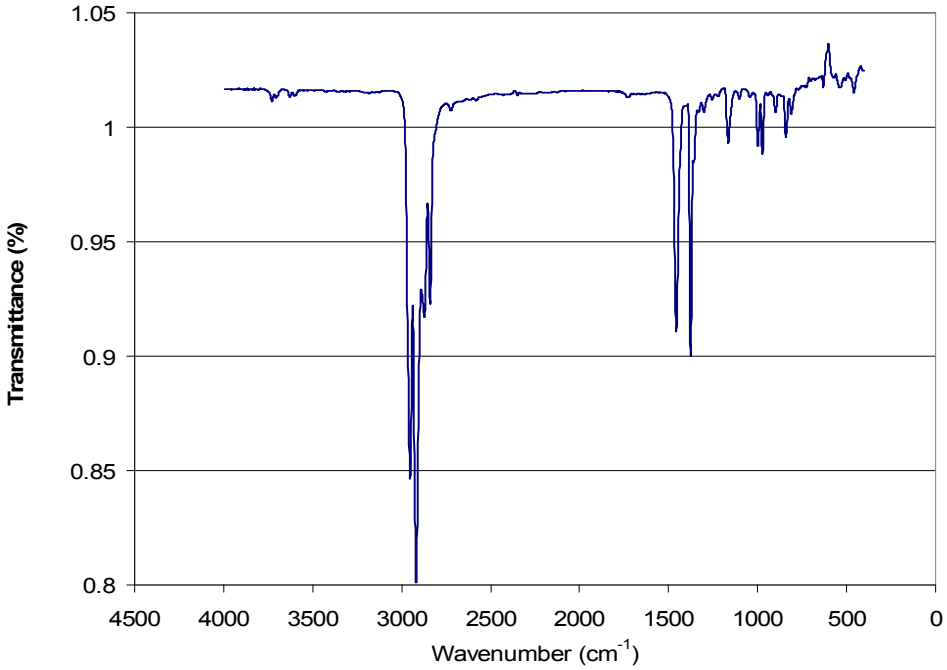

Figure A4.3: ATR-FTIR spectrum for vPP, sample #3

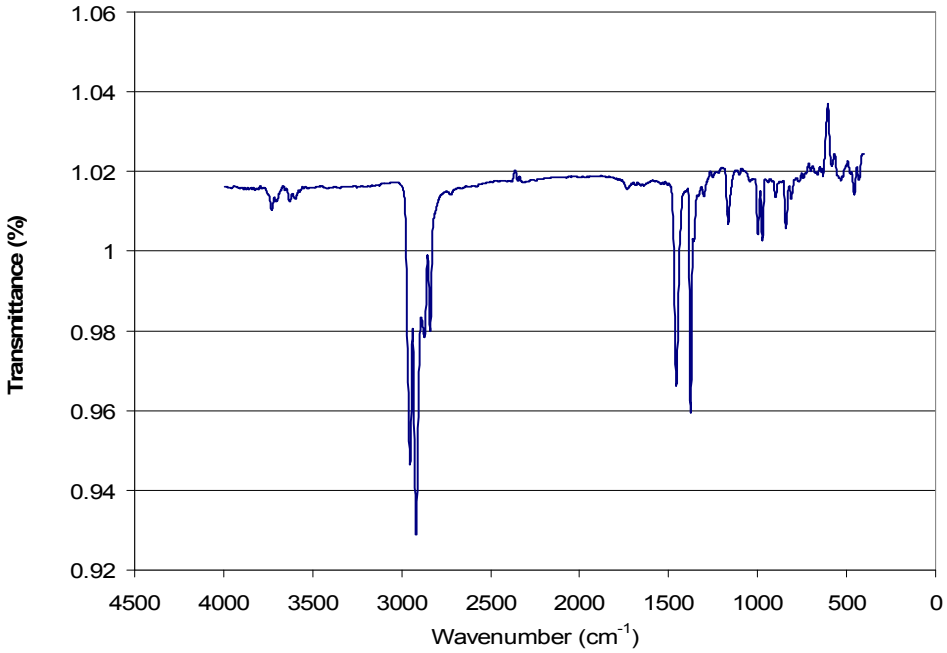

Figure A4.4: ATR-FTIR spectrum of 40gSH-60vPP-0rPP, sample #1

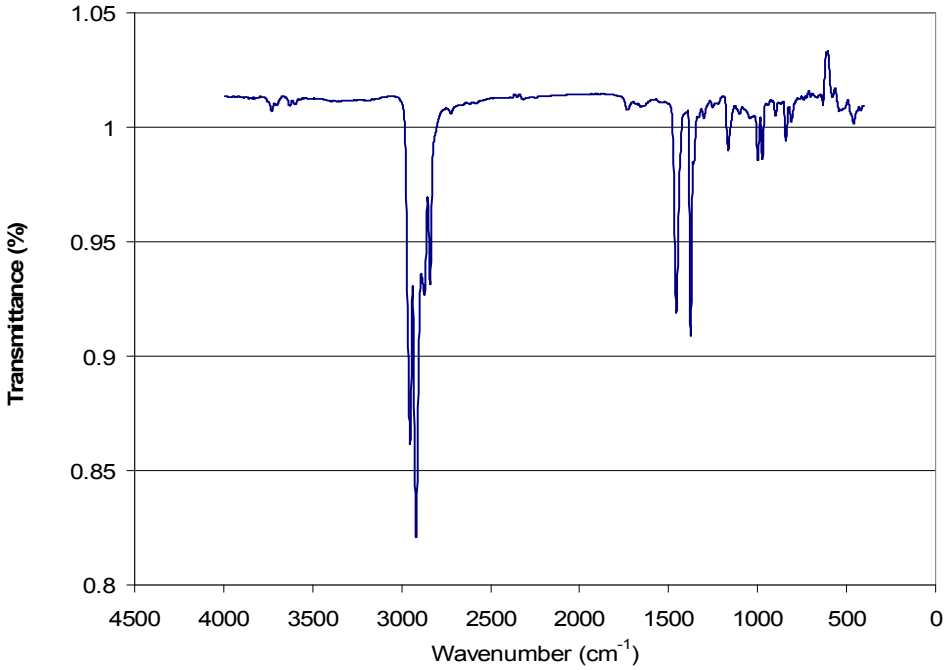

Figure A4.5: ATR-FTIR spectrum for 40gSH-60vPP-0rPP, sample #2

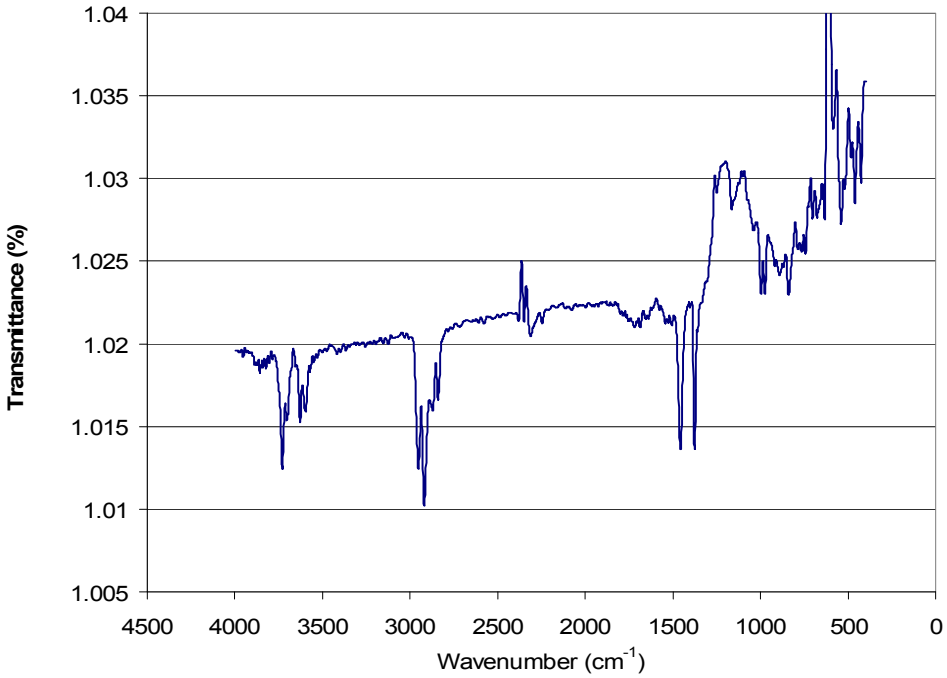

Figure A4.6: ATR-FTIR spectrum of 40gSH-60vPP-0rPP, sample #3

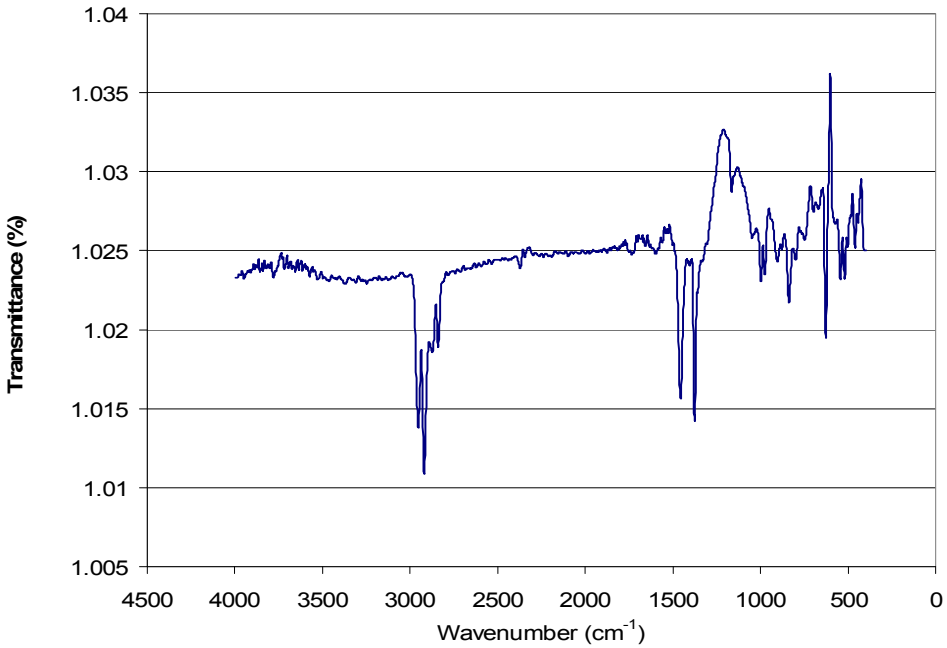

Figure A4. 7: ATR-FTIR spectrum of 40gSH-0vPP-60rPP

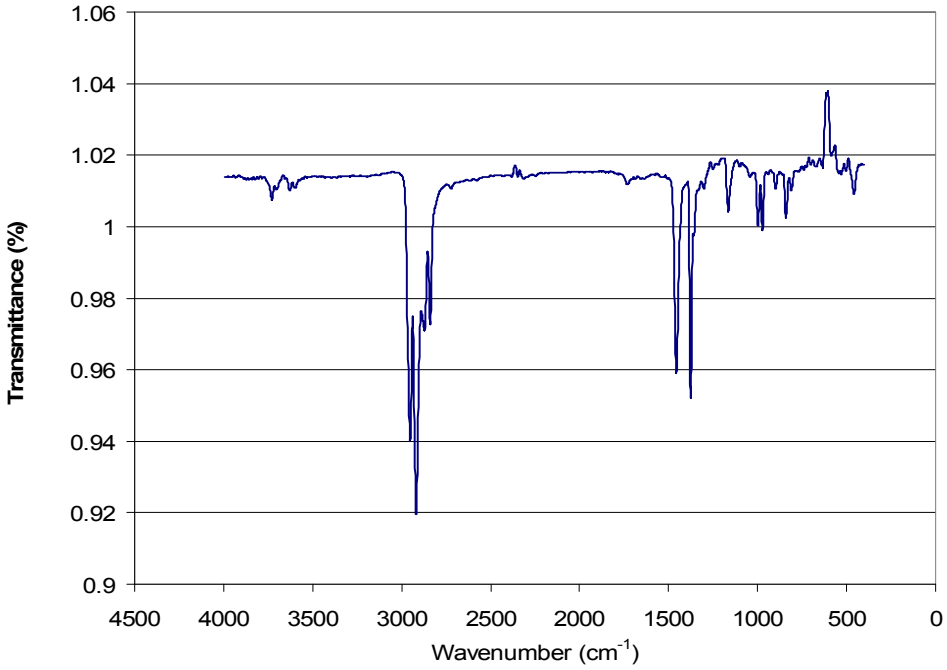

Figure A4.8: ATR-FTIR spectrum of 40SH-60vPP-0rPP

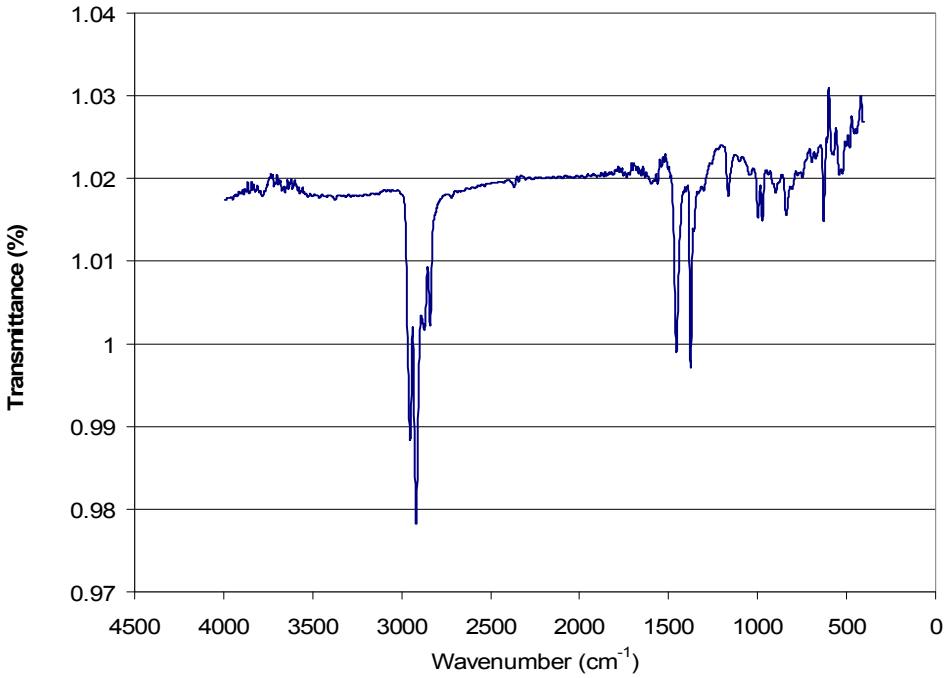

Figure A4.9: ATR-FTIR spectrum of 40SH-30vPP-30rPP

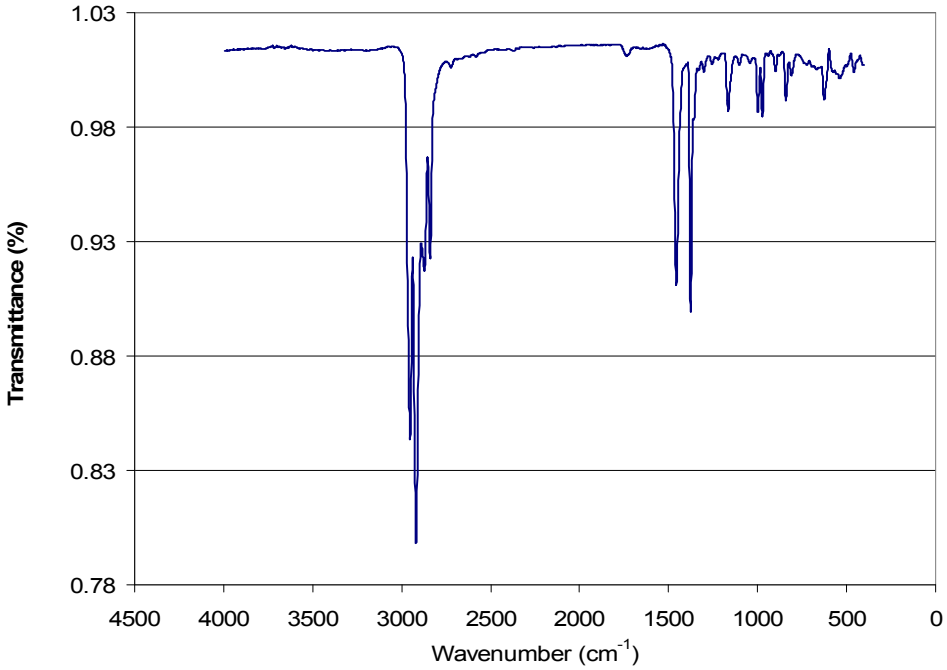

Figure A4.10: ATR-FTIR spectrum of 40SH-15vPP-45rPP

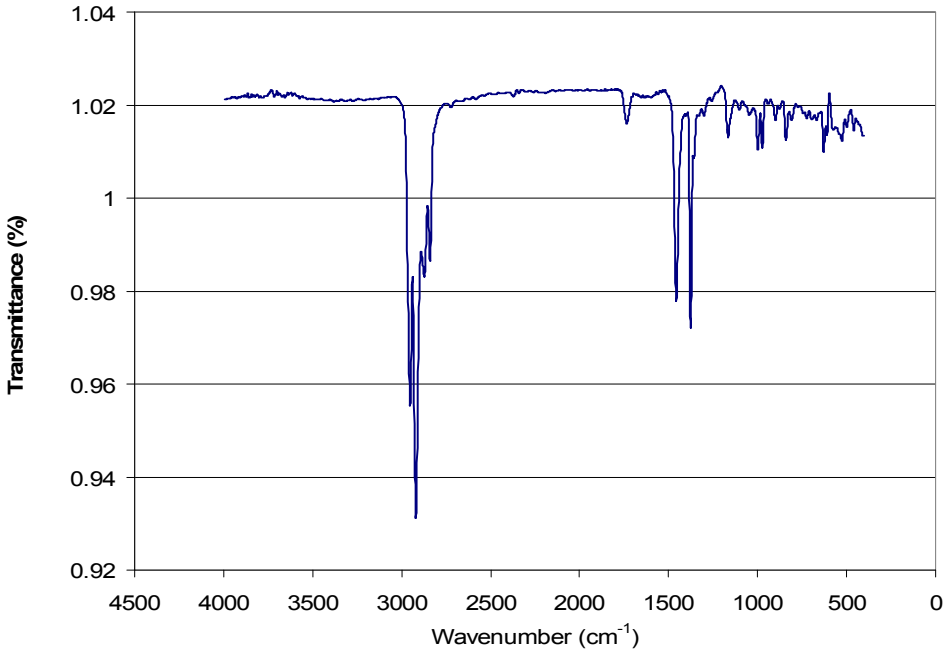

Figure A4.11: ATR-FTIR spectrum of 40SH-0vPP-60rPP

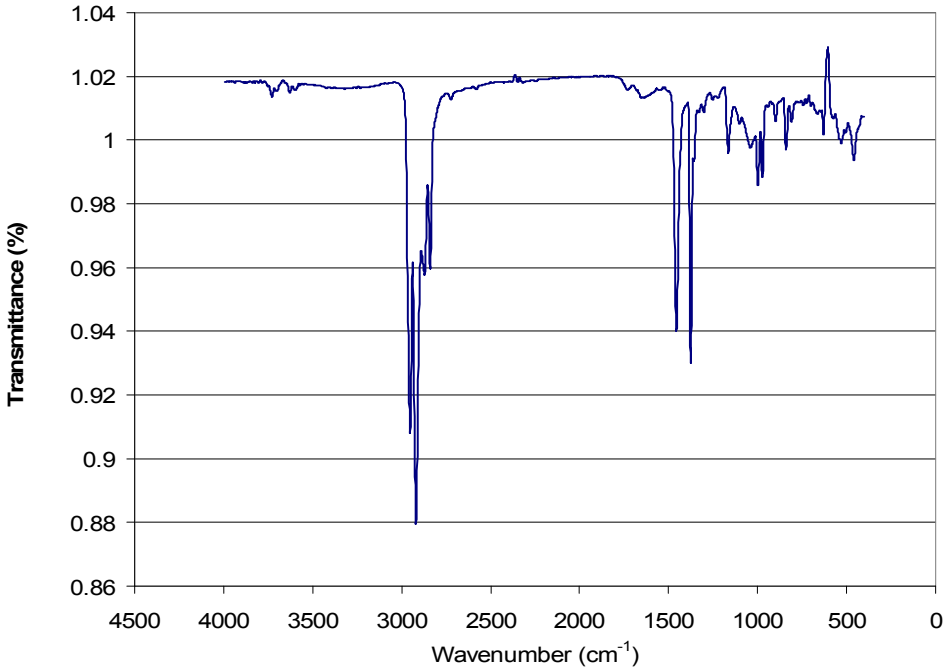

Figure A4.12: ATR-FTIR spectrum of 40SS-60vPP-0rPP

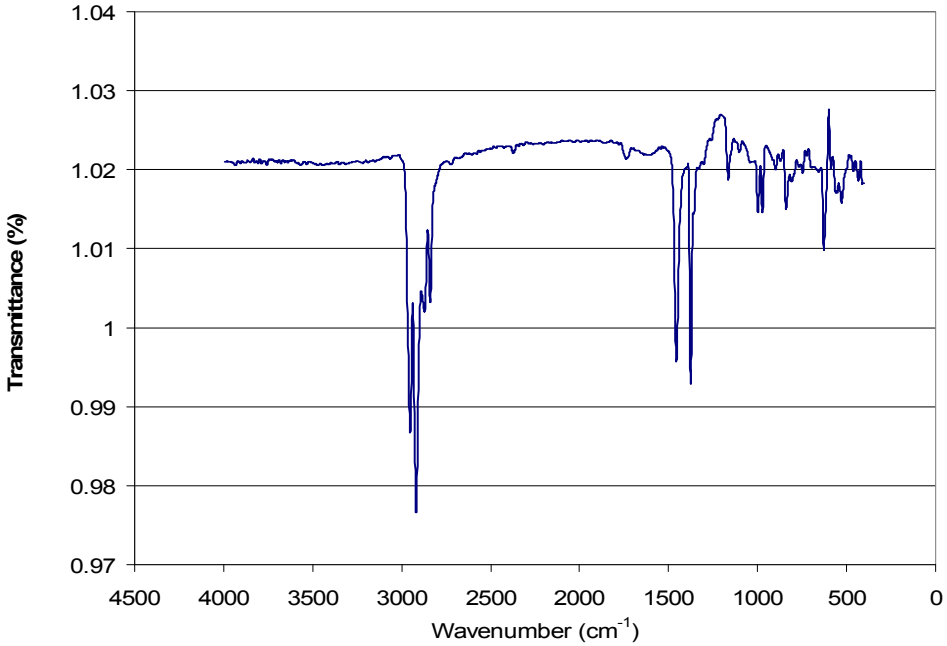

Figure A4.13: ATR-FTIR spectrum of 40SS-0vPP-60rPP

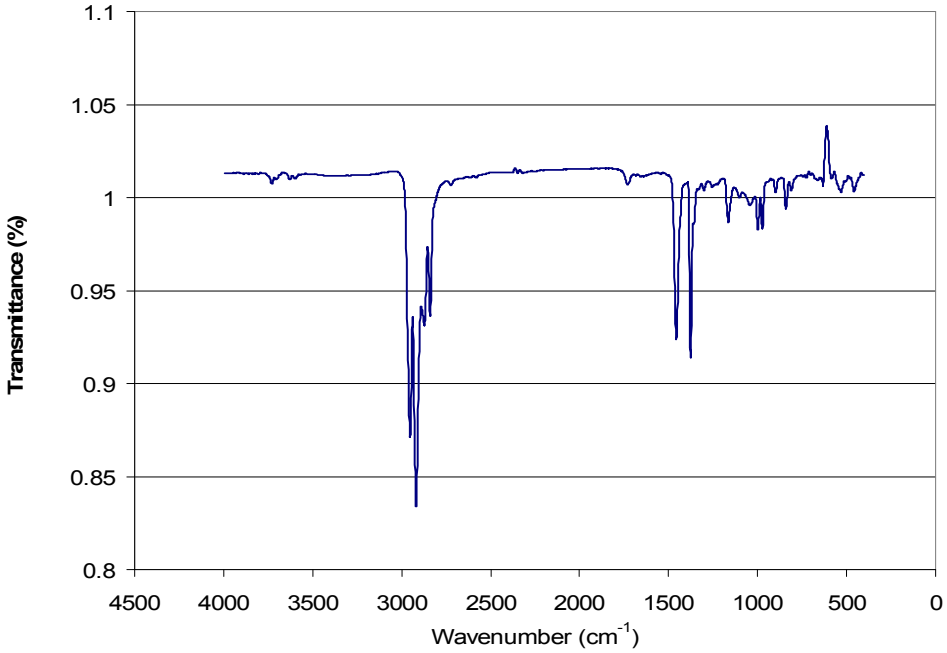

Figure A4.14: ATR-FTIR spectrum of 40WS-60vPP-0rPP

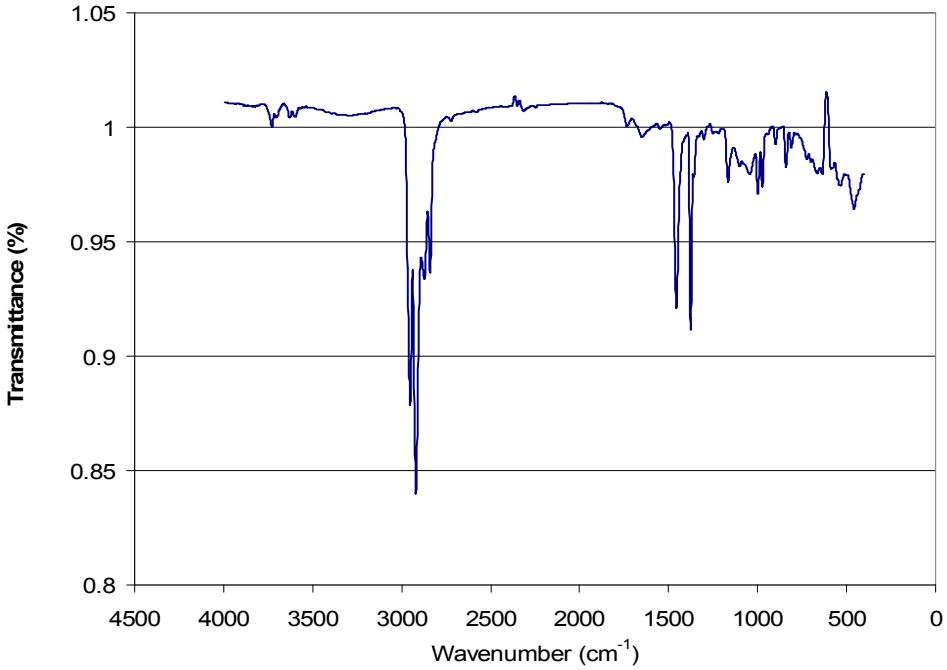

Figure A4.15: ATR-FTIR spectrum of 40WS-0vPP-60rPP

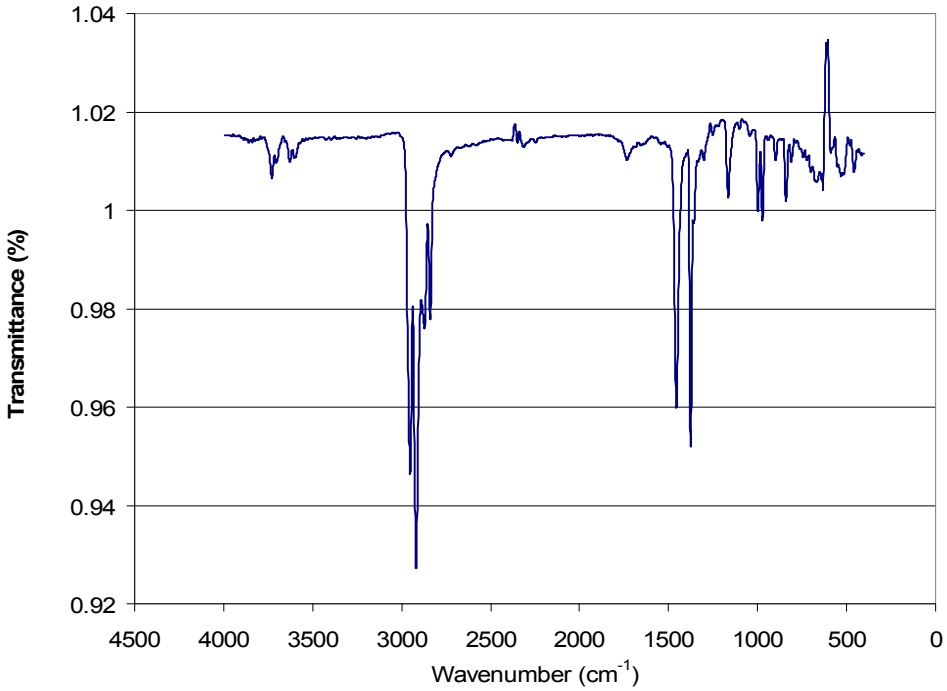

Figure A4.16: ATR-FTIR spectrum for rPP

APPENDIX E – OMAFRA public display information

This OMAFRA public display information brochure was prepared with the help of Dr. Leonardo Simon and Dr. Larry Erickson, to introduce to the public the research on AgFiller-PP composites, and to demonstrate the feasibility of such work for commercialization.

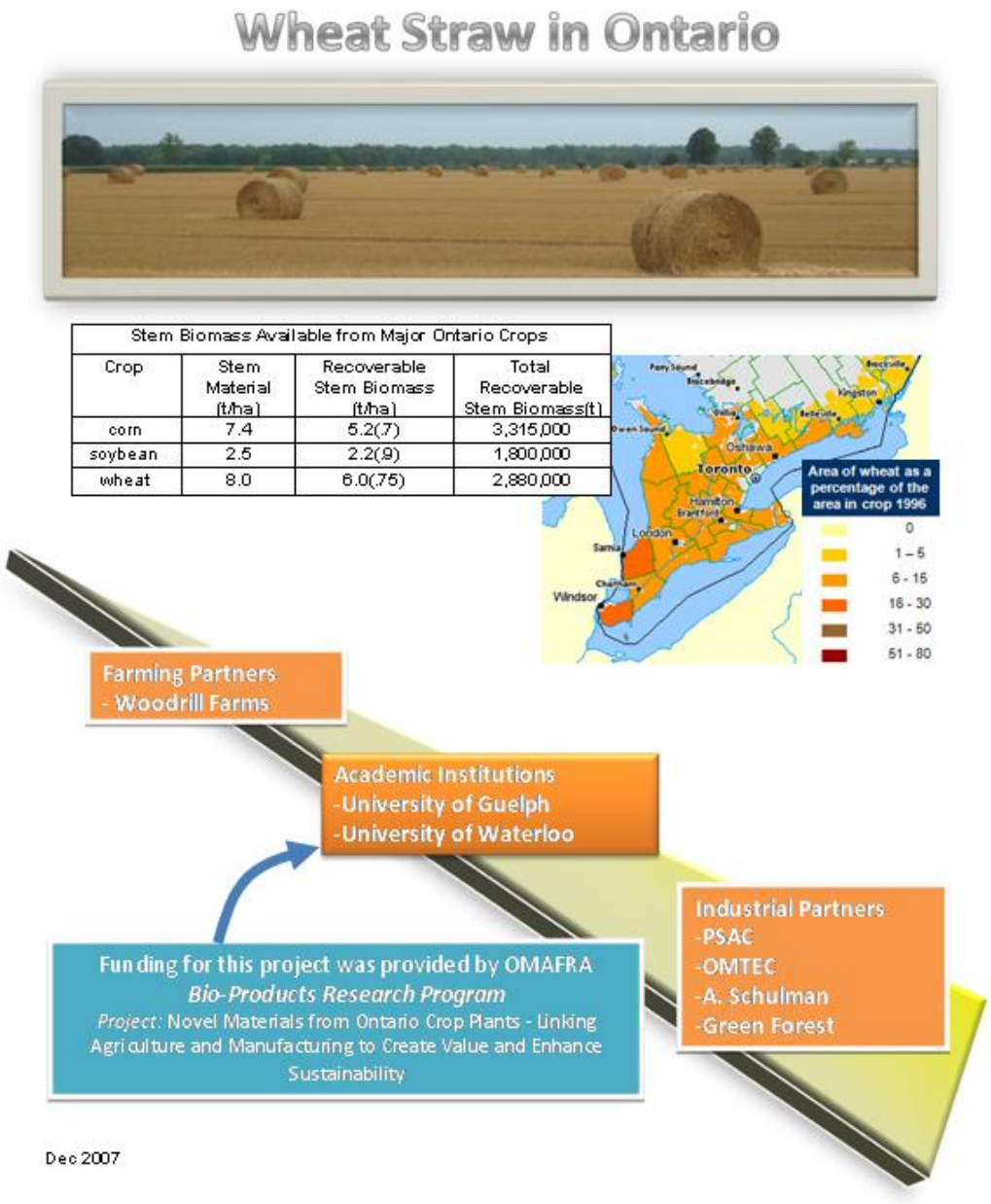

Figure A5.1: OMAFRA display information, page 1

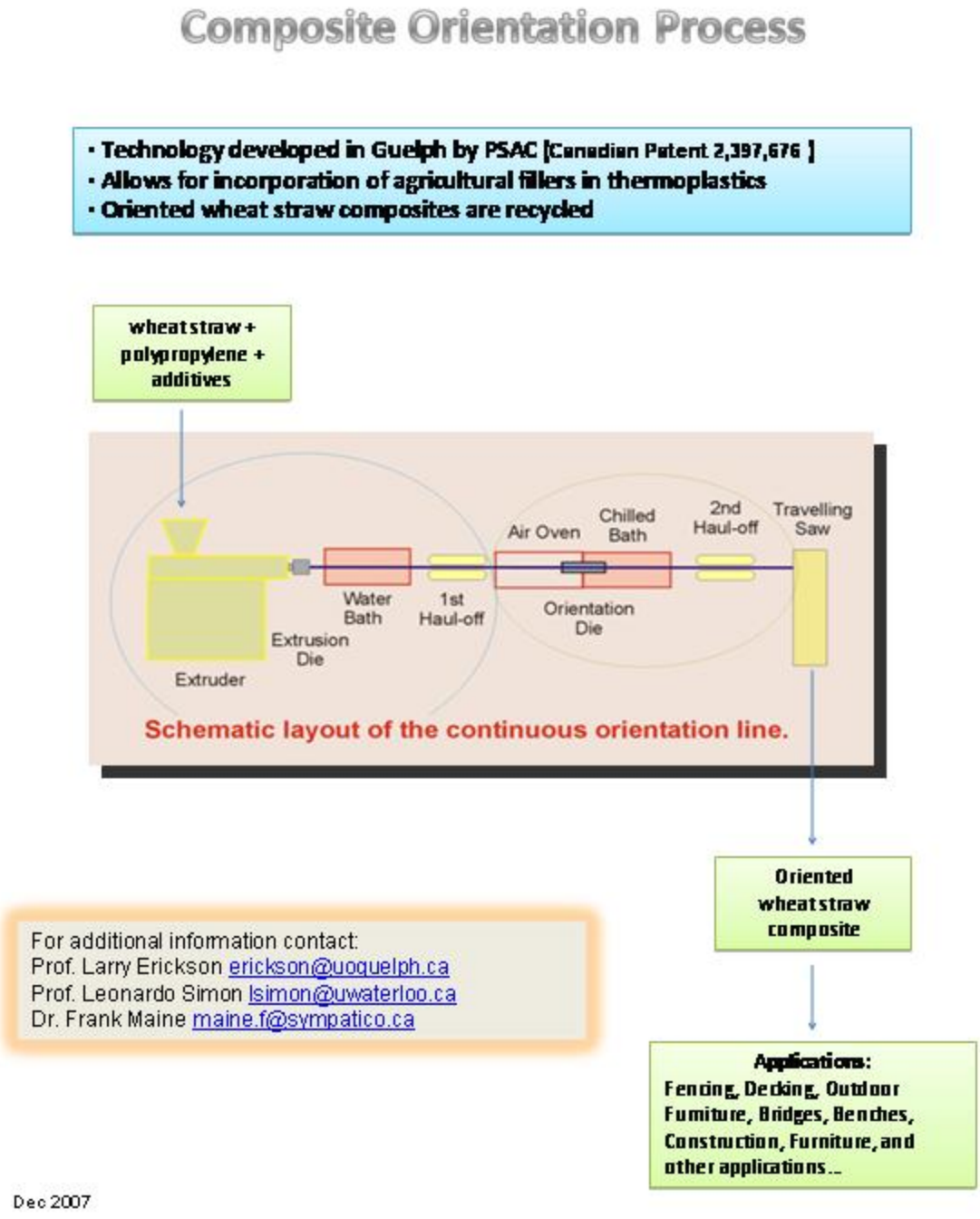

Figure A5.2: OMAFRA display information, page 2

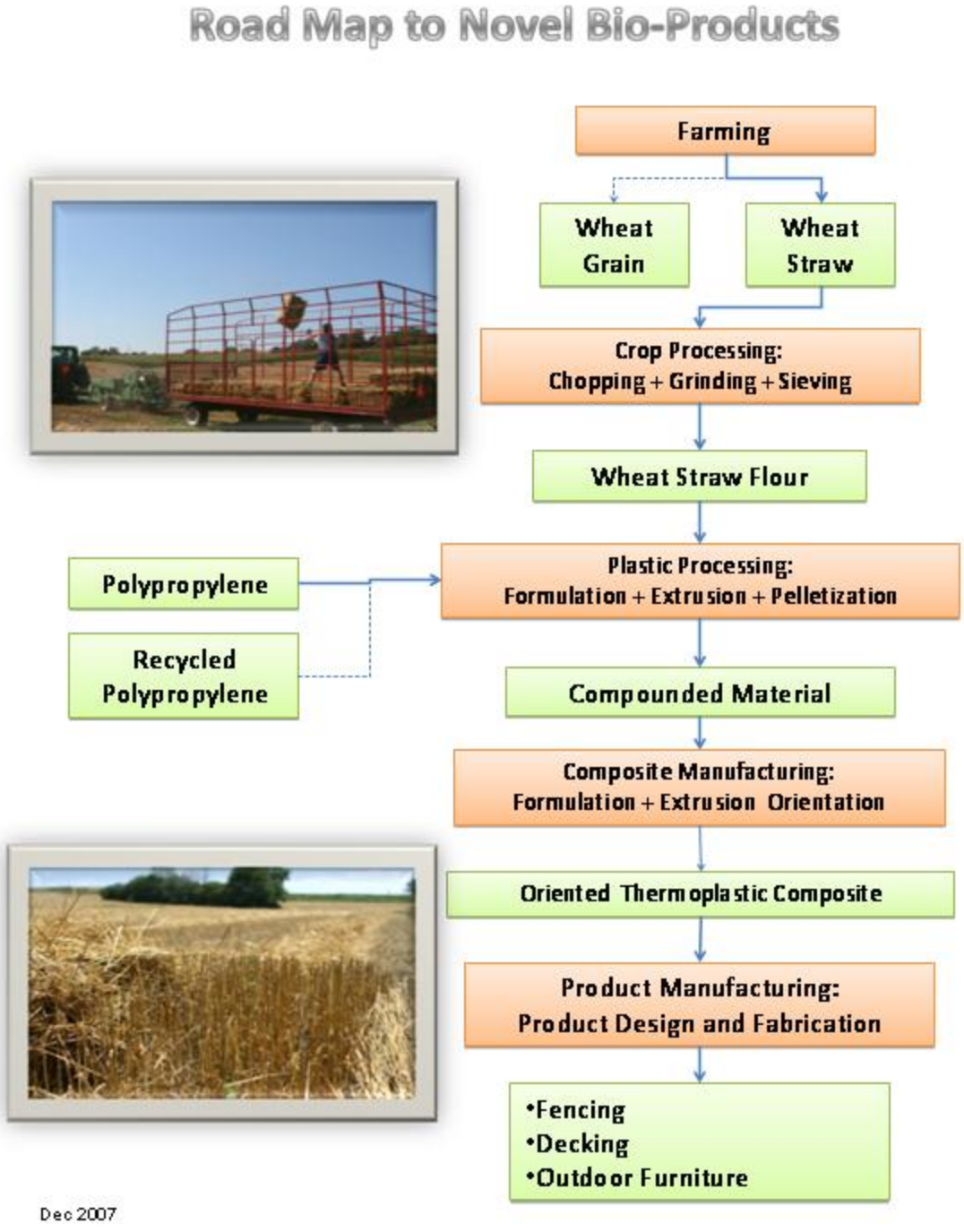

Figure A5.3: OMAFRA display information, page 3